

**KARADENİZ TECHNICAL UNIVERSITY  
THE GRADUATE SCHOOL OF NATURAL AND APPLIED SCIENCES**

**GEOLOGICAL ENGINEERING DEPARTMENT**

**THE PETROGENESIS AND GEODYNAMIC SETTING OF THE LATE CRETACEOUS  
PLUTONIC AND VOLCANIC ROCKS FROM ÇAYKARA MAGMATIC COMPLEX (ARAKLI/  
TRABZON, NE TURKEY)**

**DOCTOR OF PHILOSOPHY**

**Yaser ALMASHRAMAH**

**DECEMBER 2019  
TRABZON**



**KARADENİZ TECHNICAL UNIVERSITY  
THE GRADUATE SCHOOL OF NATURAL AND APPLIED SCIENCES**

**GEOLOGICAL ENGINEERING DEPARTMENT**

**THE PETROGENESIS AND GEODYNAMIC SETTING OF THE LATE CRETACEOUS  
PLUTONIC AND VOLCANIC ROCKS FROM ÇAYKARA MAGMATIC COMPLEX  
(ARAKLI/ TRABZON, NE TURKEY)**

**Yaser ALMASHRAMAH**

**This thesis is accepted to give the degree of  
DOCTOR OF PHILOSOPHY**

**By  
The Graduate School of Natural and Applied Sciences at  
Karadeniz Technical University**

**The Date of Submission : 05 / 11 / 2019**

**The Date of Examination : 18 / 12 / 2019**

**Thesis Supervisor : Prof. Dr. Cüneyt ŞEN**

**Trabzon 2019**

**KARADENİZ TECHNICAL UNIVERSITY**  
**THE GRADUATE SCHOOL OF NATURAL AND APPLIED SCIENCES**

**GEOLOGICAL ENGINEERING DEPARTMENT**

**Yaser ALMASHRAMAH**

**THE PETROGENESIS AND GEODYNAMIC SETTING OF THE LATE CRETACEOUS  
PLUTONIC AND VOLCANIC ROCKS FROM ÇAYKARA MAGMATIC COMPLEX  
(ARAKLI/ TRABZON, NE TURKEY).**

**Has been accepted as a thesis of**

**DOCTOR OF PHILOSOPHY**

**after the Examination by the Jury Assigned by the Administrative Board of the  
Graduate School of Natural and Applied Sciences with the Decision Number 828 dated  
19 / 11 / 2019**

**Approved By**

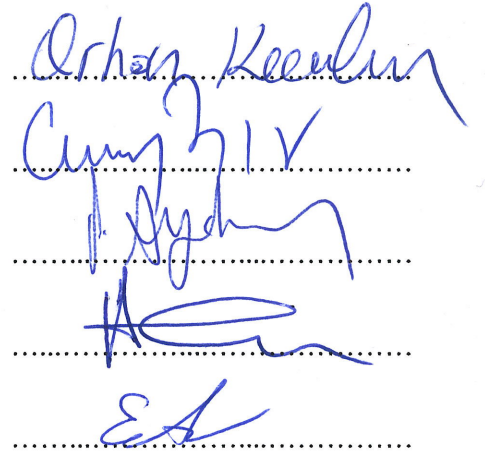
**Chairman : Prof. Dr. Orhan KARSLI**

**Member : Prof. Dr. Cüneyt ŞEN**

**Member : Prof. Dr. Faruk AYDİN**

**Member : Prof. Dr. Hakan KARSLI**

**Member : Assoc. Prof. Dr. Emre AYDINÇAKIR**



**Prof. Dr. Asim KADIOĞLU**  
**Director of Graduate School**

## ACKNOWLEDGEMENT

This project particularly take place on the aykara magmatic complex (south of Araklı, NE Turkey) aimed to study the petrological, geochronological and isotopical properties.

Thanks, are mainly due to my supervisor, Cüneyt ŐEN, who provided motivating discussions and explanations and for reviewing the manuscript. Many thanking to Associate Professor. Emre AYDINAKIR, Research assistant Ufuk Celal YAĐCIOĐLU and Muhammet OĐUZ for helping in terms of suggestion and technical stuff. I offer my regards and blessings to Professor Yener EYÜBOĐLU for help in term of age analysis of volcanic rocks. So many thanks to Professors Faruk AYDİN, Mehmet ARSLAN and Hakan KARSLI for scientific information. I would like to thank the Karadeniz Technical University Research Foundation (FDK-2017-7088) for supportive of my project.

Yaser ALMASHRAMAH  
DECEMBER-2019



## **THESIS ETHICS DECLARATION**

My PhD thesis entitle ‘The Petrogenesis and Geodynamic setting of the Late Cretaceous plutonic and volcanic rock from Çaykara Magmatic Complex (Araklı/ Trabzon, NE Turkey)’. I have done this project from start to end with sincere guidance my supervisor Prof. Dr Cüneyt ŞEN. As for the data, I have collected around 200 samples from the field and analyzed them in specialised laboratories. The information cited in text from different sources have been documented in the reference list. The work in the thesis has followed the scientific menthods. In case the thesis found to be violating the scientific method of research, I am ready to accept the decision of the committee. 18/12/2019

Yaser ALMASHRAMAH

## CONTENTS

	<b>Page No</b>
ACKNOWLEDGMENT .....	III
THESIS ETHICS DECLARATION .....	IV
CONTENTS .....	V
ÖZET .....	VIII
ABSTRACT .....	XI
FIGURE LIST .....	XII
TABLE LIST .....	XX
SYMBOL INDEX .....	XXII
1. INTRODUCTION .....	1
1.1. Aims of the Thesis .....	1
1.2. Geographical Position of the Study Area.....	2
1.3. Geological Background .....	3
1.4. Previous Works .....	6
1.4.1 Petrological Studies .....	6
1.4.2 Tectonical Studies .....	13
2. SAMPLING AND ANALYTICAL METHODS .....	16
2.1. Methodology .....	16
2.1.1 Field Studies.....	16
2.1.2. Laboratories .....	16
2.1.2.1. Microscopic Investigations .....	17
2.1.2.2 Chemical Analysis .....	18
2.1.2.2.1. Whole Rocks Major Oxides, Trace Element and REE.....	18
2.1.2.2.2 Mineral Chemistry .....	18
2.1.2.2.3. Isotope Analysis .....	18
2.1.2.3 Geochronological Dating .....	19
2.1.3. Office Works.....	20
3. RESULT .....	22
3.1. Stratigraphical and Petrographical Studies .....	22
3.1.1. Pazarcık Metamorphic Rocks .....	22
3.1.2. Berdige Formation .....	25
3.1.3. Taşlıyayla Volcanic rocks.....	26

3.1.4.	Gündoğdu Pluton .....	38
3.1.5.	Boğalı Pluton .....	38
3.1.6.	Uzuntarla Pluton .....	44
3.1.7.	Eğerler Pluton .....	45
3.1.8	Salmankaş Volcanic Rocks .....	46
3.1.9	Basic and Acidic Dykes .....	47
3.2.	Mineral Chemistry .....	48
3.2.1.	Taşlıyayla Volcanic Rocks .....	48
3.2.1.1.	Plagioclase .....	48
3.2.1.2.	Clinopyroxene.....	48
3.2.1.3.	Chlorite .....	49
3.2.2.	Gündoğdu Pluton .....	49
3.2.2.1.	Plagioclase .....	49
3.2.2.2.	K-feldspar .....	50
3.2.2.3.	Amphibole.....	51
3.2.2.4.	Biotite.....	51
3.2.2.5.	Fe-Ti oxides .....	52
3.2.2.6.	Chlorite .....	52
3.2.3.	Boğalı Pluton .....	52
3.2.3.1.	Plagioclase .....	52
3.2.3.2.	K-feldspar .....	53
3.2.3.3.	Amphibole.....	54
3.2.3.4.	Biotite.....	54
3.2.3.5.	Fe-Ti oxides .....	55
3.2.3.6.	Chlorite .....	55
3.3.	Geochemistry.....	55
3.3.1.	Taşlıyayla Volcanic Rocks .....	55
3.3.2	Gündoğdu Pluton.....	62
3.3.3.	Boğalı Pluton .....	73
3.4.	Isotope Analysis .....	81
3.4.1.	Gündoğdu Pluton .....	81
3.4.2.	Boğalı Pluton .....	81
3.5.	Geochronology.....	82
3.5.1.	Taşlıyayla Volcanic Rocks .....	82

3.5.2.	Gündoğdu Pluton .....	82
3.5.3.	Boğalı Pluton .....	85
3.5.4.	Salmankaş Volcanic .....	85
4.	DISCUSSIONS .....	88
4.1.	Taşlıyayla Volcanic Rocks .....	88
4.2.	Gündoğdu Pluton .....	97
4.3.	Boğalı Pluton .....	106
4.4.	P-T Conditions of Crystallization and Emplacement .....	116
4.4.1	Taşlıyayla Volcanic Rocks .....	116
4.4.2	Gündoğdu and Boğalı Plutons .....	118
4.5.	Geodynamic Implications .....	123
5.	CONCLUSIONS .....	128
6.	REFERENCES .....	133
7.	APPENDIX .....	147
8.	RESUME .....	186

## Doktora Tezi

### ÖZET

#### ÇAYKARA MAGMATİK KOMPLEKSİNDE (ARAKLI/ TRABZON, TÜRKİYE) GEÇ KRETASE YAŞLI PLÜTONİK VE VOLKANİK KAYAÇLARIN PETROJENEZİ VE JEOTEKTONİK ORTAMI

Yaser ALMASHRAMAH

Karadeniz Teknik Üniversitesi  
Fen Bilimleri Enstitüsü  
Jeoloji Mühendisliği Anabilim Dalı  
Danışman: Prof. Dr. Cüneyt ŞEN  
2019, 146 Sayfa, 39 Ek Sayfa

Çalışma alanı Karadeniz bölgesinin doğusunda, Araklı (Trabzon) İlçesi'nin güneyinde ve Kaçkar Batoliti'nin batı kısmında yer almaktadır. Alanda Üst Kretase yaşlı plütonik ve volkanik kayalar yüzeylenmektedir. Bu çalışmanın amacı, Araklı (Trabzon) ilçesinin güney kesiminde bulunan Çaykara Magmatik Kompleksine ait volkanik ve plütonik kayaların petrolojik, jeokronolojik ve izotopik özelliklerini incelemektir.

Çalışma alanının tabanında Geç Kretase yaşlı bazalt ve andezitlerden oluşan Taşlıyayla Volkanitleri bulunur. Taşlıyayla Volkanitleri iri taneli granit, granodiyorit, monzogranit ve diyorit bileşimli kayaların oluşturduğu Geç Kretase yaşlı Gündoğdu Plütonu tarafından kesilmiştir. Plüton içerisinde, oval yarı köşeli kayalar şeklinde diyorit ve kuvars monzodiyorit kompozisyonda mafik magmatik anklavlar (MMA) bulunur. Gündoğdu r çeşitlilik gösterir. Geç Kretase yaşlı Boğalı Plütonu granit ve monzogranitten oluşmuştur ve diyorit ile kuvars monzodiyorit bileşiminde MMA içerir. Geç Kretase yaşlı kayalar, Eosen yaşlı asidik ve bazik dayklar tarafından kesilmiştir.

Geç Kretase'de oluşmuş kayalar içerisindeki zirkon minerallerinden itibaren yapılan SHRIMP U-Pb yaş analizlerinden, Taşlıyayla Volkanitleri'nin  $92.5 \pm 2$  My (Turoniyen), Gündoğdu Plüton'un  $85.0 \pm 2.4$  My (Santoniyen) ve Boğalı Plüton'un  $83.6 \pm$  My (Kampaniyen) yaşında oldukları saptanmıştır.

Taşlıyayla volkanik kayalarının ana ve iz element içeriklerindeki farklılıklar, plajiyoklaz, klinopiroksen, klorit, Fe-Ti oksitler, apatit,  $\pm$  amfibolün bazaltik ve andezitik kayaların oluşumları sırasındaki geçirmiş oldukları fraksiyonel kristalleşmesi ile açıklanmıştır. İlksel mantoya-normalize edilmiş element diyagramlarında, büyük iyon çaplı

elementler ve hafif nadir toprak elementlerin zenginleştiği, yüksek alan enerjili elementlerin tüketildiği görülmektedir. Kondrite normalize edilmiş nadir toprak elementi desenleri birbirine benzer ve paraleldir ((La/Lu)<sub>N</sub> = 4-11). İz element modelleri volkanitleri oluşturan magmanın sığ-manto kaynağının (yani MORB benzeri spinellerzolit) düşük ila orta derecede bölümsel ergimesi ile oluştuğunu göstermektedir. Kimyasal ve izotopik bileşimleri Taşlıyayla Volkanitlerini oluşturan magmaların farklı petrolojik olaylar sonucu kimyasını değiştirdiğini (fraksiyonel kristallenme, birbiri ardından gelen mafik magmaların birbiriyle karışımı ve/veya az miktarda da olsa kabuksal kirlenmesi gibi) göstermektedir.

Gündoğdu Plütununun Al-doygunluk indisi metalüminden peralümine geçişli yönseme sunarken, Boğalı Plütunu metalümin özelliklidir. Her iki plütonda, K, Rb, Th ve U gibi büyük iyon yarıçaplı litofil elementlerce bakımından zenginleşmiş ve Nb, Ta, Sr, P ve Ti bakımından tüketilmiştir. Kondrite normalleştirilmiş lantanit grubu element diyagramlarında, (La/Lu)<sub>N</sub> oranları 5-15 arasında değişir ve belirgin negatif Eu anomalileri (Eu/Eu\* = 0.3-0.93) gösterirler. <sup>87</sup>Sr/<sup>86</sup>Sr(i), <sup>143</sup>Nd /<sup>144</sup>Nd(i) ve <sup>206</sup>Pb/<sup>204</sup>Pb(i) izotopik oranları, Gündoğdu Plütunu için sırasıyla 0.703552 ila 0.711929, 0.512222 ila 0.512084 ve 17.986 ila 18.534 arasındayken, Boğalı Plütunu için 0.706097 ila 0.706657, 0.512279 ila 0.512341 ve 18.247 ila 18.718'dir. Söz konusu izotop değerlerinden Gündoğdu için hesaplanan εNd (85) değerleri -7.58 ile -9.65 arasında, Boğalı için hesaplanan εNd (80) değerleri -3.92 ile -9.65 arasında değişmektedir. İncelenen kayaçların kimyasal özellikleri volkanik yay alanlarında bulunan granitik kayaçlarla benzer özelliklerdedir.

Plütunları oluşturan kayaçların mineral kimyasına göre belirlenen kristalleşme koşulları bunların kayaçların genellikle orta-sığ kabuk derinliklerinde kristalleştiğini göstermiştir. Gündoğdu Plütununun oluşturan magmanın kaynağı, metagrovak, amfibolit, metabazalt ve metapelitik kayaçların, litosferik mantodan türeyen magmanın etkisiyle kısmi ergimesi ve her iki ergiyiğin karışmasıyla oluşan bir magmadır. Buna karşın Boğalı Plütununun oluşturan magmanın kaynağı amfibolitik kayacın litosferik mantodan türeyen magmanın etkisiyle kısmi ergimesi ve her iki ergiyiğin karışmasıyla oluşan bir magmadır. İzotop ve iz elementlerden oluşturulan karışım modelinde Gündoğdu Plütununun oluşturan magmanın %65-60 kabuktan ve 35-40 mantodan, Boğalı Plütununun oluşturan magmanın, ~%25-35 kabuk ve ~%65-75 mantodan türetilmiş magmadan oluştuğu hesaplanmıştır.

Genel olarak Gündoğdu ve Boğalı Plütunlarının içermiş olduğu MMA'lar izotopik olarak host (ana) kayaçlarına benzerlik gösterir ve aynı oluşum süreçlerini paylaştığını

gösterir. Silisyumdioksite karşı çizilen ikili değişimde fraksiyonel kristalleşmenin (FC) plutonları oluşturan magmanın oluşumunda aktif rol oynadığını göstermektedir.

Taşlıyayla volkanik kayalar Turoniyen'de Neotetis Okyanusu'nun kapanmasının ilk aşamasında spinel içeren lerzolitlerin yüksek derecelerde sığ derinliklerde (yaklaşık 50 km) ergimesi sonucu ortaya çıkan magmadan oluşmuştur. Gündoğdu ve Boğalı plütonları, Neotetis Okyanusu'nun kapanmasının olgunluk (Santoniyen) ve son aşamalarına denk (Kampaniyen) yay üzerindeki kabuğun mantodan gelen magma ile ergimesi ve karışması sonucu oluşmuştur.

**Anahtar Kelimeler:** Sr-Nd-Pb-O izotopları, U-Pb zirkon yaşları, Geç Kretase yaşlı volkanitler, Geç Kretase yaşlı, Doğu Pontidler, Trabzon-Araklı.

PhD Thesis

THE PETROGENESIS AND GEODYNAMIC SETTING OF THE LATE  
CRETACEOUS PLUTONIC AND VOLCANIC ROCKS FROM ÇAYKARA  
MAGMATIC COMPLEX (ARAKLI/ TRABZON, NE TURKEY).

SUMMARY

Yaser ALMASHRAMAH

Karadeniz Technical University  
The Graduate School of Natural and Applied Sciences  
Geology Engineering Graduate Program  
Supervisor: Prof. Dr. Cüneyt ŞEN  
2019, 146 Pages, 39 Appendix

The study area situated in the eastern of Black Sea region, south of Araklı (Trabzon) district and occupied the western part of the Kaçkar Batholith. The aim of this study is to study petrological, geochronological and isotopically properties of volcanic and plutonic rocks. SHRIMP U-Pb age analysis, the emplacement age is  $92.5 \pm 2$  Ma (Turonian) for Taşlıyayla volcanic rock,  $85.0 \pm 2.4$  Ma (Santonian) for Gündoğdu plutonic rocks,  $83.1 \pm 2$  Ma (Campanian) for Boğalı plutonic rocks. Petrographically the Taşlıyayla volcanic rocks consist of basaltic and andesitic rocks, Gündoğdu Pluton and Boğalı Pluton varies from granite to monzogranite. Differences in chemical properties of Taşlıyayla volcanic rocks indicate to the importance of FC as a primary process during the magma generation with magma mixing and indicating to magma products of a shallow mantle source (i.e. MORB-like spinel-lherzolite). The isotopic ratios of  $^{87}\text{Sr}/^{86}\text{Sr}$ ,  $^{143}\text{Nd}/^{144}\text{Nd}$  and  $^{206}\text{Pb}/^{204}\text{Pb}$  of the rocks belonging to the Gündoğdu Pluton are between 0.703552 to 0.711929, 0.512222 to 0.512084 and 17.986 to 18.534, respectively. The isotopic ratios of  $^{87}\text{Sr}/^{86}\text{Sr}$ ,  $^{143}\text{Nd}/^{144}\text{Nd}$  and  $^{206}\text{Pb}/^{204}\text{Pb}$  for the Boğalı Pluton range from 0.706097 to 0.706657, 0.512279 to 0.512341 and 18.247 to 18.718, respectively. Chemical features of Gündoğdu and Boğalı pluton rocks indicate to dominant the FC, and magma mixing with minor amount of crustal contamination during the magma generation. The Taşlıyayla volcanic rocks formed during the first stage of closure of the Neotethyan Ocean. The Gündoğdu and Boğalı Plutons were formed during the last stage closure of the Neotethyan Ocean as result as a result of extensional arc and slab-roll back model.

**Key Words:** Sr-Nd-Pb-O isotopes, U-Pb zircon ages, Late Cretaceous volcanic, Late Cretaceous pluton, Eastern Pontides, Trabzon, Araklı.



## FIGURE LIST

	<u>Page No</u>
Figure 1. Geological map including study area (Modified from Güven. 1993) .....	2
Figure 2. Tectonic map of the north-eastern Mediterranean region showing the main blocks in relation to the Afro-Arabian and Eurasian plates (modified after Okay and Tüysüz, 1999). (b) The disturbance of the main tectonic feature in the Eastern Pontides. (Modified after Eyüboğlu et al, 2010).....	7
Figure 3. Geological map of field study.....	21
Figure 4. Generalised columnar section of the study area showing the stratigraphical units.....	23
Figure 5. Photograph showing the boundary between Pazarcık metamorphic rock and Berdiga carbonate rock 40°36'9.81"-39°57'14.27"NE. ....	23
Figure 6. Photo showing a banding of Gneiss rock in Pazarcık Formation 40°63.4.35"- 39°57'24.27"NE.....	24
Figure 7. Photomicrographic showing mineral content and foliations in Gneiss rock in Pazarcık Formations, (a, b, e,f) displays the lepidogranoblastic (Qz: quartz, Or: orthoclase, Ms: Microcline, Bio: biotite).....	24
Figure 8. Photograph taken from south to north showing the Berdiga formation in between the of Boğalı pluton and Taşlıyayalı volcanic rocks 40°36'37.07"- 40° 2'4.54"NE .....	25
Figure 9. Photograph showing the distribution of carbonate rock 40°31'21.50"- 40° 8'0.10"NE.....	26
Figure 10. Photographs taken from North of Pelitli Village 40°34'26.98"- 40° 0'2.72"NE and displays the shape of Taşlıyayalı volcanic rocks in the field with some features (a) basalt with exfoliation structure, (b) high alteration. ....	27
Figure 11. Microphotographs showing microcrystalline porphyritic, microlitic porphyritic, glomeroporphyritic, microgranular, and poikilitic, (a, b) Microlitic porphyritic texture, represent microcrystalline porphyritic displays plagioclases sieve texture,(d) plagioclase exhibits with albite twinning, and oscillatory texture,represent glomeroporphyritic and poikilitic texture, (f) microcrystalline porphyritic displays phenocryst of clinopyroxene and plagioclase, (pl: plagioclase, Amp: amphibole, Cpx: clinopyroxene, Op: opaque minerals).....	28
Figure 12. Microphotographs showing microcrystalline porphyritic, microlitic porphyritic, glomeroporphyritic texture, (a) glomeroporphyritic texture of plagioclase, (d) microlitic porphyritic displays plagioclases, (b) microcrystalline porphyritic texture contain plagioclase displays high alteration, (c, d) microlitic porphyritic texture contain Plagioclase shows oscillatory zoned.....	29
Figure 13. (a) The boundary between Boğalı and Gündoğdu pluton. (b) Microgranular enclave with dark color 40°34'38.70"-40°0'55.89"NE. ....	30

Figure 14. Modal classification of the Gündoğdu Granitoid (Streckeisen 1976). .....	31
Figure 15. General view showing the petrographically feature of granitic rock at Gündoğdu pluton: a) showing majority of mineral grain size and textural characteristics of the host rocks; b) microcrystalline porphyritic showing plagioclase altered, amphibole and anhedral epidote;; c,d) oscillatory texture, zoning in plagioclase and displays poikilitic texture; e,f) myrmekitic texture, (Q: Quartz, Pl: Plagioclase, Or: Orthoclase, Op: Opak minerals).....	33
Figure 16. General view showing the petrographically feature of granodiorite rock at Gündoğdu pluton: a) k- feldspar, Plagioclase altered showing myrmekitic texture; b) microcrystalline porphyritic texture showing high alteration, (Q: Quartz, Pl: Plagioclase, Or: Orthoclase) .....	34
Figure 17. General view showing the Petrographical feature of Synograndiorite rock at Gündoğdu pluton: a); b) phaneritic porphyritic texture microcrystalline porphyritic texture showing high alteration and zone in plagioclase (Q: Quartz, Pl: Plagioclase, Or: Orthoclase).....	34
Figure 18. General view showing the Petrographical feature of granitic rock at Gündoğdu pluton: (a) showing majority of mineral grain size and textural characteristics of the host rocks; (b) microcrystalline porphyritic showing amphibole altered and embayed quartz;(c) microcrystalline porphyritic showing plagioclase altered; d) microlitic texture, (Q: Quartz, Pl: Plagioclase, Or: Orthoclase) .....	36
Figure 19. Intersertal texture of dioritic rocks. ....	37
Figure 20. General view showing grained mafic enclave (sample) displays plagioclase altered and amphibole, (Pl: Plagioclase, Or: Orthoclase, Op: Opak minerals).....	38
Figure 21. Fine-medium grained to porphyritic textured of K-feldspar in monzogranite which forms the main body of the Boğalı Pluton containing large K-Feldspar 40°35'12.18"- 40°0'21.73"NE .....	39
Figure 22. Dacitic dayks at the road between Bahçekik and Boğalı (40°35'24.79"- 40° 0'26.25"NE).....	39
Figure 23. Modal classification of the Boğalı Granitoid (Streckeisen 1976) .....	41
Figure 24. (a,k)Microphotographs displaying certain textural features of the Boğalı monzogranite: ( a) albite plagioclase, amphibole altered and orthoclase, (b) microcrystalline texture showing Zone of plagioclase and biotite, (c) Micrographic texture and twinning in plagioclase phenocryst, (d) anhedral grain of quartz and plagioclase showing poikilitic and intersertal texture, (e) porphyritic texture showing zoning in plagioclase, and quartz, (f) Orthoclase show poikilitic texture, (Q: Quartz, Pl: Plagioclase, Or: Orthoclase, bi: Biotite).....	42
Figure 25. Microphotographs displaying the textural features of the Boğalı granitic rock: a) phaneritic porphyritic texture showing albite twinning and small grain of quartz: b) phaneritic texture showing poikilitic texture; c-d) phaneritic porphyritic texture showing albite twinning, biotite and fine	

grain of quartz, (Q: Quartz, Pl: Plagioclase, Or: Orthoclase, Op: Opak minerals) .....	43
Figure 26. Microphotographs displaying fine grained mafic enclave (sample) displays plagioclase altered and amphibole.....	44
Figure 27. Photo showing the distribution of Uzuntarla pluton and their MMEs in the west of Şeyhi plateau 40°34'17.54"N-40°11'13.09"E.....	45
Figure 28. Photographs showing the distribution of Eđerler pluton and their MMEs in the southeast of Gündođdu Village 40°30'40.53"N- 40° 8'50.71"E.....	46
Figure 29. Microphotographs in which rocks of Salmankaş volcanic rocks displaying microcrystalline porphyritic, microlitic porphyritic, glomeroporphyritic, microgranular, and intersertial texture, (a) Microlitic porphyritic texture, (b) microcrystalline porphyritic displays plagioclases and biotite, (c) plagioclase exhibits with albite twinning, (d) glomeroporphyritic texture showing plagioclase zoned and altered, (pl: plagioclase, bio: biotite, Cpx: clinopyroxene, Op: opaque minerals).....	47
Figure 30. Mineral classification of sample from Taşlıyayla volcanic rocks: (a) a ternary An-Ab-Or diagram of feldspars classification (after Deer et al. 1992), (b) classification diagram of clinopyroxene (after Morimoto et al. 1988).....	48
Figure 31. Classification of chlorites based on the diagram of Hey (1954). .....	49
Figure 32. Ternary An-Ab-Or diagram of feldspars classification for sample from Gündođdu pluton (after Deer et al. 1992).....	50
Figure 33. Scattered electron (BSE) of some plagioclase and amphibole minerals in the rocks to from Gündođdu pluton.....	50
Figure 34. Hornblend Classification diagram (after Leak et al. 1997) of the plutonic rocks from Gündođdu Pluton .....	51
Figure 35. Feldspars Classification on a ternary An-Ab-Or plot for sample from Bođalı pluton (after Deer et al. 1992).....	53
Figure 36. Scattered electron (BSE) of some plagioclase, quartz, orthoclase and amphibole minerals in from Bođalı pluton.....	53
Figure 37. Hornblend Classification diagram (after Leak et al. 1997) of the plutonic rocks from Bođalı Pluton.....	54
Figure 38. General of chemical classification of Taşlıyayla volcanic rocks, (a) log Nb/Y vs. log Zr/Ti by Pearce (1996), b) Chemical nomenclature diagram of (Le Maitre et al., 1989), separation curve between the field of subalkaline and alkaline magma after Irvine & Barager, (1971) for selected samples. Abbreviations, Ba: Basalt, And: Andesite, And/Ba: Andesite/Basalt, Rh/Da: Rhyolite/Dacite, Alk-Rh: Alkalia Rhyolite, Tr: Trachyte, Tr-An: Trachyte- Andesite, Tr-Da: Trachyte-Dacite, Alk-Ba: Alkalia Basalt, Te-Pho: Tephri-Phonolite, Pho: Phonolite, Da: Dacite, Tr-Ba: Trachy-Basalt, Te: Tephrite, Pho-te:Phonolite-tephrite, Te-pho: Tephri-Phonolite, Rh: Rhyolite. ....	56

Figure 39. (a) Classification of Altered rocks by using Immobile Trace Elements Taşlıyayla formation.....	57
Figure 40. Selected SiO <sub>2</sub> versus major oxide plots for the Taşlıyayla volcanic rocks.....	60
Figure 41. Selected SiO <sub>2</sub> versus trace elements plots for the Taşlıyayla volcanic rocks.....	61
Figure 42. (a) Chondrite normalized rare earth element patterns of Taşlıyayla 2volcanic rocks, (b) Primitive mantle-normalized trace-element patterns for samples from the Taşlıyayla volcanic rock. Normalizing values for chondrite and primitive mantle and are from Taylor and McLennan 1985 and Sun and McDonough 1989 respectively .....	62
Figure 43. General of chemical classification of Gündoğdu plutonic rocks. (a) Chemical nomenclature diagram of (Debon and Le Lort, 1982) for selected samples, (b) log Nb/Y vs. log Zr/Ti by Pearce (1996), (c) Classification diagram (Le Maitre et al., 1989) separation curve between the field of subalkaline and alkaline magma after Irvine & Barager, (1971), (d) ternary diagram between calc-alkaline and tholeiitic subalkaline series by (Irvine & Baragar, 1971). Abbreviations: Gra/Gran: Granite/Granodiorite, Ga-Dio Dio: Gabbro-Diorite Diorite, Ga: Gabbro, Alk Ga: Alkalia Gabbro, Mon: Monzonite, Q Mon: Quartz Monzonite, Fo Sy: Foid Syenite, Fo Mon: Foid Monzosyenite, Dio: Diorite, Mon dio: Monzodiorite, Mon ga: Monzogabbro.....	63
Figure 44. (a) General chemical classification of Altered plutonic rocks by using Immobile Trace Elements, (b) aluminum saturation index] (after Maniar and Piccoli (1989).....	64
Figure 45. Selected SiO <sub>2</sub> versus major oxide plots for the Gündoğdu Plutonic rocks.....	65
Figure 46. Selected SiO <sub>2</sub> versus trace element plots for the Gündoğdu plutonic rocks.....	66
Figure 47. (a,b) Chondrite normalized rare earth element patterns of Gündoğdu Plutonic rocks, (c,d) Primitive mantle-normalized trace-element patterns for samples from the Gündoğdu Plutonic rocks. Normalizing values for chondrite and primitive mantle and are from Taylor and McLennan 1985 and Sun and McDonough 1989 respectively. ....	73
Figure 48. General of chemical classification of Boğalı plutonic rocks. (a) Chemical nomenclature diagram of (Debon and Le Fort, 1982), (b) log Nb/Y vs. log Zr/Ti by Pearce, (1996) for selected samples. Abbreviations: Gra/Gran: Granite/Granodiorite, Ga-Dio Dio: Gabbro-Diorite Diorite, Ga: Gabbro, Alk Ga: Alkalia Gabbro, Mon: Monzonite, Q Mon: Quartz Monzonite, Fo Sy: Foid Syenite, Fo Mon: Foid Monzosyenite. ....	74
Figure 49. (a) Classification diagram (Le Maitre et al., 1989), separation curve between the field of subalkaline and alkaline magma after Irvine & Barager, (1971), (d) a discriminate diagram between calc-alkaline and tholeiitic subalkaline series by (Irvine & Baragar, 1971). Abbreviations: Gra: Granite, Gran: Granodiorite, Ga-Dio: Gabbro-Diorite, Dio: Diorite, Ga: Gabbro, Mon: Monzonite, Q Mon: Quartz Monzonite, Dio: Diorite, Mon dio: Monzodiorite, Mon ga: Monzogabbro.....	75

Figure 50. Selected SiO <sub>2</sub> versus major oxides plots for the Boğalı intrusions .....	76
Figure 51. Selected SiO <sub>2</sub> versus trace element plots for the Boğalı intrusions.....	77
Figure 52. a) General classification of Altered plutonic rocks by using Immobile Trace Elements, (b) aluminum saturation index (after Maniar and Piccoli (1989).....	78
Figure 53. (a)Chondrite normalized REE patterns from the Boğalı pluton, (b) Chondrite normalized rare earth element patterns for MMEs of the Boğalı pluton, (c) Primitive mantle-normalized trace-element patterns for samples from the Boğalı pluton, (d) Primitive mantle-normalized trace-element patterns for MMEs of the Boğalı pluton. Normalizing values for chondrite and primitive mantle and are from Taylor and McLennan (1985) and Sun and McDonough (1989) respectively.....	78
Figure 54. Sr-Nd-Pb isotope diagram of Gündoğdu and Boğalı plutonic rocks (a): $\epsilon\text{Nd}_{(i)}$ vs. ( $^{87}\text{Sr}/^{86}\text{Sr}$ ) <sub>(i)</sub> , (b) and (c) plots of $^{206}\text{Pb}/^{204}\text{Pb}$ (i) vs. $^{207}\text{Pb}/^{204}\text{Pb}$ (i) and $^{208}\text{Pb}/^{204}\text{Pb}$ (i) ratios. Lithospheric mantle and mantle array data are from Davies and Von Blanckenburg (1995) and Arculus and Powell (1986), McCulloch et al. (1994) and Wilson (1989) respectively. The data source from Eastern Pontides are as follows: Şışdağı pluton from Karşlı et al. (2012b); Harşıt pluton from Karşlı et al. (2010a); Maçka subvolcanic rock from Aydın 2014; and palaeozoic Köse pluton from Dokuz (2011). EM I: enriched mantle I; HIMU: high- $\mu$ ( $\mu = 238\text{U}/204\text{Pb}$ ); EM II: enriched mantle II; LC: lower crust; UC: upper crust; NHRL: Northern Hemisphere Reference Line (Hart, 1984). Lower crust (LC) from Kempton et al. (1997), HIMU, EM I and EM II from Zindler and Hart (1986).....	83
Figure 55. Concordia diagrams displaying U–Pb age results of zircons from the Taşlıyayla volcanic rocks. ....	84
Figure 56. (a) Concordia diagrams displaying U–Pb age results of zircons grain from Gündoğdu granitoid, (b) weighted average. ....	85
Figure 57. (a) Concordia diagrams displaying U–Pb age results of zircons grain from Boğalı pluton, (b) weighted average. ....	86
Figure 58. (a) Concordia diagrams displaying U–Pb age results of zircons grain from the salmankaş volcanic rocks.....	86
Figure 59. (a) Ti/100-Zr-Sr/2 diagram (Pearce ve Cann, 1973), (b) Hf/3-Th-Ta discrimination diagram (Wood et al., 1979).....	88
Figure 60. Microphotographs of the Taşlıyayla volcanic rocks (a,b,c,d) plagioclase with sieve texture and reflect the change of composition, (e,f) zoning, resorbed rims, and embayed albite in clinopyroxene, (g,h) hornblende with eroded edges and skeletal structure. ....	90
Figure 61. (a) Rb/Y versus Nb/Y for the volcanic samples (upper crust and lower crust are from, (Taylor ve McLennan (1985)), (b) Th/Yb versus Ta/Yb diagram (after Pearce et al. 1990) for the Taşlıyayla volcanic rocks. composition of continental crust and the N-MORB taken are from Taylor and McLennan (1985) and Sun and McDonough (1989) respectively.	

	Vectors displays effects of magma generation process during the evolution of Taşlıyala volcanic rocks Pearce et al. (1990). .....	91
Figure 62.	(a)Th(ppm) vs.TbN/YbN for volcanic sample of Taşlıyayla formation displays horizontal line separates fields expected for melting garnet–and spinel–lherzolite as determined for Basin and Range basalts (Wangetal.,2002), (b) Non-modal Rayleigh partial melting model used to determine the main magmas of the Taşlıyayla volcanic and Taşlıyayla Eocene volcanic rocks (chondrite normalized rare earth element distributions of the melt created by partial melting of the spinal lherzolite source in different degrees (spinal lherzolite , E-type MORB and Ocean Island basalt values are from Sun and McDonough (1989)), the modal composition and melting ratios of the mantle, are from Frey (1984), the partition coefficients are from McKenzie ve O’Nions (1991). Chondrite normalized values are from Taylor and McLennan (1985). .....	94
Figure 63.	(a) Th/Y vs Nb/Y (Pearce 1983), (b) The Nb/La vs La/Yb variation diagram, Jahn et al. 1999), (c) Nb/Th vs Nb(ppm) diagram after Hofmann (1988), (d) TiO <sub>2</sub> /Yb vs Nb/Yb digram (after Pearce,2008), indicating of the genesis of volcanic rocks. Composition of OIB and composition of lower crust is taken from Fitton et al (1991) and Chen and Arculus (1995) respectively. Dashed lines that splite the fields of asthenospheric, mixed mantle and lithospheric and the HIMU OIB field are after Smith et al.(1999) and Weaver et al. (1987),respectively, (c) Nb/Th vs Nb The compositions of MORB and OIB after Harms et al. (1997). .....	95
Figure 64.	(a, b) Nb-Y and Ta -Nb discrimination diagrams (Pearce et al. 1984) for samples from the Gündoğdu pluton, displaying the fields of volcanic-arc granites (VAG), syn- collisional granites (Syn-COLG), within-plate granites (WPG) and ocean-ridge granites(ORG), (c) Sr/Y vs Y for samples from Gündoğdu pluton, (d) Nb vs Rb/Zr diagram (Brown et al. 1984). .....	98
Figure 65.	(a)Rb/Sr vs. Ti/Zr diagram, (b) Sr/Zr vs Ti/Zr diagram for Gündoğdu pltonic rocks which indicating to mixing between two distinct geochemical end-members (i.e. mantle derived-magmas and lower crustal components. ....	100
Figure 66.	Microphotographs of the Gündoğdu plutonic rocks (a,b) plagioclase with seive texture showing the change of composition. ....	100
Figure 67.	(a) SiO <sub>2</sub> vs ISr (85 Ma); (b) SiO <sub>2</sub> vs eNd (85 Ma) (c) 1/Sr vs ISr (85 Ma) and (d) La/Yb ratio vs La (ppm) content for the Gündoğdu pluton. ....	101
Figure 68.	Diagrams of Nb–Y–Ga*3 (Eby, 1992) for Gündoğdu pluton explained the magma source. ....	104
Figure 69.	Chemical composition of the Gündoğdu plutonic rocks. (a) (Na <sub>2</sub> O <sub>3</sub> K <sub>2</sub> O FeO MgO TiO <sub>2</sub> ) vs (Na <sub>2</sub> O <sub>3</sub> K <sub>2</sub> O)/FeO TiO <sub>2</sub> MhO), (b) ASI vs Molar K <sub>2</sub> O Na <sub>2</sub> O <sub>3</sub> , (c) SiO <sub>2</sub> vs Mg#. abbreviation, MB metabasalts; MA meta-andesites; MGW metagreywackes; MP metapelites; AMP amphibolites. sources of data: Vielzeuf and Holloway (1988), Patinˆo Douce and Johnston (1991), Rapp et al. (1991), Gardien et al. (1995), Rapp (1995),	

	Rapp and Watson (1995), Patinˆo Douce and Beard (1996), Stevens et al. (1997), Skjerlie and Johnston (1996), Patinˆo Douce (1997, 1999), Patinˆo Douce and McCarthy (1998).....	105
Figure 70.	(a,b) discrimination diagrams of Nb vs Y and Ta vs Nb (Pearce et al. 1984) of Boğalı pluton, (c) Sr/Y– Y for samples from the Boğalı pluton. (d) Nb vs Rb/Zr diagram (Brown et al. 1984). abbreviation; volcanic-arc granites (VAG), syn- collisional granites (Syn-COLG), within-plate granites (WPG) and ocean-ridge granites (ORG).....	107
Figure 71.	(a) Diagram of Rb/Sr vs. Ti/Zr, (b) linear correlation between Sr/Zr vs Ti/Zr for Boğalı pltonic rocks indicating to mixing process. ....	109
Figure 72.	(a) SiO <sub>2</sub> vs ISr (82 Ma); (a) SiO <sub>2</sub> vs eNd (82 Ma) and (c) 1/Sr vs ISr (82 Ma) for the Boğalı pluton. ....	109
Figure 73.	Microphotographs of the Boğalı plutonic rocks (a,b) plagioclase with seive texture showing the change of composition, (c,d) hornblende with eroded edges and skeletal structure .....	110
Figure 74.	Chemical composition of the Boğalı pltonic rocks, (a) (Na <sub>2</sub> O <sub>3</sub> K <sub>2</sub> O FeO MgO TiO <sub>2</sub> ) vs (Na <sub>2</sub> O <sub>3</sub> K <sub>2</sub> O)/FeO TiO <sub>2</sub> MnO), (b) ASI vs Molar K <sub>2</sub> O Na <sub>2</sub> O <sub>3</sub> , (c) SiO <sub>2</sub> vs Mg#, (d) Nb–Y–Ga*3 (Eby, 1992). Different diagrams for samples from the Boğalı pluton explained the magma source. Abbreviation, MB metabasalts; MA meta-andesites; MGW metagreywackes; MP metapelites; AMP amphibolites. Data sources: Vielzeuf and Holloway (1988), Patinˆo Douce and Johnston (1991), Rapp et al. (1991), Gardien et al. (1995), Rapp (1995), Rapp and Watson (1995), Patinˆo Douce and Beard (1996), Stevens et al. (1997), Skjerlie and Johnston (1996), Patinˆo Douce (1997, 1999), Patinˆo Douce and McCarthy (1998).....	114
Figure 75.	<sup>143</sup> Nd/ <sup>144</sup> Nd(represent) vs. <sup>87</sup> Sr/ <sup>86</sup> Sr(represent) plot for samples from the Boğalı and Gündoğdu plutons with simple source mixing lines between basaltic mantle (BM; Aydın et al., 2017) and local lower crustal (LCC, Gnesis of a Paleozoic age from Tübitak 114Y219, 2018) end members by using two component equation of (Langmuir et al, 1978) and AFC equation of ( Depaolo 1981), UUC from Taylor and McLennan (1985). ....	115
Figure 76.	Ternary diagram An–Ab–Or by using the method of (Fuhrman and Lindsley 1988) for the feldspar compositions of Taşlıyayla formation. ....	117
Figure 77.	Ternary diagram of An–Ab–Or using the method of (Fuhrman and Lindsley 1988) for the feldspar compositions for Gündoğdu and Boğalı pluton. ....	119
Figure 78.	The minnum tempreture for melting by this digram SiO <sub>2</sub> and P <sub>2</sub> O <sub>5</sub> according to pressure (Watson ve Green, 1982).....	120
Figure 79.	Proposed geodynamic model for Late Cretaceous volcanic and plutonic rocks and evolution of the ESZ (NE Turkey). Explanations: (a) The initiation of a northward-directed subduction leading Incorporation of slab-derived fluids to the mantle wedge and area of metasomatised spinel-lherzolite mantle and generation of the Taşlıyayla basaltic melt.	

This subduction would have started to subduct at a relatively higher angle because the subducting oceanic lithosphere would have been the oldest. (b) Subduction angle less angle due to the age and density of oceanic lithosphere and significant amounts of heat flow input from MOR leading to partial melting of the metasomatised mantle and generation of Gündoğdu pluton. (c) An increasing age of the subducting oceanic crust, the subduction angle becoming increasingly upright due to the “roll-back” must have caused the volcanism to immigrate from the arc towards the fore-arc basin and the magma source area to immigrate deeper and deeper and leading to generation of Boğali pluton. ....127





## TABLE LIST

	<u>Page No</u>
Table 1. Mineral modes that in the sample collected in Gündoğdu pluton (more than 1500 grain has been counted), Q=Quartz, K-F= K-Feldspar, Pl= Plagioclase, Amph= Amphibole, Bio=Biotite, Mu=Muscovite, İl=İlmenite, Epi= Epidote, Matrix= uncounted grains, Opak= opak minerals.....	32
Table 2. Mineral modes that in the sample collected in Boğalı pluton (more than 1500 grain has been counted), Q=Quartz, K-F= K-Feldspar, Pl= Plagioclase, Amph= Amphibole, Bio=Biotite, Mu=Muscovite, İl=İlmenite, Epi= Epidote. ....	40
Table 3. Whole-rock major oxides ICP-MS analyses of samples from the Taşlıyaylı volcanic rocks. ....	58
Table 4. Whole-rock rare earth element (ppm) ICP-MS analyses of samples from Taşlıyaylı volcanic. ....	59
Table 5. Whole-rock major oxides ICP-MS analyses of samples from the Gündoğdu pluton. ....	67
Table 6. Whole-rock rare earth element (ppm) ICP-MS analyses of samples from Gündoğdu pluton. ....	70
Table 7. Whole-rock major oxides ICP-MS analyses of samples from the Boğalı pluton. ....	79
Table 8. Whole-rock rare earth element (ppm) ICP-MS analyses of samples from the Boğalı pluton. ....	80
Table 9. Sr and Nd isotope composition of sample from Gündoğdu and Boğalı Plutons. ....	87
Table 10. Pb isotope composition of sample from Gündoğdu and Boğalı plutons. ....	87
Table 11. Estimation the degree of partial melting and magma composition for Taşlıyayla volcanic rock and Taşlıyayla Eocene volcanic rock by using non-modal Rayleigh partial melting model (Equation 1) and normalized to Chondrite by using the Rare Earth Element. ....	96
Table 12. Comparison of calculated P (kbar) and T (°C) conditions after Putirka (2008) using c clinopyroxeneliquid in basaltic and andesitic rocks from the Taşlıyayla volcanic rocks (Arakli) area. ....	117
Table 13. Chlorite temperature according to Cathelineau (1988) and Jowett (1991) .....	118
Table 14. Comparison of calculated temperatures (T, °C) conditions after Fuhrman ve Lindsley, (1988) for two feldspar, hornblend-plagioclase (Blundy and Holland, 1990; Holland and Blundy, 1994), for Zircon (after Mşller et al,2003), Using whole-rocks major oxides for 7,5 k bar after Watson ve Green (1982) and and lower than 1 atmosphere pressure after Watson (1979) .....	122

Table 15. Comparison of calculated pressures (P, kbar) conditions after Hammarstrom and Zen (1986), Hollister et al. (1987), Johnson and Rutherford (1989), Schmidt (1992), and Anderson and Smith (1995) using hornblendes in Granitoid rocks and MME from the Gündoğdu and Boğalı plutons .....	122
App Table 1. Description all information about the taken sample from Gündoğdu and Boğalı pluton .....	147
App Table 2. Microprobe analysis results of Plagioclase in the Taşlıyayla formation. ....	156
App Table 3. Microprobe analysis results of Clinopyroxene in the Taşlıyayla formation.....	160
App Table 4. Microprobe analysis result of Chlorite in the Taşlıyayla formation .....	163
App Table 5. Microprobe analysis of Plagioclase in the Gündoğdu pluton and their MMEs .....	167
App Table 6. Microprobe analysis of K-feldspar in the Gündoğdu pluton and their MMEs .....	170
App Table 7. Amphibole, Biotite, Chlorite and Fe-Ti Oxides microprobe analysis result of Gündoğdu pluton and their MMEs.....	171
App Table 8. Plagioclase microprobe analysis of Boğalı pluton and their MMEs. ....	174
App Table 9. K-Feldspar microprobe analysis of Boğalı Pluton and their MMEs.....	177
App Table 10. Amphibole microprobe analysis of Boğalı Pluton and MMEs.....	179
App Table 11. Fe-Ti oxides microprobe analysis of Boğalı Pluton and MMEs.....	180
App Table 12. Biotite and Chlorite microprobe analysis .....	181
App Table 13. SHRIMP U-Pb zircon age result Of Taşlıyayla volcanic rocks.....	182
App Table 14. SHRIMP U-Pb zircon age result Of Gündoğdu Pluton .....	183
App Table 15. SHRIMP U-Pb zircon age result Of Boğalı Pluton .....	184
App Table 16. SHRIMP U-Pb zircon age result Of Salman Kaş volcanic rocks .....	185

## SYMBOL INDEX

Ab	:Albit
AFC	:Asimilation and Fractional Crystalization
Alk-Ba	:Alkalia Basalt
Alk Ga	:Alkalia Gabbro
Alk-Rh	:Alkalia Rhyolite
Amp	:Amphibol
An	:Anorthite
And	:Andesite
And/Ba	:Andesite/Basalt
App	:Appendix
ASI	:Aluminum Saturation Index
Ba	:Basalt
Bio	:Biotite
CA	:Calc-alkaline
CAB	:Continental Arc Basalt
Da	:Dacite
Dio	:Diorite
Ep	:Epidote
E	:East.
EMI	:Enriched mantle
FC	:Fractional Crystalization
Fo Mon	:Foid Monzosyenite
Fo Sy	:Foid Syenite
Ga	:Gabbro
Ga-Dio Dio	:Gabbro-Diorite Diorite,
Gra/Gran	:Granite/Granodiorite
HFSE	:Heavy Field Strength Element
HRS	:Host Rocks
ICP-ES	:Inductively Coupled Plasma Emission Spectroscopy)
ICP-MS	:Inductively Coupled Plasma Mass Spectrometry
IAB	:Island Arc basalt
I (sr)	:Sr isotop analysis

Kbar	:Pressure in kilobars
LILE	:large-ion Lithophile Elements
LC	:Lower Crust
LREE	:Light Rare Earth Elements
Ma	:Milyon yıl
Mg#	:Magnisum Number= $100 \times \text{Mg}/(\text{Mg} + \text{Fe}^{2+})$
MMEs	:Mafic Microgranular enclaves
Mon	:Monzonite
Mon ga	:Monzogabbro
Mon dio	:Monzodiorite,
MORB	:Mide Oceanic Ridge Basalt
My	:Million Year
Nu	:Namber
NW	:North West
NE	:North East
NHRL	:North Hemisphere Reference line
Op	:Opaque Minerals
Or	:Orthoclase
OFB	:Oceanic Floor Basalt
OIB	:Oceanic Island Basalt
ORG	:Oceanic Ridge Granite
P	:Pressure
Pho	:Phonolite
Pho-te	: Phonolite-tephrite
Pl	:Plagioclase
Q	:Quartz
QAP	:Quartz- Alkalia feldspar- Plagioclase model classification
Q Mon	:Quartz Monzonite
REE	:Rare earth element
Rh	:Rhyolite
Rh/Da	:Rhyolite/Dacite
T	:Temerature (°C )
TDM	:Plaka ortası granitoyidleri

Te	:Tephrite
Te-pho	:Tephri-Phonolite
TH	:Tholiitic
Tr	:Trachyte
Tr-An	:Trachyte- Andesite
Tr-Ba	:Trachy-Basalt
Tr-Da	:Trachyte-Dacite
UC	:Upper Crust
W	:West
WPG	:Within Plate Granite



## **1. INTRODUCTION**

Eastern Pontides are the most important area in the Alpine-Himalayan orogenic belt which is characterized by wide spread of volcanic and plutonic rocks. There are a lot of intrusions formed in the region ranged from the Permo-Carboniferous to the Eocene (Fig 1). This study particularly takes place on the Çaykara magmativ complex (south of Araklı, NE Turkey), which is part of the composite Kaçkar Batholith in the Eastern Pontides (Figure 1). The area of the present study contains plutonic and volcanic rocks range from Upper Cretaceous to Eocene in age which displays different petrographical, mineralogical and geochemical features. These variations which can be related to different causes will be examine and evaluate in this study.

The reasons to the selection of the study area are that: (a) petrogenetic evolution of Kaçkar Batholith is closely related with the Pontides's evolution during post-Paleozoic time span, (b) the plutonic rocks of the Çaykara magmatic complex exposing in the western part of the Kaçkar Batholith will provide an important contribution to better understanding the Late Mesozoic to Cenozoic geodynamic evolution of the eastern Pontides, (c) The magmatic complex subjected to this study has not investigated in detail so far in the region by using modern analytical techniques, (d) The data related to petrological properties and crystallization ages of these magmatic rocks are still absent. In addition, cessation and polarity of subduction during Cretaceous time, initiation of collision between Pontides and Tauride-Anatolide platform, the time of extensional processes, magma dynamics and mantle-crustal processes in the study area are also controversial (Robinson et al., 1995; Okay and Şahintürk, 1997; Şen et al., 1998; Bektas et al., 1995; 1999; Şengör et al., 2003; Topuz et al., 2005; Boztuğ et al., 2006; Karlı et al., 2007).

### **1.1. The Aims of the Thesis**

This project aims to study the petrological, geochronological and isotopical properties of eastern part of the Kaçkar intrusive located in southern part of the Araklı (Trabzon) village, which locally and regional tectonics setting have not been studied in detail. In addition to that, this study is carried out to determine the implication of subduction during late Cretaceous and try to figure out the geodynamic model of this event.

The purpose of the project is to study and interpret the Çaykara Intrusive Complex by using data that will be obtain by using the new methods listed as below:

- a) To study the contact relation between the plutonic and volcanic rocks and to examine the mechanism of magma generation (subduction, collosion, etc.)
- b) To evaluate the magma that formed the rocks and make up the complex (degree of partial melting, magma mixing, assimilation, differentiation, magmatic processes, etc.).
- c) Using new data in order to look for the possibility to revise the dynamic model that was used to test the relation of age.
- d) (To examine/ To follow up/ To observe) the Geodynamic event that occurs from the beginning to the end of complex.
- e) To examine and create new details about the complex which the most of these rocks in Eastern Pontides show similar properties such as age.

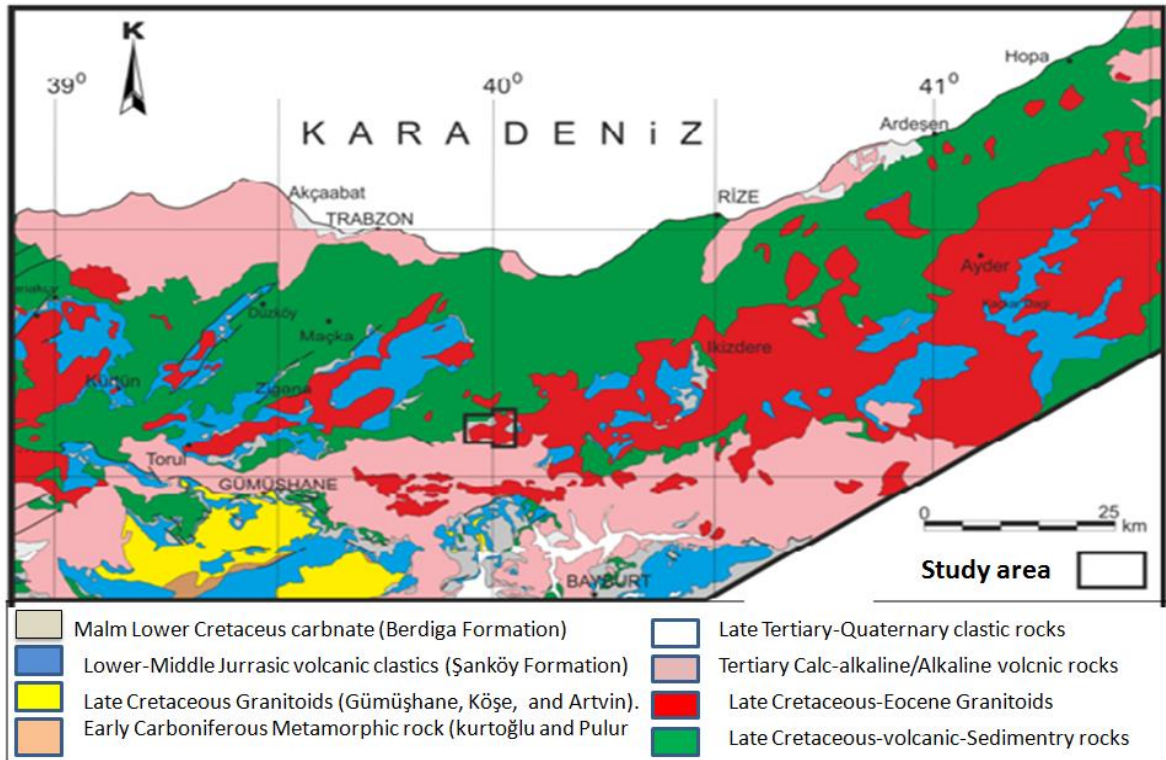


Figure.1. Geological map including study area (Modified from Güven. 1993)

## 1.2. Geographical Position of the Study Area

The area of the present study is situated in the south of Araklı (Trabzon) from the

eastern part of the Black Sea region, south of Araklı (Trabzon) district. The study area is approximately 60 km away from the centre of Araklı town and 110 km away from the Trabzon city. In the study area, which has a rough morphology, the altitude varies from about 1500 m to 2500 m. The most important settlements are Bahçecik, Gögören and Güneyler neighborhood while the most important elevations in the study area are Kaban Hill (2466 m), Küçükbağ Hill (2448 m), Çakıralı Hill and Kilise Hill. Important creeks such as Gögören, Aslanca and Asma Creeks are the side branches of the Karadere.

### **1.3. Geological Background**

The area of the present study is situated in the northeastern part of İzmir-Ankara-Erzincan suture zone, between Black Sea and Anatolide-Tauride Platform (Figure 2a). The eastern Pontides is eastern part of the Sakaraya Zone, which is extending along the west to east Black Sea coast with a length of about 500 km and width of 200 km. It has been named by Hamilton, (1842) as the Pontide. Ketin, (1966) also named it as the Pontide based on tectonic evolution of Turkey and determine the geographical boundaries. Ketin and Canitez, (1972) rearranged to tectonic units of Turkey and divided to Pontides as eastern and western Pontides based on variations of lithological features. Later, Gedikoğlu, (1978) and Gedikoğlu et al., (1979) separated the eastern Pontides as northern and southern zones. Bektaş et al., (1995) and then Eyüboğlu et al., (2006) divided into three subgroups: northern, southern, and axial zones, based on the variations of lithological units, and tectonic characteristics. The Paleozoic rocks represent the basement of the Eastern Pontides and are composed of metamorphic lithologies and granitic intrusions. These rocks are dominated in the southern zone of the Eastern Pontides (Zankl, 1961; Agar, 1977; Gedikoglu, 1978) and are rarely found in the northern zone of the Eastern Pontides (Turkish-Japanese team, 1985; Boynukalin, 1990; Kaygusuz et al., 2012).

These Paleozoic metamorphic rocks have been cut by Paleozoic intrusion (Çoğulu, 1975; Topuz et al., 2010; Dokuz, 2011). Granitoidic rocks are found by large plutonic masses found in Gümüşhane and Köse regions (Tokel, 1972; Çoğulu, 1975; Yılmaz, 1977; Özdoğan, 1992; Dokuz, 2011), with metamorphic rocks in the southern zone. Part of Giresun (Schultze-Wetsrum, 1961).



Generally, the northern zone occupied by volcanoclastic and volcanic rocks of Late Cretaceous and Middle Eocene, whereas pre-Late Cretaceous rocks are most common in the southern zone. The basement contains metamorphic rocks (schist, gneiss, and marble) which are cross-cut by Permo-Carboniferous plutons which are probably Devonian-Carboniferous age, (Okay and Şahintürk, 1997; Topuz et al., 2010; Dokuz, 2011; Kaygusuz et al., 2012).

There is a general unanimity that the belt is a paleo-magmatic arc in character, developed above the northward-dipping subduction zone of northern branch of Neo-Tethys Ocean ( Okay et al., 1994 and 2001; Yılmaz et al., 1997; Tüysüz, 1999; Okay and Tüysüz, 1999; Rojay et al., 2001; Kaymakçı et al., 2003; 2007; Keskin et al., 2008; Karlı et al., 2010; 2011; 2012; Topuz et al., 2005; 2010). Three magmatic cycles such as, Jurassic, Upper Cretaceous and Eocene, make up to the geodynamic evolution of Eastern Pontides (Adamia et al., 1977; Korkmaz et al., 1995; Camur et al., 1996; Arslan et al., 1997, 2000; Dokuz, 2011). It has been indicated by several of geological and geophysical data that each zone is separated by vertical faults trending NW, NE and E-W trending in the eastern Pontides (Bektaş et al., 1995).

Early-Middle Jurassic, volcanic and volcanoclastic rocks formed as result to an extensional regime that was possibly related to rifting in the arc setting and just before to the subduction (Okay and Şahintürk, 1997; Şen, 2007; Topuz et al., 2010). Early-Middle Jurassic volcanic and volcanoclastic rocks is conformably cover by the Late Jurassic-Early Cretaceous carbonates (e.g., Okay and Şahintürk, 1997; Eyüboğlu et al., 2006). Late Jurassic-Early Cretaceous carbonates rocks are overlain by the Late Cretaceous sedimentary rocks that consist of sandy limestone, red limestone and clastic rocks in the south (Eren, 1983; Pelin, 1977; Eyüboğlu, 2015), the volcanic and associated pyroclastic rocks in the north of eastern Pontides (Güven, 1993; Eyüboğlu, 2010; Eyüboğlu et al., 2014). Lithologies are seen in the north formed in two different cycles during Late Cretaceous (Turonian-Santonian-Campanian-Maastrichtian). The first cycle represented by Çatak formation and Kızılkaya formation occurs in Turonian–Coniacian–Santonian time and shows range in rocks content starting from basaltic-andesitic volcanic and pyroclastic rocks and grades upward into the felsic volcanic and pyroclastic rocks. The lithologies belonging to the first cycle is covered by Santonian (?) aged Danişman Formation

consisting mainly of limestone, and reddish biomicrites interbedded with volcanoclastic rocks (Eyüboğlu et al., 2014). The second cycle of the Late Cretaceous volcanic activity displays a thick sequence begins with basaltic-andesitic lithologies (Çağlayan Formation) and continues with biotite-rich felsic rocks units (Çayırbağ or Tirebolu Formation). The volcanic- and pyroclastic-dominated Late Cretaceous sequence is covered by Late Maastrichtian-Paleocene Bakırköy Formation including mainly limestone and sandstone. The Eocene age of Pontides usually starts with basal conglomerates over the Cretaceous and Paleocene units and these Eocene units are dominated by series of andesite, and pyroclastites. Volcano-sedimentary rocks belong to Eocene are widespread in both the northern and southern parts of the Eastern Pontides (Güven, 1993; Aslan et al., 2014). The Eocene and post-Eocene volcanic rocks are divided into two sub-provinces: an alkaline province in the northern part and a calc-alkaline province in the southern part (Arslan et al., 2003; Aydın et al., 2008). Oligocene formations have been found in Trabzon, Ünye and Fatsa regions (Schultz-Westrum, 1961; Özsayar, 1971). The sediments belong to Neogene are present near Trabzon-Akçaabat and Rize-Pazar beaches (Yalçınlar, 1952; Özsayar, 1971). Quaternary aged formations consist of siltstones and travertine rock, (Özsayar, 1971).

Geotectonic evolution and the direction of the subduction of the eastern Pontides is still under discussion. The limited of geochemical, geological, isotopic and geochronological data cause all this scientific discussion. Three subduction models were offered to explain geotectonic development for the eastern Pontides. Adamia et al. (1977), Dewey et al., (1973), Ustaömer & Robertson, (1996), Okay and Leven, (1996) proposed subduction to northward from the Paleozoic to the end of the Eocene. They argued that the ultramafic rocks which found in the southern part of the eastern Pontides, represents the residual part of the Paleotethys Ocean. Şengör and Yılmaz, (1981), Karlı et al., (2010), Dokuz et al., (2011) suggested that Palaeotethys was situated north of the Pontides Orogenic Belt, and consequently, early-mid Jurassic subduction were placed to toward south. They also suppose a changing of subduction polarity, toward north during the Late Mesozoic-Early Cenozoic. Conversely, some authors proposed that the northern part of Turkey was shaped by in a southerly direction subduction of Paleotethys oceanic lithosphere that was situated in the north of the Pontides (Dewey et al., 1973; Chorowicz et al., 1998; Bektaş et al., 1999; Eyuboglu, 2010). According to this model, Black Sea

represents the remainder of Paleotethys and the ultramafic belt in the south of the magmatic arc represents portions of a well-preserved back-arc basin (Figure 2b). As another suggestion is that Palaeotethys was situated north of the Pontides, and hence, a southward subduction operated from the Paleozoic until the mid-Jurassic (Şengör and Yılmaz, 1981; Karşlı et al., 2010a; Dokuz, 2011). They also suppose a reversal of subduction polarity, with northward subduction during the Upper Cretaceous until the end of the Eocene. Contrariwise, Dewey et al., (1973), Chorowicz et al., (1998), Bektaş et al., (1999) and Eyuboglu, (2010) support a southward subduction model for the whole period from the Paleozoic to the end of the Eocene. The Black Sea according to this model, represents the remnant of Paleotethys and the ultramafic belt represents portions of a preserved back-arc basin (Figure 2b).

#### **1.4. Pervious Work**

##### **1.4.1. Petrological Studies**

The geological maps of the Araklı and Çaykara regions including the study area its vicinity (1/100000 and 1/25000) have been done by MTA. The geochemical data covering the whole rock major oxides, trace, and rare earth elements, and also isotope data indicate that the parental magmas that was produced the Upper cretaceous granitic and volcanic bodies has different sources such as mixing of crustal sources and lithospheric and/or asthenospheric mantle sources or fractional crystallization of lithospheric and asthenospheric mantle-derived magmas and Assimilation fractional crystallization processes.

Turkish-Japanese team (1974), by MTA Institute they have studied the geology of Trabzon region and have the geological map of 1 / 50.000 scale. According to their studies the Upper Cretaceous units based on volcanic activity and sedimentary cycle were divided into four different stratigraphic units. These units have been named upwardly from top to bottom for A1, D1, A2, D2 formations. Formation A1 represents the large part and consists of andesite and pyroclastic rocks. The D1 formation overlies the A1 and consists of dacitic lava and pyroclastic rocks. A2 formation consists of andesitic lava and pyroclastic rock.

Hacıbrahimoğlu, (1986) studied the place of Dağbaşı-Araklı and found that these rocks belong to the Jurassic-Lower Cretaceous in age, and he found that the marble-shaped marble and dacitic rocks came in succession and cut all of Dağbaşı granitoid rock.

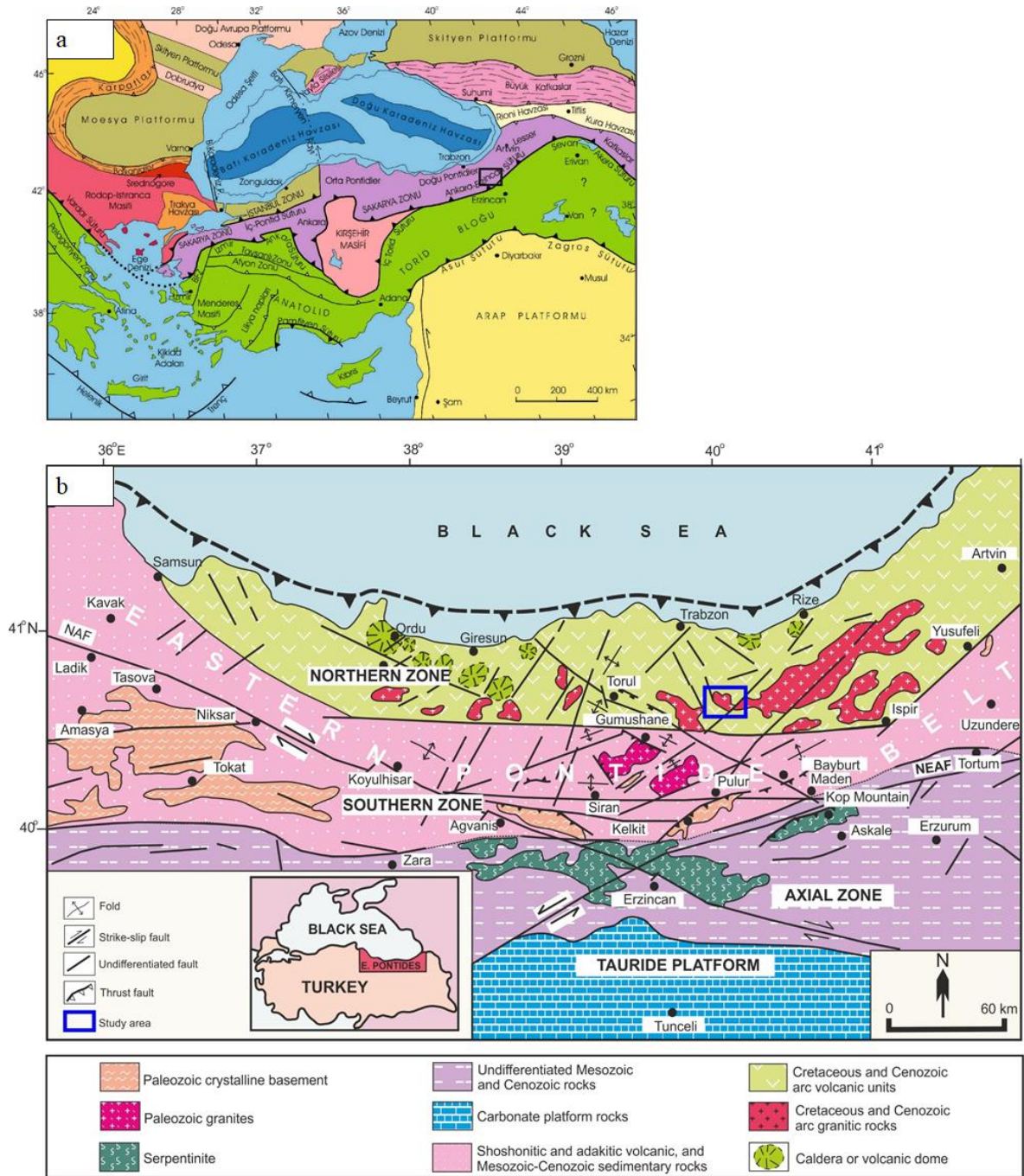


Figure 2. a) Tectonic map of the north-eastern Mediterranean region showing the main blocks in relation to the Afro-Arabian and Eurasian plates (modified after Okay and Tüysüz, 1999). b) The disturbance of the main tectonic feature in the Eastern Pontides, (modified after Eyüboğlu et al, 2010).

Kargi (1987) studied the geotectonic and Petrographical features of Granitoid rocks of Araklı-Bahçecik area and found that main body of intrusion consist of granite and

monzonite and the limestone rock of lower Cretaceous cut the volcanic rock of lower Jurassic.

Şen, (1988) studied the petrographical- geochemical properties of formation of sub-basic -Granitoid rocks which ranging from Jurassic to upper Cretaceous in Dağbaşı (Trabzon). He concludes that the main body of intrusion consists of granodiorite and quartz diorite and have tholeiitic-calc alkaline affinity in composition.

Güven, (1993) concluded that the volcanism of Late Cretaceous in the eastern part of the Sakarya Zone is composed of four different phases. The first and second volcanic phases belong to (Turonian -Santonian?) and represent by Çatak and Kizilkaya formations, whereas the third and fourth volcanic phases are represented by Çağlayan and Tirebolu formations and belong to (Santonian – Campanian and Maastrichtian?) and these magmatic phases are represented by different rocks.

Arslan et al., (1997) studied the volcanic rocks of Kale (Gumushane) and they found that these rocks chemically are calc-alkaline in composition, displays moderate potassium enrichment, and mainly consists of dacite-rhyolite and partly consist of basaltic-andesitic rocks.

Boztuğ, (2001) and Boztuğ, et al., (2003a,) interpreted the petrogenesis of the composite Kaçkar Batholith. They identified several intrusive units derived from different geodynamic environments, starting from Early and Late Cretaceous to Eocene. These intrusive chemically range from tholeiitic to calc-alkaline metaluminous granitoids and peraluminous leucogranites and reflect arc-collisional through syn-collisional crustal thickening to postcollisional extensional regimes. They also concluded that the granitoid rocks of Early/Late Cretaceous to Early Palaeocene arc-related, chemically displays calc-alkaline, metaluminous affinity, I-type, granodiorite, and granite compositions with well-preserved characterisation indicated to magma mingling–mixing processes between coeval mafic and felsic magma sources Cretaceous.

Kaygusuz and Şen, (2011) used the U–Pb zircon ages, geochemical and Sr–Nd isotopic compositions to study the Köprübaşı pluton. They discovered that the main body of pluton consists of granodiorites and monzogranites formed by partial melting of mafic lower crustal sources, as a result to the subduction of the Neotethyan Ocean beneath the Eurasian plate through the Cretaceous–Paleocene times.

Karlı et al., (2004) tried to explain the origin of the İkizdere KFM (K-feldspar megacrysts) by using textural relationships and mineral compositions and they concluded

that the KFMs are magmatic in origin and not porphyroblast due to the similarities in composition of inclusions and host minerals, felsic and mafic silicate inclusion morphology and the distribution of crystal inclusions. They also found that the central part of the K-feldspar has low content of BaO, indicating that they are undecomposed crystal remnant in a melt after a period of crustal-derived felsic and mantle-derived mafic magma interaction processes.

Şahin, (2005) studied the granitic rocks of the studied area by using K–Ar dating and petrology properties. She called these granitic rocks as the Gündoğdu Altered Microgranite, Boğalı K-feldspar-megacrystic monzogranite, and Uzuntarla porphyritic granodiorite. She also interpreted the process as shallow-seated plutons based on textural and structural properties, and according to K–Ar ages determinations indicate from 75.71.55 through 61.41.47 to 561.19 Ma ages for the Boğalı pluton, and 42.40.87 and 41.20.89 Ma ages for the Uzuntarla granodiorite.

Şahin, (2008) tried to investigate chemical interaction between MMEs–host rock pairs by using various geochemical diagrams. In particular, she studied mafic microgranular enclaves in the Late Cretaceous Tamdere Quartz Monzonite in the south of Dereli/Giresun because it considered as an ideal opportunity to pursue these types of geological phenomena. She found out that the MMEs are composed of diorite, monzodiorite and quartz diorite, whereas the felsic host rocks comprise mainly quartz monzonite, granodiorite and rarely monzogranite on the basis of both mineralogical and chemical compositions. The mafic microgranular enclaves (MMEs) ranging from spheroidal to ellipsoidal in shape, and from a few centimeters to decimeters in size. She also found out that an exchange between the MMEs and the felsic host in the distribution of major, trace and REE elements due to thermal, mechanical and chemical interactions between coeval felsic host magma and mafic magma. In addition, she found some elements that displays transference between from felsic host magma to mafic magma blob is that of alkalis such as Na and K. LILEs such as Rb, Sr, Ba and some HFSEs such as Nb, Y, Zr and Th have been migrated from felsic host magma to MMEs. She also found that the felsic and mafic magma sources behave as concordia and visco-plastic materials, where the small MMEs behave as a closed system due to immediate rapid cooling, whereas the bigger MMEs suffer greater diffusion from the felsic host magma due to slow cooling. Petrological features also indicated that hybrid rocks produced by magma mingling and subsequent chemical exchange between the mafic and felsic melts.

Boztuğ et al., (2005) studied the the composite Kaçkar batholith and they found out that it represents of five different magmatic associations have different ages. They found their age ranging from Early Cretaceous to Late Eocene and represents by early to mature arc through syn- and post-collisional lithospheric delamination to postcollisional extension geodynamic settings. They found the Early Cretaceous intrusive unite is unconformably overlain by the Turonian Ardıçlı Formation whereas the Late Eocene intrusive units cut pre-Late Eocene intrusive units and are unconformably overlain by the Miocene Şebinkarahisar Formation. They also found that the tectonic uplift of this huge composite batholith in the Miocene was a result of NE-SW trending faults. On the basis of petrochemical properties, they found that Kaçkar batholith reflects the early and mature stages of arc plutonism of Early and Late Cretaceous age, respectively. Finally, they concluded that all these intrusives represent different stages of a convergence system, i.e. subduction, extension, syn-collision, and post-collision.

Boztuğ et al., (2006) tried to date the formation of the composite Kaçkar batholith by using the titanite and zircon fission-track dating. They concluded that the Çamlıkaya Granitoid ( $112.4 \pm 1.6$  Ma) was emplaced during an immature-arc magmatic episode of Early Cretaceous age, the Sırtıyayla ( $57.1 \pm 1.2$  Ma), Marselevat ( $52.9 \pm 1.3$  Ma) granitoids are late products of a Late-Palaeocene mature-arc episode. Besides Ayder granitoid ( $46.4 \pm 1.0$  Ma) is the result of middle- to late-Eocene post-collisional magmatism related to slab break-off, the Halkalıtas, Quartz diorite ( $43.7 \pm 2.3$  Ma) and the Güllübağ monzonite ( $38.1 \pm 0.9$  Ma) is a Middle- to Late-Eocene episode related to post-collisional extension. They also identified different lithodem units result from consecutive igneous episodes from titanite and zircon fission-track ages.

İlbeyli, (2008) studied the geochemical properties of the Sebinkarahisar Granitoids rocks in the eastern Pontides. She concluded that the main body of these rocks consist of granite and monzonite and she related the generation of this pluton to partial melting of mafic lower crustal sources as a resulte to normal to mature stages of the subduction of the northern branch of the Neo-Tethyan Ocean beneath the Eurasian plate through Cretaceous–Paleocene times.

Karşlı et al., (2008) tried to investigate the chemical compositions of the oxides and he tried to study the application of these oxides as a geothermobarometer effect the magma interactions causing the generation of hybrid granitoids. They concluded that thermal equilibrium can occur between two different magma in different proportions so that

possibility of interaction between felsic and mafic magma occurred in a convectively dynamic magma chamber during crystallization of the plutons. So that the generation of the hybrid plutons can be related or interpreted to these reasons.

Kaygusuz and Aydınçakır, (2011) studied the Dağbaşı pluton and they found that the main body of pluton consists of tonalite, granodiorite and Monzogranite including MMEs with gabbro dioritic and tonalitic compositions. They also found out that the Dağbaşı pluton were formed as result of partial melting of mafic lower crustal sources whereas MMEs formed as a result of magma mingling.

Kaygusuz et al., (2013, and 2014) studied Turnagöl and Camiboğazı plutons in the Late Cretaceous of eastern Pontides and based on geochemical and isotopic data. They concluded that these plutons were formed as a result of partial melting of mafic lower crustal sources in arc-related geodynamic regime through subduction of the Neotethyan Ocean beneath the Eurasian plate during Late Cretaceous times.

Evcimen, (2011) studied geochronology, petrology, and geodynamic significance of İkizere pluton during his master thesis and he found that the main body of pluton comprises of granite, granodiorite, tonalite, minor diorite, and minor gabbroic diorite mafic micro-granular enclaves. He interpreted the origin of this pluton by the partial melting of lower crust by melting the lithospheric mantle-derived basaltic melt first than mixing with granitic magma of crustal origin.

Karlı et al., (2012) studied the A-type granitoid from the Eastern Pontides and tried to evaluate the production of hybrid A-type rocks in a subduction-related environment. They found that the A-type Pirnalli pluton originated from a hybrid source. According to the model calculation of Sr–Nd isotopic compositions, they conclude that the composition of the pluton occurs between two end-member, mafic lower crust (82–90%) and chemically enriched lithospheric mantle (10–18%). They also concluded that the A-type Pirnalli pluton formed by mixing of these two magmas, then this hybrid magma underwent a limited fractional crystallization during the ascending of the hybrid magma to the upper crust. Besides they also, thought that the A-type Pirnalli pluton in the Eastern Pontides formed as result to Back-arc extensional events due to northward subduction of the Neotethyan oceanic crust throughout late Cretaceous.

Karlı et al., (2012) tried to decipher the shoshonitic monzonites with I-type characteristic, of the pluton of Sıldağı and he attributed the shoshonitic melt to partial melting lithospheric thinning and following the upwelling of hot asthenospheric material



beneath the region. Then this melt underwent to different processes such as fractional crystallization and assimilation leading to the generation of this pluton.

Eyüboğlu et al., (2014) attempted to characterize the metallogeny through a comprehensive overview of the importance of volcanogenic massive sulfide (VMS) mineralizations in the belt. They separated the VMS deposits in the northern part of the eastern Pontides to two different stratigraphic horizons consisting mainly of felsic volcanic rocks within the Late Cretaceous sequence and they also detected that the VMS ages ranging between  $91.1 \pm 1.3$  and  $82.6 \pm 1$  Ma. They conclude that the felsic rocks of the first and second horizons reflect the geochemical characteristics of subduction-related calc-alkaline and shoshonitic magmas, respectively, in continental arcs and represent the immature and mature stages of a late Cretaceous magmatic arc. They also concludes that the volcanogenic massive sulfide (VMS) deposits were generated either in intra-arc or near arc region of the eastern Pontides during the southward subduction of the Tethys oceanic lithosphere based on detailed analyses of the geological, geophysical, and geodynamic information.

Aydin, (2014) studied the subvolcanic of Maçka area in the eastern part of the Sakarya zone, and he found that these subvolcanic rocks were generated in Late Cretaceous (Campanian) time. He investigated the main body of this intrusion entirely composed of tonalite), with mafic micro-granular enclaves (MMEs) consisting of gabbro-diorite. He found also that both the Maçka subvolcanic rocks and their MMEs are displays similar petrographically and chemically features, and also conclude, based on the geochronology and geochemistry data that the Maçka subvolcanic rocks are hybrid in origin, generated as result of interactions between enriched lithospheric mantle with lower crust in an extensional arc setting.

Eyüboğlu, (2015) emphasized that the evolution of Eastern Pontides take time starting from Paleozoic go through Mesozoic till Cenozoic as result to the subduction of an oceanic lithosphere toward south, depending on the systematical geological, petrochemical, geochronological and geochronological data. He supported his model with the migration toward south and an increase in potassium content of the late Cretaceous arc volcanism and the existence of south-dipping reverse fault systems extending parallel to the southern coast of Black Sea.

### 1.4.2. Tectonical Studies.

The Eastern Pontides is magmatic arc in characters formed to the subduction of the Neo-Tethyan oceanic crust beneath the eastern Pontide. The beginning of subduction and the collision between Pontides and the TAP are both still under discussion. There is a unanimity indicated that the late Cretaceous igneous activity is subduction-related, but the direction of subduction is still argumentative.

Dewey et al., (1973) conclude that the Eastern Pontides developed as a result of a southward subduction zone of Paleotethys, and he also stated that the Black Sea coast situated between the Anatolian Plate which was located to the south of the Tethyan Ocean, and Eurasian and Afro-Arabian plate.

Şengör and Yılmaz, (1981) studied the evolution of the Tethyan in Turkey and they divided the evolution of Tethyan into two main phases, and they named as a Palaeo-Tethyan and a Neo-Tethyan. They said that evolution of first phase Palaeo-Tethyan evolution controlled by the southward subduction of Palaeo-Tethys beneath northern Turkey through the Permo-Liassic interval postulate and they state that the Eastern Pontides Orogenic Belt illustrate the southern active of Eurasia. According to their opinion, they advocated that a model of subduction from the Paleozoic until the Mid-Jurassic was southward in direction and followed by northward subduction model from the Upper Cretaceous until the end of the Eocene dominates. They also interpreted the Gümüşhane Pluton is as the result to this event.

Bektaş, (1984) study the eastern Pontide and he found that the eastern Pontide divided to three zone, North, South and axial zones which separated by E-w, NE-SE and NW-SE trending fault zones. He found that the volcanic and plutonic rocks occupied the northern zone, whereas the southern zone dominated by carbonate sediment rocks. The Cadera and Dom structure represent one of the magmatic structure features that appears in the Northern zone. The northern of axial zone is bordered by Northern Anatolian fault and Eastern Anatolian fault. He said that the southward subduction of Paleotethys oceanic lithosphere subducted toward south and this subduction starts from Paleozoic and continues until the Eocene. It described that these events as the main tectonic event that leads to the evolution of the Eastern Pontides Orogenic. He supported this idea by paleomagnetic and magmatic data.

Okay et al., (1994) studied the the opening history and the effect of the opening of the Black Sea on the surrounding regions and he fined the Black Sea contains two oceanic basins west and east and separated by the ridge of mid-Black Sea. He also concluded that the west basin opened as result to back-arc rifting of hercynian continental sliver during the Late cretaceous, whereas the opening of the east Black Sea was during the middle cretaceous as result to counterclockwise rotation of east black sea.

Okay and Şahintürk, (1997), studied the Geology of the Eastern Pontides and they found the Eastern Pontide belt shows several common stratigraphic features resulting from a common Mesozoic-Tertiary tectonic history. They concluded the stratigraphical features of Eastern Pontides during the Mesozoic is associated with the northward emplacement of an ophiolitic over the passive continental margin of the Eastern Pontides. They also concluded the obduction of ophiolitic melange is a result of partial subduction of the Eastern Pontides continental margin in a south-dipping intra-oceanic subduction zone. They also found that the volcanism shows a general silica enrichment, with time, ranging from basalts and andesites to dacites. Finally they concluded that the rifting of the volcanic arc axis during the Maastrichtian time represent the reason for the opening of the Eastern Black Sea Basin.

Bektaş, (1999) tried to explain the immigration of Subduction-related volcanism towards the back-arc basin through Cretaceous time and he found that the Cretaceous TH-CA bimodal arc volcanic rocks in the northern zone of the eastern Pontides comprises a lower and upper volcanic cycle along the Black Sea coast whereas in the southern zone, the type and timing of the Cretaceous volcanism are different and there is no bimodal volcanism. He also found out that the southern zone of the Late Cretaceous volcanism began much later than that in the northern zone, which implies that southward migration of the active Late Cretaceous volcanism occurred above the south-dipping subduction zone along the eastern Pontides magmatic arc.

Arslan and Aslan, (2006) tried to evaluate the geodynamic model of Eastern Pontides by studied the petrological properties of the Tertiary granitic intrusions in the Eastern Pontides, and they supported the idea of a post-collisional, extensional tectonic setting in the Eocene for the Eastern Pontides.

Eyüboğlu, (2010), also suggested that the Late Cretaceous High-K Volcanism in the southern part of the Eastern Pontides occurred in two distinct cycles as in the northern part. Campanian shoshonitic trachyandesites and associated pyroclastics represent the first

cycle, resting on Middle Cretaceous olistostromal ophiolitic mélangé, and is covered by rudist-bearing limestones, whereas the second cycle of the Late Cretaceous volcanic arc displays potassic and/or ultrapotassic analcimitized leucitite-bearing volcanics that are the Maastrichtian in the age. He also emphasized that the progressive shallowing in the southern of the Eastern Pontides during the Late Cretaceous reveals that Late Cretaceous high-K volcanism developed during the final stage of a pull-apart basin development.

Karlı et al., (2010a) tried to test the possibility to generate the adakitic magma by partial melting of lower continental crust in collision settings. Moreover, they tried to investigate the time and influence the evolution of eastern Pontide by the collision event between the Eurasian plate and Taurid–Anatolid block. They concluded that the mafic lower continental crust beneath the region firstly thickened then delaminated through the periods from Late Cretaceous until Late Paleocene-Early Eocene time. They correlated these to the initial stage of crustal thinning caused by crustal extensional events in the Eastern Pontides and rules out the possibility of an extensional regime before ~ 50 Ma in the region during the Late Mesozoic to Early Cenozoic.

Dokuz et al., (2010), tried to investigate the source of magma, petrogenetic processes and pre- and post-collisional event that leads to generation of granitoid rocks in the Yusufeli area, north eastern of Turkey during the Jurassic age. They conclude that there are succession of events starting with rifting following by post-collisional uplift during the period of early to late Jurassic respectively. They related all of these events to subduction of old Paleotethyan crust toward south and placed beneath the Pontides, and following by breakoff shortly due to collision event between Laurasia and Pontides.

Karlı et al., (2010b) tried to investigate the source of magma and geodynamic evolution of the Harşit pluton, from the Eastern Pontides (NE Turkey). They detected the main body of this pluton varies from granite to diorite, with MMEs. They related the generation of this pluton to subduction setting and they conclude according to geochemical features that unlikely to attribute this kind of magma to the Post-collision setting because this magma has a mixed-origin formed as result to subduction events.

## **2. SAMPLING AND ANALYTICAL METHODS**

### **2.1. Methodology**

The geological maps of the Çaykara and its vicinity (1/100000 and 1/25000) have been done by MTA. In this study, we will use these geological maps with some revisions. This project took place in Çaykara intrusion and aimed to investigate the petrological, geochemical, petrographical, isotopic and geochronological properties. Sampling involved collection from various localities taking particular care to ensure that the samples were clean and fresh. This project contains field work, laboratories, microscope investigation, chemical and isotopic analysis.

#### **2.1.1. Field Work**

The field work forms the first step of this study. This part contains identification of the units in the region, the identification of boundary between the different intrusions, and studied the traces of the local and regional tectonic of area followed by determining the mechanism of settlement and uplift. During the field work the samples collected with respect to elevation and location and all of units photograph it. To achieve the purpose of the project, 200 samples have been collected from plutonic and volcanic rocks.

#### **2.1.2. Laboratories**

Sampling involved collection of fresh unweathered rocks from different localities taking particular care to ensure that the samples were clean. Samples were collected as widely as possible from different level and represent all magmatic complex. Thin section to 200 samples prepared and these thin sections sections have been analysed for mineral assemblages, proportions of minerals and matrix, rock texture and grain size distribution. All of the stuff tested under an optical microscope to determine the petrographical features and weathering stage for all samples. These thin sections were prepared at the labs of Department of Geology Engineering, Karadeniz Technical University.

Samples were selected for geochemical analysis to determine the whole-rock major-trace- and rare earth element (REE) analyses. The whole samples prepared at the labs of Geology Department, Karadeniz Technical University, then sent to ACME (Bureau Veritas Minerals) for analysis at laborator of Geology Engineering Ankara Laboratories. The first step consists of reducing the size of the samples into small, typically 0.8x0.5 cm chips and then crushing down in a steel jaw crusher and then powdered in an agate mill to a grain size of <200 mesh. Whole-rock analyses were carried out at Analytical Laboratories of ACME (Ankara). Major and trace element compositions were determined by using the inductively coupled plasma atomic emission spectroscopy (ICP-ES). The inductively coupled plasma mass spectrometry (ICP-MS) used to analyze the REE.

To prepare the sample to microprobe analysis the sample should cut to small plate 1,25 cm and take shape of semicircular shape where two semicircular shape displays one circle. Samples placed in a circular mould and poured into epoxy and formed into a round pattern. Then, samples were corroded with corrosive powder in various dimensions. Thus finially smaples were prepared for mineral chemistry analyses polishing with aluminium oxide powder.

#### **2.1.2.1. Microscopic Investigations**

Thin sections to 200 samples were prepared and these thin sections sections under an optical microscope have been analyzed for mineral assemblages, proportions of minerals and matrix, rock texture and grain size distribution. 80 samples were studied for Granitoid rocks of Boğalı and Gündoğdu pluton, 10 samples for the enclave and 70 for volcanic rocks and 20 samples for dykes. All of these analyses referred to the locations, formations, textures and elevation. The mineralogical modal of selected samples was detected by point counting with a Swift automatic counter fitted to a polarizing microscope. Around 1200-1500 points were counted to each thin-section, then normalized to 100%. For the grain size investigation, the microscope had a calibrated eye-piece micrometer. Throughout the study, modal analyses were made using a polarizing microscope with a Swift automatic point counter unit attached to its stage. All of these analyses are given in Tables (1 and 2) and referred in different figure numbers.

## **2.2. Chemical Analysis**

### **2.2.1. Whole Rocks Major oxides, Trace Element and REE Analysis**

Whole-rock analyses have been done at ACME Analytical Laboratories (Vancouver, Canada). The inductively coupled plasma atomic emission spectroscopy (ICP-ES) was used to determine major and trace element compositions, whereas the inductively coupled plasma mass spectrometry (ICP-MS) was used to analyze the REE. The detection limits ranged from 0.01 to 0.1 wt% for major oxides, 0.1 to 10 ppm for trace elements, and 0.01 to 0.5 ppm for the REE. It has been used the STD GS311-1, STD OREAS45EA, STD SO-18 and STD GS910-4 as standards. The samples also put at the oven in 105°C for 24 hours to determine the loss of volatile element, for example, before getting the platinum it should measure the cabinet weight than put gr of platinum and measure the wight again. After than put it in the oven for two hours and temperture 1000°C than take it out of oven and wait for 15 minutes to cooled and measure the wight again. The vartion of wight before heating and after heating represents the loss voltaile.

### **2.2.2. Mineral Chemistry**

Electron microprobe analyses of the main rock-forming minerlas were carried out on diamond polished and carbon-coated thin sections using a Munich Ludwig Maximilian University (Germany) by using of CAMECA SX 100 electronic microprobe laboratory. An accelerating voltage should be constant to measure feldspar and mafic minerals 20nA and 15 KV respectively. A point beam of for feldspar minerals 10 µm and 1µm for mafic minerals. These analyses measured in comparison with standard minerals.

### **2.2.3. Isotope Analysis**

Sr-Nd and Pb isotopic data of the HRs and MMEs have been analysed at the department of Geology in the University of New Mexico State. All the isotopic analyses were measured on a VG Sector 30 thermal ionization mass spectrometer using TIMS (Thermal Ionization Mass Spectrometry) method. All the analyzed samples were filled onto the rhenium filaments on the Cathodian beads or on the edge flap of the triple filament

group. The reproducibility of the  $^{87}\text{Rb} / ^{86}\text{Sr}$  and  $^{147}\text{Sm} / ^{144}\text{Nd}$  ratios are in the range of 0.3% and occur between  $\pm 0.000025$  and  $\pm 0.00003$  for  $^{87}\text{Sr} / ^{86}\text{Sr}$  and  $^{143}\text{Nd} / ^{144}\text{Nd}$  respectively. The  $^{87}\text{Sr}/^{86}\text{Sr}$  ratios were adjusted to the NBS-987 Sr standard =0.710226 (11), 0.710213 (13), 0.710219 (10) ve 0.710260 (11), The neodymium (Nd) was purified by using HDHEP coated resin and 0.25N HCl. Nd-isotope values were measured with MC-ICPMS device working with 7 Faraday collectors in 2% HNO<sub>3</sub> solution. Nd-isotope values were normalized to  $^{146}\text{Nd} / ^{144}\text{Nd} = 0.7219$  and are corrected by the Sm content. Pb isotope ratios of samples were analyzed using the middle of the triple cathode tips, Ramos, (1992).

#### 2.2.4. Geochronological Dating

Zircon minerals in two granitic of Gündoğdu and Boğalı plutons and one sample of Taşlıyayla volcanic rock samples were determined for U-Pb zircon dating. Heavy mineral enrichment was made by hydro-separation of the chosen samples, and after the concentrate enriched by magnetic separation, it was investigated in a binocular microscope and the zircon minerals were selected. After that the separated zircon minerals were placed in epoxy and were investigated in terms of optical and cathodoluminescence images, and they were analysed using U-Pb method via the “SHRIMP-IIe/mc” brand ion microscope in Granada University for plutonic samples whereas the volcanic sample was analysed in Laboratory of Mineral Laser Microprobe Analysis, China University of Geosciences, Beijing.

Details of the analytical method was given in Williams and Claesson (1987) and can be accessed at “[www.ugr.es/~ibersims](http://www.ugr.es/~ibersims)”. The U concentration was calibrated using SL13 zircon standard (U: 238 ppm). U/Pb ratio was calibrated by reading TEMORA-1 zircon standard (417 Ma; Black et al. 2003) once in every four measurements (Aiglsperger et al.2015). Common lead value of minerals with low U/Pb ratio were corrected by measuring the  $^{204}\text{Pb}/^{206}\text{Pb}$  value using continental lead production model proposed by Cumming and Richards (1975). The error margins in 95% confidence interval, which are determined by re-measurement of TEMORA standard that was measured during zircon measurements, are  $\pm 0.23\%$  for  $^{206}\text{Pb}/^{238}\text{U}$  and  $\pm 0.46\%$  for  $^{207}\text{Pb}/^{206}\text{Pb}$ . Data arrangement was carried out using “SHRIMPTOOLS” ([www.ugr.es/~fba](http://www.ugr.es/~fba)) software which is compiled in “STATA<sup>TM</sup>” programming language.



### **2-3. Office Work**

The office work went through the evaluation of our result based on the data obtained from fieldwork and according to Petrographical, petrological, geochemical, isotope analysis and geochronological analysis. The rocks will be chemically and petrographically classified, petrogenesis interpreted and draw in the map. Different programs such Graphic, and Corel Draw are used to displays the variation of data.





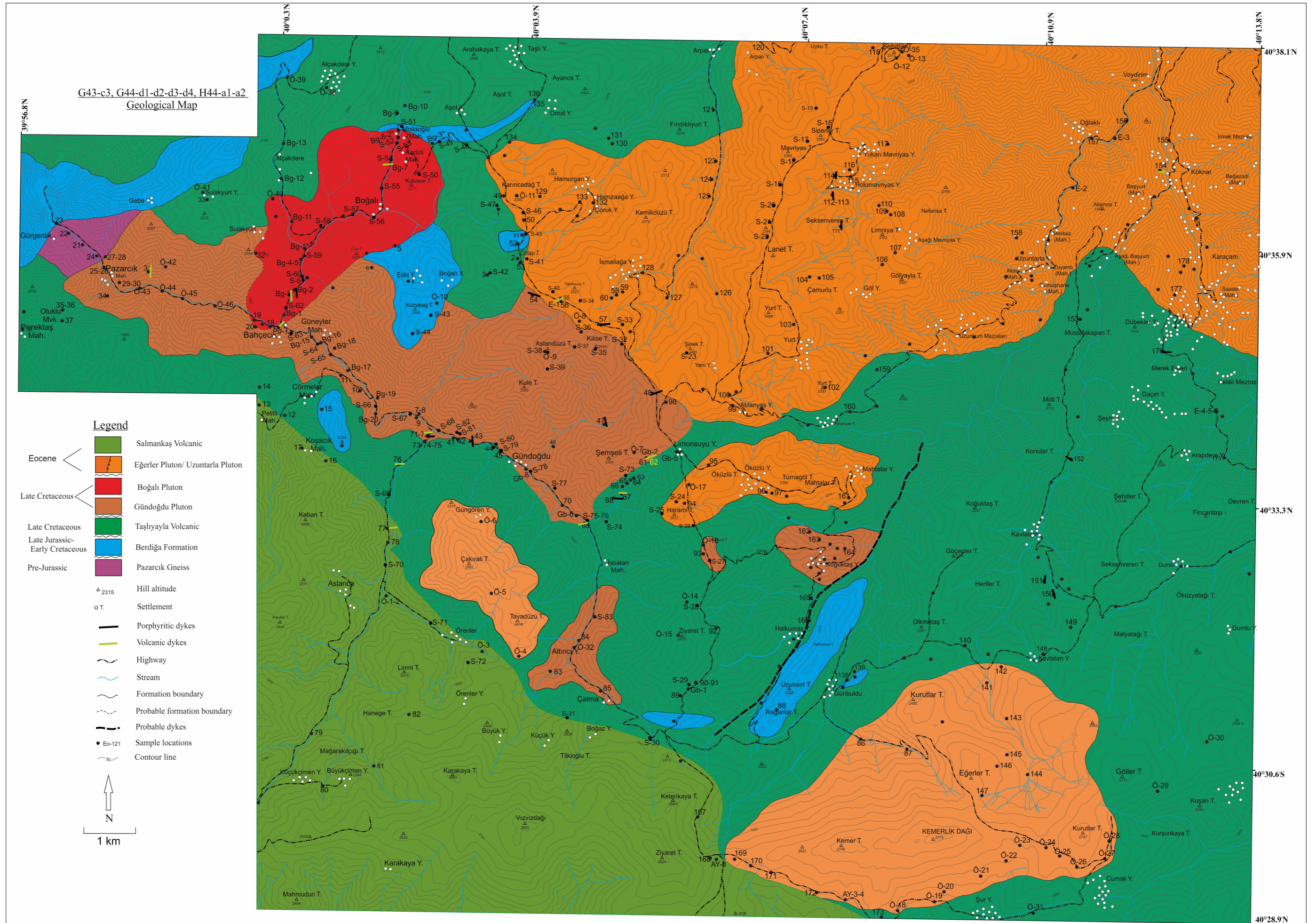


Figure 3. Geological map of field study, modified from Tübitak project 114Y219.



### 3. RESULTS

#### 3.1. Stratigraphically and Petrographical Studies

The rocks in the area of the present study distribute around the boundary between Trabzon-Gümüşhane and Bayburt on the eastern of the Karadeniz Region. It includes a wide range of rocks ranging from pre-Jurassic (Pazarcık gneiss) to Upper Cretaceous (Boğalı and Gündoğdu plutonic rocks) to the dykes of Eocene (Figure 4). The stratigraphic sequence and the lithological information about rocks that appears in the investigation area are as follows.

- 1- Pazarcık Gneiss
- 2- Berdiga Formation
- 3- Taşlıyayla Volcanic Rocks
- 4- Gündoğdu Pluton
- 5- Boğalı Pluton
- 6- Uzuntrla Pluton
- 7- Eđerler Pluton
- 8- Salmankaş volcanic rocks
- 9- Young acidic and basic dykes

##### 3.1.1. Pazarcık Gneiss

The basement unite of the study area contains a gneiss metamorphic rocks composed of coarse-grained, quartz, feldspar, biotite, and muscovite minerals. It occupies small area (less than 1,5 km<sup>2</sup>) and is located in the northwestern part of Pazarcık village. It has been named by Şahin (2005) as Pazarcık Metamorphic Formation and it has been aged Pre-Jurassic. This formation is in contact with Berdiga limestones in the north and the north west, Taşlıyayla volcanic rocks from the southwest and with Gündoğdu granitoid rocks from the south and east (Figure 5). All boundaries are faulted. The Gneiss rocks display variation of color, where the light color bands consist of medium-grained of quartz; plagioclase, orthoclase and lesser amount of muscovite whereas the dark colored bands dominated by large amount of biotite with small amounts of amphiboles (Figure 6 and 7). In some samples, contain quartz and plagioclase have a near granoblastic texture with

aligned biotite crystals. The lepido-granoblastic and banding are observed in the sections studied.

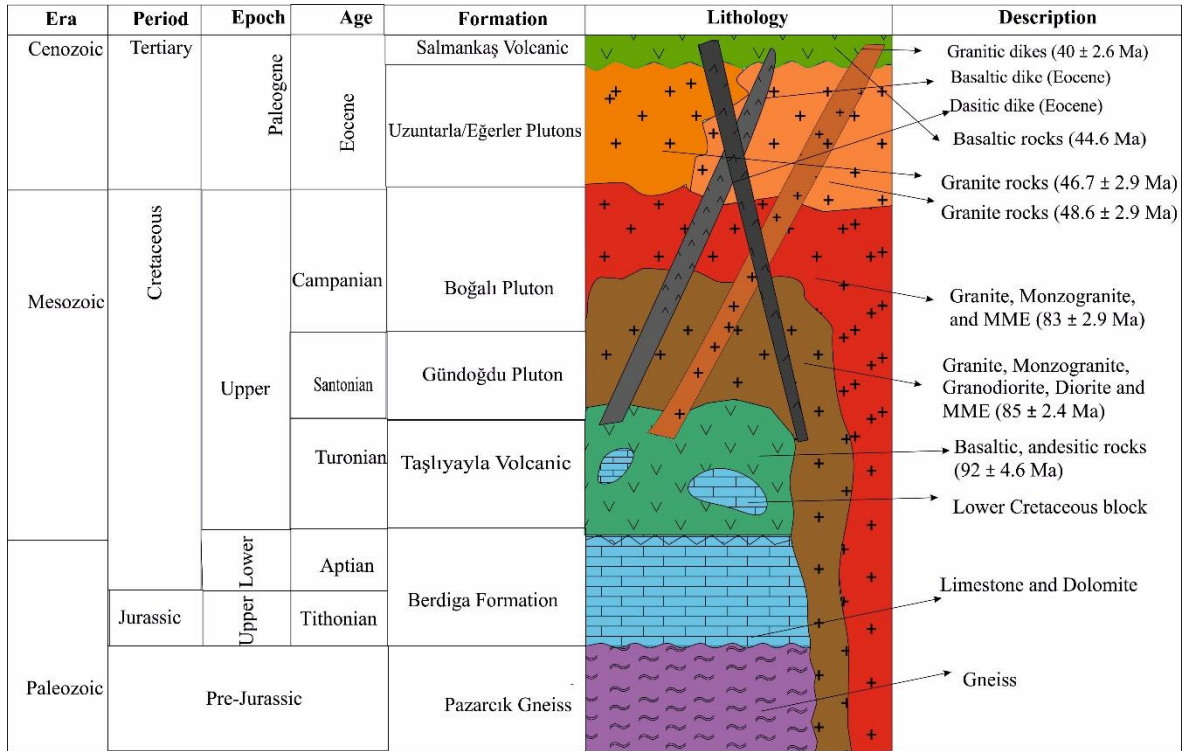


Figure 4. Generalised columnar section showing the stratigraphical units of the study area.

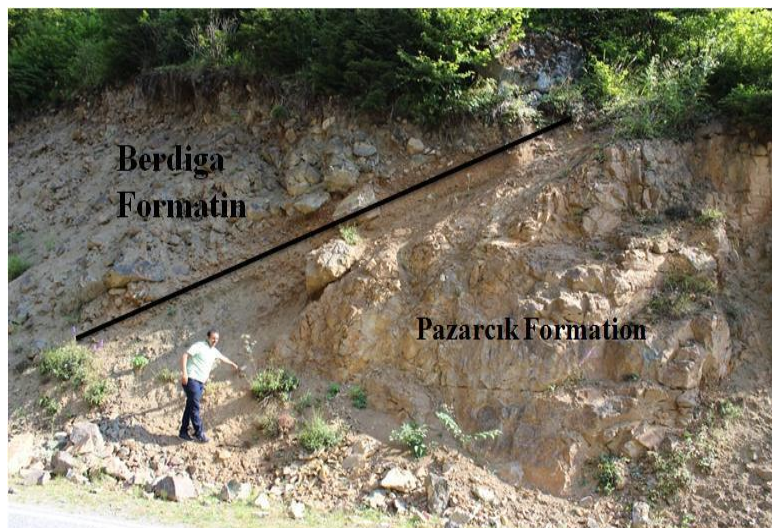


Figure 5. Photograph showing the boundary between Pazarcık Gneiss rock and Berdiga carbonate rock,  $40^{\circ}36'9.81''$ - $39^{\circ}57'14.27''$ NE.





Figure 6. Photo showing a banding in Pazarçık Gneissic rock,  $40^{\circ}63.435''$ - $39^{\circ}57'24.27''$ NE.

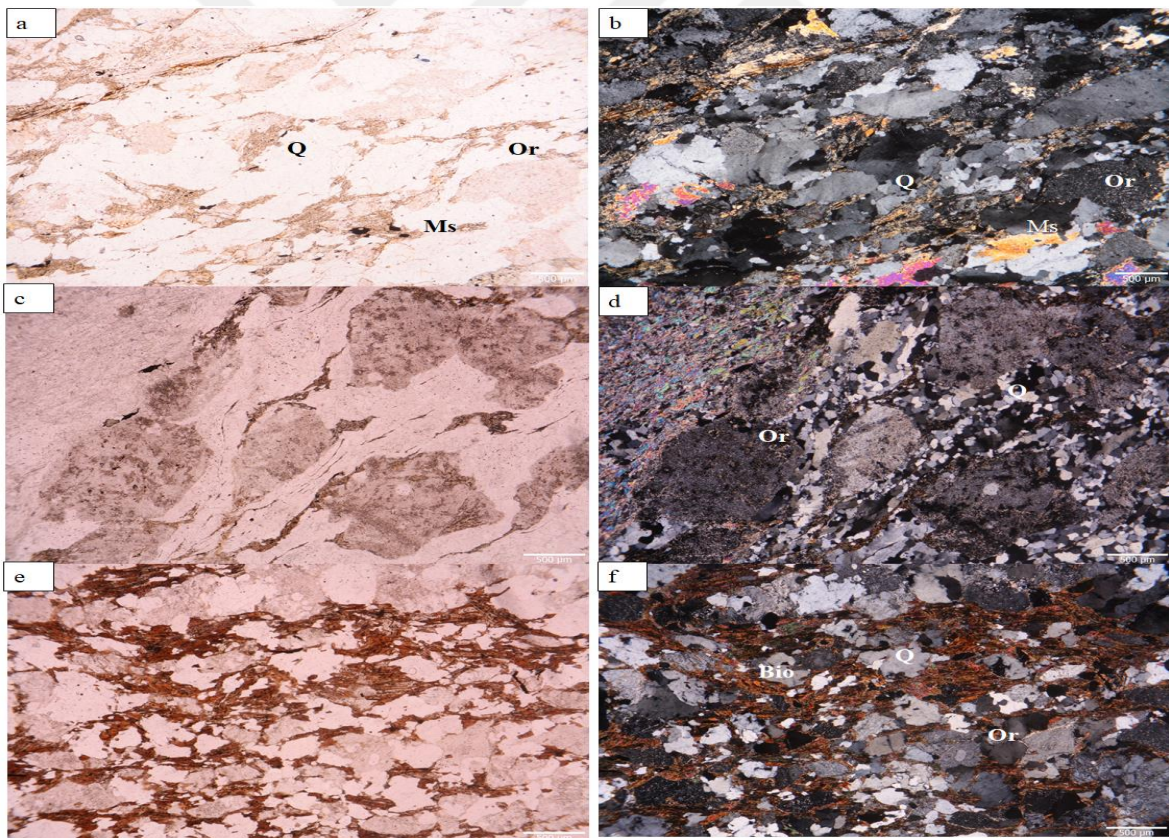


Figure 7. Photomicrographic showing mineral content and foliation in Pazarçık Gneissic rock, (a- f) displays the lepidogranoblastic texture (Qz: quartzs, Or: orthoclas, Ms: muscovite, Bio: biotite).

### 3.1.2. Berdiga Formation

The study area contains small area of carbonate rocks mainly composed of massive bedded limestone and dolomitic limestones with gray- beige color. These carbonates are found in huge blocks in different areas of the study area (Figure 8 and 9). It appears in the eastern part of Boğalı Village, Mollaoğlu Village, eastern of Halkuas Plateau, southeast of the Cörmeler Village, and eastern of Boğalı Plateau. This sedimentary unit has been named and classified by Pelin (1977), in the Giresun-Alucra area and the carbonates have been studied by different researcher and they were given age to Malm-Lower Cretaceous.

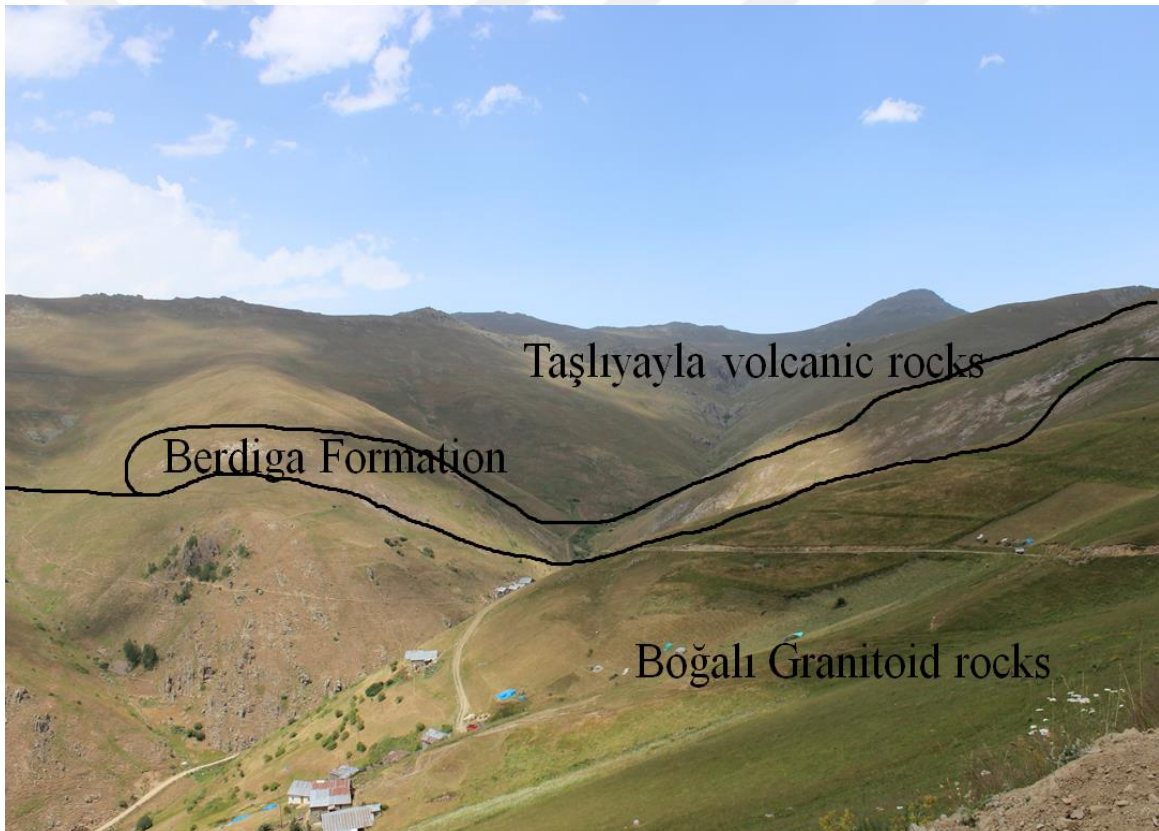


Figure.8. Photograph take from south to north showing the Berdiga limestone in between the Boğalı pluton and Taşlıyayla volcanic rocks,  $40^{\circ}36'37.07''$ -  $40^{\circ} 2'4.54''$ NE.



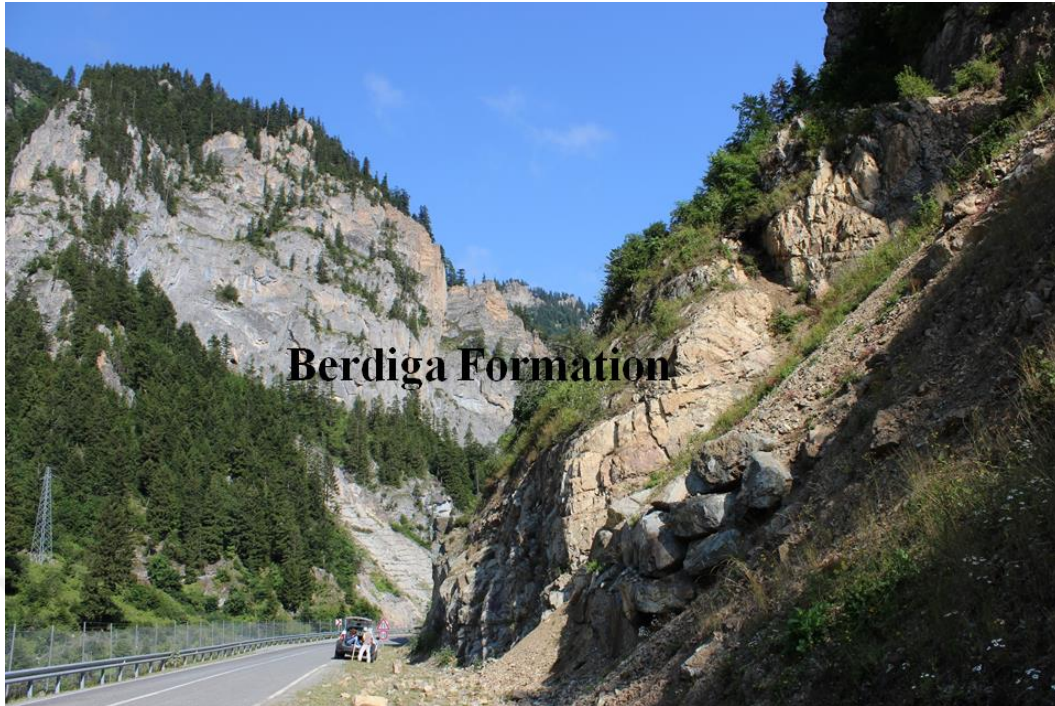


Figure 9. general view the distribution of the Berdiga carbonates, 40°31'21.50"- 40° 8'0.10"NE

### 3.1.3. Taşlıyayla Volcanic Rocks

The study area contains widespread volcanic rocks with different ages. These volcanic rocks cover most of the study area and cut by Upper Cretaceous and Eocene plutons. The name of the Taşlıyayla volcanic rocks is given by Şahin (2005).

The main body of Taşlıyayla volcanic rocks shows high diversity in composition and texture in which consist of basaltic and andesitic rocks. This formation also includes granitic-porphyry, basaltic and dacitic dykes and displays exfoliation structure. Minerallogically they generally consist of plagioclase, clinopyroxene, hornblende, biotite and include some of the secondary minerals such as chlorite and epidote. These rocks have greyish-blackish aphanitic texture characterized by microcrystalline porphyritic, microlitic porphyritic, glomeroporphyratic, microgranular, vesicular, poikilitic, ophiolitic, and intersertal textures. It has been also observed some microlitic rocks contains cracks, fracture, and decomposition in the contact with plutonic rocks. Exfoliations structure are observed around Pelitli area (Figure 10). Alterations such as chloritization, sericitization,

and epidotization represent the most common hydrothermal alteration types associated with the rocks here.

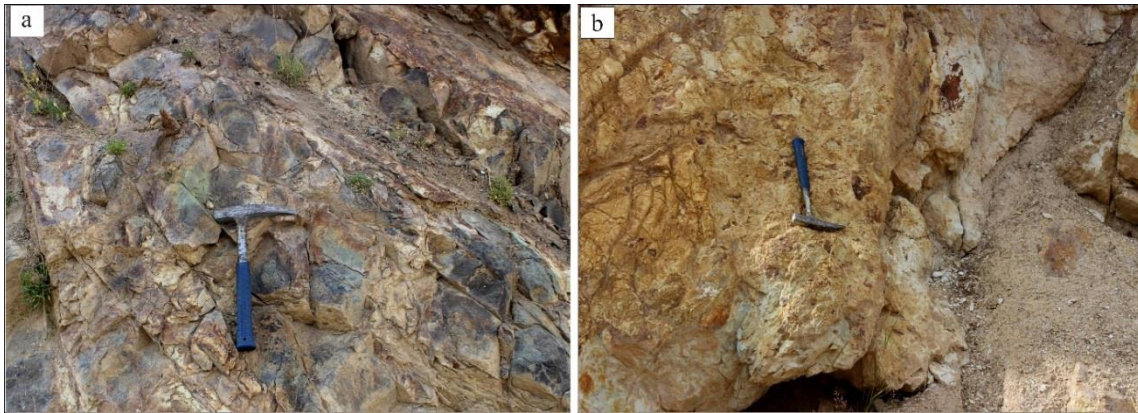


Figure 10. Photographs taken from North of Pelitli Village, 40°34'26.98"- 40° 0'2.72"NE and displays some features of Taşlıyayla volcanic rocks in the field, (a) basalt with exfoliation structure, (b) hydrothermal alteration.

Basaltic rocks represent the majority of volcanic rocks that distributed in the area of the present study. These basaltic rocks were studied in terms of minerals content and textures features. These rocks consist of plagioclase ( $An_{60-80}$ ), clinopyroxene, hornblende, biotite and opaque minerals. Chlorite, epidote, sericite, carbonate, prehnite, zeolite, and Fe–Ti oxide are secondary minerals. Generally, these rocks display diversity in color, grain size and texture which the grain range from fine to medium grained rocks displays microcrystalline porphyritic, microlitic porphyritic, glomeroporphyritic, microgranular and vesicular, ophitic, and intersertial textures (Figure 11). It also shows epidotization and chloritization alteration type.

Andesites represents a part of extrusion rocks distribute in the area. These unit displays porphyritic and microlitic porphyritic textures. The mineral content of andesitic rocks is dominated by phenocryst of quartz, plagioclase ( $An_{40-44}$ ), amphibole, and opak minerals with matrix of quartz plagioclase, epidote and amphibole. The andesites also characterized by epidotization, carbonation and sericitization hydrothermal alteration types (Figure 12).

Plagioclase is present both as phenocrysts and microlites textures and found as euhedral-to-subhedral crystals displaying albite twinning, oscillatory zoning and sieve texture (Figure 11a). Clinopyroxenes phenocrysts are euhedral-to-subhedral grains, rounded. Clinopyroxene in few samples found as overgrowth rims on earlier formed



plagioclase Crystals. It also partly fragmented, but relatively unaltered including inclusions of opaque minerals and apatite. Hornblendes display an opaque rim and chloritization and found as euhedral-to-subhedral, tabular, prismatic and acicular crystals. Biotite occur as euhedral and subhedral reddish-brown. Alteration product of chlorites are green color, rimmed by fine-grained magnetite occurs in the matrix as a replacement of mafic minerals – possibly amphiboles (?). The groundmass is composed of subhedral plagioclase microlites, epidotes and chlorites.

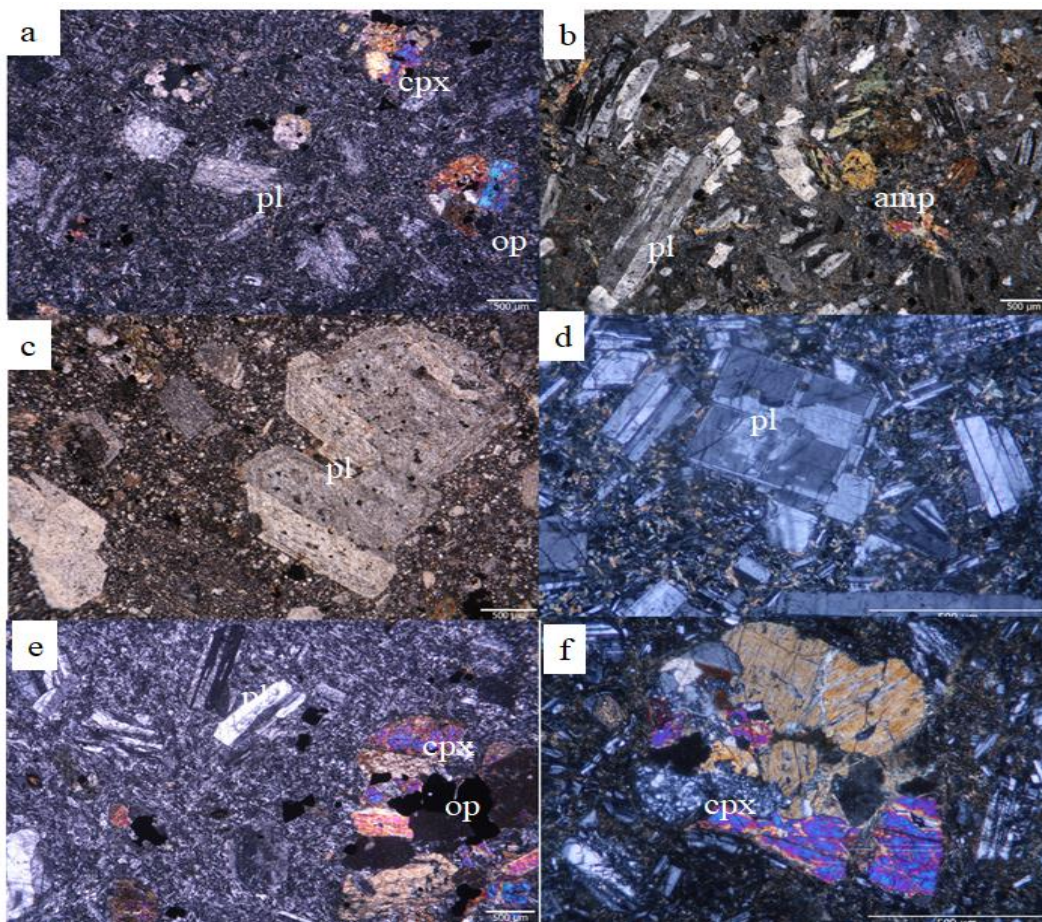


Figure.11. Microphotographs of Taşlıyayla volcanic rocks showing microcrystalline porphyritic, microlitic porphyritic, glomeroporphyrific, microgranular and poikilitic, (a, b) microlitic porphyritic texture, (c) microcrystalline porphyritic displays plagioclases sieve texture,(d) plagioclase exhibits with albite twinning and oscillatory texture, (e) glomeroporphyrific and poikilitic texture, (f) microcrystalline porphyritic displays phenocryst of clinopyroxene and plagioclase, (Pl: plagioclase, amp: amphibole, Cpx: clinopyroxene, Op: opaque minerals).



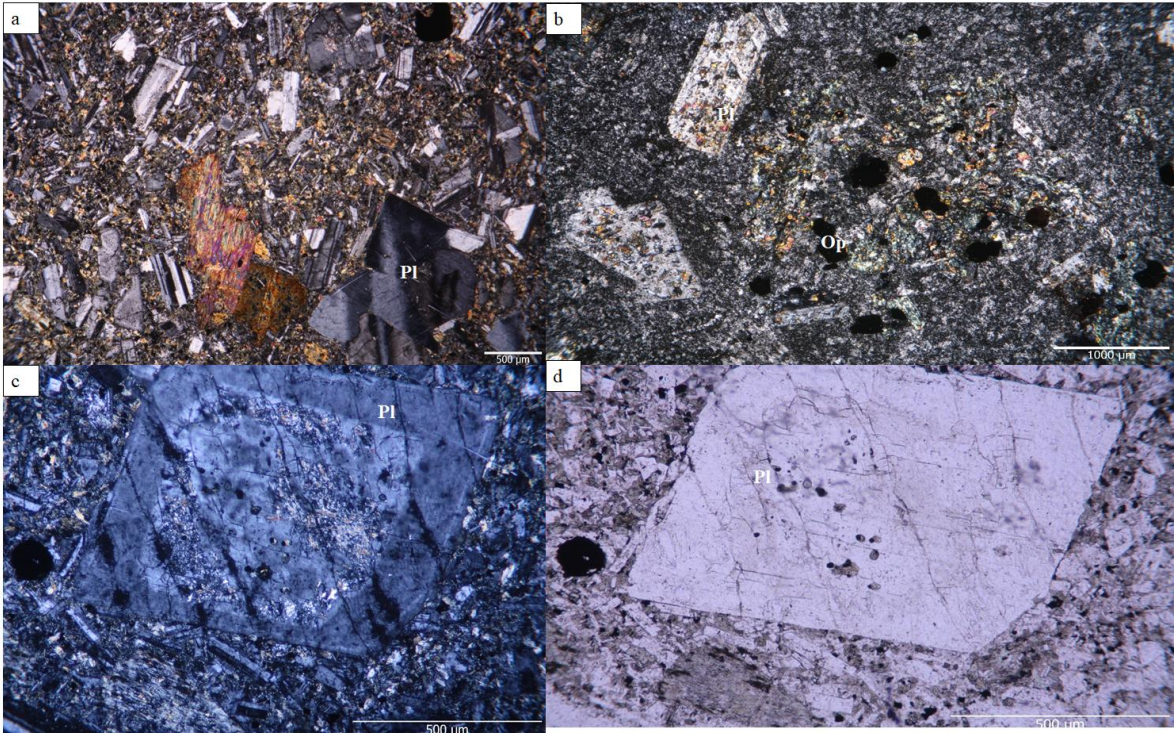


Figure 12. Microphotographs of Taşlıyayla volcanic rocks showing microcrystalline porphyritic, microlitic porphyritic, glomeroporphyritic texture, (a) glomeroporphyritic texture of plagioclase, (b) microcrystalline porphyritic texture contain plagioclase displays high alteration, (c, d) microlitic porphyritic texture contain Plagioclase shows oscillatory zoned.

#### 3.1.4. Gündoğdu Pluton

The rocks belonging to Gündoğdu Pluton take place between Pazarcık village and Güngören village and settled by cutting the Taşlıyayla volcanic rocks. It is in faulty contact with Pazarcık metamorphic rocks from the North West. The pluton cut by Late Cretaceous Boğalı pluton and Eocene age of acidic and basic dykes (Figure 13). The pluton has been named by Şahin, (2005) as Gündoğdu alter microgranite whereas in this study we use it as Gündoğdu Pluton. The main body of pluton show high diversity in composition and texture in which consist of fine grain granitic and granodiorite rocks. Generally, this pluton displays large porphyritic texture. On the contact there are porphyritic aphanitic textures are common whereas inside the pluton there are porphyritic phaneritic textures are seen. Under microscope these seen as poikilitic, graphic and rarely myrmekitic textures. This

pluton especially in the edge zones contain from centimeters to dimeter oval/circular shaped mafic microgranular enclave consisting of quartz diorite and monzodiorite.



Figure 13. (a) The boundary between Boğalı and Gündoğdu pluton. (b) Microgranular enclave with dark color in Gündoğdu pluton, photo is taken in 40°34'38.70"-40°0'55.89"NE.

The mineralogical modal of granitoids samples that represent the pluton are given in the Table 1. The classification modal of Streckeisen (1976) QAP (quartz–alkali feldspar–plagioclase) is used here to classify the rocks. The granitoid rocks of the Gündoğdu pluton plotted in the granite, granodiorite, syanogranite and diorite fields in the QAP diagram (Streckeisen, 1976) (Figure14). The modal mineralogy of Gündoğdu pluton is 10-48% plagioclase, 7-56% orthoclase, 23-45% quartz, 3-12% amphibole, 0.6-4.1% Biotite, 0.8-2.8% opaque minerals, 0.1-5.1% Muscovite with secondary minerals such as apatite, and zircon. Chlorite, sericite, epidote are accessory minerals. Alterations such as chloritization, sericitization, epidotization, and muscovitization represent the most common hydrothermal alteration types associated with the rocks here. The rocks of the Gündoğdu pluton displays variations on minerals content and properties and can be explained as follow.



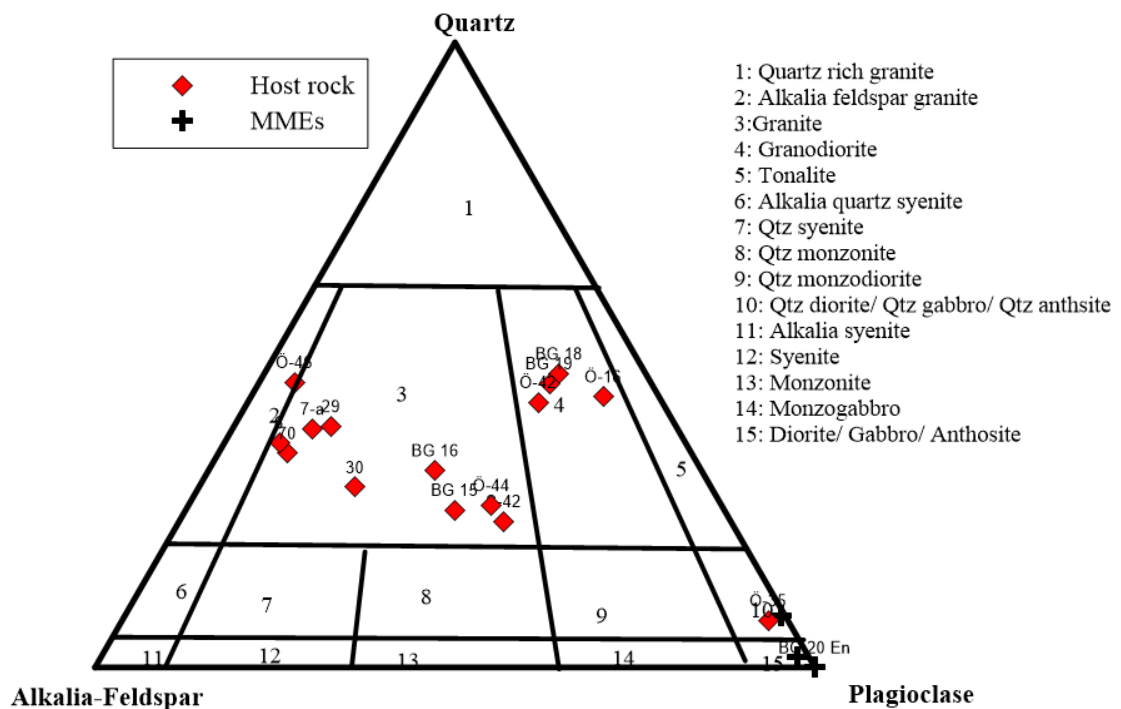


Figure 14. Modal classification of the Gündoğdu pluton (Streckeisen 1976).

**Granitic rocks** are light in color displays fine-to medium grained, microgranular porphyritic, and poikilitic textures. Generally, these rocks show variations in terms of texture which they display microcrystalline porphyritic, phaneritic porphyritic and phaneritic texture. They also display poikilitic, graphic and myrmekitic textures.

These granitic rocks in different sample such as (7a, 29, 30, Ö44 and BG 16) mainly contain 29-38% quartz, 21-29% plagioclase, 17-56% orthoclase and microcrystalline matrix composed of plagioclase, quartz, K-feldspar, zircon and apatite. It shows plagioclase (albite) with twinning and polycrystalline twinning and K-feldspar with alteration in the rims. Plagioclase displays diversity of characters which displays oscillatory zoned, albite twinning, reversely zoned prismatic-cellular growth and sieve texture (Figure 15). The dominant alteration is sericitization hydrothermal alteration.

Table 1. Mineral modes that in the sample collected in Gündoğdu pluton (more than 1500 grain has been counted), Q=Quartz, K-F= K-Feldspar, Pl= Plagioclase, Amph= Amphibole, Bio=Biotite, Mu=Muscovite, İl=İlmenite, Epi= Epidote, Matrixes= uncounted grains, Op= opaque minerals.

Sam	Q	K-F	Pl	Amph	Bio	Mus	İl	Epi	Matrix	Op	Q%	K-F%	Pl%
<b>S-42</b>	21.1	28.4	40.7	6.1	0.6	---	---	---	---	2,8	23.39	31.49	45.1
<b>7-a</b>	34.5	45.7	10.1	3	0.6	5.1	---	---	---	1,6	38.21	50.61	11.18
<b>29</b>	35.5	44	12.44	7.64	---	---	---	---	---	0,5	38.61	47.86	13.53
<b>70</b>	31.3	51.2	8.8	7.7	---	---	---	---	---	0,8	34.28	56.08	9.64
<b>6</b>	35.4	55.5	7.5	---	0.6	---	---	---	---	1	35.98	56.40	7.62
<b>30</b>	24.5	42	18.5	12.8	---	---	---	---	---	1,7	28.82	49.41	21.76
<b>BG 15</b>	20.1	19.9	30.05	4.95	---	---	2	---	---	---	29	29	43
<b>BG16</b>	10	15	10	2	---	---	---	---	63	---	29	43	29
<b>BG18</b>	40	10	35	10	---	---	2	3	---	---	47	12	41
<b>BG19</b>	38.0	12	34	10	---	---	---	---	---	6	45	14	40
<b>BG-20 en</b>	---	---	55	35	---	---	---	---	---	10	0	0	100
<b>O-9</b>	3.3	0.2	36.6	6.6	2.3	---	---	0.8	---	2	8	0	91
<b>Ö-16</b>	17.0	3.0	19.0	0.4	0.4	---	---	0.3	59.9	---	44	8	49
<b>Ö-35</b>	2.7	1.0	32.3	2	2	---	---	0.3	59.7	---	8	3	89
<b>Ö-40</b>	19.3	27.6	36.4	1.7	2.3	---	---	---	10.1	---	23	33	44
<b>Ö-44</b>	15.0	19.3	25.4	4.1	0.9	---	---	---	33.8	---	25	32	43
<b>Ö-46</b>	29.7	32.2	3.2	8.8	0.8	---	---	---	24.62	---	46	49	5

Plagioclase may contain small acicular apatite crystals, indicating to local saturation of apatite or magma mixing (Wyllie et al., 1962; Frost and Mahood, 1987; Hibbard, 1991; Salonsaari, 1995; Arslan and Aslan, 2006). Quartz displays embayed crystal and variations in grain size which appear as phenocryst in some granitic rocks and as porphyritic texture on the others, whereas plagioclase reflects a high of alteration (Figure15a). Quartz exhibits undulose extinction, embayed and corroded at the outer part of crystal. It fills interstices between other minerals forming a granophyric texture. K-feldspar displays an anhedral, to subhedral crystals. Large phenocrysts are heterogeneously distributed within the various rock types. These minerals display a poikilitic texture in which large K-feldspar contain some grain of quartz (Figure 15c, d). In some samples some K feldspar crystals shows sericitization and chloritization alteration types. Hornblende displays euhedral to subhedral tabular, prismatic and acicular crystals. It shows color range from pale yellow, yellowish

green to pale green. Hornblende displays chloritization alteration types. Some of hornblende crystals include small grain of biotite and orthoclase inclusions. Zircon is not much visible in most samples but in some samples displays a small crystal (less than 100  $\mu\text{m}$ ), very high relief and shows vertical extinction in sections parallel to the extension.

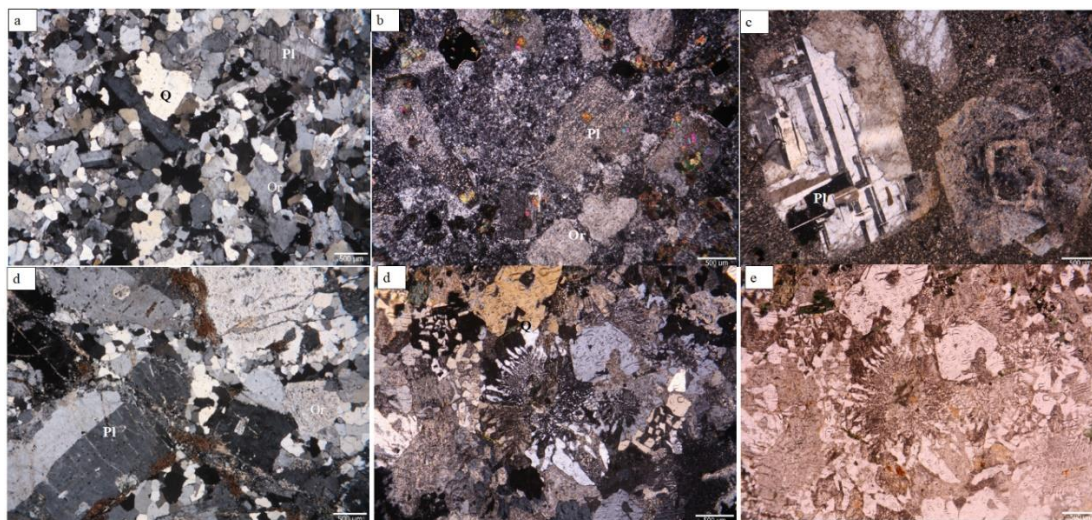


Figure.15. General views showing the petrographically feature of granitic rocks in Gündoğdu pluton, (a) showing majority of mineral grain size and textural characteristics of the host rocks, (b) microcrystalline porphyritic showing plagioclase altered, amphibole and anhedronal epidote, (c, d) oscillatory texture, zoning in plagioclase and displays poikilitic texture, (e,f) myrmekitic texture, (Q: Quartz, Pl: Plagioclase, Or: Orthoclase, Op: opaque minerals).

**Granodiorite rocks** (samples like Ö42, Ö16, BG18 and BG19) are founded as microcrystalline porphyritic and phaneritic porphyritic texture (Figure 16). It is light grey in color and have medium to coarse grained. It contains a approximately phenocryst of quartz 47-49%, plagioclase 30-50%, K- feldspar 8-14%, Amphibole 2% with a microcrystalline matrix composed of plagioclase + amphibole and displays hydrothermal alteration types such as high sericitization. The plagioclase has an (20-25%) in composition, commonly shows albite twinning and displays sericitization alterations. Quartz found as anhedronal to rarely subhedronal in shape displays embayed crystal and found as fine grain. K-feldspar displays an anhedronal, to subhedronal crystals shape of orthoclase altered to carbonate and chlorite. Hornblende displays euhedronal to subhedronal tabular crystals which is increasingly altered to chlorite.



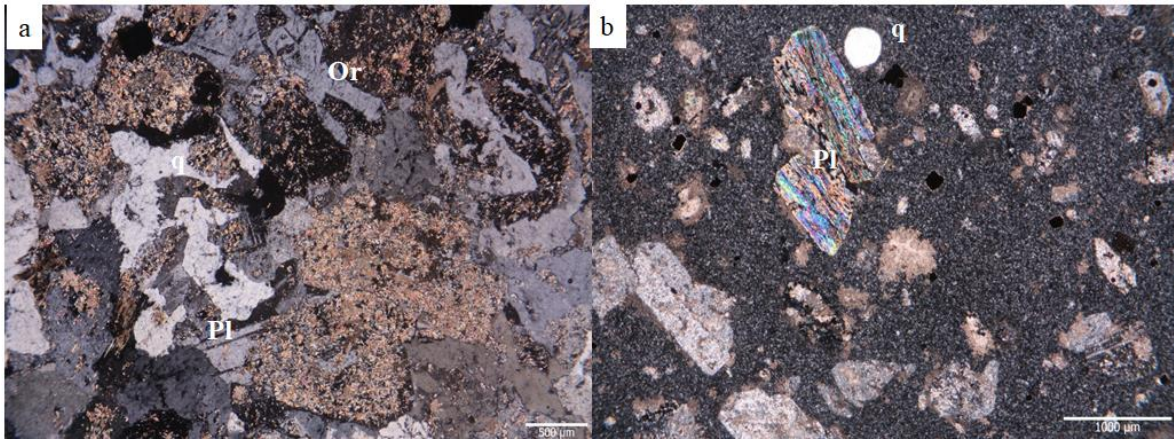


Figure 16. General view showing the petrographically feature of granodiorite rock at Gündoğdu pluton, (a) k- feldspar, Plagioclase altered showing myrmekitic texture, (b) microcrystalline porphyritic texture showing high alteration, (Q: Quartz, Pl: Plagioclase, Or: Orthoclase).

**Syanogranite rocks** (samples Ö46, 29, 7a and 70) show light to small dark in color displays a phaneritic and microcrystalline porphyritic texture contain fine-grained crystal. It contains a phenocryst of quartz 30-46%, K- feldspar 47-56 %, plagioclase 5-13%, amphibole 10%, opak minerals 2%, Biotite 5% and epidote %3 and it displays inclusion of calcite and sericitization hydrothermal alteration types (Figure 17)..

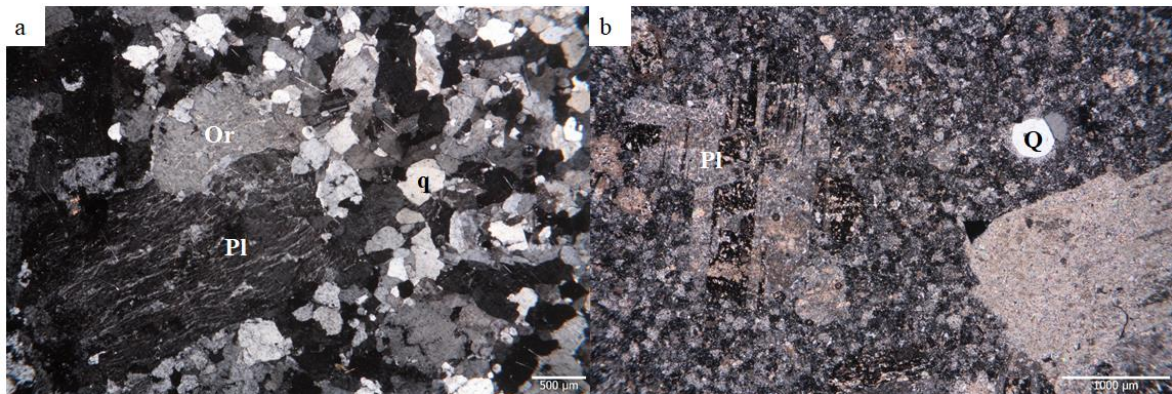


Figure 17. General view showing the petrographical feature of synograndiorite rock at Gündoğdu pluton, (a, b) phaneritic porphyritic texture microcrystalline porphyritic texture showing high alteration and zone in plagioclase (Q: Quartz, Pl: Plagioclase, Or: Orthoclase).

Quartz occurs as embayed crystal and has an anhedral shape. Quartz represent the majority of minerals. It is found as fine grain displays anhedral to rarely subhedral in shape and displays embayed crystal. The plagioclase commonly shows albite twinning and

has been altered to sericite. K-feldspar grain displays are anhedral, to subhedral crystals shape of orthoclase and has been also altered to sericite

**Monzogranites rocks** (samples Ö 40. Bg 15 -S42) displays similar properties to granite rocks in terms of mineral content but they show more appearance to biotite minerals. They contain light colored minerals such as plagioclase, quartz and orthoclase, they usually show light gray and pinkish gray colors. This unit medium to fine grained displays microcrystalline porphyritic and phaneritic porphyritic texture, contain 23-29 % Quarts, 29-31% Orthoclase, 43-45% Plagioclase (An<sub>25-28</sub>), Amphibole approximately 0,9%, Fe-Ti oxides %0.2, and opaque minerals and microcrystalline matrix are composed of amphibole ± biotite and/or quartz. Grain size of plagioclase are ranging from 0.2 mm for inclusions to 2.5 mm for large crystals. It commonly displays the twinning of albite, sieve texture, reversely zoned and displays a high sericitization alterations (Figure 18). Quartz occur as embayed crystals displays anhedral shape and fine to medium grains. K-feldspar and plagioclase also occur as Euhedral to subhedral shapes and displays poikilitic textures. Orthoclase form anhedral, to subhedral crystals displays poikilitic texture displays high of sericitization alteration. Hornblend dispalys euhedral to subhedral tabular crystals. They are generally more abundant than biotite. It displays variation of colour brownish, yellowish green to pale green. Hornblende is altered to chlorite. Biotite varies in crystal shapes from subhedral to euhedral, brown- reddish and forms prismatic crystals and lamellas. Large crystals of biotite showing poikilitic texture in which contain small plagioclase and opaque minerals. Epidote and sericite are most abundant accessory mineral and they present a common alteration product of plagioclase.



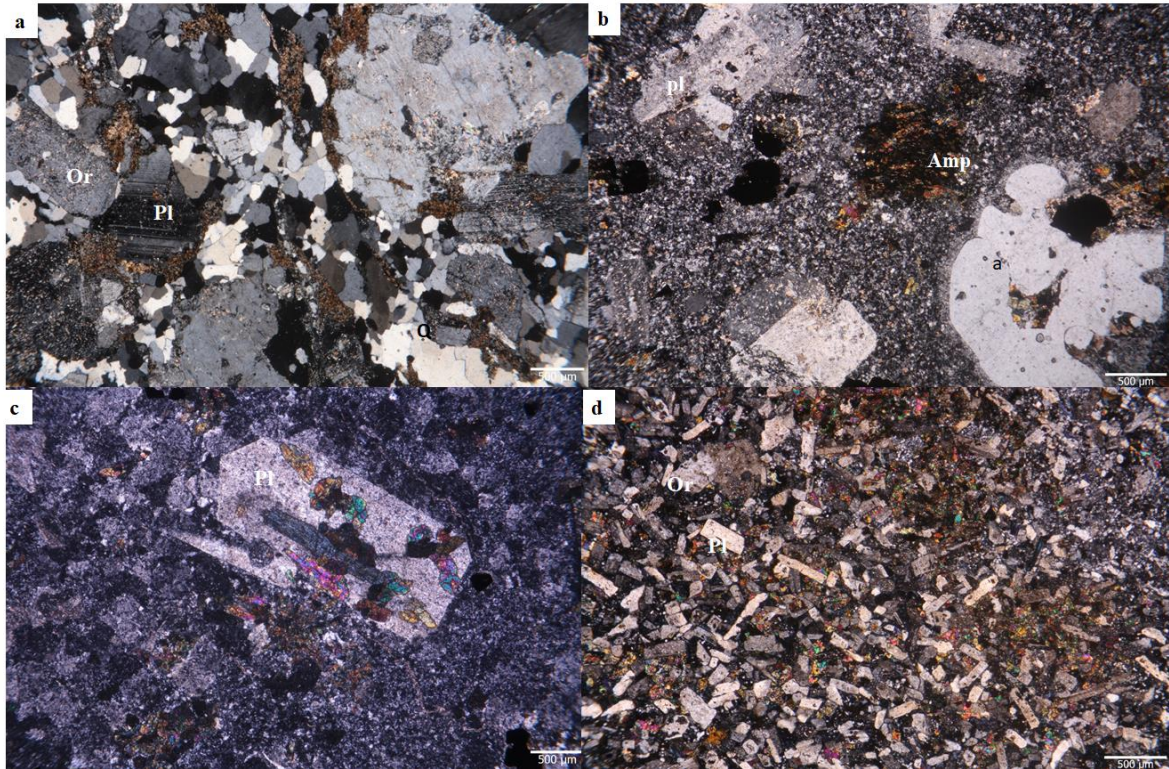


Figure 18. General view showing the petrographical feature of monzogranitic rocks in Gündoğdu pluton: (a) showing majority of mineral grain size and textural characteristics of the host rocks; (b) microcrystalline porphyritic showing amphibole altered and embayed quartz; (c) microcrystalline porphyritic showing plagioclase altered; (d) microlitic texture, (Q: Quartz, Pl: Plagioclase, Or: Orthoclase).

**Diorites** (samples Ö 9 and Ö45) having porphyritic texture also contain fine-grained crystals, plagioclase phenocryst with fine to medium grains of amphibole and biotite and show poikilitic, ophitic and intersertal textures (Figure 19). It shows high alteration intensity in which the plagioclase representing the majority of minerals that formed the diorite rocks with euhedral shapes altered to sericite. It displays diversity of characters which displays oscillatory zoned, twinning of albite and also displays a sieve texture. Biotite also show alteration where the crystals have been altered to chlorite.



Figure 19. General view showing the petrographical feature of dioritic rocks in Gündoğdu pluton and displays an intersertal texture.

MME's are oval in shape and display fine-grained compared to the host rock. They have diorite and quartz monzodiorite in compositions. They consist of plagioclase, amphibole, quartz (0,00-0,2%), biotite, opaque minerals and accompanied by accessory such as apatite, zircon and magnetite (Figure 20). The alteration pattern of the rocks shows that chloritization and sericitization represent the most common hydrothermal alteration types. Plagioclase is subhedral, oscillatory zoned, and has albite-law twinning. Quartz occurs as embayed crystals and partly corroded rims. Biotite shows chloritization and is abundant at contacts between enclaves and host rock. Mafic microgranular enclaves (MMEs) occurring at the boundary between Gündoğdu pluton and Uzuntarla pluton have a basaltic composition and contain plagioclase amounts of  $\geq 2\%$  and 98% microcrystalline matrix that is composed of microlitic plagioclase ( $an_{52}$ ) and Fe-Ti oxides.



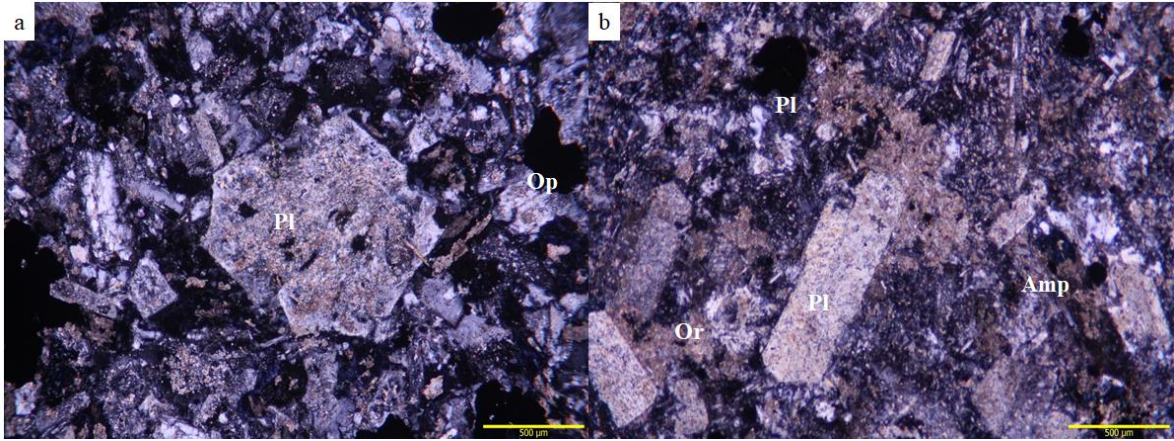


Figure 20. General view showing grained mafic enclave (sample) displays plagioclase altered and amphibole, (Pl: Plagioclase, Or: Orthoclase, Op: opaque minerals).

### 3.1.5. Boğalı Pluton

Boğalı pluton located to the north-east part of Çaykara intrusive is complex and extend to 7km<sup>2</sup>. To the North of Boğalı pluton there are a Taşlıyayla Volcanic rock and Berdiga carbonate rocks. Gündoğdu pluton cut by the Boğalı pluton from south and west. Pluton has been named by (Şahin, 2005) as Boğalı\_ K-feldspar-megacrystic monzogranite. In this study we call it only Boğalı pluton. The main body of pluton show a high diversity in composition and texture in which consist of Phenocryst-K feldspar Monzogranite and fine grain granitic rocks (Figure 21). It includes microgranular porphyritic rock which occur at the edge of pluton. The pluton of Boğalı contain elliptical/circular shaped microgranular enclave. The pluton cut by acidic dykes of 5 to 10 meters' thickness and mafic dykes of 1-2 meters' thickness (Figure 22). The modal mineralogy of selected samples in Boğalı pluton is given in the (Table 2).

The classification modal of (Streckeisen 1976) QAP is used here to classify the rocks. The rocks of the Boğalı pluton are plotted in the granite, quartz monzodiorite, quartz monzonite and quartz syenite fields in the QAP modal classification diagram (Streckeisen, 1976) (Figure 23). The modal mineralogy is mainly 10-49% plagioclase, 30-57% Orthoclase, 15-27% quartz, 2-11% amphibole, 0.5-2.3% Biotite, 0.5-2.5% opaque minerals, with accessory minerals such as apatite, and zircon. Chlorite, sericite, and epidote minerals. These rocks have been altered and the chloritization, sericitization, and

epidotization, represent the most common hydrothermal alteration types. The alteration processes have more appearance toward the contact with Gündoğdu pluton.

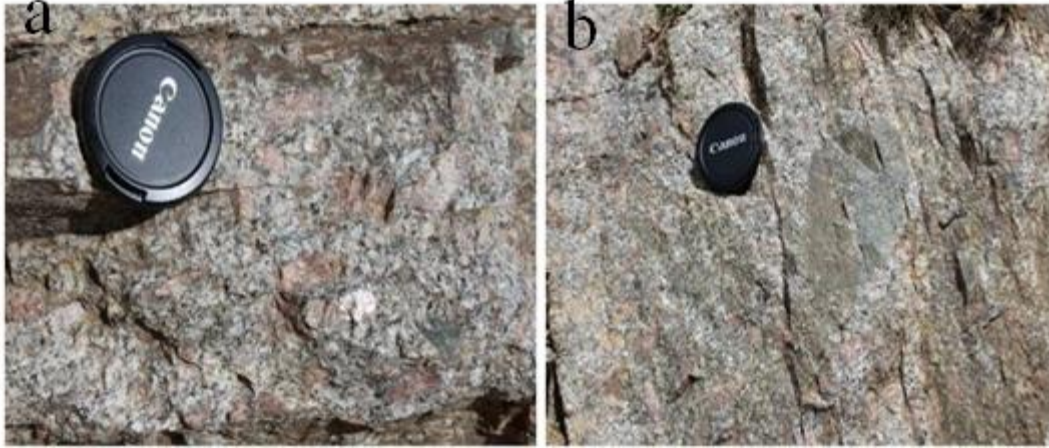


Figure 21. Fine-medium grained to porphyritic textured of K-feldspar in monzogranite which forms the main body of the Boğalı Pluton containing large K-Feldspar  $40^{\circ}35'12.18''$ -  $40^{\circ}0'21.73''$ NE.



Figure 22. Dasitic deyke at the road between Bahçecik and Boğalı ( $40^{\circ}35'24.79''$ -  $40^{\circ}0'26.25''$ NE).

Petrographically, this pluton shows diversity in grain size, color, and texture. Generally, they have poikilitic, graphic and rarely myrmekitic textures. The rock of the Boğalı pluton displays variation on minerals content and properties and can be mainly classified to monzogranite, and granite as explained as follow.

Table 2. Mineral modes in the samples collected in Boğalı pluton (more than 1500 grain has been counted), Q=Quartz, K-F= K-Feldspar, Pl= Plagioclase, Amph= Amphibole, Bio=Biotite, Mu=Muscovite, İl=Ilmenite, Epi= Epidote, Op= opaque minerals.

Sample	Q	K-F	Pl	Amph	Bio	Epi	Op	Q%	Or%	P%
<b>Bg1*</b>	27.3	41.0	23.5	---	---	---	---	29.7	44.6	25.6
<b>Bg1b*</b>	16.1	22.5	49	11.8	---	---	0.6	18.38	25.68	55.94
<b>19</b>	20.9	53.5	13.1	10	---	---	0.7	23.89	61.14	14.97
<b>S-59</b>	17	55.0	23.6	2	0.5	---	1.1	17.78	57.53	24.69
<b>Bg-1</b>	22.8	43.1	22.3	7.1	---	0.5	0.9	25.9	48.7	25.34
<b>S-58A</b>	27.4	36.2	40	7.65	---	---	0.9	26.45	34.9	38.61
<b>32</b>	28.5	29.3	32.6	7.9	---	---	1.6	31.53	32.4	36.06
<b>S-54</b>	14.42	56.57	26.97	1.59	0.48	---	0.69	14.72	57.7	27.53
<b>S-53</b>	28.7	51.5	17.4	1.4	---	---	1	29.41	52.7	17.83
<b>S-52</b>	13.5	43.85	37.2	4.07	0.4	---	0.98	14.28	46.3	39.34
<b>Bg11</b>	18.5	50	23.8	4	---	---	1.6	20.04	54.17	25.79
<b>S-55</b>	33.4	37.7	23.5	3.8	---	---	1.3	35.31	39.85	24.84
<b>S-56</b>	17.7	50.6	26.5	4.1	---	---	1.1	18.67	83.38	27.95
<b>S-61</b>	16.5	37.3	38.5	4.8	0.9	---	1.5	17.88	40.41	41.71
<b>S-57</b>	20.9	45.8	26.2	5.3	0.3	---	1.3	22.5	49.3	28.2
<b>O-40</b>	21.4	30	38.5	1.34	2.38	---	3.1	23.8	33.37	42.83

**Monzogranites** (sample such 19, Bg1, Bg11, S58, S54, S59, S61, S52, Ö40) are dark pink and pinkish gray in color. This unit displays phaneritic porphyritic texture. These rocks are medium to fine grained porphyritic texture, contain 14-23% quartz 17-42% plagioclase (An<sub>32</sub>), 33- 46% Orthoclase, 4.8-11% amphibole, 0.4-2% biotite and 0.1% opaque minerals. Orthoclase forms anhedral, to subhedral crystals displays poikilitic texture in which phenocryst of orthoclase includes small inclusion of quartz (Figure 24). Plagioclase displays diversity of characters which displays albite twinning, sieve texture, oscillatory zoned, reversely zoned prismatic-cellular growth and also displays a sericitization hydrothermal alteration type. Quartz crystal in some monzogranitic rocks displays embayed crystal and found as fine to medium grain. Generally, these rocks display different colours, sizes and textures which the grain ranging from fine to medium-coarse grained showing graphic, poikilitic and rarely myrmekitic textures. Hornblende shows an euhedral



to subhedral crystals. It displays pleochroism feature from Pale green to yellowish green to pale Brown and highly altered to chlorite.

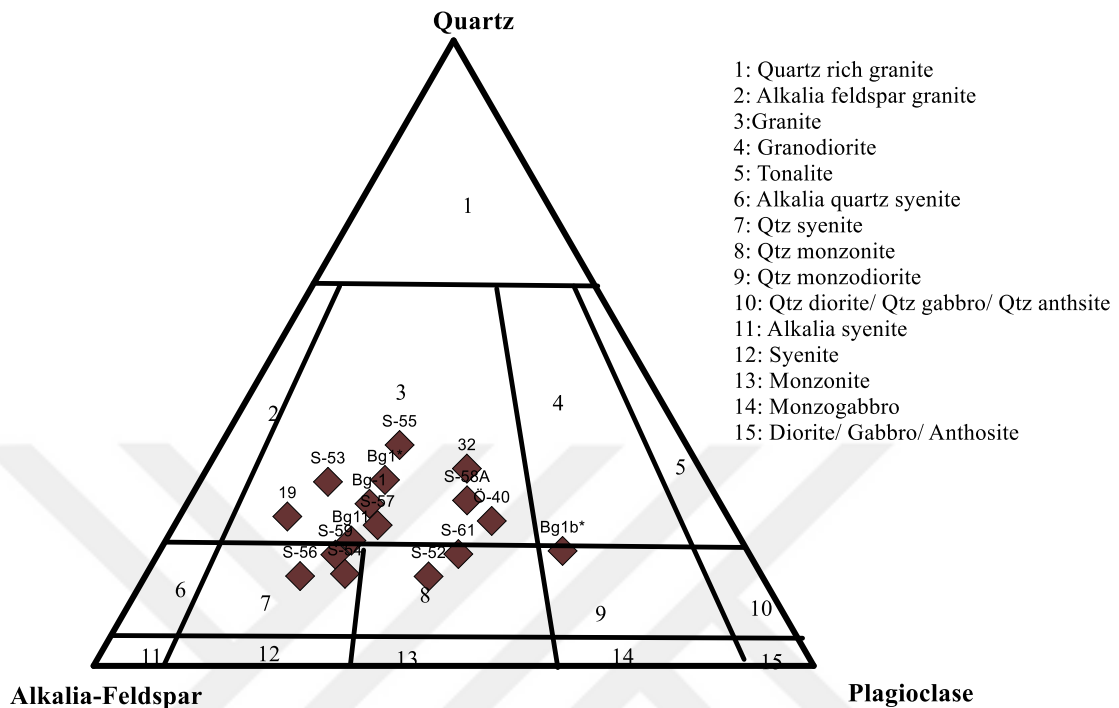


Figure 23. Modal classification of the Boğalı Pluton samples (Streckeisen 1976).

Biotite is abundant in this unit in comparison of other rocks displays varies in crystal shape range from euhedral to subhedral, with reddish-brown in color reflecting shape of prismatic and lamellas. Biotite displays chloritization alteration type, and epidote along the cleavage planes. Some large crystals of biotite showing poikilitic texture in which large crystal may contain opaque minerals.

**Granites** (sample number 32, Bg1, Bg11, S53, S55, S58a,) display light to light grey in color and displays a phaneritic porphyritic- microcrystalline porphyritic texture contains fine- grained crystal of plagioclase, orthoclase, quartz, with small amount of biotite and amphibole. It contains 15-33% quartz 22-49% plagioclase, 22-57% Orthoclase with a microcrystalline matrix consist of different minerals such as plagioclase, amphibole, quartz, K-feldspar and zircon. Generally, these rocks also show variations in terms of color, and size and texture and displays poikilitic, graphic and rarely myrmekitic textures.

Plagioclase commonly displays oscillatory zoned, sieve texture, prismatic- cellular growth displays twinning of albite and may include a small acicular apatite crystal. (Figure

25b). Some of granitic rocks in this pluton displays plagioclase crystals mostly altered to sericite and clay. Some plagioclase crystals have poikilitic textures in which large plagioclase crystals may contain small crystals of another minerals such as orthoclase or quartz. K-feldspar displays crystals shape varies from anhedral, to subhedral. The mineral shows a poikilitic texture in which orthoclase enclose some grain of quartz and plagioclase (Figure 26b, d). Some K feldspar crystals shows sericitization and chloritization alteration. Quartz is found as anhedral to rarely subhedral shape, fine to medium grain in size and commonly exhibits undulose extinction. It fills interstices between other minerals forming granophyric and myrmekitic texture.

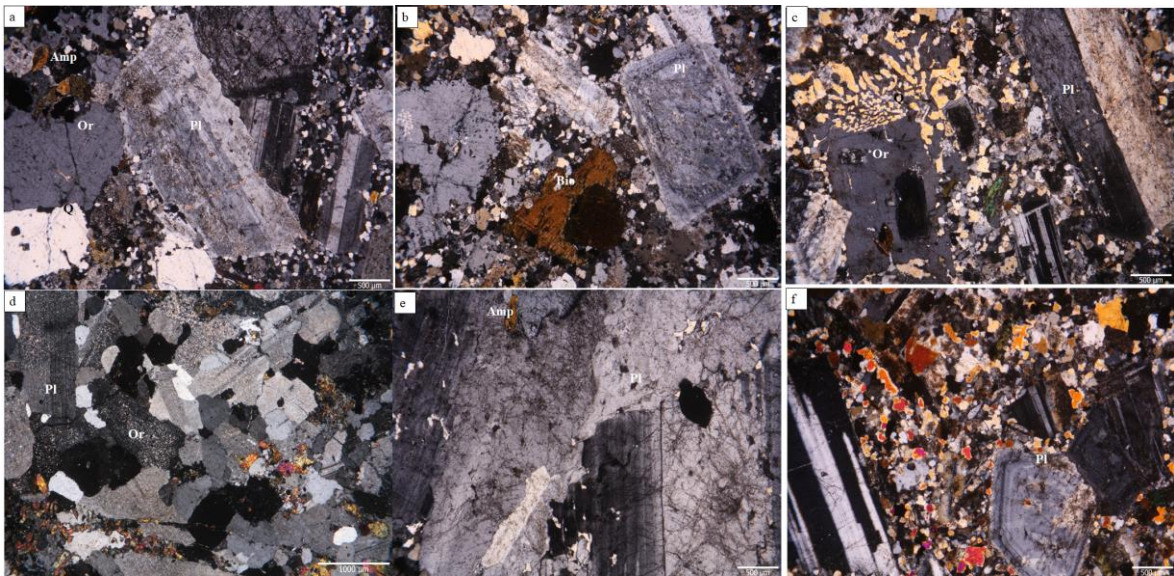


Figure 24. (a, k) Microphotographs displaying certain textural features of the Boğali monzogranite, (a) albite plagioclase, amphibole altered and orthoclase, (b) microcrystalline texture showing zone of plagioclase and biotite, (c) Micrographic texture and twinning in plagioclase phenocryst, (d) anhedral grain of quartz and plagioclase showing poikilitic and intersertal texture, (e) porphyritic texture showing zoning in plagioclase, and quartz, (f) Orthoclase show poikilitic texture, (q: Quartz, Pl: Plagioclase, Or: Orthoclase, Bio: Biotite, Amp: Amphibole).

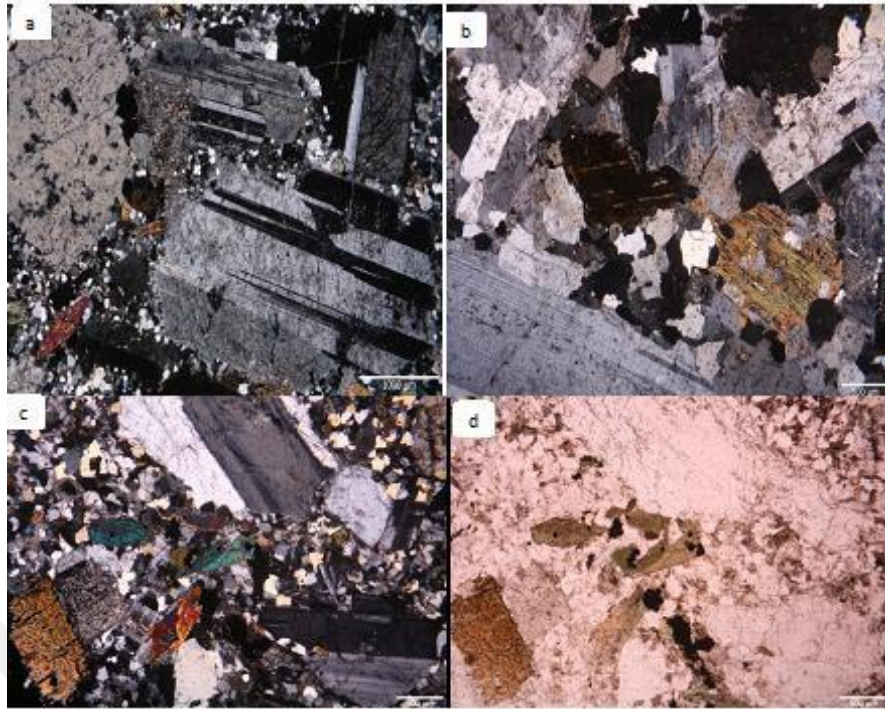


Figure 25. Microphotographs displaying the textural features of the Boğalı granitic rock, (a) phaneritic porphyritic texture showing albite twinning and small grain of quartz: b) phaneritic texture showing poikilitic texture; c-d) phaneritic porphyritic texture showing albite twinning, biotite and fine grain of quartz, (q: Quartz, Pl: Plagioclase, Or: Orthoclase, Op: Opaque minerals).

Hornblende occurs as euhedral to subhedral tabular, prismatic and acicular crystals, which are abundant in the monzonite and granite. It shows color of with pale green to pale yellow. To the margin of the Boğalı pluton the hornblende highly altered to chlorite, and calcite. Biotite is found as small amount and occurs as euhedral and subhedral reddish-brown and forms prismatic crystals and lamellas (Figure 26c). Apatite present as acicular in plagioclase and quartz. Titanite is observed as subhedral in all rock types. Epidote and sericite are most abundant accessory mineral and they present a common alteration product of plagioclase. Zircon displays in some sample as subhedral crystals, very high relief and shows vertical extinction in sections parallel to the extension.

MME's are elliptical in shape and very fine-grained compared to the host rock. They have diorite and monzodiorite compositions. They consist of plagioclase, orthoclase, quartz (0,00-2%), biotite, hornblende and accompanied by accessory such as apatite, zircon and magnetite (Figure 26).. The rocks show alterations and the chloritization, and



sericitization represent the most common hydrothermal alteration types. Plagioclase is subhedral, andesine to labradorite ( $An_{26-74}$ ) in composition and has albite-law twinning. The boundary between the Boğalı pluton and Taşlıyayla volcanic rocks contain Dykes as granite porphyry and dacit.

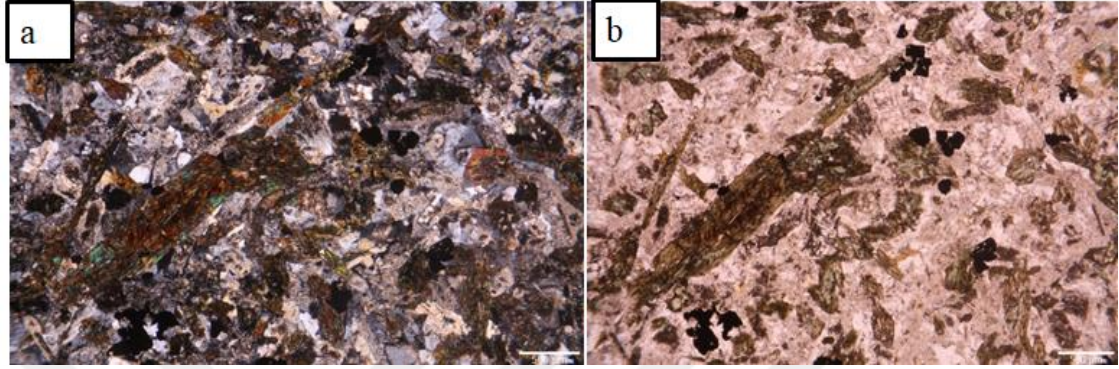


Figure 26. Microphotographs displaying fine grained mafic enclave displaying plagioclase altered and amphibole.

In The scope of the area of the present study there are different plutonic and volcanic rocks and different dykes belong to the Eocene time. These formations and dykes were not studied in detail because of the primary aims on this thesis is to study and evaluate the Upper Cretaceous formations.

### 3.1.6. Uzuntarla Pluton

Uzuntarla Pluton take place in the study area from plateau of İsmailağa to Köknar (Geological Map of study area, Figure 3). Uzuntarla Pluton settled by cutting the Gündoğdu Pluton and Berdiga Limestone in the west of the study area, and Taşlıyayla volcanic rocks in the south (Figure 3). It has been named by Şahin (2005) as "Uzuntarla porphyritic granodiorite" than named by (Şen et al 2017) as Uzuntarla Pluton. In general Uzuntarla Pluton (47-40 Ma) shown as apophyses and dikes cut the Upper Cretaceous Plutons and displays petrographical composition varies from diorite to granodiorite rock and (Şen et al 2017). This pluton also contains from centimeters to diameter oval/circular shaped mafic microgranular enclaves (diorite, monzodiorite composition) (Figure 27).



Figure 27. Photo showing the distribution of Uzuntarla pluton and their MMEs in the west of Şeyhi plateau 40°34'17.54"N-40°11'13.09"E.

### 3.1.7. Eđerler Pluton

Eđerler Pluton ( $49 \pm 2$  Ma) located to the southpart of the area of the present study, extending to 25km<sup>2</sup> and are in contact with Taşliyayla volcanics in the north (Figure 28). This unit displays variation in petrographical properties in which varies from granite, granodiorite, monzogranite to quartz monzodiorite composition and contains from centimeters to dimeter abundant of oval/circular shaped mafic microgranular enclaves (Figure 28).



Figure 28. Photographs showing the distribution of Eđerler pluton and their MMEs in the southeast of Gőnbuldu Village 40°30'40.53"N- 40° 8'50.71"E.

### 3.1.8. Salmankaş Volcanic rocks

These rocks are situated in the upper of Taşlıyayla volcanic rock and are in contact with Granitic Eocene age. The main body of volcanic rocks show high diversity in composition and texture in which consist of basalt rocks. This formation is also cutting by prophyritic granitic and dacitic dykes. They generally consist of plagioclase, clinopyroxene, quartz, k- feldspar, biotite and etc. It has been observed in the contacts places with plutonic rocks some metamorphism scars rocks contain epidote and clinopyroxene.

Generally, these rocks show variations in terms of color, size and texture which the grain range from fine to medium-coarse grained rocks displays microcrystalline porphyritic, microlitic porphyritic, glomeroprophyritic, microgranular, and intersertial textures (Figure 29). It also shows epidotization alteration type. This formation includes in some places a dacitic rocks which represents a part of intrusion rocks distribute in the area.



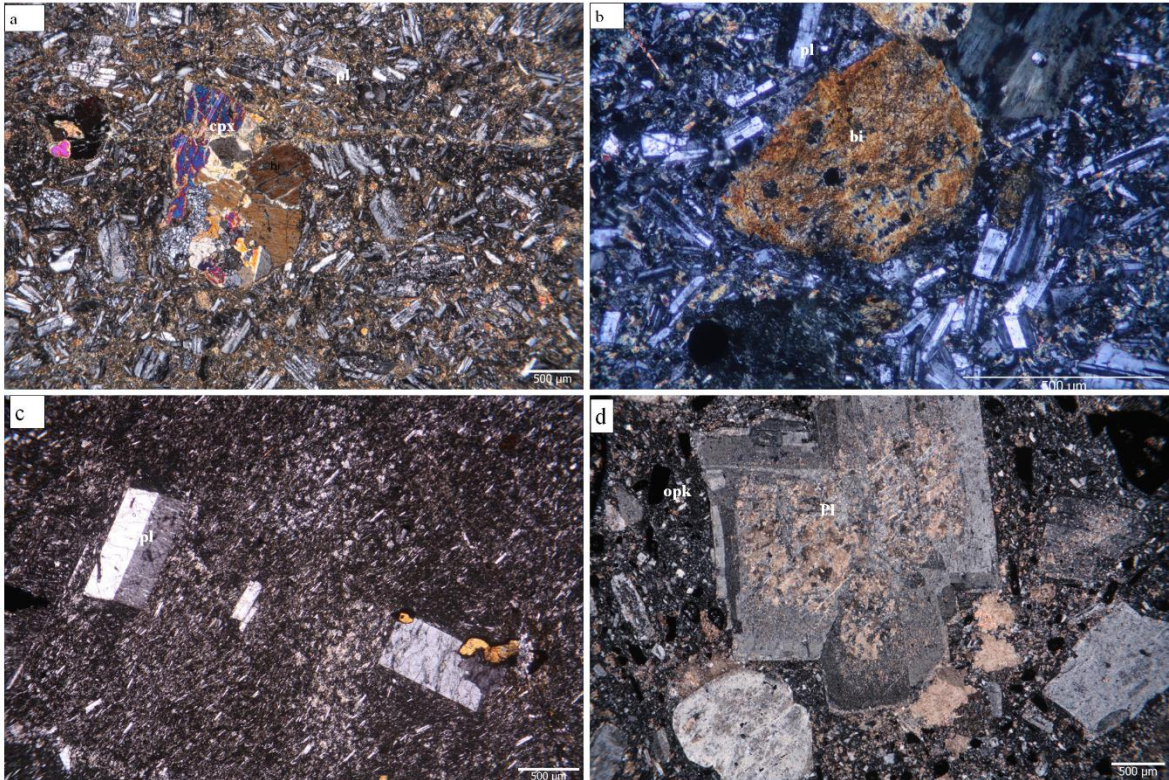


Figure 29. Microphotographs in which rocks of Salmankaş volcanic rocks displaying microcrystalline porphyritic, microlitic porphyritic, glomeroporphyritic, microgranular, and intersertial texture, (a) Microlitic porphyritic texture, (b) microcrystalline porphyritic displays plagioclases and biotite, (c) plagioclase exhibits with albite twinning, (d) glomeroporphyritic texture showing plagioclase zoned and altered, (pl: plagioclase, bio: biotite, Cpx: clinopyroxene, Op: opaque minerals).

### 3.1.7. Young Acidic and Basic Dykes

The plutonic and volcanic rocks of the area of the present study host numerous dykes with acidic and basic composition (Figure 22). These dykes generally extend from NE-to SW cuts these formations. They distributed around the area and have more appearance in the Gündoğdu pluton and Taşlıyayla volcanic rocks border along the Gündoğdu Village road. These dykes classified to basic and acidic dykes. The acidic dykes petrographically classified to dacitic dykes and granitic -porphyritic dykes whereas the basic dykes classified as basaltic dykes. Dacitic dykes vary in thickness from 6 m to 10m (Figure 22), textures whereas Basaltic dykes vary in thickness from 22 m to 35m. Granitic porphyritic dykes' rocks are distributed and cut all volcanic and plutonic rocks and are vary in thickness from 13m to 20m and grey to light grey in color, displays fine-to medium grained, microgranular porphyritic, and microlitic texture.

## 3.2. Mineral Chemistry

### 3.2.1. Taşlıyayla Volcanic Rocks

#### 3.2.1.1. Feldspar

The chemical compositions of feldspars from basaltic and andesitic rocks are provided in (App Table 2) and are offered in a ternary plot of the An-Or-Ab system (Figure 30a). The plagioclase composition Na-rich, occurs between Albite to Anorthite with An content ranging from 5 to 45. The K-Feldspar displays different compositions in orthoclase content, ranging from Or<sub>88</sub> to Or<sub>96</sub> (Figure 30a; App Table 2). The composition ranges from Or<sub>78</sub> to Or<sub>92</sub> basaltic rocks.

#### 3.2.1.2. Clinopyroxene

Clinopyroxenes are the most abundant mafic phase displaying euhedral to subhedral, shape. These clinopyroxenes are homogeneous with compositions of Wo<sub>28-47</sub> En<sub>35-45</sub> Fs<sub>4-36</sub> and classified as diopside and augite (Morimoto et al. 1988; Figure 30b and Supplemental App Table 3).

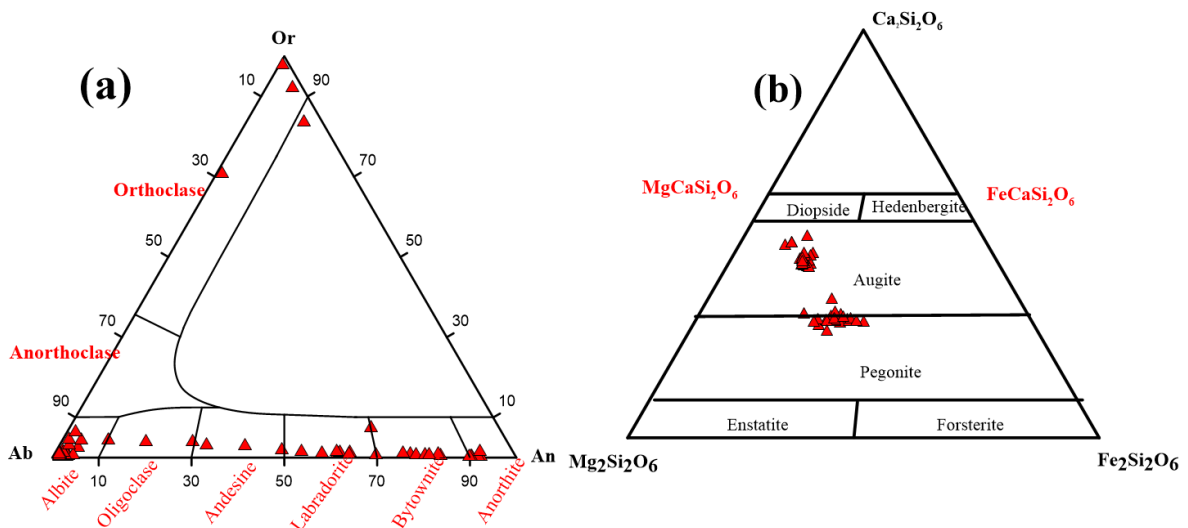


Figure 30. Mineral classification of sample from Taşlıyayla volcanic rocks, (a) a ternary An-Ab-Or diagram of feldspars classification (after Deer et al., 1992), (b) classification diagram of clinopyroxene (after Morimoto et al., 1988).

### 3.2.1.3. Chlorite

The composition of chlorites in basaltic rocks are provided in App table 4, They are mostly concentrated Pikanoklorit and Ripidolite field with high FeO (12,82-18,15 wt%) (Figure 31).

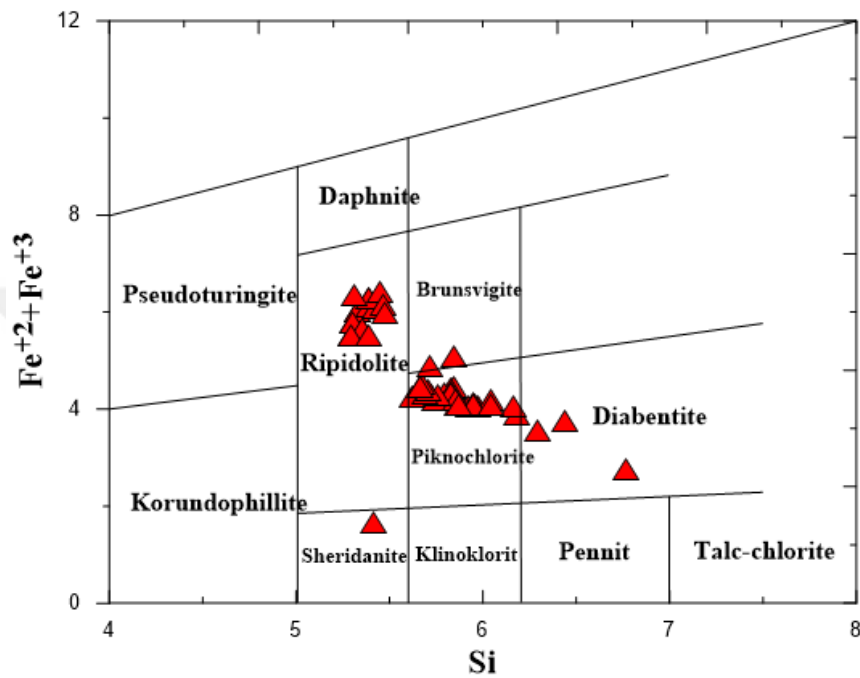


Figure 31. Classification of chlorites of sample from Taşlıyayla volcanic rocks by using the diagram of Hey, (1954).

### 3.2.2. Gündoğdu Pluton

#### 3.2.2.1. Plagioclase

Plagioclase compositions from monzogranite, diorite, monzodiorite and MMEs (quartz monzodiorite) are provided in (App table 5) and are offered in a ternary plot of the An-Or-Ab system (Figure 32a: 33). The plagioclase composition is generally Na-rich, occur between albite to oligoclase with An content ranging from 4 to 30 for Monzogranite rocks and between Albite to Bytownite for Diorite rocks, whereas the MMEs displays more calcic plagioclase (An<sub>9</sub> to An<sub>72</sub>) than their host rocks, and occur within oligoclase, andesine, labradorite and bytownite. The Gündoğdu granitoid rocks have Albit composition between An<sub>2.67-7.92</sub> Ab<sub>91.36-95.91</sub> Or<sub>0.43-0.82</sub>, Oligoclas composition occur between An<sub>11.95-29.89</sub> Ab<sub>68.84-87.80</sub> Or<sub>0.25-1.27</sub>, andesine composition occur between An<sub>30.59-49.96</sub> Ab<sub>48.69-66.91</sub> Or<sub>0.28-2.78</sub>,

labradorite composition occur between  $An_{50.39-65.22}$   $Ab_{33.79-47.73}$   $Or_{0.99-1.87}$ , bytonite composition occur between  $An_{83.62-90.00}$   $Ab_{9.81-15.95}$   $Or_{0.17-0.43}$  and Anorthite composition occur between  $An_{90.00-90.42}$   $Ab_{9.41-9.81}$   $Or_{0.17-0.19}$ . The MME has Oligoclase composition occurring between  $An_{19.36-28.92}$   $Ab_{69.82-80.25}$   $Or_{0.40-1.43}$ , Andesine composition occurs between  $An_{36.82-46.22}$   $Ab_{48.23-60.91}$   $Or_{2.26-5.55}$ , Labradorite composition occurs between  $An_{51.73-72.72}$   $Ab_{26.49-46.36}$   $Or_{0.79-1.98}$ .

### 3.2.2.2. K-Feldspar

The composition of K-Feldspar ranges from  $Or_{65}$  to  $Or_{92}$  in monzogranite rocks and  $Or_{92}$  quartz monzodiorite (MMEs) (Figure 32b; App table 6).

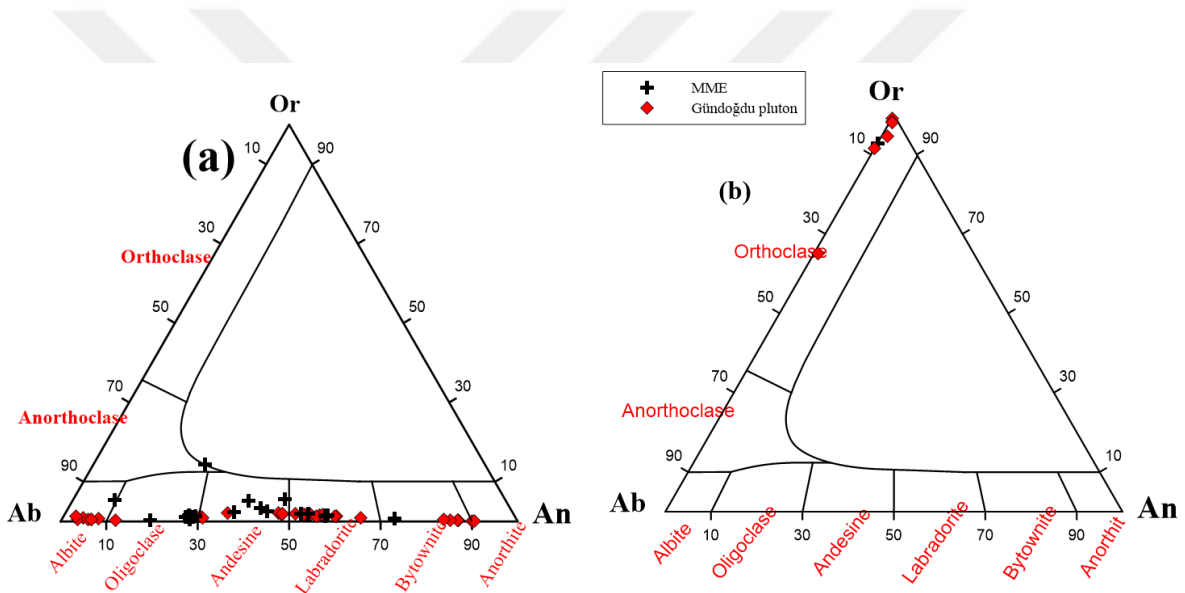


Figure 32. a ternary An-Ab-Or diagram of feldspars classification for sample from Gündoğdu pluton (after Deer et al., 1992).

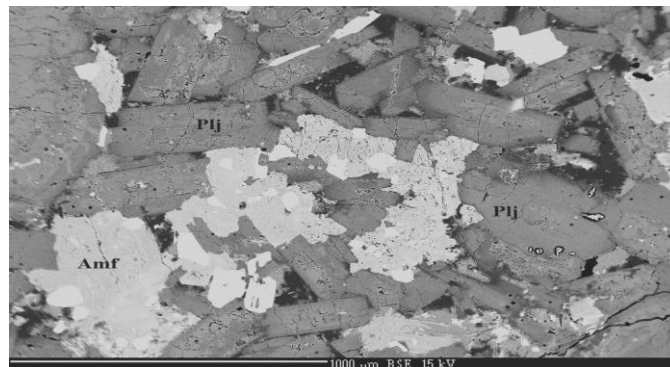


Figure 33. Scattered electron (BSE) of some plagioclase and amphibole minerals in the rocks of Gündoğdu pluton.



### 3.2.2.3. Hornblende

Representative samples are provided in App Table (7) and are explained in (Figure 34). According to ((Ca+Na) vs Na) diagram of (Leake et al., 1997) the hornblendes samples has a calcic composition. Hornblende composition of whole rocks are plotted in the field of magnesio-hornblende and actinolite with high SiO<sub>2</sub>(51,26 -53,41 wt. %), relatively high MgO (13,71-16,11 wt.%) content and Mg-number range from 63 to 74.

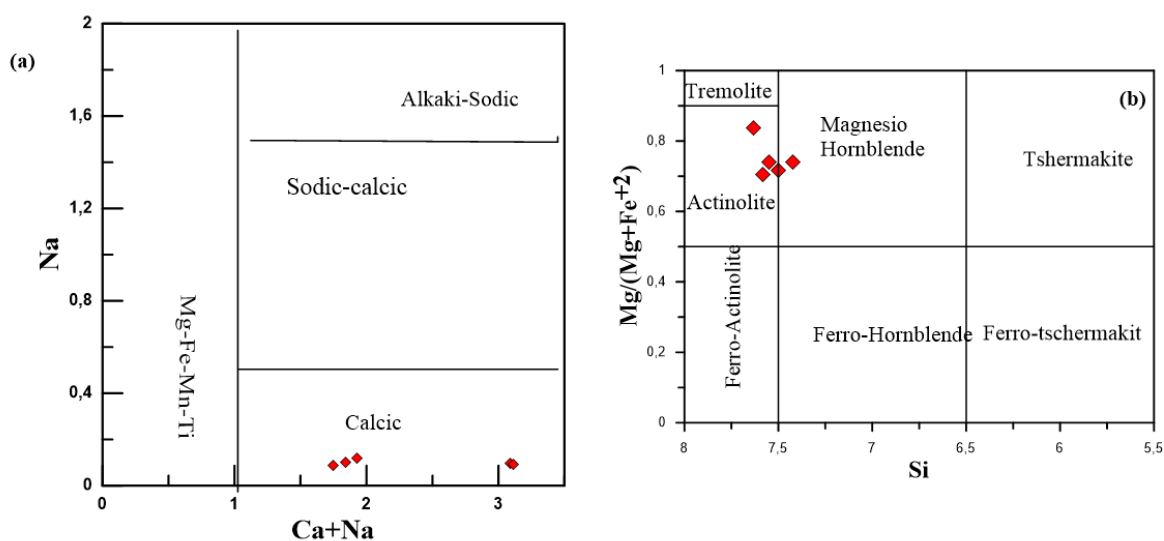


Figure 34. Hornblende classification of the plutonic rocks from Gündoğdu Pluton (after Leake et al., 1997).

### 3.2.2.4. Biotite

The biotite composition is provided in App Table 7, according to the value of TiO<sub>2</sub> (FeO(t), MnO) and MgO they display a composition of primary Biotite for monzogranite sample, whereas monzodiorite (MME) has composition of re-equilibrated primary biotite according to discrimination diagram of (Nachit et al. 2005). The biotite of monzogranite and MMEs (Monzodiorite) is Fe rich ( $Fe^{2+}/(Fe^{2+}+Mg) = 0.36-0.39$ ; with high TiO<sub>2</sub> (0,12-4,42 wt%). Their FeO and MgO content vary between 3,08-16,09 wt% and 2,95-13,61 wt% respectively. The Mg-number (Mg#) varies between 60,5 and in monzogranite and between 64,15 in the MMEs (App Table 7).



### 3.2.2.5. Fe-Ti Oxides

Iron Oxides are disseminated throughout Fe<sub>2</sub>O<sub>3</sub>-TiO<sub>2</sub>-FeO triangular diagram for monzogranite, diorite and MME (App Table 7). Fe- Ti oxides are plotted in the field of magnetit-ulvospinel series and ilmenite (FeTiO<sub>3</sub>) mineral according to diagram of (Bacon and Hirschmann 1988). The Magnetic from Monzogranite, and diorite displays low concentration of Al<sub>2</sub>O<sub>3</sub> (0.09-1.33) and (0.00-1.80 wt%) respectively. MME has Al<sub>2</sub>O<sub>3</sub> (0.06-1.27) and MnO (0.32- 1.45 wt%).

### 3.2.2.6. Chlorite

The compositions of chlorites in monzogranite and monzodiorite (MME) are mostly concentrated in Pikanoklorit field with high FeO (17.70-19.31 wt%) (App Table 7).

## 3.2.3. Boğalı Pluton

### 3.2.3.1. Plagioclase

Plagioclase composition from biotite-hornblende monzonite, porphyritic granites and MMEs are given in (App Table 8). The plagioclase composition generally Na-rich, occurs between oligoclase to labradorite with An content ranging from 11 to 66 for biotite hornblende monzonite, porphyritic granites whereas the MMEs displays more calcic plagioclase (An<sub>26</sub> to An<sub>74</sub>) than their host rocks (biotite-hornblende monzonite, porphyritic granites) which occur within oligoclase, andesine, labradorite and bytownite (Figure 35a).

The Boğalı granitoid rocks has oligoclase composition occurs between An<sub>11-29</sub> Ab<sub>65.49-88.46</sub> Or<sub>0.12-4.59</sub>. Andesine composition occurs between An<sub>31.17-46.58</sub> Ab<sub>51.13-66.78</sub> Or<sub>0.91-3.36</sub>. Labradorite composition occurs between An<sub>60.92-66.28</sub> Ab<sub>33.11-38.37</sub> Or<sub>0.61-0.70</sub> Ab<sub>51.13-66.78</sub> Or<sub>0.91-3.36</sub>. The Boğalı MME has Oligoclase composition occurs between An<sub>25.96-26.67</sub> Ab<sub>71.77-72.01</sub> Or<sub>1.56-2.03</sub>, Andesine composition occurs between An<sub>33.22-34.94</sub> Ab<sub>63.71-65.19</sub> Or<sub>1.35-1.58</sub>, Labradorite composition occurs between An<sub>55.14-57.96</sub> Ab<sub>25.96-44.01</sub> Or<sub>0.85-16.08</sub> and Bytownite composition occur between An<sub>74.07</sub> Ab<sub>25.36</sub> Or<sub>0.57</sub>.

### 3.2.3.2. K-Feldspar

The composition of K-Feldspar composition is characterized by a difference in orthoclase content, which range from Or<sub>74</sub> to Or<sub>96</sub> (Figure 35b; App Table 9). The composition ranges from Or<sub>78</sub> to Or<sub>92</sub> in biotite hornblende monzonite, Or<sub>94</sub> to Or<sub>96</sub> in porphyritic granitic and Or<sub>80</sub> to Or<sub>93</sub> in MMEs.

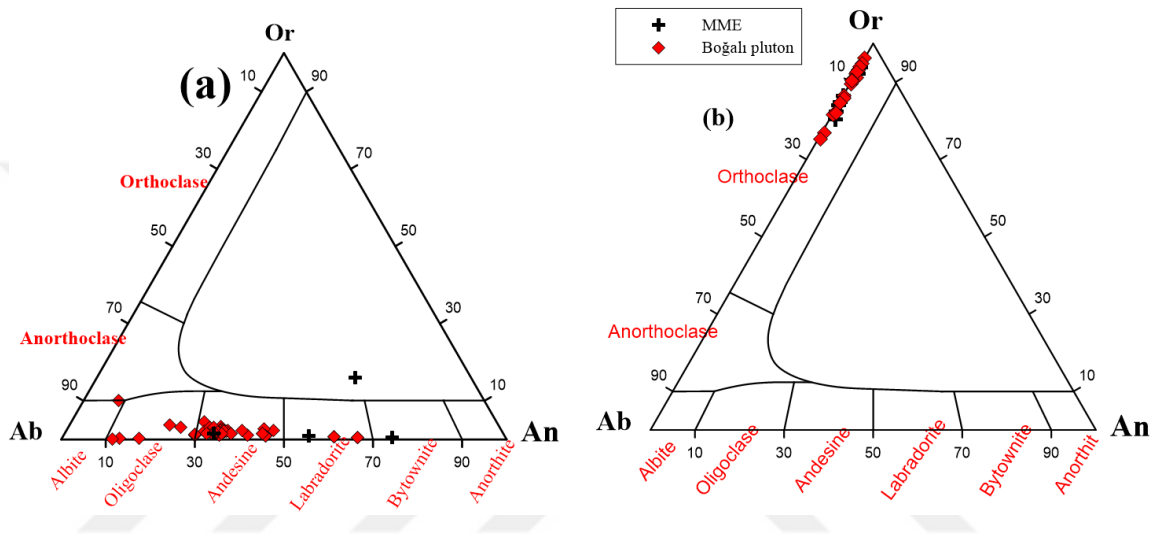


Figure 35. Feldspars Classification on a ternary An-Ab-Or plot for sample from Boğalı pluton (after Deer et al., 1992).

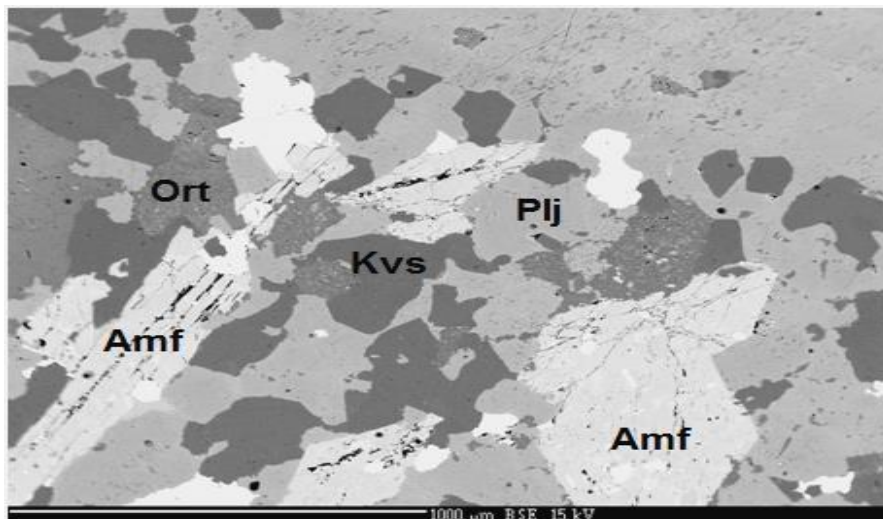


Figure 36. Scattered electron (BSE) image of some plagioclase, quartz, orthoclase and amphibole minerals in the studied rocks.

### 3.2.3.3. Hornblende

Representative samples are given in (App Table 10) and are illustrated in (Figure, 37). According to ((Ca+Na) vs Na) diagram of (Leake et al. 1997) the hornblende samples it has a calcic composition. Hornblende of whole rocks plotted in the field of magnesio-hornblende and actinolite with high SiO<sub>2</sub> (50-54 wt. %) and relatively high MgO (12-17 wt. %) content. The Mg-number range from 66 to 75 to biotitehornblende monzonite, porphyritic granites and from 69 to 75 for MMEs.

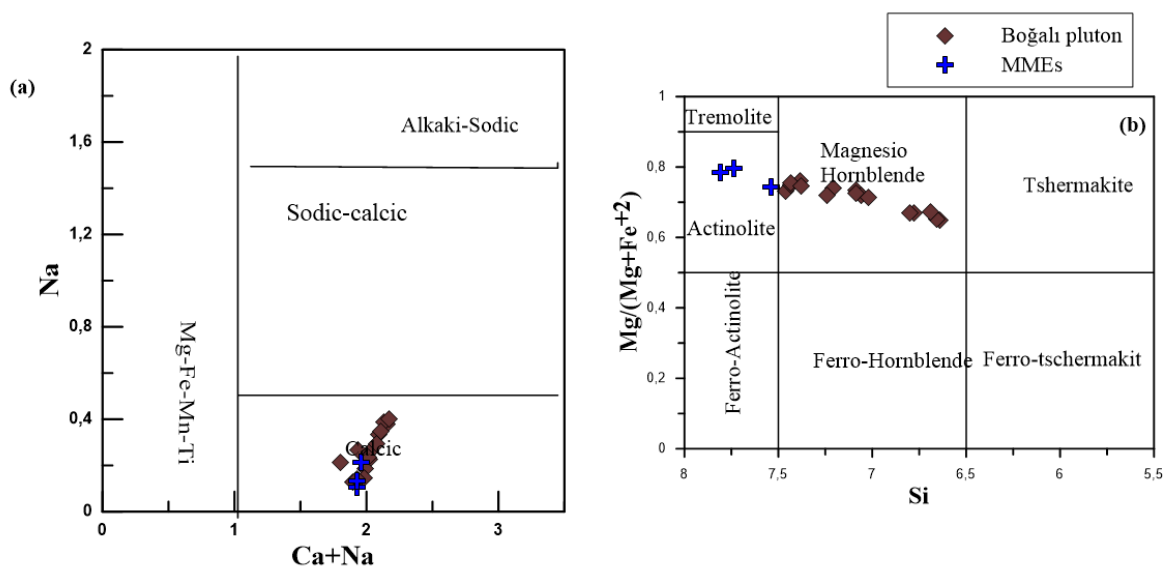


Figure 37. Hornblende classification of the plutonic rocks from Boğalı Pluton diagram (after Leake et al., 1997).

### 3.2.3.4. Biotite

Representative samples are given in (App Table 12). The chemical compositions of biotites quartz monzonite and MMEs according to the ternary diagram of (Nachit et al. 2005)  $10xTiO_2(FeO(t) + MnO) - MgO$  within the field of primary Biotite, and in the re-equilibrated primary biotite. The biotite of quartz monzonite and MMEs (monzodiorite) is Fe-rich ( $Fe^{2+}/(Fe^{2+}+Mg) = 0.38-0.41$ ; with high TiO<sub>2</sub> (3.21- 4.59 wt%) and their composition plotted in the Biotite field. Their FeO and MgO content varies between 13.99-16.27 wt% and 12.83-13.35 wt% respectively. The Mg-numbers (Mg#) differs in all rock types and are between 50.27-62 in the MME's (App Table 12).

### 3.2.3.5. Fe-Ti Oxides

Iron oxides are disseminated throughout the biotite-hornblende monzonite, porphyritic granites and MME. Fe- Ti oxides are magnetite in composition according to diagram of (Bacon and Hirschmann, 1988). The magnetic from biotite-hornblende monzonite, porphyritic granites and MME displays low concentration of  $Al_2O_3$  (0,06-0,45) and (0,1-0,85 wt%) respectively. -hornblende monzonite, porphyritic granites and MME have MnO (0,1-5,08 wt%), (0,040-0,57wt%) respectively (App Table 11).

### 3.2.3.6. Chlorite

The composition of chlorite in biotite-hornblende monzonite, porphyritic granites are mostly concentrated Pikanoklorit field with high FeO (17,82-19,15 wt%) (App Table 12).

## 3.3. Whole-rock Composition and Classification

### 3.3.1. Taşlıyayla Volcanic Rocks

The major oxides, trace element and RREs of volcanic samples from the Taşlıyayla Formations are provided in Tables 3 and 4. Taşlıyayla volcanic rocks displays variation with  $SiO_2$  contents spread from 45 to 61 wt.% and Mg# varies from 21 to 49 (Table 3).

In the log Nb/Y versus. log Zr/Ti by Pearce, (1996) diagram, the Taşlıyayla volcanic rocks plotted in the fields of andesite/basalt and basalt (Figure 38a). In the diagram of total alkali–silica (Figure 38b), the Taşlıyayla volcanic rocks plotted in the fields of basaltic andesite, andesite, basalt, dacites, trachy-basalt, basaltic trachy-andesite and trachy-andesite. Chemical classification diagram of Middlemost (1994) indicates that some of Taşlıyayla volcanic rocks are of subalkaline affinity whereas others are Alkaline affinity. AFM diagram and Th versus Co diagram further indicate that the volcanic samples are calc- alkaline show high-K and shoshonitic affinity (Figure 39). In general, the variation of  $SiO_2$  content in the Taşlıyayla volcanic rocks, indicating the bimodal distribution of compositions. Most of volcanic rocks of Taşlıyayla formation are metaluminous, and few are paraluminous with aluminum saturation index (ASI) values varies from 0.68 to 1,1. (Table 3).

Harker variation diagrams of Taşlıyayla volcanic rocks shows chemical trends, reflecting negative and positive correlations with SiO<sub>2</sub> content indicated to fractional crystallization processes. These analyzed samples generally display decreasing in the amount of Al<sub>2</sub>O<sub>3</sub>, CaO, MgO, Fe<sub>2</sub>O<sub>3</sub>tot, TiO<sub>2</sub>, P<sub>2</sub>O<sub>5</sub>, Yb, Y, Sr, and Co with increasing SiO<sub>2</sub> whereas K<sub>2</sub>O, Na<sub>2</sub>O, Rb, Ba, Zr, Nb, and Th, exhibited positive correlation with increasing SiO<sub>2</sub> (Figure 40 and 41). The negative correlation between SiO<sub>2</sub> and MgO, CaO Fe<sub>2</sub>O<sub>3</sub> indicate to clinopyroxene and plagioclase fractional crystallization. The decreasing of Fe<sub>2</sub>O<sub>3</sub> and TiO<sub>2</sub> indicating to Fe-Ti oxides. Decreasing of P<sub>2</sub>O<sub>5</sub> and Al<sub>2</sub>O<sub>3</sub> indicating to apatite and amphibole respectively. The positive relation between SiO<sub>2</sub> with Rb, Ba, Th and Hf elements can be attribute to Feldspar fractionation. Decreasing of CaO with increasing SiO<sub>2</sub> refers to clinopyroxene fractionations.

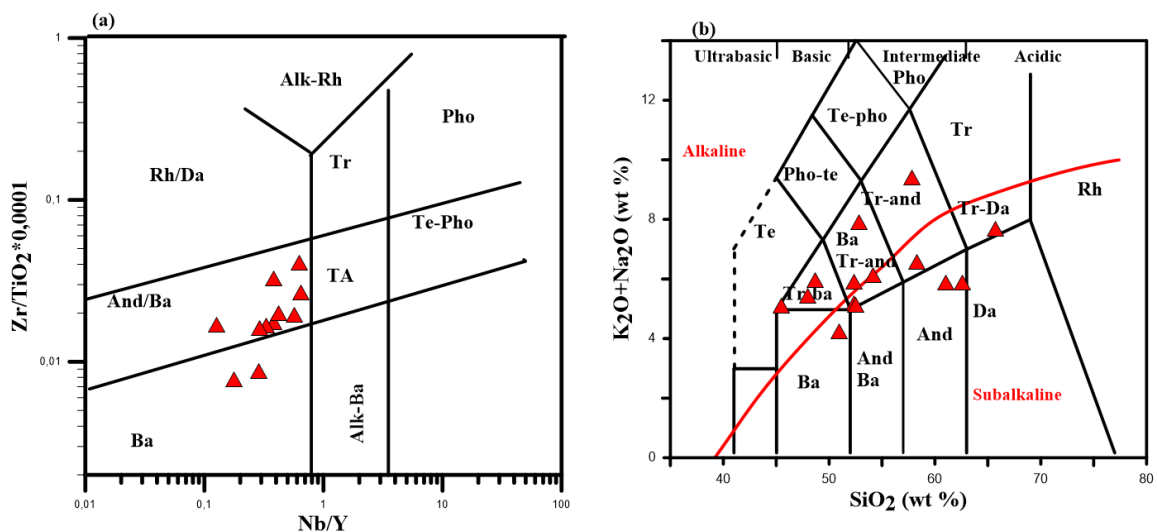


Figure 38. General of chemical classification of volcanic rocks, (a) log Nb/Y vs. log Zr/Ti by Pearce (1996), b) Chemical nomenclature diagram of (Le Maitre et al., 1989), separation curve between the field of subalkaline and alkaline magma after Irvine & Barager, (1971) for selected samples. Abbriaviation, Ba: Basalt, And: Andesite, And/Ba: Andesite/Basalt, Rh/Da: Rhyolite/Dacite, Alk-Rh: Alkalia Rhyolite, Tr: Trachyte, Tr-An: Trachyte- Andesite, Tr-Da: Trachyte-Dacite, Alk-Ba: Alkalia Basalt, Te-Pho: Tephri-Phonolite, Pho: Phonolite, Da: Dacite, Tr-Ba: Trachy-Basalt, Te: Tephrite, Pho-te:Phonolite-tephrite, Te-pho: Tephri-Phonolite, Rh: Rhyolite.

The studied Taşlıyayla volcanic rocks displays an enrichment in large ion lithophile elements (LILE; e.g. Rb, Ba, Th, U, K), and light rare earth elements (LREE), whereas high field strength elements (HFSE; e.g. Nb, Ta, P, Ti), and heavy rare earth elements



(HREE) displays depletion in terms of primitive mantle and chondrite (Figure 42a). The primitive mantle normalized element concentration diagram showing a general trend (Figure 42b). All rocks reflect an enrichment of large ion lithophile element (LILEs) and depletion of high field strength element (HFSEs). The depletion of HFSEs is best expressed by negative of Nb, Ta, P, and Ti anomalies with positive of Pb and Th anomalies and these features can be attributed to magma generated at subduction zone (Taylor and McLennan, 1985). In chondrite-normalized rare earth element (Boynton, 1984; Figure 42a) REE patterns displays an enrichment in LREE, relative to HREE ((La/Sm)<sub>N</sub> = 3.4-12). Chondrite-normalized rare earth element patterns display concave-upward shape exhibited negative Eu anomalies with Eu/Eu\* varies from 0.49 to 1.14 and by (La/Lu)<sub>N</sub> value 3.49-12.6 (Figure 45a; Table 12). The small negative Eu anomalies indicate to insignificant of plagioclase fractionation in the generation of the Taşlıyaylı volcanic rocks, or possible due to high oxygen fugacity (Gill, 1981). The concave-upward shape and enrichment of LREE indicate to fractional crystallization of hornblende and the similarity of shape indicate to same magma source for all basic and moderated silica rocks. The value of HREE indicate to the absent of garnet minerals from the mantle source.

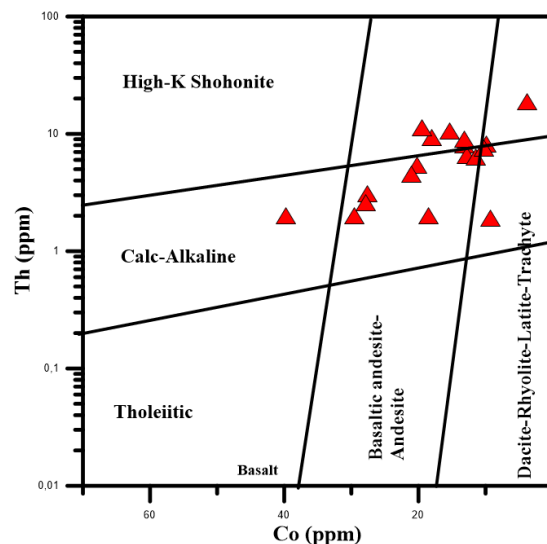


Figure 39. Chemical classification of altered volcanic rocks of Taşlıyaylı Formation, (diagram of Hastie et al., 2007).

Table 3. Whole-rock major oxides ICP-MS analyses of samples of Taşlıyayla volcanic rocks. Major oxides as weight (wt%), Trace elements as (ppm).

Sample	175	160	121	3	153	78	38-b	134	66	61	67	38a	BG-10	E6	E4	16	44
SiO <sub>2</sub>	52.35	45.48	52.33	48.01	50.97	52.84	55.4	52.52	48.65	58.26	42.08	54.13	57.81	62.56	61.02	65.71	59.45
Al <sub>2</sub> O <sub>3</sub>	18.67	17.21	19.77	16.85	17.97	17.03	16.1	17.99	17.15	16.38	16.13	15.67	18.87	16.03	16.11	16.34	15.62
Fe <sub>2</sub> O <sub>3</sub>	8.77	11.03	7.38	9.54	8.6	7.14	6.12	6.45	8.75	6.86	11.52	6.13	5.73	4.72	5.09	3.76	5.59
MgO	2.75	5.07	2.43	6.67	4.81	2.86	2.06	6.44	3.92	3.69	7.27	1.65	2.7	1.9	2.17	1.48	2.53
CaO	7.82	8.23	8.24	6.21	5.99	4.6	5.78	9.57	6.77	2.61	10.25	7.12	3.41	5.22	5.28	1.37	5.57
Na <sub>2</sub> O	4.39	3.08	0.72	4.63	2.75	5.01	3.77	3.17	4.47	3.46	1.67	3.24	6.82	3.26	3.31	4.32	2.72
K <sub>2</sub> O	0.71	1.93	5.1	0.72	1.41	2.8	2.74	1.87	1.41	3.04	2.34	2.79	2.5	2.54	2.48	3.28	3.06
TiO <sub>2</sub>	0.84	0.98	1.13	1.21	0.72	0.67	0.54	0.62	0.71	0.57	1	0.55	0.6	0.39	0.42	0.35	0.46
P <sub>2</sub> O <sub>5</sub>	0.07	0.29	0.27	0.23	0.13	0.31	0.21	0.1	0.34	0.12	0.13	0.23	0.2	0.14	0.14	0.13	0.16
MnO	0.07	0.2	0.14	0.14	0.19	0.22	0.14	0.1	0.19	0.12	0.16	0.17	0.12	0.12	0.13	0.1	0.11
Cr <sub>2</sub> O <sub>3</sub>	0.02	<0.002	0.005	0.021	0.014	<0.002	0.002	0.015	<0.002	0.003	0.006	0.003	<0.002	0.03	0.003	0.002	<0.002
LOI	3.4	6.2	2.2	5.5	6.3	6.3	6.9	0.8	7.3	4.7	7.1	8	1	2.8	3.6	2.9	4.5
Sum	99.85	99.66	99.73	99.72	99.81	99.74	99.75	99.7	99.62	99.83	99.72	99.86	99.78	99.85	99.85	99.88	99.73
Sc	33	27	26	26	20	17	16	21	17	18	42	17	11	9	11	5	13
Ba	104	906	1148	372	235	664	1073	245	1579	661	707	1441	497	1079	970	1033	1047
Be	<1	1	2	1	<1	2	<1	<1	<1	5	2	<1	2	<1	<1	<1	2
Co	9.3	27.6	20.2	29.5	18.5	18	12.8	27.9	21	19.5	39.8	11.4	13.1	9.9	10.2	6	13.1
Cs	1.8	1.3	3.9	0.5	3.2	2.2	1.1	4.2	3.8	4.2	4.4	1.1	0.6	0.9	0.8	1.1	2.1
Ga	17	16.8	14.9	15.1	16.4	17.5	13.4	17.2	16.9	18.3	15.3	14	17.3	15	15.4	14.3	14.3
Hf	1.8	2.6	3.7	2.5	1.9	3.2	2.8	3.1	2.8	3.2	1.6	2.6	5.1	2.7	2.3	3.2	2.8
Nb	3.1	5.3	5.7	6	4.2	7.1	5.3	1.5	5.5	5.4	2.6	5.1	8.6	7.8	7.4	7.8	6
Rb	29.1	43.6	157.2	21.7	52.2	70.1	63.5	50.6	57.8	131.6	70.7	59	33.5	60.1	57.1	73.6	71.3
Sn	4	<1	<1	<1	<1	<1	<1	<1	<1	2	<1	<1	1	<1	<1	<1	<1
Sr	235.2	571.2	163.1	599.3	247.2	342.3	461	929.7	481.6	187.6	414.1	388.4	388.3	523.2	471.9	338.8	527.8
Ta	0.1	0.3	0.2	0.4	0.2	0.4	0.3	0.1	0.2	0.5	<0.1	0.4	0.5	0.7	0.6	0.4	0.5
Th	1.9	3.1	5.4	2	2	9.3	6.5	2.6	4.5	11.3	2	6.3	9	8.2	7.5	9.6	8
U	0.5	0.6	1.5	0.4	0.6	2.5	1.2	0.6	1	4.4	0.6	1.1	2.6	2.6	2.3	22	2.8
V	245	283	261	175	165	167	95	176	197	153	361	106	118	95	105	59	141
W	0.7	0.6	1.5	0.5	1.1	5.3	0.6	1.4	1.9	2.6	0.5	0.5	0.7	0.9	0.6	0.6	1.1
Zr	63.4	97.7	127.6	101.9	70.2	113.9	107.3	101.7	110.9	109.4	51.2	88.9	189.2	100.3	79	137.4	96.2
Y	17.5	22.3	23.1	20.9	18.4	18.6	15	11.9	19	12.9	15.6	15.4	22.4	12.1	13	12.4	12.1
Mg#	38.3	47.6	39.4	58.0	52.5	44.2	39.9	66.4	47.01	51.5	55.5	34.7	48.2	44.4	43.8	43.8	47.2

Mg# = 100 X Mg/(Mg + Fe<sup>2+</sup>)

Table 4. Whole-rock rare earth element (ppm) ICP-MS analyses of samples from the Taşlıyayla volcanic rocks.

Sample	La	Ce	Pr	Nd	Sm	Eu	Gd	Tb	Dy	Ho	Er	Tm	Yb	Lu
175	9.4	20.9	2.51	10.6	2.72	1.04	2.83	0.5	3.24	0.69	1.97	0.3	1.96	0.28
160	19.8	45	5.45	23.2	5.15	1.37	4.95	0.73	4.03	0.82	2.42	0.32	2.1	0.32
121	19.6	41.4	5.18	22	4.54	1.09	4.48	0.71	4.26	0.91	2.36	0.38	2.59	0.37
3	12.8	28.9	3.64	16.5	3.54	1.16	3.85	0.65	4.09	0.84	2.31	0.33	2.17	0.31
153	12.9	26.8	3.34	13.9	3.2	1.06	3.43	0.57	3.52	0.74	2.15	0.32	2.16	0.33
78	27.8	57	6.42	26.5	4.94	1.24	4.29	0.64	3.57	0.7	1.83	0.28	1.89	0.27
38-b	24.3	47.5	5.48	21.6	4.21	1.2	4.03	0.49	2.87	0.52	1.52	0.24	1.51	0.24
134	9.5	21.1	2.72	11.6	2.29	0.82	2.28	0.34	2.26	0.44	1.23	0.2	1.26	0.2
66	23	47.3	5.89	23.6	4.71	1.27	4.25	0.58	3.64	0.65	1.98	0.26	1.96	0.29
61	21.5	42.1	4.8	17.9	3.3	0.75	2.74	0.4	2.29	0.52	1.52	0.2	1.37	0.22
67	10.7	22.6	3.12	13.9	3.48	1.06	3.4	0.53	3.12	0.61	1.6	0.24	1.41	0.2
38a	27.9	50.5	6.06	23.3	4.41	1.28	4.02	0.54	3.19	0.56	1.66	0.23	1.6	0.26
BG-10	34.3	66.5	7.46	28.7	5.09	1.35	4.6	0.64	3.73	0.72	2.25	0.34	2.46	0.38
E6	28.2	45.3	4.85	16.9	2.91	0.81	2.5	0.36	2.16	0.4	1.27	0.18	1.31	0.23
E4	25.9	43.8	4.74	16.6	2.96	0.85	2.57	0.38	2.12	0.43	1.34	0.19	1.31	0.22
16	32.5	49.2	5.23	17.9	2.78	0.82	2.41	0.33	1.97	0.42	1.23	0.17	1.24	0.21
44	19.8	38.5	4.07	15.8	2.85	0.78	2.55	0.38	2.17	0.41	1.17	0.19	1.34	0.21

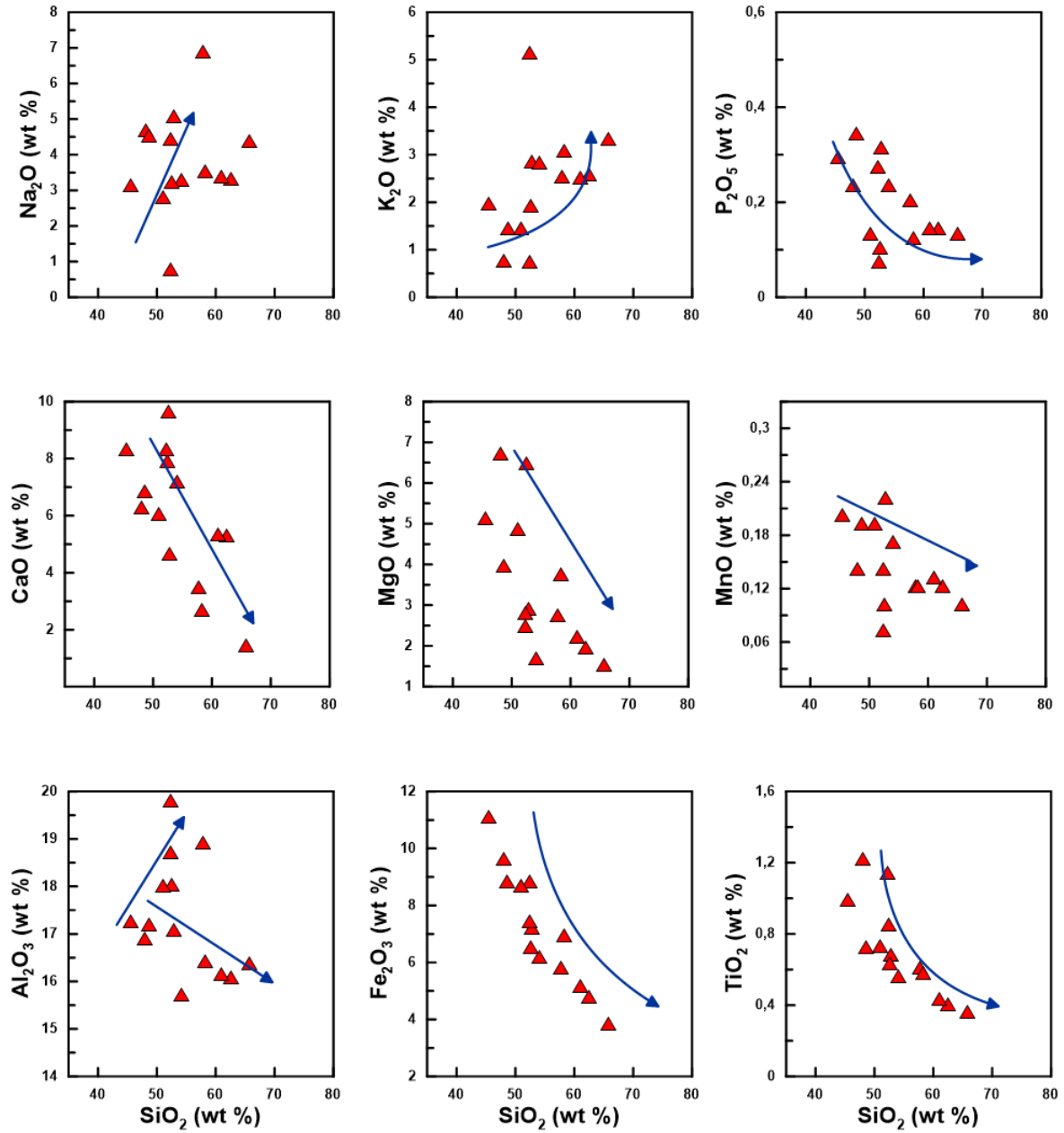


Figure 40. Selected  $\text{SiO}_2$  versus major oxide plots for the Taşhyayla volcanic rocks.

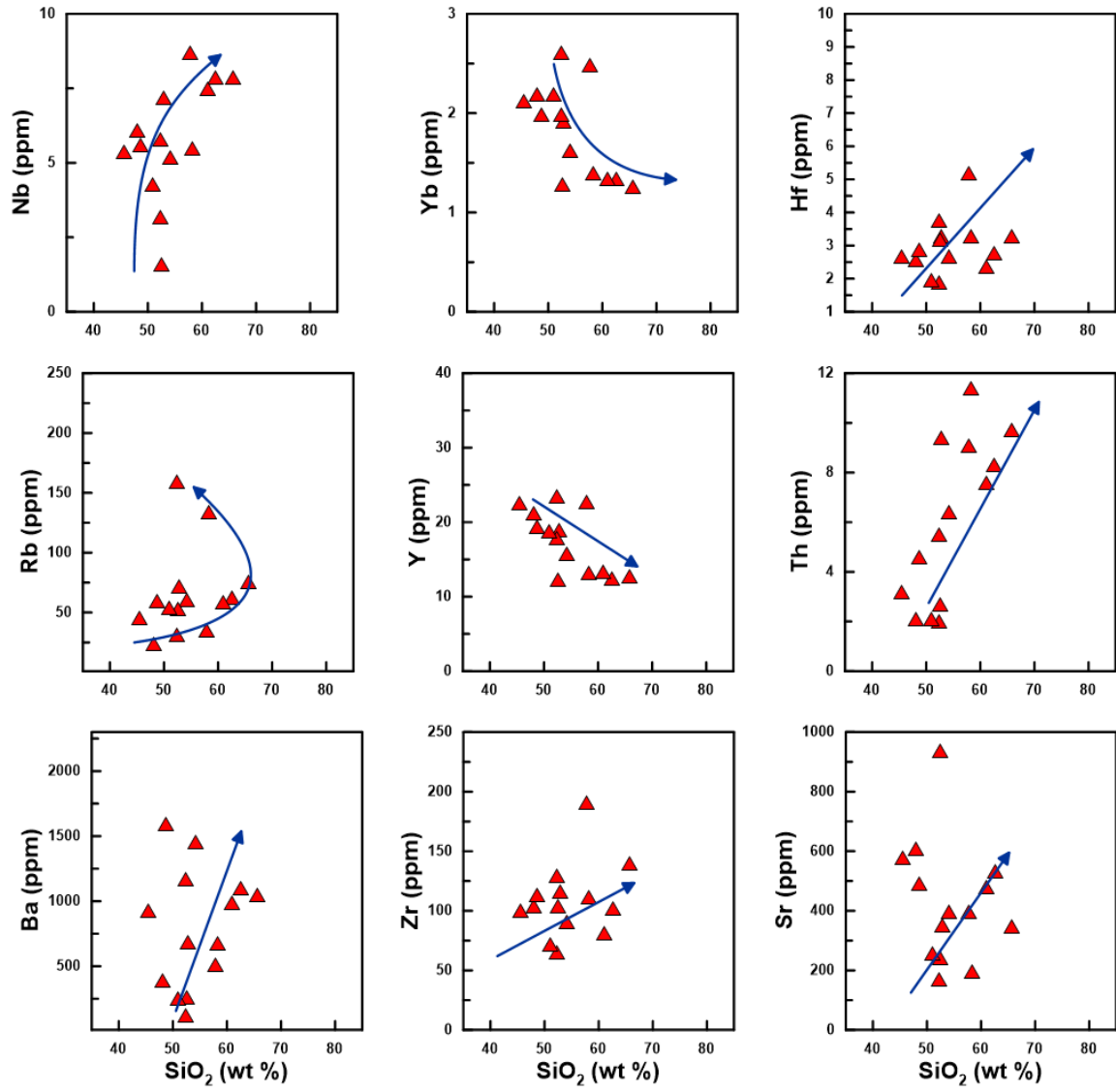


Figure 41. Selected  $\text{SiO}_2$  versus trace elements plots for the Taşlıyayla volcanic rocks.



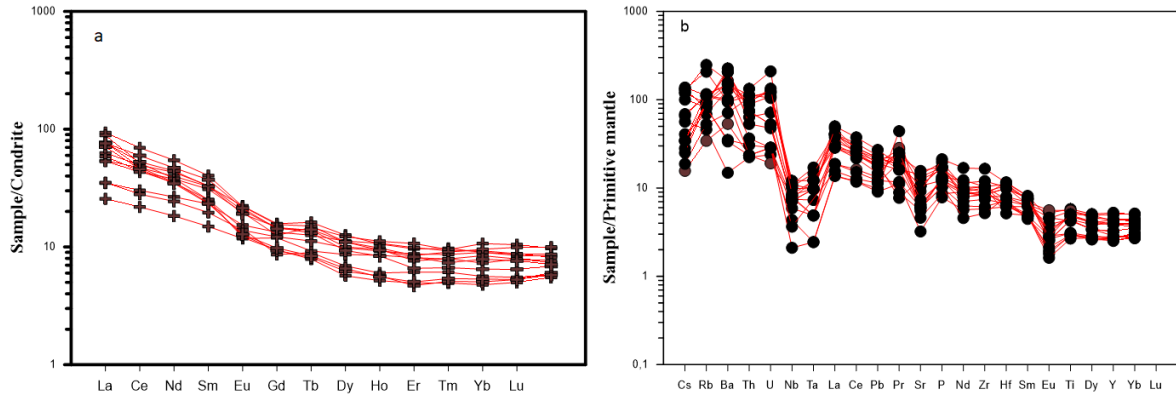


Figure 42. (a) Chondrite normalized rare earth element patterns diagrams of Taşlıyayla volcanic rocks, (b) Primitive mantle-normalized trace-element patterns for samples from the Taşlıyayla volcanic rock. Normalizing values for chondrite and primitive mantle and are from Taylor and McLennan, 1985 and Sun and McDonough, 1989 respectively.

### 3.3.2. Gündoğdu Pluton

The major oxides, trace element and REEs of granitoid rocks of the Gündoğdu pluton are provided in Tables 5 and 6. According to major oxides the Gündoğdu pluton rocks are plotted in chemical nomenclature of (Debon and Le Fort, 1983) and fall in the field of granite, monzogranite (adamellite), quartz monzonite and quartz syenite fields, which approximately consistent with the QAP classification (Figure 43a). It has been used the term of monzogranite Instead of term “adamellite” because it is obsolete term (Le Maitre et al. 1989). The MMEs plotted in diorite/gabbro and monzodiorite fields (Figure 43a). MMEs (monzodiorite and diorite/gabbro) displays  $\text{SiO}_2$  content ranging from (44–52%wt).  $\text{K}_2\text{O}/\text{Na}_2\text{O}$  ratios in Gündoğdu plutonic rocks and MMEs vary between 0.2 to 2.8 and 0.8 to 2, respectively (Table 5). MMEa rocks have lower  $\text{SiO}_2$  content than their host rocks. In the classification diagram of Nb/Y vs  $\text{Zr}/\text{TiO}_2 \cdot 0,0001$ , the sample plot in the field of granite, quartz monzogranite, monzonite and diorite (Figure 43b).

The sample rocks also plotted in the classification diagram of Middlemost, (1994), and fall in field of granite, monzogranite, quartz monzonite, and granodiorite. It is approximately consistent with the QAP classification (Figure 43c). The MMEs plotted in the monzodiorite field. Most of granitoids rocks of Gündoğdu pluton and their MMEs are peraluminous to metaluminous, with (ASI) [molar  $\text{Al}_2\text{O}_3/(\text{CaO} + \text{Na}_2\text{O} + \text{K}_2\text{O})$ ] values vary from 0.62 to 1.37 (Figure 44a). Chemical classification diagram of Middlemost

(1994) indicates that the granitoid rocks of Gündoğdu pluton are of subalkaline affinity whereas MMEs are alkaline affinity. AFM diagram and Th versus Co diagram further indicate that the granitoid samples are calc-alkaline which shows High-K and shoshonitic affinity (Figure 44a). In general, the variation of SiO<sub>2</sub> content in the Gündoğdu granitoid rocks and MMEs, indicating the bimodal distribution of compositions.

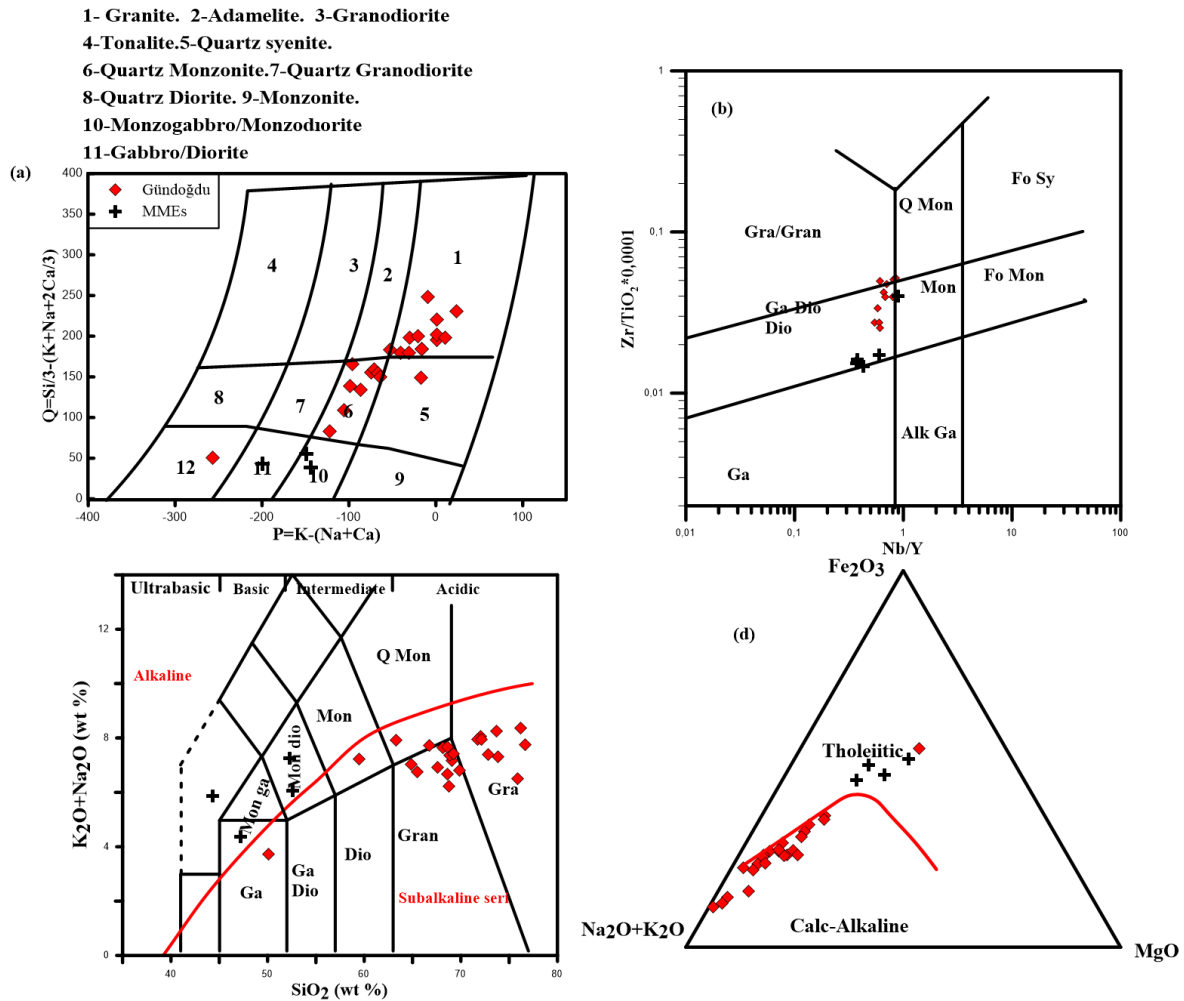


Figure 43. General of chemical classification of Gündoğdu plutonic rocks, (a) Chemical nomenclature diagram of (Debon and Le Lort, 1982) for selected samples, (b) log Nb/Y vs. log Zr/Ti by Pearce (1996), (c) Classification diagram (Le Maitre et al., 1989) separation curve between the field of subalkaline and alkaline magma after Irvine & Barager, (1971), (d) ternary diagram between calc-alkaline and tholeiitic subalkaline series by (Irvine & Baragar, 1971). Abbreviations: Gra/Gran: Granite/Granodiorite, Ga-Dio Dio: Gabbro-Diorite Diorite, Ga: Gabbro, Alk Ga: Alkalia Gabbro, Mon: Monzonite, Q Mon: Quartz Monzonite, Fo Sy: Foid Syenite, Fo Mon: Foid Monzosyenite, Dio: Diorite, Mon dio: Monzodiorite, Mon ga: Monzogabbro.

In the Harker variation plots (Figure 45), both pluton samples exhibit negative correlation of  $\text{Al}_2\text{O}_3$ ,  $\text{Fe}_2\text{O}_3$ ,  $\text{MgO}$ ,  $\text{TiO}_2$ ,  $\text{CaO}$ ,  $\text{MnO}$ , and  $\text{P}_2\text{O}_5$  with increasing  $\text{SiO}_2$ , whereas  $\text{K}_2\text{O}$  displays positive correlation with  $\text{SiO}_2$ .  $\text{Na}_2\text{O}$  displays constant or irregular increasing with increasing  $\text{SiO}_2$ . In terms of trace elements the Rb, Ba, Th, Hf, and Nb displays positive correlations, whereas Sr, Ba and Y displaying negative correlations with increasing  $\text{SiO}_2$  (Figure 46). Zr and Yb display constant or irregular increasing with increasing  $\text{SiO}_2$ . The MMEs are distinguished by moderate to high values of  $\text{MgO}$  and  $\text{Fe}_2\text{O}_3$  in comparison with host rocks. Some trace elements show an irregular correlation trend and that can be attributed to alteration processes.

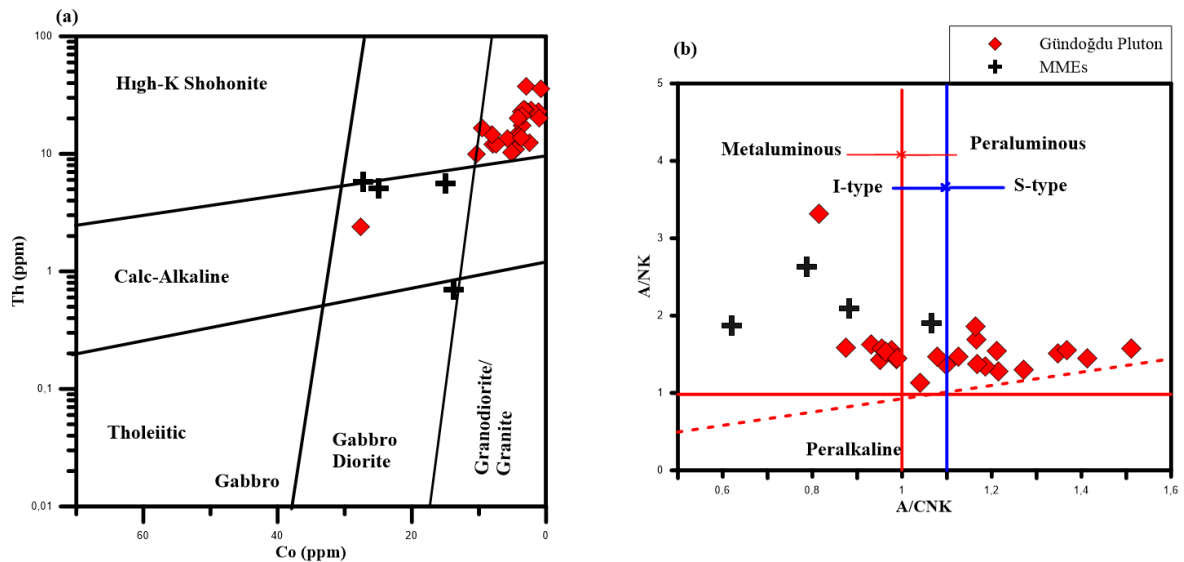


Figure 44. (a) General chemical classification of Altered plutonic rocks by using Immobility Trace Elements diagram of (Hastie et al., 2007) (b) aluminum saturation index] (after Maniar and Piccoli, (1989).

The primitive mantle normalized element concentration diagram showing a general trend (Figure 47c). All rocks of Gündoğdu pluton reflect an enrichment of large ion lithophile element (LILEs) and depletion of high field strength element (HFSEs; e.g. Nb, Ta, P, Ta). MMEs show small Ba Negative anomalies (Figure 47d). Granitic rock are more enriched in incompatible elements. All of granitic rock and MMEs display the same properties and these features can be attributed to magma generated at subduction zone (Taylor and McLennan, 1985).

Chondrite-normalized rare earth element patterns of all of Gündoğdu plutonic rock represent by an enrichment of LREE than HREE ( $(\text{La}/\text{Sm})_{\text{N}} = 3.3-9.6$ ;  $(\text{Gd}/\text{Lu})_{\text{N}} = 0.45-1.55$ ). Chondrite-normalized rare earth element patterns of Gündoğdu pluton and MMEs

have concave-upward shape characterized by negative Eu anomalies with  $\text{Eu}/\text{Eu}^*$  ranging from 0.51 to 1,1 and by  $(\text{La}/\text{Lu})_N$  value 3.5-22.2 (Figure 47a, b; Table 4).

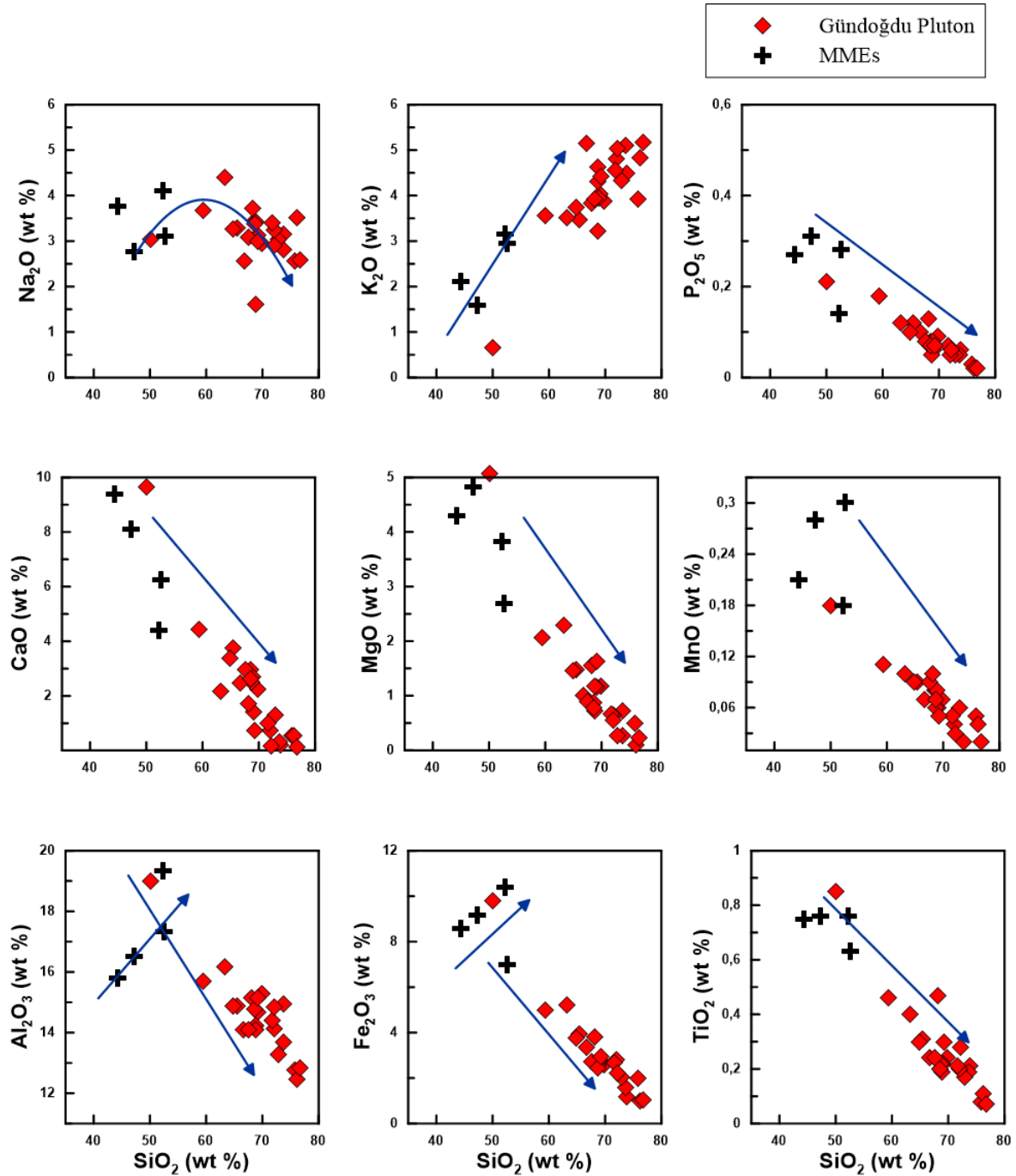


Figure 45. Selected  $\text{SiO}_2$  versus major oxide plots for the Gündoğdu Plutonic rocks.

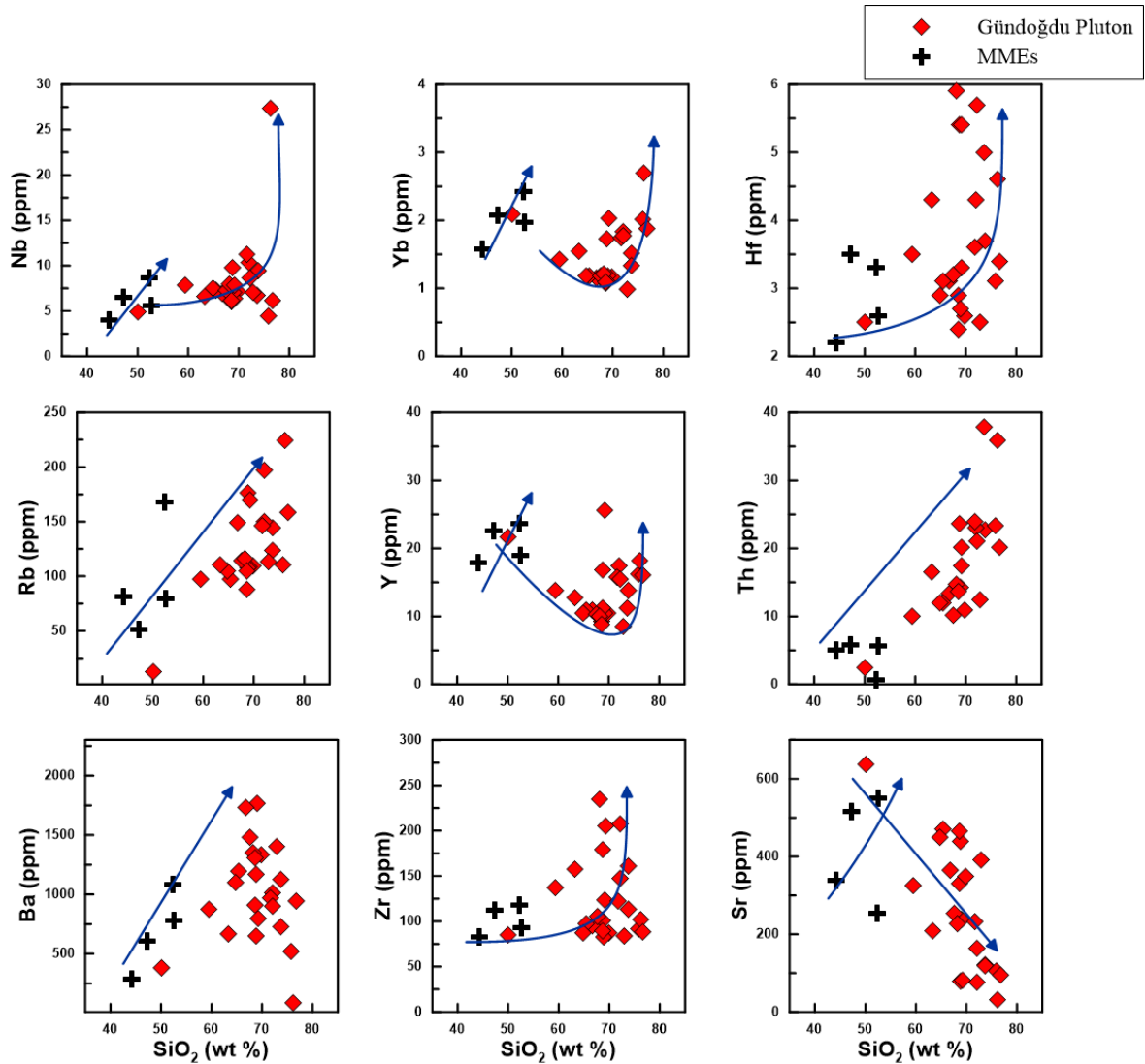


Figure 46. Selected  $\text{SiO}_2$  versus trace element plots for the Gündoğdu plutonic rocks.

The negative Eu anomalies indicate to fractionation of plagioclase. The concave-upward shape and enrichment of LREE indicate to fractional crystallization of Hornblende. The value of HREE indicates to the absence of Garnet minerals from the mantle source. MME shows similar properties to granitoid of Gündoğdu pluton and which it displays an enrichment of LREE than HREE ( $(\text{La}/\text{Sm})_N = 5.2-8.2$ ;  $(\text{Gd}/\text{Lu})_N = 1.09-1.4$ ),  $(\text{La}/\text{Lu})_N$  value range from 8.3 to 13.14 and negative Eu anomalies ( $(\text{Eu}/\text{Eu}^*)_N = 0.90-0.91$ ).



Table 5. Whole-rock major oxides (wt%) ICP-MS analyses of samples of Gündoğdu Pluton.

Sample Sample N	Gündoğdu Plütönu													
	BG-19	GB-6	29	26	83	BG-18	63	6	63-1	S-28	S-64	S-66	S-75	S-76
SiO <sub>2</sub>	68.61	73.81	73.7	75.85	50.07	69.85	72.87	76.21	69.12	68.78	68.87	66.72	72.05	71.71
Al <sub>2</sub> O <sub>3</sub>	14.2	14.95	13.69	12.78	18.98	15.27	13.29	12.47	14.67	14.24	14.08	14.09	14.11	14.4
Fe <sub>2</sub> O <sub>3</sub>	2.58	1.16	1.58	1.98	9.8	2.6	2.04	1.01	2.68	2.57	2.77	3.34	2.82	2.69
MgO	0.88	0.26	0.73	0.49	5.07	1.17	0.27	0.1	1.16	1.18	0.72	1.01	0.65	0.67
CaO	2.96	0.22	0.32	0.55	9.65	2.23	1.31	0.54	1.43	2.52	2.7	2.46	0.75	1.01
Na <sub>2</sub> O	3.45	2.81	3.14	2.57	3.05	2.95	3.05	3.51	3.13	1.61	3.42	2.56	3.24	3.39
K <sub>2</sub> O	3.22	4.5	5.11	3.93	0.66	3.87	4.34	4.84	4.04	4.62	3.95	5.15	4.81	4.55
TiO <sub>2</sub>	0.2	0.21	0.19	0.08	0.85	0.24	0.17	0.11	0.22	0.22	0.19	0.24	0.2	0.21
P <sub>2</sub> O <sub>5</sub>	0.08	0.06	0.05	0.03	0.21	0.09	0.05	0.02	0.06	0.05	0.08	0.1	0.05	0.07
MnO	0.08	<0.01	0.02	0.05	0.18	0.07	0.06	0.04	0.06	0.06	0.08	0.07	0.04	0.05
LOI	3.6	1.9	1.3	1.6	1.2	1.4	2.3	1.1	3.2	4	3	4	1.1	1.1
Sum	99.86	99.88	99.83	99.91	99.72	99.74	99.75	99.95	99.77	99.85	99.86	99.74	99.82	99.85
Ba	907	726	1126	522	380	1338	1406	83	1766	650	1165	1730	1016	968
Be	<1	<1	2	<1	<1	1	<1	3	<1	3	2	<1	1	2
Co	4.6	1.1	2.9	2.2	27.6	4.5	2.5	0.8	3.5	3.1	4	5.7	3.7	3.3
Cs	0.9	2.6	1.3	1.9	0.5	1.2	3.2	4.7	3.2	2.7	1	1.9	1.5	1.5
Ga	11.6	14.6	13.2	11.9	19.5	13.2	10.1	13.4	12.9	15.7	12.9	12.6	14.9	14.4
Hf	2.9	3.7	5	3.1	2.5	2.6	2.5	4.6	3.3	5.4	2.7	3.1	4.3	3.6
Nb	6	9.5	6.7	4.5	4.9	7.2	7	27.4	6.4	9.8	7.1	6.9	10.3	11.2
Rb	87.9	123.3	144	110.9	12.9	109.1	113.5	224.6	108.2	176.3	108	148.9	150.4	145.8
Sn	<1	2	2	<1	<1	<1	<1	2	2	2	<1	<1	3	3
Sr	330.9	120.2	119.4	105	638.3	349.6	390.8	31.5	236.6	79.8	438.4	363.9	163.4	232.9
Ta	0.6	0.8	0.9	0.6	0.2	0.7	0.7	2.4	0.6	1	0.7	0.7	0.9	1
Th	14	22.7	37.8	23.4	2.4	10.9	12.5	35.9	17.5	23.6	14.2	13.4	23	23.9
U	4.6	4.6	4.5	4.2	0.6	4.1	3.9	14.8	3.4	6.7	4.4	4.3	5.1	5
V	44	23	13	<8	274	56	27	<8	28	16	38	54	24	24
W	2.5	2.9	1.1	0.6	<0.5	1.2	0.9	3.6	2.4	2	2.1	2.7	1.1	1.8
Zr	100.6	113.6	160.7	92.3	85.1	87.7	84.3	102.2	123.2	179.5	82.9	95	147.5	122.8
Y	9.3	13.8	11.2	16.2	21.7	10.5	8.5	18.2	10.5	16.8	11.2	10.9	17.4	15.7
Mg#	25.43	18.31	31.60	19.84	34.10	31.03	11.69	9.01	30.21	31.47	20.63	23.22	18.73	19.94

Table 5. Continue

Sample	GB-1	GB-2	68	EO17	GB5	63A	77	O7	65	76	36	63B	BGg13	S-79	S-81	41
SiO2	70.11	71	71.59	75.02	71.49	73.44	77.75	73.27	71.29	74.8	72.98	69.41	59.61	65.47	64.86	67.61
Al2O3	14.22	13.18	13.81	13.4	13.61	13.79	12.63	13.91	13.84	13.45	12.57	14.69	17.55	14.87	14.89	14.08
Fe2O3	2.13	1.73	1.8	1.72	1.53	1.93	1.01	1.71	2.17	1.88	1.37	2.71	5.91	3.96	3.77	2.72
MgO	0.81	0.55	0.29	0.38	0.47	0.23	0.31	0.24	0.67	0.25	0.6	1.12	3.03	1.48	1.45	0.89
CaO	1.46	3.32	2.23	0.28	1.86	0.93	0.1	1.3	1.51	0.92	2.65	1.37	6.39	3.75	3.39	2.97
Na2O	2.29	2.32	2.73	5.72	2.8	3.1	1.71	2.49	2.16	4.56	2.6	3.06	3.2	3.28	3.27	3.08
K2O	6.26	3.5	3.99	1.97	5.03	4.48	4.54	4.27	5.6	1.87	2.5	4.21	1.53	3.48	3.75	3.83
TiO2	0.21	0.16	0.17	0.16	0.13	0.16	0.09	0.16	0.17	0.16	0.13	0.24	0.74	0.31	0.3	0.24
P2O5	0.04	0.05	0.06	0.06	0.04	0.05	0.02	0.05	0.05	0.04	0.02	0.07	0.23	0.12	0.1	0.08
MnO	0.06	0.07	0.07	0.08	0.13	0.05	0.01	0.06	0.05	0.03	0.09	0.05	0.15	0.09	0.09	0.09
LOI	2.2	4	3	1.1	2.6	1.6	1.7	2.3	2.3	1.9	4.3	2.8	1.4	3	3.9	4.2
Sum	99.8	99.86	99.92	99.93	99.92	99.9	99.91	99.92	99.91	99.92	99.94	99.9	99.8	99.81	99.77	99.79
Ba	1180	770	1347	508	1574	1338	845	1081	1073	355	1227	1587	497	1196	1096	1483
Be	2	<1	<1	3	<1	3	<1	2	2	4	<1	2	<1	1	1	2
Co	2.4	2.7	2.7	2.2	1.5	3	0.5	2.9	2.4	2.1	2.2	3.8	15.6	7.9	7.5	5.1
Cs	3.7	2.6	4	0.2	2.9	3.4	1.8	1.9	2.6	1.6	2.8	2.8	1	2.9	3	2.4
Ga	13.6	9.9	12	10	11.9	10.9	10.7	11.7	12.7	11.9	9.6	13.1	16	13.9	13	11.4
Hf	5.5	2.8	3.2	2.7	2.4	2.6	2.2	2.6	3.8	4.7	2.3	3.5	4.8	3.1	2.9	3.2
Nb	8.6	7.1	7.9	7.3	7.6	7.9	9.7	7.9	9.9	12.2	9.3	7.1	8.2	7.3	7.5	7.3
Rb	218.3	107.8	123.2	56.2	128.7	122.7	123.4	135.1	184.9	79.4	76.1	107.1	28.3	96.9	104.4	114.1
Sn	2	<1	<1	<1	<1	<1	<1	<1	6	1	<1	2	1	<1	<1	<1
Sr	103.5	272.7	259.5	250.3	287.8	383.3	55.2	296.7	135.1	208.5	85.4	204.9	490.3	471.6	448.8	254.5
Ta	0.8	0.6	0.9	0.7	0.6	0.7	0.8	0.8	1.1	1.2	0.9	0.6	0.6	0.7	0.6	0.7
Th	23.7	12.7	12.9	15.2	15.2	12.6	15.3	13.3	26.8	23.2	14.6	18.9	11	12	12	10.2
U	7.2	3	3.8	4.2	4	4.1	3.3	4.2	8.6	5.3	4.1	3.6	3.3	3.3	3.6	2.5
V	22	27	29	22	19	22	9	23	12	<8	15	29	149	83	78	47
W	2.8	2	1	3	1.6	0.9	1.3	0.6	2.8	2.1	1.2	1.6	0.5	1.6	1.7	2
Zr	199.6	95.6	102.2	95.1	77.6	93.4	64.7	98.4	136.6	165.6	72	130.2	177.3	97.1	87.1	105
Y	16.4	8.9	9.2	6.9	8.7	9	10.2	9	13.7	15.9	12.5	10.9	23.6	11	10.5	10.3
Mg#	42.9	38.6	24.2	30.4	37.8	19.1	37.8	21.8	37.9	20.8	46.4	45.0	50.4	27.21	27.78	24.65

Table 5. Continue

Sample N	Gündoğdu pluton										MME			
	30	93	BG-20	70	85	92	84	S-80	30a	93a	BG-20a			
SiO <sub>2</sub>	68.17	59.44	68.63	76.7	72.17	69.21	63.28	47.24	52.27	44.29	52.61			
Al <sub>2</sub> O <sub>3</sub>	15.16	15.69	14.79	12.82	14.83	15.15	16.18	16.5	19.32	15.8	17.33			
Fe <sub>2</sub> O <sub>3</sub>	3.8	5	2.43	1.06	2.2	2.93	5.22	9.18	10.37	8.58	6.99			
MgO	1.56	2.07	0.77	0.23	0.55	1.63	2.29	4.83	3.83	4.29	2.69			
CaO	1.71	4.42	2.61	0.14	0.15	0.74	2.18	8.08	4.39	9.37	6.24			
Na <sub>2</sub> O	3.71	3.68	3.37	2.58	2.9	3	4.39	2.77	4.1	3.76	3.11			
K <sub>2</sub> O	3.93	3.55	4.31	5.16	5.04	4.43	3.52	1.59	3.15	2.11	2.94			
TiO <sub>2</sub>	0.47	0.46	0.2	0.07	0.28	0.3	0.4	0.76	0.76	0.75	0.63			
P <sub>2</sub> O <sub>5</sub>	0.13	0.18	0.07	0.02	0.06	0.07	0.12	0.31	0.14	0.27	0.28			
MnO	0.1	0.11	0.07	0.02	0.03	0.05	0.1	0.28	0.18	0.21	0.3			
LOI	1	5.2	2.5	1.1	1.6	2.3	2.1	8.2	1.2	10.3	6.4			
Sum	99.74	99.8	99.75	99.9	99.81	99.81	99.78	99.74	99.71	99.73	99.52			
Ba	1355	875	1309	943	905	800	668	603	1079	289	778			
Be	<1	1	1	2	5	3	5	1	2	<1	1			
Co	8.1	10.4	3.7	1	3.6	4.2	9.5	27.3	13.8	25	15			
Cs	1.4	1.9	1.5	2.7	3.1	4.3	1	3.9	3.5	1.7	2.2			
Ga	15.2	14.2	11.3	9.7	14.1	13.7	16.3	20.4	22.1	17	17.5			
Hf	5.9	3.5	2.4	3.4	5.7	5.4	4.3	3.5	3.3	2.2	2.6			
Nb	8	7.9	6.1	6.2	8.7	7.8	6.6	6.5	8.7	4	5.6			
Rb	116.3	97.1	104.4	158.6	196.9	169.5	110.7	51.4	167.5	81.1	79.2			
Sn	1	<1	<1	1	5	4	3	2	3	1	1			
Sr	226.6	325.4	464.1	94.2	76.4	81.4	207.6	514.7	253.8	338.4	550			
Ta	0.4	0.6	0.6	0.8	0.7	0.7	0.6	0.4	0.5	0.3	0.4			
Th	14.7	10	13.7	20.2	21	20.1	16.5	5.8	0.7	5.1	5.6			
U	2.9	2.4	3.8	4.3	7	4.9	6.3	3.6	0.8	1.7	1.8			
V	67	118	41	<8	18	26	70	247	197	224	170			
W	0.6	1	2.2	1	2.8	2	2.2	3	0.6	1.1	4.4			
Zr	235.1	137.3	89.2	88	207	204.7	157.4	111.6	118.2	82.1	92.6			
Y	10	13.8	8.8	16	15.5	25.6	12.8	22.5	23.7	17.9	18.9			
Mg#	29.10	29.28	24.06	17.83	20.00	35.75	30.49	34.48	26.972	33.333	27.789			

Table 6. Whole-rock rare earth element (ppm) ICP-MS analyses of the samples of Gündoğdu Pluton.

Sample	Gündoğdu Pluton													
	BG-19	GB-6	29	26	83	BG-18	63	6	63-1	S-28	S-64	S-66	S-75	S-76
La	21.7	35	41.9	23.6	16.7	23.4	26.7	16.1	40.1	33.6	25.2	23.2	36.3	36.8
Ce	37.9	60.1	75.9	45.9	35.3	38.3	43.2	28.8	65.8	65.7	40.9	38.3	64.2	63
Pr	3.46	5.92	7.21	4.65	4.47	3.93	3.96	2.9	6.18	7.39	4.15	4.04	6.69	6.57
Nd	11.4	18.8	22.8	16.2	18.4	13.4	12.7	9.5	20.1	24.6	12.7	13.3	20.8	19.6
Sm	1.85	3.3	3.52	3.28	4.39	2.37	1.93	1.84	2.62	4.17	2.09	2.33	3.7	3.44
Eu	0.48	0.5	0.63	0.55	1.19	0.6	0.44	0.21	0.74	0.63	0.55	0.56	0.58	0.58
Gd	1.55	2.7	2.65	2.76	4.11	2.02	1.52	1.73	2.31	3.15	1.8	1.95	3.28	2.96
Tb	0.24	0.42	0.38	0.47	0.65	0.31	0.22	0.33	0.31	0.49	0.27	0.3	0.5	0.44
Dy	1.48	2.42	2.07	2.62	3.99	1.82	1.3	2.46	1.85	2.76	1.56	1.83	2.74	2.59
Ho	0.32	0.47	0.37	0.6	0.78	0.39	0.25	0.54	0.34	0.54	0.33	0.34	0.56	0.52
Er	0.93	1.33	1.26	1.66	2.16	1.14	0.77	2.07	1.12	1.71	0.98	1.02	1.76	1.62
Tm	0.16	0.24	0.19	0.3	0.32	0.18	0.14	0.36	0.17	0.28	0.16	0.19	0.28	0.25
Yb	1.07	1.51	1.33	2.01	2.09	1.17	0.99	2.7	1.19	1.73	1.1	1.16	1.83	1.75
Lu	0.19	0.25	0.23	0.32	0.33	0.19	0.18	0.47	0.19	0.29	0.2	0.19	0.3	0.29
(La/Lu) <sub>N</sub>	11.86	14.53	18.91	7.66	5.25	12.79	15.40	3.56	21.91	12.03	13.08	12.68	12.56	13.17
(Eu/Eu*)	0.84	0.50	0.61	0.54	0.84	0.82	0.76	0.35	0.90	0.51	0.85	0.78	0.50	0.54

Eu\*=(Sm+Gd)/2, CN= Condirite value has been normalized according to (Taylor ve McLennan, 1985).

Table.6. Continue.

Sample	Gündoğdu Pluton																
	63a	GB-1	GB-2	68	EO17	GB5	14	63A	77	O7	65	76	36	Bg-13	S-79	S-81	41
La	46.4	37	22	24	21	25.4	11.3	23.4	31	25.9	37.7	38	25.2	28.9	22.8	22.7	18.3
Ce	70.5	69.8	33.9	39.5	35.3	39.3	20.7	36.9	49.2	39	62.1	62.8	41.5	57	38.7	38.9	30.1
Pr	6.65	7.59	3.42	3.9	3.24	3.74	2.21	3.69	4.64	3.86	5.78	6.07	4.11	7.01	4.16	4.11	3.16
Nd	20.3	25.4	11.9	12.8	10.5	11.6	7.6	12.1	14.7	12.3	17.7	19.8	14.2	27	13.7	12.6	11.4
Sm	2.96	4.19	1.76	2.12	1.64	1.73	1.37	1.82	2.23	2.02	2.86	2.89	2.07	5.45	2.4	2.38	2.05
Eu	0.78	0.61	0.45	0.5	0.39	0.44	0.29	0.53	0.4	0.46	0.49	0.34	0.4	1.17	0.67	0.65	0.55
Gd	2.34	3.27	1.57	1.74	1.44	1.51	1.37	1.58	1.81	1.66	2.31	2.46	1.93	4.84	2.19	1.99	1.71
Tb	0.31	0.44	0.22	0.26	0.18	0.21	0.26	0.22	0.27	0.23	0.35	0.39	0.31	0.71	0.32	0.31	0.26
Dy	1.81	2.7	1.36	1.36	1.05	1.31	1.93	1.36	1.49	1.52	2.09	2.52	1.95	4.04	1.95	1.84	1.54
Ho	0.38	0.53	0.26	0.31	0.24	0.26	0.47	0.28	0.32	0.3	0.47	0.57	0.41	0.85	0.38	0.34	0.32
Er	1.22	1.66	0.88	0.9	0.81	0.9	1.72	0.93	1.01	0.95	1.62	1.69	1.35	2.65	1.11	1	0.97
Tm	0.16	0.28	0.13	0.16	0.14	0.14	0.26	0.14	0.16	0.15	0.25	0.27	0.21	0.35	0.18	0.17	0.16
Yb	1.1	1.82	1.01	1.1	1.05	1.15	2.01	1.14	1.18	1.08	1.76	1.79	1.42	2.4	1.18	1.19	1.18
Lu	0.19	0.27	0.18	0.19	0.18	0.18	0.32	0.19	0.2	0.19	0.29	0.31	0.23	0.39	0.2	0.19	0.18
(La/Lu) <sub>N</sub>	13.4	14.2	12.6	13.1	12.1	14.6	3.6	12.7	16.09	14.15	13.4	12.7	11.3	7.69	11.83	12.40	10.55
(Eu/Eu*)	0.87	0.48	0.82	0.77	0.75	0.81	0.64	0.93	0.59	0.74	0.56	0.38	0.60	0.68	0.88	0.89	0.88

Eu\*=(Sm+Gd)/2, CN= Condirite value has been normalized according to (Taylor ve McLennan, 1985).



Table 6. continue

Sample	Gündoğdu Pluton										MME	
	30	93	BG-20	70	85	92	84	S-80	30a	93a	BG-20a	
La	36.5	29	26.2	25	34.2	39.2	29.4	29.9	13.5	24.6	25.2	
Ce	69.1	51.3	42.1	46.5	66.1	68.4	53.7	61.6	31.1	40.3	48.7	
Pr	7	5.45	4.09	4.91	6.74	8.22	5.69	7.79	4.79	5.27	5.61	
Nd	23.2	18.5	13.2	17.1	22.8	28.7	18.6	30.1	21.5	21.2	22.5	
Sm	3.22	3.07	2.01	2.97	3.67	4.58	3.31	5.69	5.04	4.16	4.3	
Eu	1.06	0.9	0.53	0.38	0.57	0.87	0.74	1.62	1.11	1.26	1.19	
Gd	2.48	2.89	1.59	2.54	3.09	4.37	2.79	5.05	5.04	4.19	4.39	
Tb	0.33	0.4	0.23	0.39	0.43	0.61	0.37	0.73	0.73	0.55	0.59	
Dy	1.83	2.44	1.41	2.63	2.66	3.42	2.36	3.88	4.34	2.98	3.61	
Ho	0.35	0.48	0.28	0.53	0.49	0.7	0.44	0.75	0.83	0.61	0.64	
Er	1	1.4	0.88	1.71	1.58	1.96	1.4	2.02	2.39	1.69	1.91	
Tm	0.16	0.21	0.15	0.27	0.25	0.28	0.22	0.32	0.36	0.25	0.3	
Yb	1.22	1.43	1.09	1.88	1.77	2.03	1.54	2.07	2.42	1.58	1.97	
Lu	0.17	0.24	0.18	0.31	0.27	0.31	0.24	0.33	0.37	0.23	0.29	
(La/Lu) <sub>N</sub>	22.29	12.54	15.11	8.37	13.15	13.13	12.72	9.41	3.79	11.10	9.02	
(Eu/Eu*)	1.11	0.91	0.88	0.41	0.50	0.59	0.73	0.91	0.67	0.91	0.83	

Eu\*=(Sm+Gd) /2, CN= Condirite value has been normalized according to (Taylor ve McLennan, 1985).

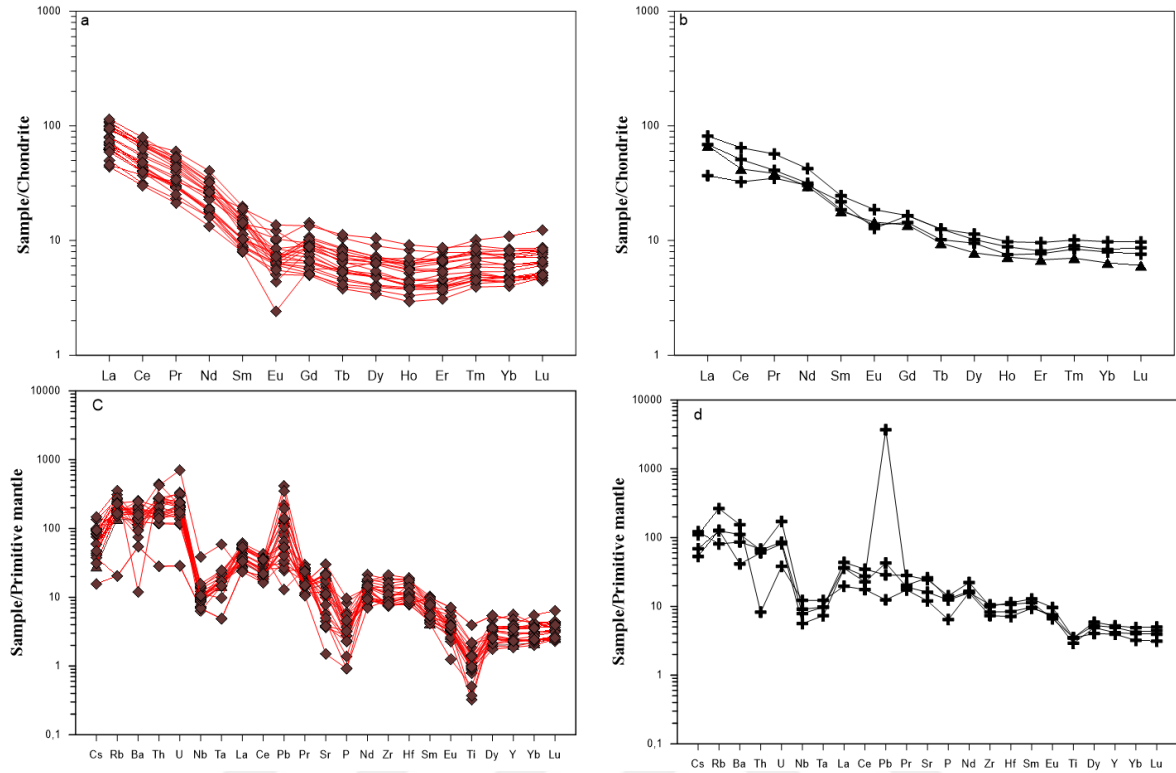


Figure 47. (a, b) Chondrite normalized rare earth element patterns of Gündoğdu Pluton, (c, d) Primitive mantle-normalized trace-element patterns for samples from the Gündoğdu Pluton. Normalizing values for chondrite and primitive mantle and are from Taylor and McLennan, 1985 and Sun and McDonough, 1989 respectively.

### 3.3.3. Boğalı Pluton

The major oxides, trace element and RREs of granitoid rocks of the Boğalı pluton are provide in Tables 5 and 6. Severals discrimination diagram has been done to classify the samples of Boğalı pluton. Based on major oxides of Boğalı plutonic rocks they fall in the field of monzogranite (adamellite), quartz monzonite and granodiorite fields in the diagram of (Debon and Le Fort, 1983), (Figure 48a). The MMEs plotted in monzodiorite and diorite/gabbro fields (Figure 48a). In the classification diagram of Nb/Y vs  $Zr/TiO_2 \cdot 0.0001$  (Winchester and Floyd, 1977, revised by Pearce, 1996), the sample plotted in the field of monzonte, quartz monzonite, diorite and granite/granodiorite (Figure 48b). MME (monzodiorite and diorite/gabbro).  $K_2O/Na_2O$  ratios in Boğalı granitoid rocks and their MMEs vary between 0.18 to 1.81.21 and 0.54 to 1.53, respectively (Table 9). MME rocks have lower  $SiO_2$  content than the the other rock types.

The sample also plotted in the diagram of Le Martre et al., (1989), the same samples plotted in monzogranite, quartz monzonite, and granodiorite. They are approximately symmetrical with the QAP classification (Figure 49a). The MMEs plotted in the monzodiorite (Figure 49a). Most of granitoid rocks of Boğalı pluton and MMEs classified as metaluminous have (ASI) values varies from 0.82 to 1.09. Monzodiorite, monzogranite rocks display metaluminous to slightly peraluminous affinity, with ASI values ranging from 1.01 to 1.06 respectively (Figure 52b, Table 7). Chemical classification diagram of (Le Maitre et al., 1989) indicates that the of Boğalı pluton rocks are of subalkaline affinity whereas MMEs are Alkaline affinity (Figure 49a).

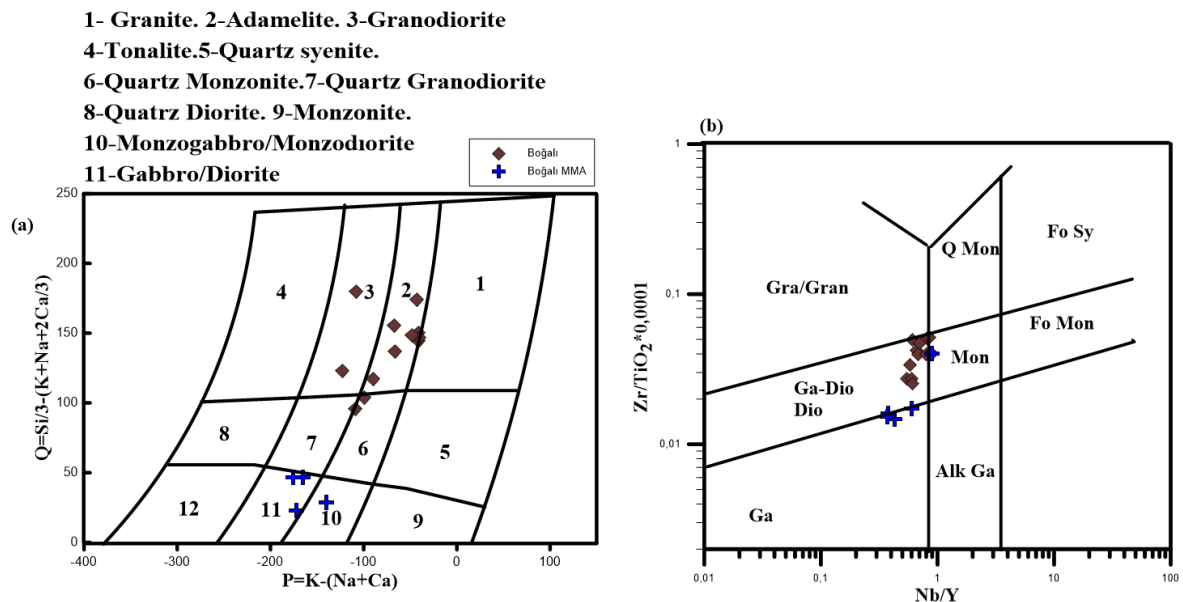


Figure 48. General of chemical classification of Boğalı plutonic rocks, (a) Chemical nomenclature diagram of (Debon and Le Fort, 1982), (b) log Nb/Y vs. log Zr/Ti by Pearce, (1996) for selected samples. Abbreviations: Gra/Gran: Granite/Granodiorite, Ga-Dio Dio: Gabbro-Diorite Diorite, Ga: Gabbro, Alk Ga: Alkalia Gabbro, Mon: Monzonite, Q Mon: Quartz Monzonite, Fo Sy: Foid Syenite, Fo Mon: Foid Monzosyenite.

AFM diagram and Th versus Co diagram further indicate that the samples are high-K and shoshonitic affinity (Figure 52a,b). Generally, the Boğalı plutonic rocks displays variation in the silica content vary from 64 to 70 wt.% for the Boğalı granitoid rocks and from 53 to 54 wt.% for the MMEs. In Harker variation plots (Figure 50), both most major and some trace elements in plutonic rocks show a linear-like trend. The Boğalı plutonic rocks characterize by decreasing of  $Al_2O_3$ ,  $Fe_2O_3$ , MgO,  $TiO_2$ , CaO, MnO, and  $P_2O_5$  with increasing  $SiO_2$ , whereas  $Na_2O$ , and  $K_2O$  are positively correlated with silica content

(Figure 50). Trace elements, like Nb, Rb and Th displays a positive correlation with silica content, whereas Sr, Zr, Ba and Y have negative correlations (Figure 51). Generally, the MMEs are distinguished by moderate to high values of MgO and Fe<sub>2</sub>O<sub>3</sub> in comparison with host rocks. Some trace elements show an irregular correlation trend and that is can be attributed to alteration processes.

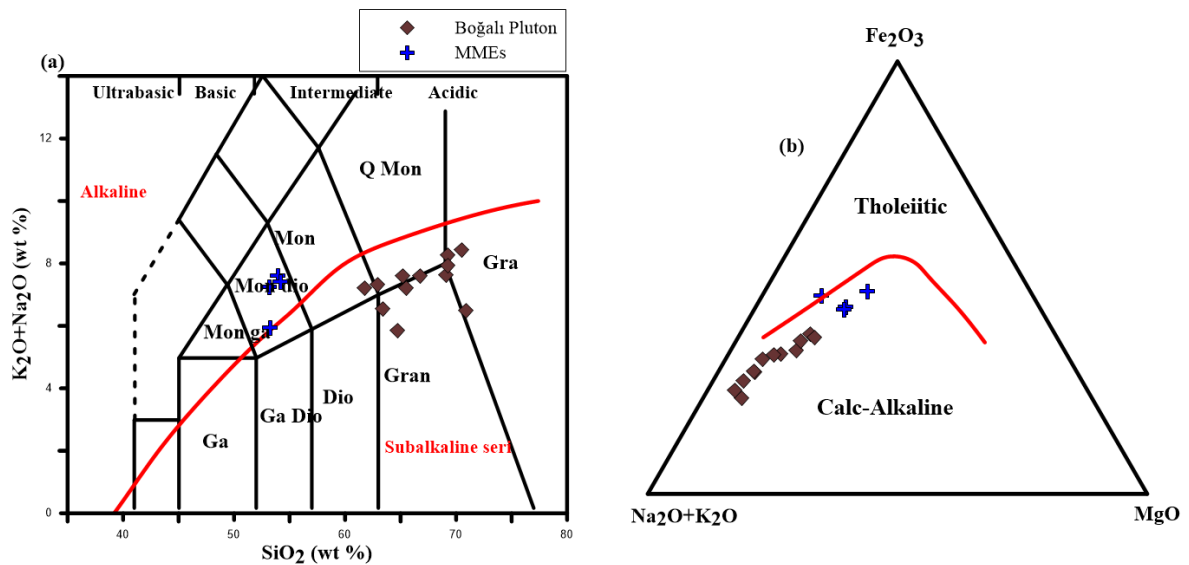


Figure 49. (a) Classification diagram of samples from Boğalı plutonic rocks (Le Maitre et al., 1989), separation curve between the field of subalkaline and alkaline magma after Irvine & Barager, (1971), (b) a discriminate diagram between calc-alkaline and tholeiitic subalkaline series by (Irvine & Barager, 1971). Abbreviations: Gra: Granite, Gran: Granodiorite, Ga-Dio: Gabbro-Diorite, Dio: Diorite, Ga: Gabbro, Mon: Monzonite, Q Mon: Quartz Monzonite, Dio: Diorite, Mon dio: Monzodiorite, Mon ga: Monzogabbro.

Chondrite-normalized rare earth element patterns of Boğalı pluton and MMEs represent by an enrichment of LREE than HREE ( $(La/Sm)_N = 4.68-8.76$ ;  $(Gd/Lu)_N = 0.96-1.62$ ) and have concave-upward shape distinguished by negative Eu anomalies with  $Eu/Eu^*$  vary from 0.55 to 0.90 and by  $(La/Lu)_N$  value 8.97-15.82 for Boğalı pluton (Figure 53a,b ; Table 10).. The concave-upward shape and enrichment of LREE indicate to fractional crystallization of Hornblend and the fractionation of plagioclase can be induced by the negative Eu anomalies. The value of HREE indicates the absent of Garnet minerals from the mantle source. MME shows a similar properties to Boğalı pluton and which it displays an enrichment of LREE than HREE ( $(La/Sm)_N = 3.63-5.59$ ;  $(Gd/Lu)_N = 1.28-2.31$ ),  $(La/Lu)_N$  value range from 8.97 to 96.84 and negative Eu anomalies ( $(Eu/Eu^*)_N = 0.56-0.91$ ). The primitive mantle normalized element concentration diagram

showing a general trend of in (Figure 53c,d). All of Boğalı plutonic rocks reflect an enrichment of large ion lithophile element (LILEs) expressed by negative of Nb, Ta, P, and Ti anomalies with positive of Pb anomalies, and depletion of high field strength element (HFSEs). MMEs show small Ba Negative anomalies (Figure 53c,d). All of granitic rock and MMEs in the boğalı pluton show same properties and these features can be attributed to magma generated at subduction zone (Taylor and McLennan, 1985).

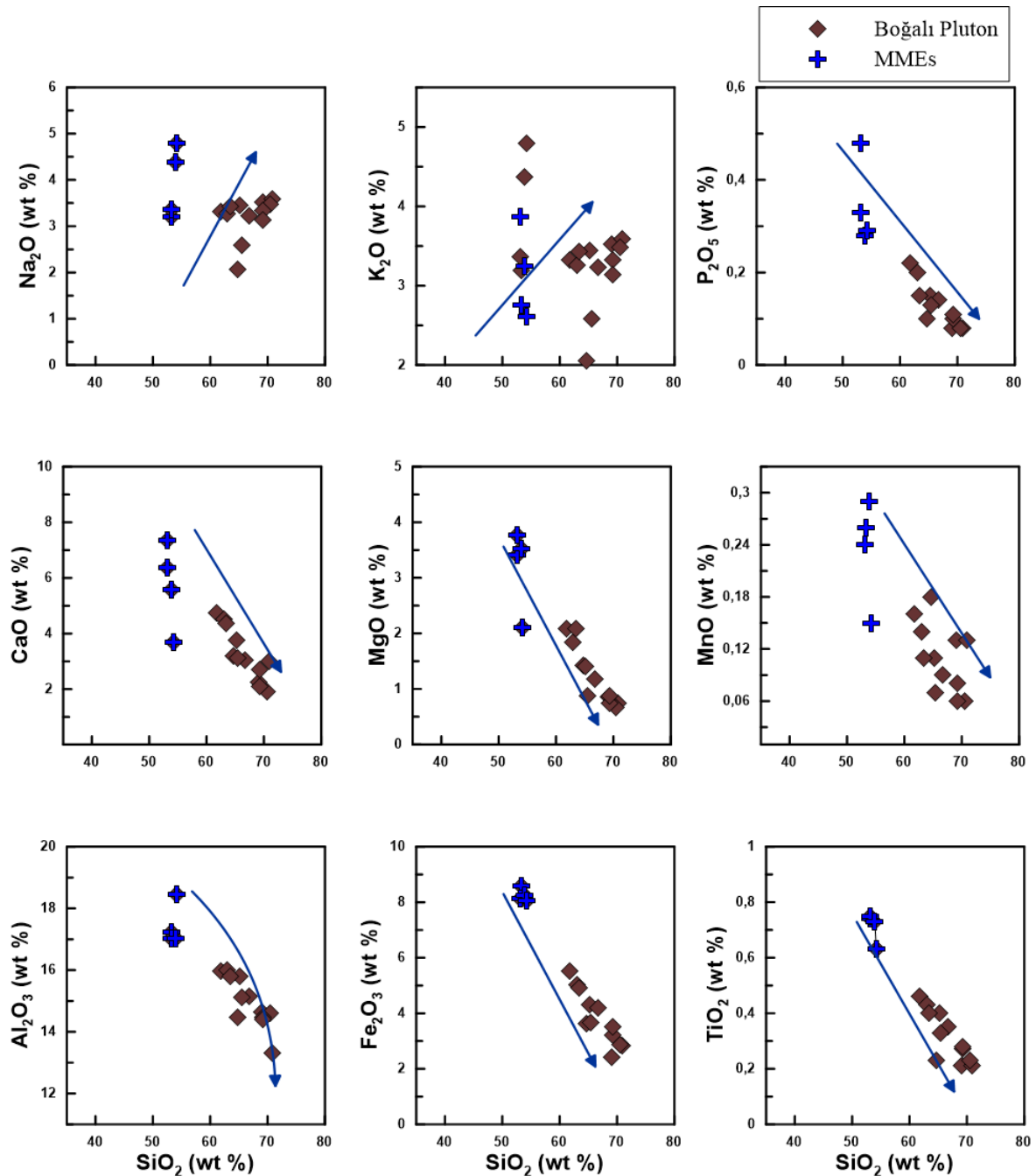


Figure 50. Selected SiO<sub>2</sub> versus major oxides plots for the Boğalı intrusion.



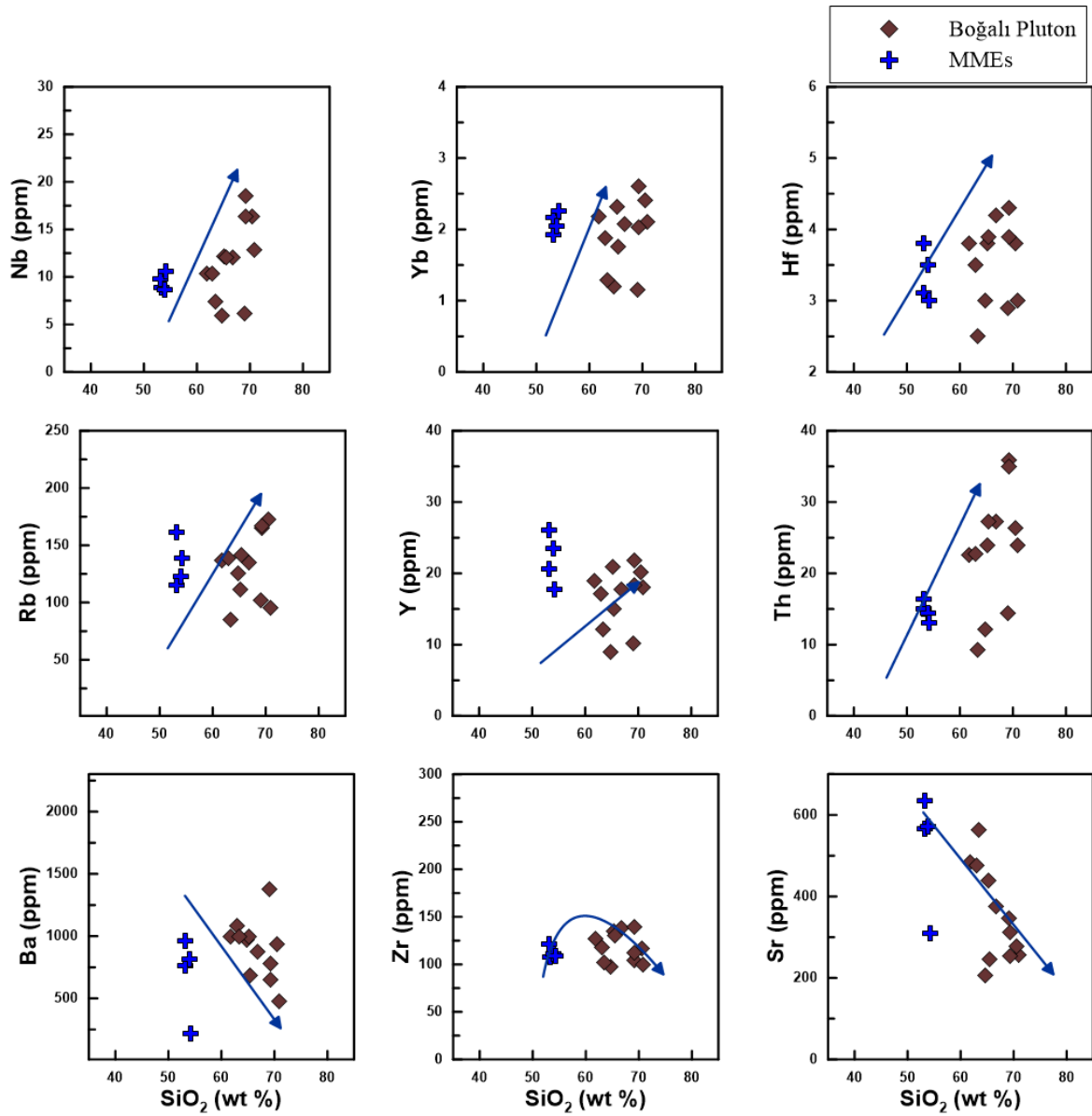


Figure 51. Selected  $\text{SiO}_2$  versus trace element plots for the Boğalı intrusion.

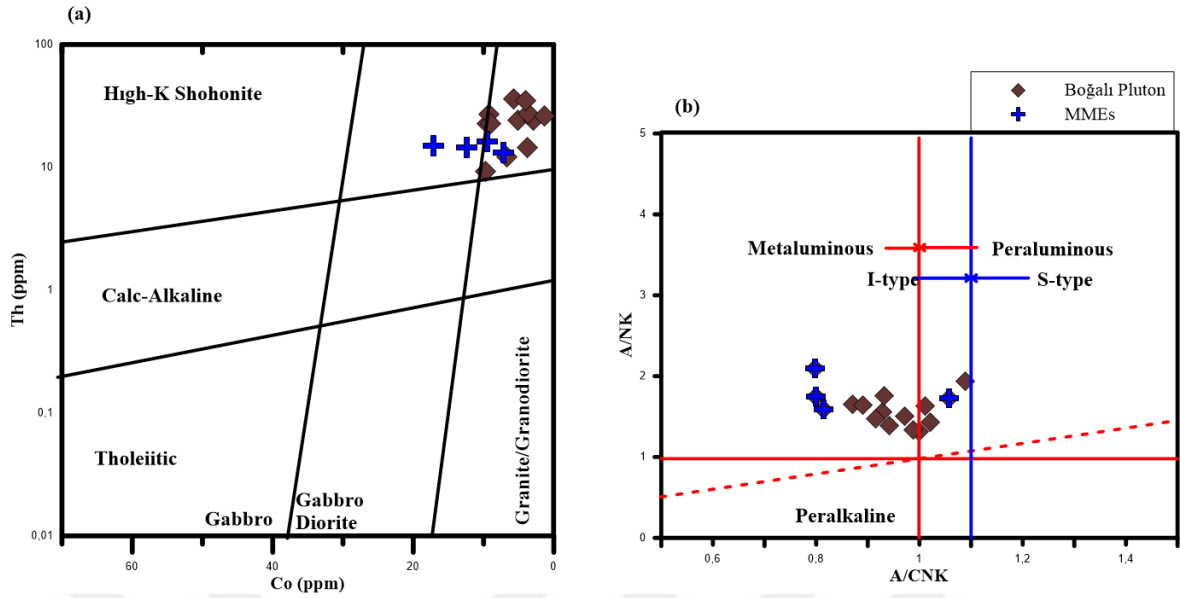


Figure 52. (a) General classification of Altered plutonic rocks by using Immobible Trace Elements diagram of (Hastie et al., 2007), (b) aluminum saturation index (after Maniar and Piccoli, (1989)).

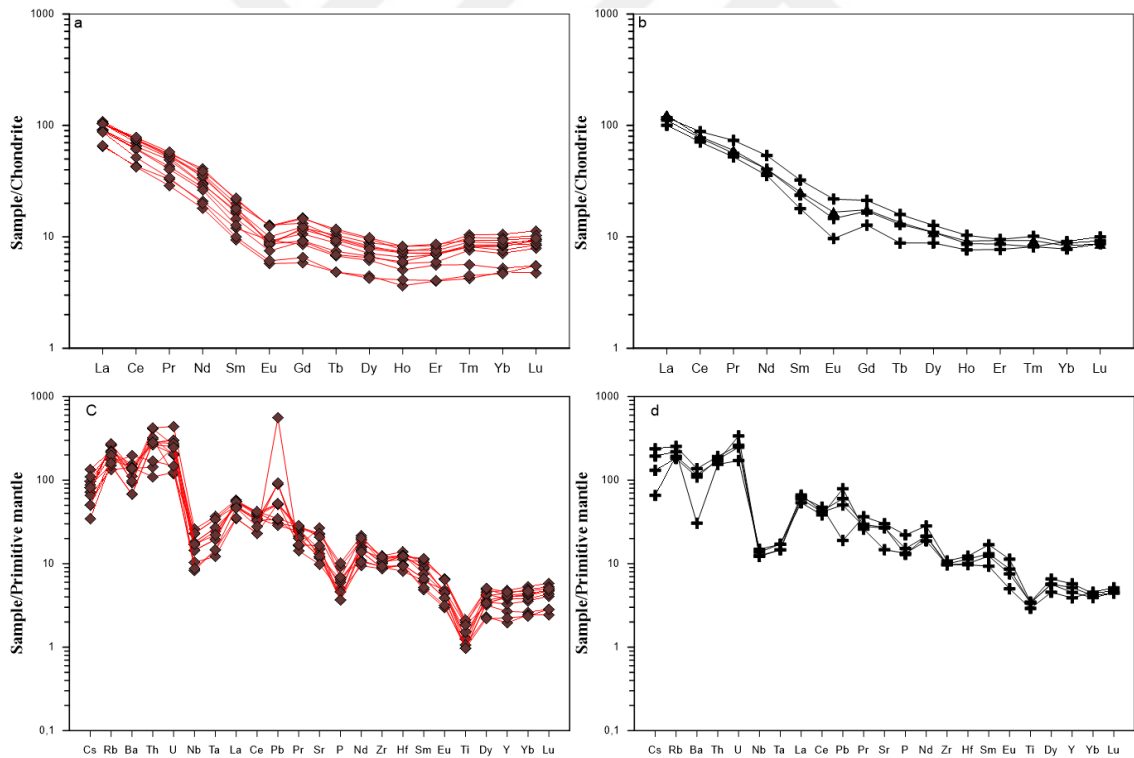


Figure 53. (a) Chondrite normalized REE patterns from the Boğalı pluton, (b) Chondrite normalized rare earth element patterns for MMEs of the Boğalı pluton (c.) Primitive mantle-normalized trace-element patterns for samples from the Boğalı pluton, (d) Primitive mantle-normalized trace-element patterns for MMEs of the Boğalı pluton. Normalizing values for chondrite and primitive mantle and are from Taylor and McLennan, (1985) and Sun and McDonough, (1989) respectively.

Table 7. Whole-rock major oxides ICP-MS analyses of samples from Boğalı Pluton. Major oxides (wt %) present and trace element (ppm).

Rocks	Boğalı Pluton										MME									
	20	BG-1	32	BG-4B	19	BG-1-2	BG-4a	BG-11	S-50	S-52	S-54	S-58A	BG-4a ank	S-59	S-60	BG-1 ank				
Sample nu																				
SiO <sub>2</sub>	69.09	64.72	65.2	61.81	70.88	66.75	62.98	65.49	63.45	70.49	69.25	69.25	53.24	53.17	53.94	54.21				
Al <sub>2</sub> O <sub>3</sub>	14.64	14.48	15.8	15.98	13.31	15.15	16.01	15.11	15.8	14.59	14.47	14.41	17.23	17.03	17.01	18.44				
Fe <sub>2</sub> O <sub>3</sub>	2.43	3.63	4.32	5.5	2.85	4.18	5.04	3.66	4.9	2.87	3.21	3.51	8.57	8.11	8.25	8.06				
MgO	0.85	1.43	1.41	2.09	0.74	1.18	1.84	0.88	2.09	0.67	0.75	0.88	3.77	3.4	3.52	2.1				
CaO	2.24	3.19	3.76	4.76	3.02	3.05	4.51	3.12	4.36	1.92	2.1	2.72	7.35	6.37	5.59	3.7				
Na <sub>2</sub> O	3.53	2.06	3.44	3.32	3.59	3.23	3.26	2.59	3.43	3.48	3.33	3.14	3.19	3.37	4.37	4.8				
K <sub>2</sub> O	4.11	3.79	4.18	3.91	2.9	4.37	4.07	4.62	3.12	4.97	4.95	4.8	2.76	3.87	3.25	2.61				
TiO <sub>2</sub>	0.21	0.23	0.4	0.46	0.21	0.35	0.43	0.33	0.4	0.23	0.27	0.28	0.74	0.75	0.73	0.63				
P <sub>2</sub> O <sub>5</sub>	0.08	0.1	0.15	0.22	0.08	0.14	0.2	0.13	0.15	0.08	0.1	0.11	0.33	0.48	0.28	0.29				
MnO	0.13	0.18	0.11	0.16	0.13	0.09	0.14	0.07	0.11	0.06	0.06	0.08	0.26	0.24	0.29	0.15				
LOI	2.4	6	1	1.5	2.2	1.3	1.3	3.8	2	0.5	1.4	0.6	2.3	2.9	2.5	4.9				
Toplam	99.71	99.81	99.77	99.71	99.91	99.79	99.78	99.8	99.81	99.86	99.89	99.78	99.74	99.69	99.73	99.89				
Ba	1373	966	994	994	473	872	1080	682	992	936	778	649	762	959	818	213				
Be	2	1	2	1	1	1	2	3	1	3	4	3	3	2	1	4				
Co	3.8	6.7	5.1	9.5	2.9	9.2	9	3.6	9.7	1.3	5.7	4	17.1	9.5	12.4	7.1				
Cs	1.1	2.6	1.6	3.5	1.6	2.8	3.1	4.3	2.1	2.3	2.6	2.3	4.2	7.6	2.1	6.2				
Ga	12.1	12.2	12.6	13.1	12.6	12.7	12.1	11.8	13.7	13.5	13.5	13.4	14.9	16.2	17.4	19.3				
Hf	2.9	3	3.8	3.8	3	4.2	3.5	3.9	2.5	3.8	4.3	3.9	3.1	3.8	3.5	3				
Nb	6.2	5.9	12.2	10.3	12.8	12.1	10.3	12	7.4	16.4	18.5	16.3	8.9	9.8	8.7	10.6				
Rb	102.2	125.5	111.2	136.8	95.6	135.3	138.8	141.8	84.8	172.8	165.4	167.2	115.2	160.9	122.3	138.8				
Sn	<1	<1	2	2	2	2	1	1	<1	2	1	1	2	5	4	4				
Sr	347.7	206.7	438	484.4	256.5	374.4	476	244.8	564.4	278.4	252.5	311.8	565.2	635.1	570.5	310.2				
Ta	0.6	0.6	0.9	0.8	1.1	1.1	0.8	1	0.5	1.4	1.5	1.4	0.6	0.7	0.6	0.7				
Th	14.4	12.2	24	22.5	24	27.2	22.7	27.3	9.3	26.4	35.9	35	15	16.3	14.4	13.1				
U	3.1	5.2	5.8	5.3	6.3	4.3	4.3	4.2	2.6	2.5	9.2	5.5	5.2	5.5	7.1	3.6				
V	43	59	78	114	38	64	106	70	96	34	39	48	211	187	211	152				
W	1.6	2.4	3.3	4.3	2.1	0.7	3.1	3.7	1.3	<0.5	2.1	1.2	2.3	1.7	7.4	5.4				
Zr	104.1	97.1	135	126.4	99.4	138.8	117.8	130.1	101.7	116.7	139.2	112.3	108.2	120.7	111.4	108.9				
Y	10.2	8.9	20.9	19	18.1	17.7	17.2	15	12.2	20.1	21.8	18.3	20.6	26.1	23.5	17.7				
Mg#	25.91	28.26	24.61	27.54	20.61	22.01	26.74	19.38	29.90	18.93	18.94	20.05	30.55	29.54	29.91	20.67				
A/CNK	1.19	1.39	1.16	1.14	1.13	1.18	1.15	1.25	1.22	1.14	1.14	1.12	1.16	1.10	1.08	1.31				

Table 8. Whole-rock rare earth element (ppm) ICP-MS analyses of samples from the Boğalı Pluton.

Rocks Sample nu	Boğalı Pluton											MMA				
	20	BG-1	32	BG-4B	19	BG-1-2	BG-4a	BG-11	S-50	S-52	S-54	S-58A	BG-4a ank	S-59	S-60	BG-1 ank
La	32	24.2	38	38.1	32.5	38.4	38.2	33.3	23.8	33.7	39.8	38	40.8	43.1	45.5	36.8
Ce	49.3	40.5	74.7	71.3	58.6	72.5	70.3	59.2	41.2	62	72.1	67	73.8	84.3	75.9	67.9
Pr	4.63	3.93	7.89	7.61	5.55	7.14	7.33	5.85	4.5	6.71	7.52	7.04	7.71	10.06	8.19	7.14
Nd	14.2	12.8	27.6	29.1	18.7	25.3	26	19.8	14.8	21	24.1	21.3	28.8	38.2	28.8	25.3
Sm	2.3	2.17	5.11	4.94	2.93	4.15	4.58	3.36	2.76	3.96	4.29	3.81	5.47	7.47	5.83	4.14
Eu	0.53	0.5	1.08	1.09	0.65	0.87	1.11	0.75	0.81	0.77	0.74	0.8	1.27	1.9	1.45	0.84
Gd	1.99	1.79	4.44	4.54	2.79	3.76	4.05	2.82	2.61	3.55	3.68	3.25	5.2	6.5	5.35	3.9
Tb	0.28	0.28	0.68	0.65	0.4	0.54	0.57	0.43	0.39	0.56	0.6	0.51	0.75	0.92	0.78	0.51
Dy	1.62	1.7	3.73	3.64	2.48	2.97	3.16	2.55	2.34	3.05	3.36	2.7	4.17	4.83	4.19	3.35
Ho	0.35	0.31	0.7	0.65	0.51	0.61	0.61	0.49	0.43	0.63	0.7	0.56	0.74	0.88	0.78	0.65
Er	1.01	1	2.14	1.87	1.75	1.78	1.75	1.48	1.39	1.97	2.07	1.72	2.14	2.36	2.31	1.92
Tm	0.16	0.15	0.33	0.32	0.3	0.29	0.29	0.27	0.2	0.35	0.37	0.29	0.29	0.36	0.33	0.29
Yb	1.16	1.2	2.31	2.18	2.1	2.08	1.88	1.76	1.29	2.41	2.61	2.03	1.93	2.17	2.05	2.25
Lu	0.21	0.18	0.37	0.35	0.36	0.33	0.32	0.3	0.21	0.39	0.43	0.35	0.33	0.35	0.33	0.38
(La/Lu) <sub>N</sub>	15.82	13.96	10.66	11.30	9.37	12.08	12.39	11.52	11.77	8.97	9.61	11.27	12.84	12.78	14.31	96.84
(Eu/Eu*)	0.74	0.75	0.68	0.69	0.69	0.66	0.77	0.73	0.91	0.62	0.56	0.68	0.72	0.82	0.78	0.63

Eu\*=(Sm+Gd)/2, KN=Condirite normalized according to (Taylor ve McLennan, 1985).

### 3.4. Sr–Nd–Pb Isotope Compositions

#### 3.4.1. Gündoğdu Pluton

The isotopic data of Sr- Nd- and Pb of Gündoğdu pluton are offered in Tables 9 and 10. Initial  $^{87}\text{Sr}/^{86}\text{Sr}$  ratios of ( $I_{\text{Sr}}$ ) and  $\epsilon\text{Nd}_{(\text{T})}$  values has been calculated by using the age of 85 Ma obtained in this pluton. The  $I_{\text{Sr}}$  values of Gündoğdu Granitoid rocks and their MMEs are 0.7082–0.7118 and 0.7034– 0.7085, respectively, whereas the  $\epsilon\text{Nd}$  values of Gündoğdu plutonic rocks and their MMEs are more radiogenic (–9.7 to –6.1) and (–8.7 to –7.7) respectively (Table 9). The relatively young two-stage Nd model ages are symmetrical with these data (TDM; 1.32–1.52 Ga for the HRs and 1.32– 1.39 Ga for the MMEs, Table 12). The studied rocks are, in general, characterized by high  $^{87}\text{Sr}/^{86}\text{Sr}$  and very low  $^{143}\text{Nd}/^{144}\text{Nd}$  and are plotted systematically in the enriched quadrant within a lithospheric mantle array diagram of  $\epsilon\text{Nd}_{(\text{T})}$  vs  $^{87}\text{Sr}/^{86}\text{Sr}(\text{i})$  (Figure 54a).

These data of Gündoğdu Granitoid plotted at the same trend as the data of Camiboğazı pluton, Maçka subvolcanic rock, and Harşit pluton which their age belong to Late Cretaceous. They show values not close to the Late Cretaceous plutons but displays values somehow close to Palaeozoic Köse pluton. They have higher  $^{87}\text{Sr}/^{86}\text{Sr}$  ratios than the Late Cretaceous Camiboğazı pluton indicating to inhomogeneous source rocks. The Gündoğdu Granitoid are relatively more homogeneous in lead isotopic compositions of  $^{206}\text{Pb}/^{204}\text{Pb}$ ,  $^{207}\text{Pb}/^{204}\text{Pb}$  and  $^{208}\text{Pb}/^{204}\text{Pb}$  isotopic ratios compared to  $^{87}\text{Sr}/^{86}\text{Sr}(\text{i})$  and similar to the late Cretaceous plutons from Harşit and Camiboğazı. Lead isotopic ratios of this Granitoid rocks are  $^{206}\text{Pb}/^{204}\text{Pb} = 18.45\text{--}18.50$ ,  $^{207}\text{Pb}/^{204}\text{Pb} = 15.62\text{--}15.65$ ,  $^{208}\text{Pb}/^{204}\text{Pb} = 38.12\text{--}38.64$  (Figure 54b and c). The data plotted in the lower crust field above the Northern Hemisphere Reference Line (Hart, 1984). The MMEs displays similar Pb isotopic values compared to their host rocks and plotted also in the lower crust field at the same field of their host rocks.

#### 3.4.2. Boğalı Pluton

The isotop analysis of Sr- Nd- and Pb of Boğalı Pluton offered in Tables 9 and 10 and illustrated in Figure 54. Initial isotopic ratios ratios of ( $I_{\text{Sr}}$ ) and  $\epsilon\text{Nd}_{(\text{T})}$  of has been calculated back to the crystallization age of the Boğalı pluton 83Ma. The  $^{87}\text{Sr}/^{86}\text{Sr}$  ratios values of Boğalı rocks are (0.7061 to 0.7065) (Table 9), whereas the MMEs has  $^{87}\text{Sr}/^{86}\text{Sr}(\text{i})$  value (0.7061). The Nd isotopic ratios of the Boğalı plutonic rocks reflected

by negative  $\epsilon\text{Nd}_{(T)}$  values ( $-5.1$  to  $-3.9$ ) whereas the MMEs are ( $-5.3$ ) (Table 12). The TDM ages of the Boğalı granitoid indicate to Proterozoic age of the source rocks (Table 12). The studied plutonic rocks are, broadly, displays high  $^{87}\text{Sr}/^{86}\text{Sr}$  and low  $^{143}\text{Nd}/^{144}\text{Nd}$ , and in a classical  $\epsilon\text{Nd}_{(T)}$  vs  $^{87}\text{Sr}/^{86}\text{Sr}(i)$  diagram they plotted in the enriched quadrant within a lithospheric mantle array at the same trend to data of late cretaceous such as Camiboğazı, Maçka subvolcanic rocks, and Harşit plutons. The samples plot near the Harşit plutons which its age is Late Cretaceous. They have lower  $\epsilon\text{Nd}_{(T)}$  values than the Early Cenozoic formation but significantly higher  $\epsilon\text{Nd}_{(T)}$  values than the Köse plutons which belong to Palaeozoic age (Figure 54a). The studied samples display values share similar characters and plotted in the same field as same to the Late Cretaceous aged Harşit pluton indicating to magma mixing processes between the material of the lower crustal as a major component and a small component from lithospheric mantle (Karşlı et al., 2010a).

The Boğalı sample are relatively homogeneous in lead isotopic compositions ranging between  $^{206}\text{Pb}/^{204}\text{Pb} = 18.18\text{--}18.70$ ,  $^{207}\text{Pb}/^{204}\text{Pb} = 15.62\text{--}15.64$ ,  $^{208}\text{Pb}/^{204}\text{Pb} = 38.05\text{--}38.58$  (Figure 54b and c). These plutonic samples and their MMEs are fall in the field of lower crust field above the Northern Hemisphere Reference Line and show trend toward the EMII (Hart, 1984). Which reflect similar Pb-isotopic compositions to another Cretaceous pluton from Harşit and Camiboğazı (Figure 54b, c).

### **3.5. U-Pb Zircon Dating**

#### **3.5.1. Taşlıyayla Volcanic Rocks**

Photomicrographs zircon grains with zircon U-Pb SHRIMP data of Taşlıyayla volcanic rocks are dated (App table 13). The  $2\sigma$  represent the doubts about the isotopic ratios and U-Pb ages. Five zircon grain has been analyzed and detected the  $^{238}\text{U}\text{--}^{206}\text{Pb}$  ages are concentrated at  $\sim 92,5 \text{ Ma} \pm 2.3$  (MSWD = 8.5) (Figure 55a and b). Contamination of Pb, Pb-loss, or appearance of older detrital grains has not been detected.

#### **3.5.2. Gündoğdu Pluton**

Previously has been dated to Gündoğdu pluton to Late Cretaceous according to stratigraphic criteria and relationships contact (Güven,1993; Yalçınalp, 1992). Granitoid



rocks from the Gündoğdu intrusion include abundant of colorless, euhedral and long-short prismatic zircon grains.

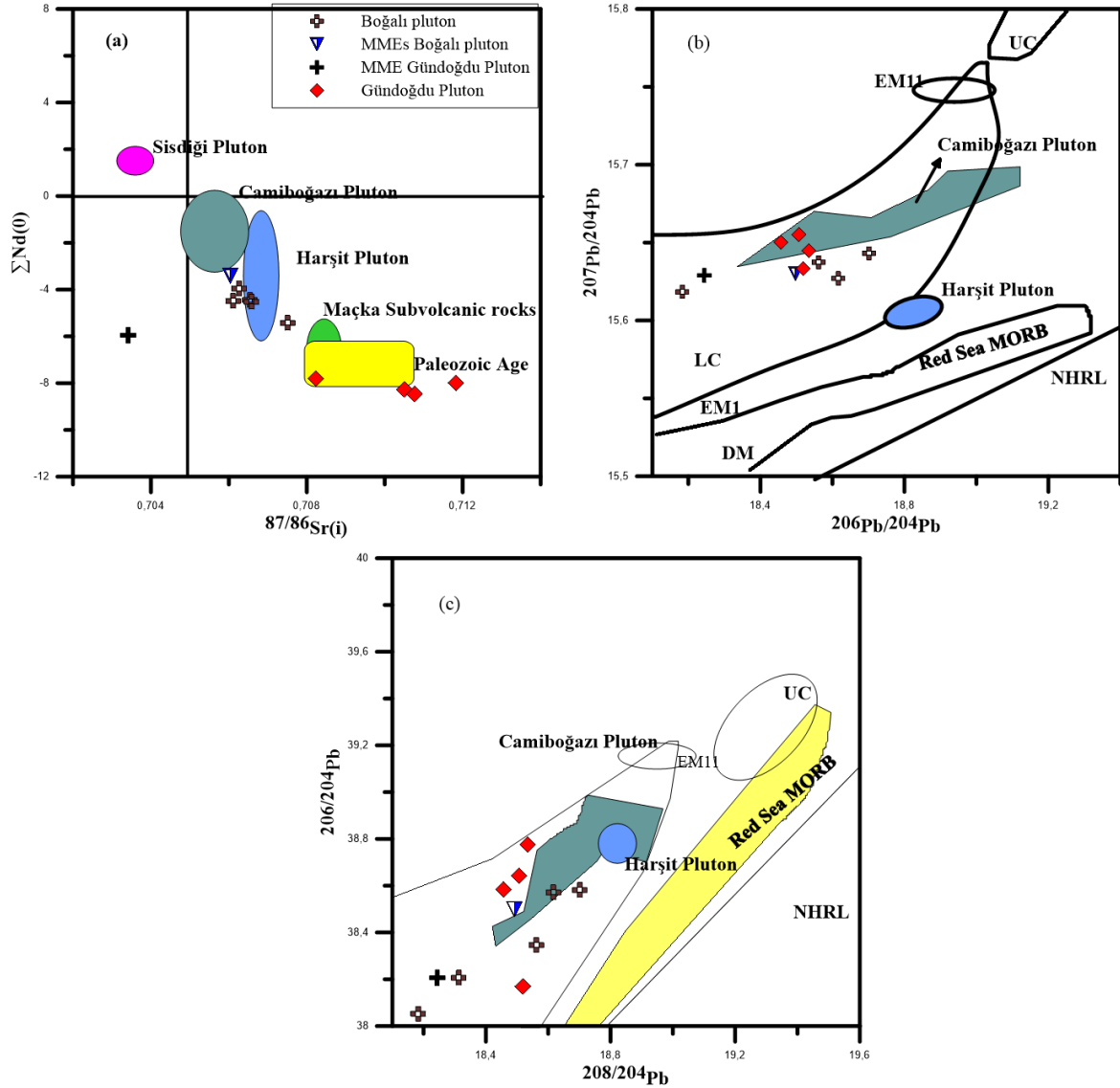


Figure 54. Sr-Nd-Pb isotope diagram of Gündoğdu and Boğalı plutonic rocks, (a)  $\epsilon_{Nd}(i)$  vs.  $(^{87}Sr/^{86}Sr)(i)$ , (b) and (c) plots of  $^{206}Pb/^{204}Pb$  (i) vs.  $^{207}Pb/^{204}Pb$  (i) and  $^{208}Pb/^{204}Pb$  (i) ratios. Lithospheric mantle and mantle array data are from Davies and Von Blanckenburg, (1995) and Arculus and Powell, (1986), McCulloch et al., (1994) and Wilson, (1989) respectively. The data source from Eastern Pontides are as follows: Şişdağı pluton from Karlı et al., (2012b); Harşit pluton from Karlı et al., (2010a); Maçka subvolcanic rock from Aydın 2014; and palaeozoic Köse pluton from Dokuz (2011). EM I: enriched mantle I; HIMU: high- $\mu$  ( $\mu = ^{238}U/^{204}Pb$ ); EM II: enriched mantle II; LC: lower crust; UC: upper crust; NHRL: Northern Hemisphere Reference Line (Hart, 1984). Lower crust (LC) from Kempton et al., (1997), HIMU, EM I and EM II from Zindler and Hart, (1986).

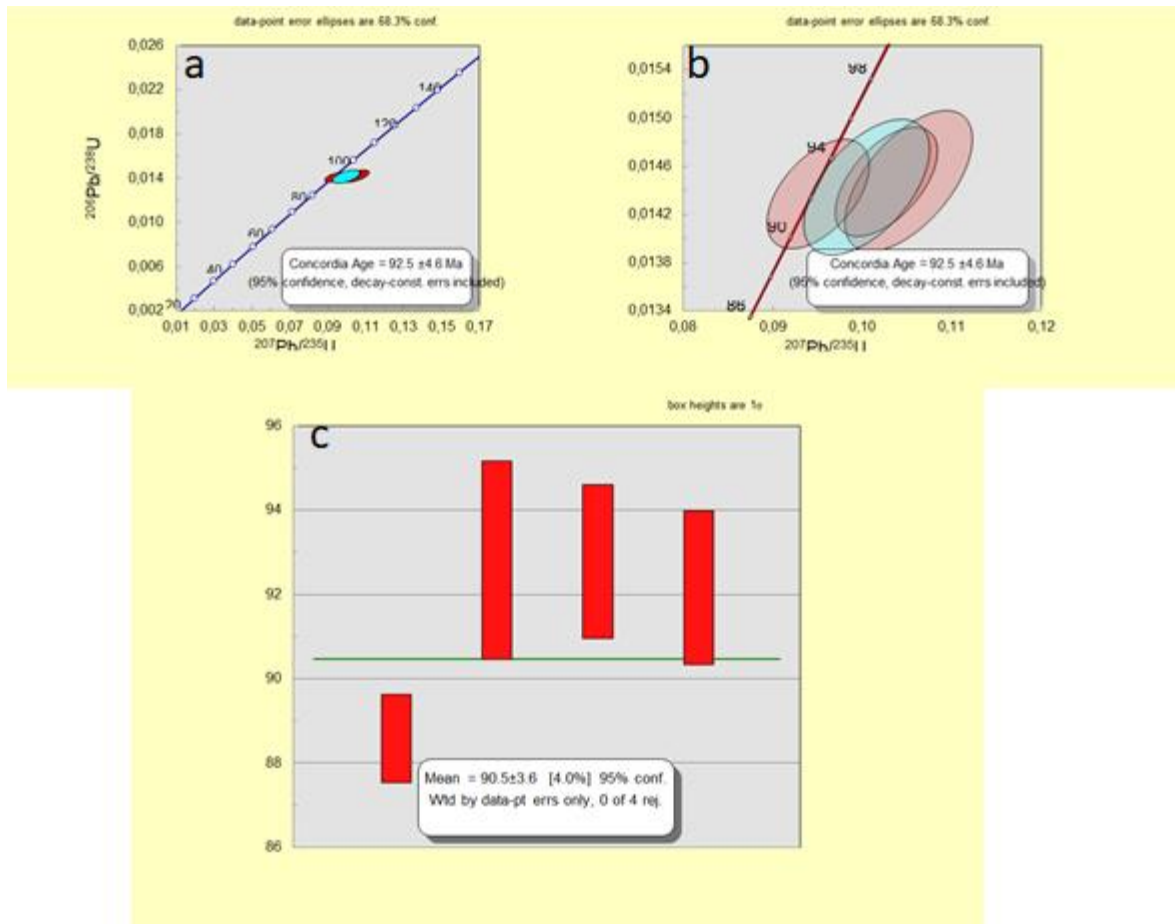


Figure 55. Concordia diagrams displaying U–Pb age results of zircons from the Taşlıyayla volcanic rocks.

These grains of zircon have been dated by LA-ICP-MS U-Pb and given in (App Table 14) and illustrate in different Concordia diagrams as shown in (Figure 56). Around 28 points from different crystals were analyzed yielded concordant ages. These concordant ages have been calculated both using  $^{207}\text{Pb}/^{235}\text{U}$  vs  $^{206}\text{Pb}/^{238}\text{U}$  ratios and plot (Wetherill Plot), and  $^{207}\text{Pb}/^{206}\text{Pb}$  vs  $^{206}\text{Pb}/^{238}\text{U}$  and (Tera-Wasserburg Plot), and both ages are concordant. The degree of uncertainties of the result represent by  $2\sigma$ . Most of the results indicate concordant data between the  $^{206}\text{Pb}/^{238}\text{U}$  and  $^{207}\text{Pb}/^{235}\text{U}$  ratios (Figure 56a and b), and the  $^{238}\text{U}$ – $^{206}\text{Pb}$  ages are concentrated at  $\sim 85,2$  Ma (MSWD = 0.9) (Figure 56a and b). Most of 28 spot analyses from a granite rocks yielded  $^{206}\text{Pb}/^{238}\text{U}$  ages varies from (80-122) Ma and a weighted mean age of  $85.2$  Ma  $\pm$   $2.4$  Ma (MSWD = 0.9) (Figure 67a and b). Contamination of Pb, Pb-loss and appearance of older detrital grains has not been detected. consequently, the weighted mean U–Pb ages from Gündoğdu granitoid are symmetrical

with magma emplacement during the Late of Cretaceous and with field observations and regional stratigraphy.

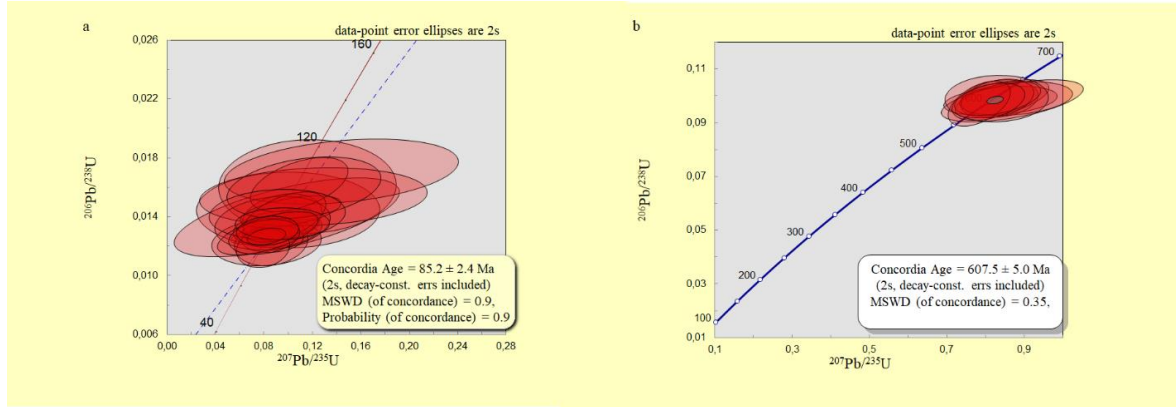


Figure 56. (a) Concordia diagrams displaying U–Pb age results of zircons grain from Gündoğdu granitoid, (b) weighted average.

### 3.5.3. Boğalı Pluton

Granitoid rocks from the Boğalı intrusion include abundant of colorless, euhedral and long-short prismatic zircon grains. These grains of zircon have been dated by LA-ICP-MS U-Pb and given in (App Table 15) and illustrate in different Concordia diagrams as shown in (Figure 57). Around 27 points from different crystals were analyzed yielded concordant ages. The degree of uncertainties of the result represent by  $2\sigma$ . Most of the results indicate concordant data and yielded the  $^{238}\text{U}$ – $^{206}\text{Pb}$  ages are concentrated at  $\sim 83,1$  Ma (MSWD = 0.9) (Figure 68a and b). Most of 27spot analyses from a granite rocks yielded  $^{206}\text{Pb}/^{238}\text{U}$  ages varies from (76-93) Ma and a weighted mean age of  $83.01$  Ma  $\pm 2.4$  Ma (MSWD = 0.46) which is symmetrical with magma emplacement during the Late of Cretaceous and field observations (Figure 57a-b). Contamination of Pb, Pb-loss, and the appearance of older detrital grains has not been detected.

### 3.5.4. Salmankaş Volcanic rock

A result of U–Pb zircon dating of Salmankaş volcanic rocks are available are offered in (App Table 16) and plotted as concordia diagrams in Figure 58. The Concordant ages of this volcanic rock has been calculated both using  $^{207}\text{Pb}/^{235}\text{U}$  vs  $^{206}\text{Pb}/^{238}\text{U}$  ratios and plot (Wetherill Plot), and  $^{207}\text{Pb}/^{206}\text{Pb}$  vs  $^{206}\text{Pb}/^{238}\text{U}$  and (Tera-Wasserburg Plot), and both ages

are concordant. The degree of uncertainties of the result represent by  $2\sigma$ . These results are represented by concordant diagram and yielded  $^{206}\text{Pb}/^{238}\text{U}$  and  $^{207}\text{Pb}/^{235}\text{U}$  ratios ages equal to  $\sim 44,61$  Ma (MSWD = 0.0018) (Figure 58). All of 27 spot analyses of Dacitic rocks give  $^{206}\text{Pb}/^{238}\text{U}$  ages ranging from (43-46) Ma and a weighted mean age of  $44,61$  Ma  $\pm 0,51$  Ma (MSWD = 0,0018) (Figure 69).

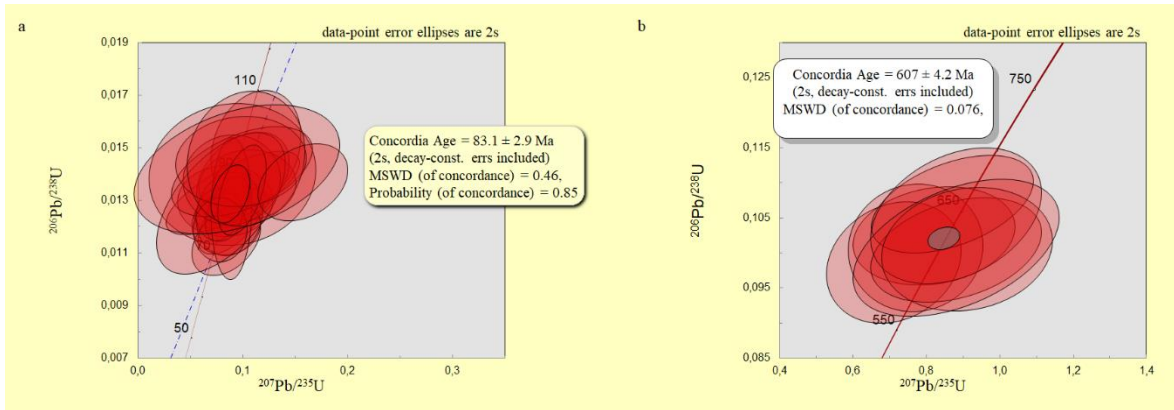


Figure 57. Concordia diagrams displaying U–Pb age results of zircons grain from Boğalı pluton (b) weighted average.

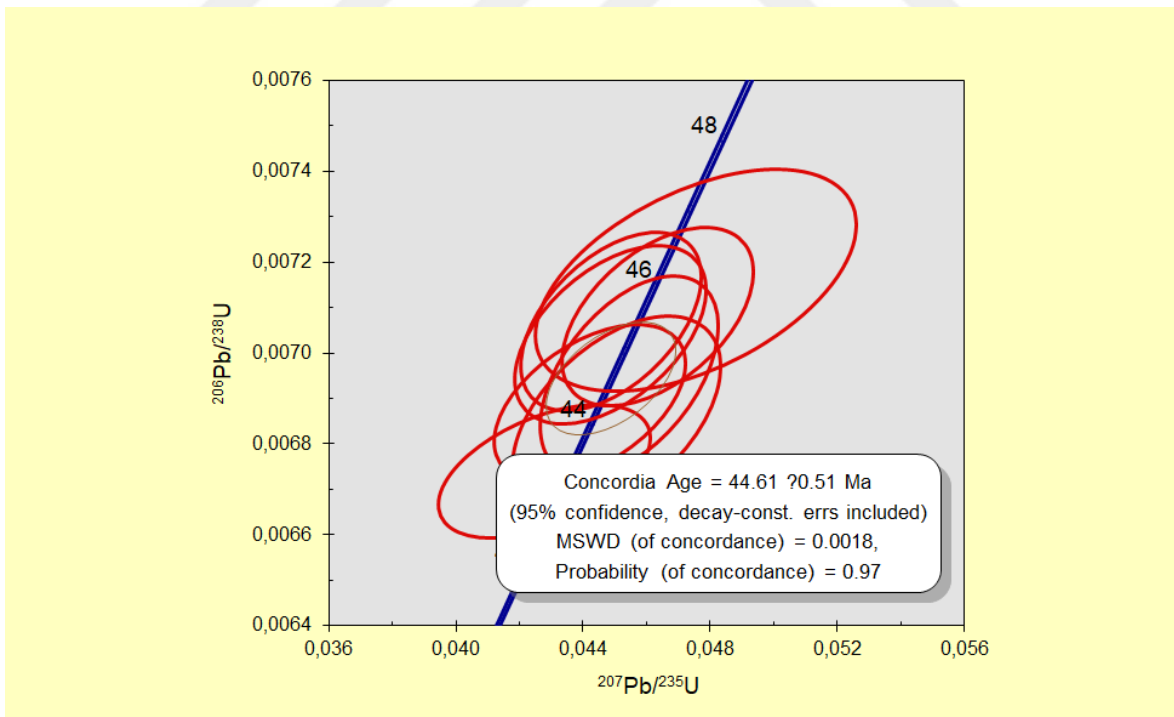


Figure 58. Concordia diagrams showing the U–Pb age results of Salmankaş volcanic rocks.

Table 9. Sr and Nd isotope composition of sample from Gündoğdu and Boğalı plutons.

Sample	Age	Rb/Sr	Sm	Nd	$^{87}\text{Rb}/^{86}\text{Sr}$	$^{87}\text{Sr}/^{86}\text{Sr}$	$^{87}\text{Sr}/^{86}\text{Sr}$ (i)	$^{147}\text{Sm}/^{144}\text{Nd}$	$^{143}\text{Nd}/^{144}\text{Nd}$	$^{143}\text{Nd}/^{144}\text{Nd}$ (i)	eNd(T)	eNd(0)	TDM**
<b>Gündoğdu pluton</b>													
70	85	1.684	3	6.2	4.87430	0.71412	0.70858	0.29379	0.51224	0.51208	-8.80	-7.80	1.47
30	85	0.513	3.2	8	1.48579	0.71362	0.71193	0.24287	0.51223	0.51210	-8.47	-8.00	1.48
84	85	0.533	3.3	6.6	1.54350	0.71237	0.71061	0.30358	0.51221	0.51206	-9.36	-8.27	1.51
97	85	0.282	3.4	6.6	0.81610	0.71175	0.71082	0.31278	0.51220	0.51204	-9.65	-8.47	1.52
30-MME	85	0.660	5.1	8.7	1.90909	0.70572	0.70355	0.35594	0.51233	0.51215	-7.58	-5.95	1.32
<b>Boğalı pluton</b>													
BG-4A	83	0.292	4.6	10.3	0.84363	0.70725	0.70625	0.27118	0.51244	0.51229	-4.75	-3.96	1.15
BG-1*	83	0.361	4.2	12.1	1.04557	0.70776	0.70653	0.21076	0.51241	0.51230	-4.60	-4.45	1.19
32	83	0.254	5.1	12.2	0.73453	0.70744	0.70657	0.25383	0.51241	0.51227	-5.13	-4.53	1.20
19	83	0.373	2.9	12.8	1.07831	0.70736	0.70609	0.13757	0.51241	0.51233	-3.86	-4.49	1.19
BG-4A-MME	83	0.204	5.5	8.9	0.58965	0.70673	0.70603	0.37524	0.51246	0.51226	-5.31	-3.41	1.11

Table 10. Pb isotope composition of sample from Gündoğdu and Boğalı Plutons.

Sample	Pb	U	Th	$^{206}\text{Pb}/^{204}\text{Pb}$	$^{206}\text{Pb}/^{204}\text{Pb}$ (206/204) <sub>i</sub>	$^{207}\text{Pb}/^{204}\text{Pb}$	$^{207}\text{Pb}/^{204}\text{Pb}$ (207/204) <sub>i</sub>	$^{208}\text{Pb}/^{204}\text{Pb}$	$^{208}\text{Pb}/^{204}\text{Pb}$ (208/204) <sub>i</sub>
<b>Gündoğdu pluton</b>									
70	20.4	4.3	20.2	18.665	18.496	15.654	15.645	38.786	38.526
30	4.5	2.9	14.7	19.038	18.518	15.658	15.633	39.033	38.169
84	40.8	6.3	16.5	18.63	18.506	15.661	15.655	38.749	38.643
97	31.5	5.7	15.9	18.601	18.456	15.657	15.650	38.716	38.583
30-MME	2.3	0.8	0.7	18.813	18.534	15.658	15.644	38.856	38.775
<b>Boğalı Pluton</b>									
BG-4A	9.6	4.3	22.7	18.931	18.557	15.655	15.637	38.986	38.338
BG-1*	19.1	4.3	27.2	18.887	18.699	15.652	15.643	38.966	38.576
32	6.4	5.8	24	18.931	18.174	15.654	15.617	39.068	38.040
19	16.5	6.3	24	18.931	18.612	15.642	15.626	38.964	38.565
BG-4A-MME	9.3	5.2	15	18.958	18.491	15.652	15.629	38.94	38.498

## 4. DISCUSSION

### 4.1. Taşlıyayla Volcanic Rocks

Different diagrams are used here to evaluate the tectonic setting of the Taşlıyayla volcanic rocks. The rocks are plotted within the field of volcanic arc basalt (VAB) as shown in the Ti/100-Zr-Sr/2 diagram (Pearce and Cann, 1973), and Hf/3-Th-Ta discrimination diagram (Wood et al., 1979) (Figure 57a, b).

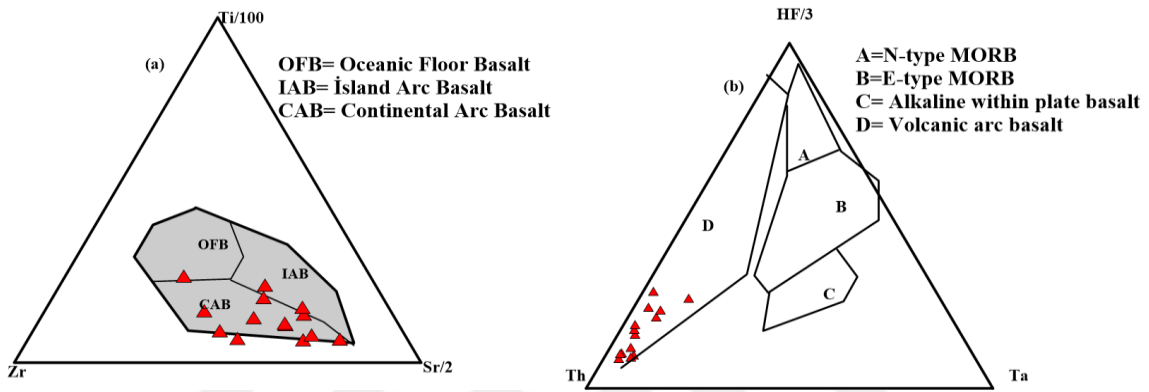


Figure 59. (a) Ti/100-Zr-Sr/2 diagram (Pearce and Cann, 1973), (b) Hf/3-Th-Ta discrimination diagram (Wood et al., 1979).

Taşlıyayla volcanic rocks distinguished by enrichment of  $\text{SiO}_2$ , LILE's with negative Ti, Ta, and Nb anomalies which reflect the subduction zone features and are generally attributed to magma source come from a lithospheric mantle. This magma during the subduction influenced by metasomatic fluids originate from subducted slab or sediments. These indicate an interaction with continental crust material during the raising of main magma and suggested generation of Taşlıyayla volcanic rocks can not be related to only fractional crystallization.

Various diagram like Nb/Y vs Rb/Y used here to identify the magma processes and to examine relation between the source modified by fluids of subduction zone, effect of crustal assimilation and fractional crystallization (Figure 61a). In this diagrams, Taşlıyayla volcanic rocks seem to have vertical directions indicating subduction zone enrichment and contamination of crust. The Ta/Yb vs Th/Yb diagram (Pearce, 1983) in Figure (61b) also has been used here to assess the sources of mantle and to identify the impact of subduction and/or crustal contamination during the magma generation. In this diagram, volcanic rocks are parallel to the mantle direction. Furthermore, according to these graphs, the magma derived from metasomatized source of subduction components. The Taşlıyayla formation



also characterized by Th content (1.9-11), U content (0.5-4.4) and Th/Ce ratio (0.06-0.26) which are indicative of the crustal contamination at a varying extent. The role of differentiation (FC) in the development of rocks indicates to magma derived from a source associated with subduction zone (Figure 61a and b).

The rocks textures of Taşlıyayla volcanic rock and their minerals compositions indicated to the several types of magma genesis occur during the generation of volcanic rock. Generally, some of the petrographic properties of plagioclases and clinopyroxene can be used to identify the main magma mixing processes (Dungan & Rhodes, 1978; Stimac & Pearce, 1992). The Taşlıyayla volcanic rocks displays sieved textured indicate to the importance of magma mixing processes during the development of magma or formed as result of decompression when the magma goes up to a shallower depth (Tsuchiyama, 1985; Nelson and Montana, 1992; Figure 60a and b).

The clinopyroxenes in the Taşlıyayla volcanic rocks shows various shape of disequilibrium textures, such as zoning and embayed crystals and breakdown clinopyroxenes megacryst which indicate to magma mixing (Hibbard, 1981; Simonetti Shore, and Bell, 1996; Streck, 2008; (Figures 60e, f and g). These texture criteria of clinopyroxenes are present both type of rocks, suggesting the presence of magma mixing. Hornblende phenocrysts are partly opaque and partly fragmented and with eroded edges and sometimes skeletal structure indicating that the magma mixture can be effective in the development of these rocks (Figure 60g and i). As a summary the magma that form the Taşlıyayla volcanic rocks generated metasomatized mantle wedge and contaminated, fractionated and mixed with middle/upper continental crust and erupted.

Chemical analysis of Taşlıyayla volcanic rocks displays negative correlation between  $\text{SiO}_2$  and  $\text{MgO}$ ,  $\text{CaO}$ ,  $\text{Fe}_2\text{O}_3$  indicating to fractionation of plagioclase and clinopyroxene. The decreasing of  $\text{Fe}_2\text{O}_3$  and  $\text{TiO}_2$  indicates Fe-Ti oxides. Decreasing of  $\text{P}_2\text{O}_5$  indicates apatite. The decreasing of  $\text{Al}_2\text{O}_3$  could be related to the effect of amphibole fractionation during the generation of volcanic rocks. The positive relation between  $\text{SiO}_2$  with Rb, Ba, Th and Hf elements can be attributed to feldspar fractionation. Decreasing of CaO with increasing  $\text{SiO}_2$  refers to clinopyroxene fractionations (Figure 40 and 41).

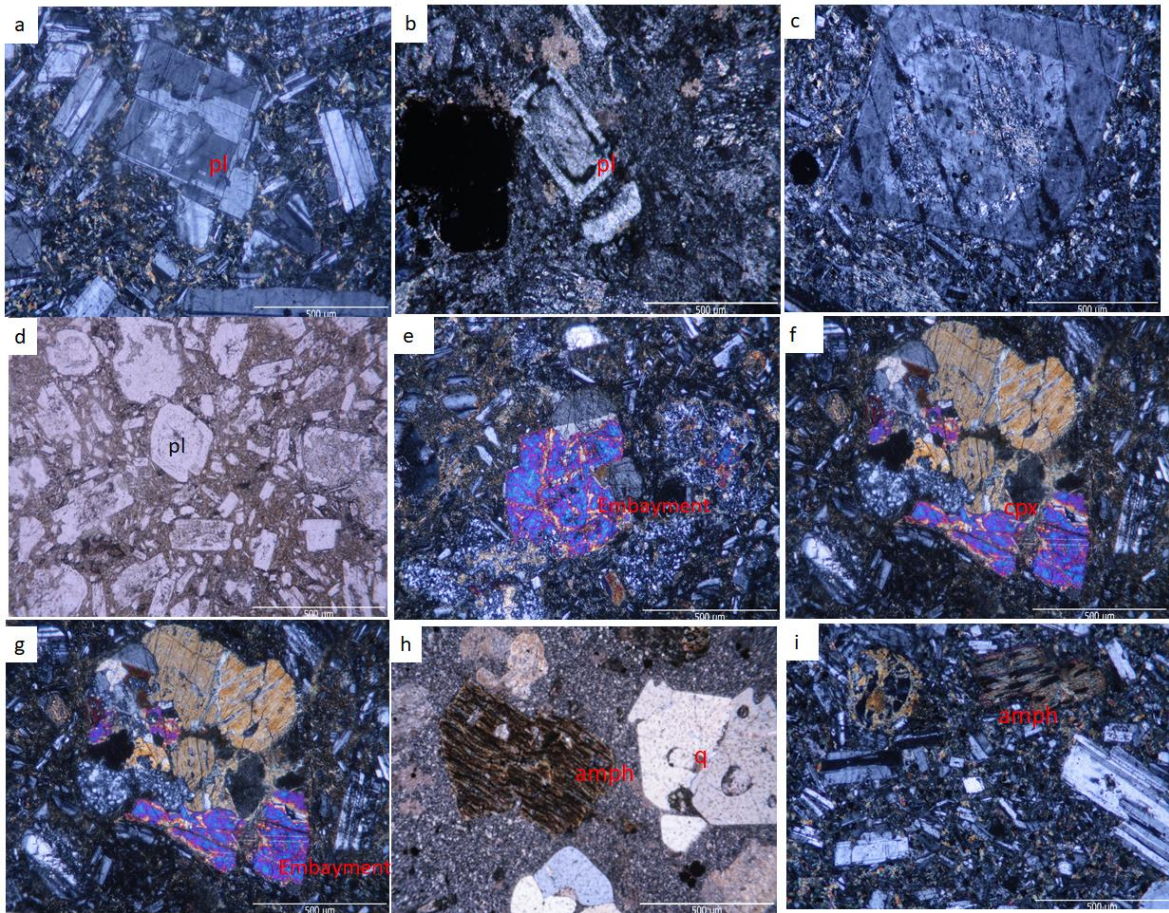


Figure 60. Microphotographs of the Taşlıyayla volcanic rocks (a, b, c, d) plagioclase with sieve texture and reflect the change of composition, (e, f) zoning, resorbed rims, and embayed albite in clinopyroxene, (g, h) hornblende with eroded edges and skeletal structure.

Generally based to the major oxides and trace element of Taşlıyayla volcanic rocks and their relationship with increasing of  $\text{SiO}_2$  pointed out to fractionation of plagioclase, clinopyroxene, hornblende, Fe-Ti oxides, and apatite. Variation on the major and trace element content is an indication that fractional crystallization represents one of the most important processes during the generation of these volcanic rocks and it is also provided by the depletion in Sr, and Eu anomalies. The negative Eu anomalies and the decrease in Sr with increase in silica, indicate the importance of plagioclase as fractionating phase. Additionally, the importance of hornblende and clinopyroxene as fractionating phases during the generation of the Taşlıyayla volcanic rocks can be identified by downward-concave shape of the REE pattern and also by petrography features. The increasing of Zr with increasing Y and Nb and decreasing  $\text{TiO}_2$  indicated that the fractional crystallization

hornblende, Clinopyroxene, magnetite and plagioclase. The positive relation between  $\text{TiO}_2$  and Ni is related to fractional crystallization of clinopyroxene and magnetite.

The fractional crystallization of accessory phases such as titanite, magnetite and zircon can be related to the depletion of Y. The negative Ti anomalies in spiderdiagrams indicated to the titanite fractionation and crustal contamination. The enrichment of LILE element relatively to HFSE and pronounced negative of Nb-Ta, Ti, P anomalies on Taşlıyayla volcanic rocks accompanied with positive of Pb, Th anomalies, indicates to subduction signature zone and contribution of crustal through the magma evolution (Taylor and McLennan, 1985; Kaygusuz, et al., 2014). The effect of crustal contamination can be induced by enrichment of Th and Pb, in which the Taşlıyayla volcanic rocks show high Th (2-9ppm) and Pb (5,3-19,1 ppm) and also by mixing texture (Taylor and McLennan, 1985).

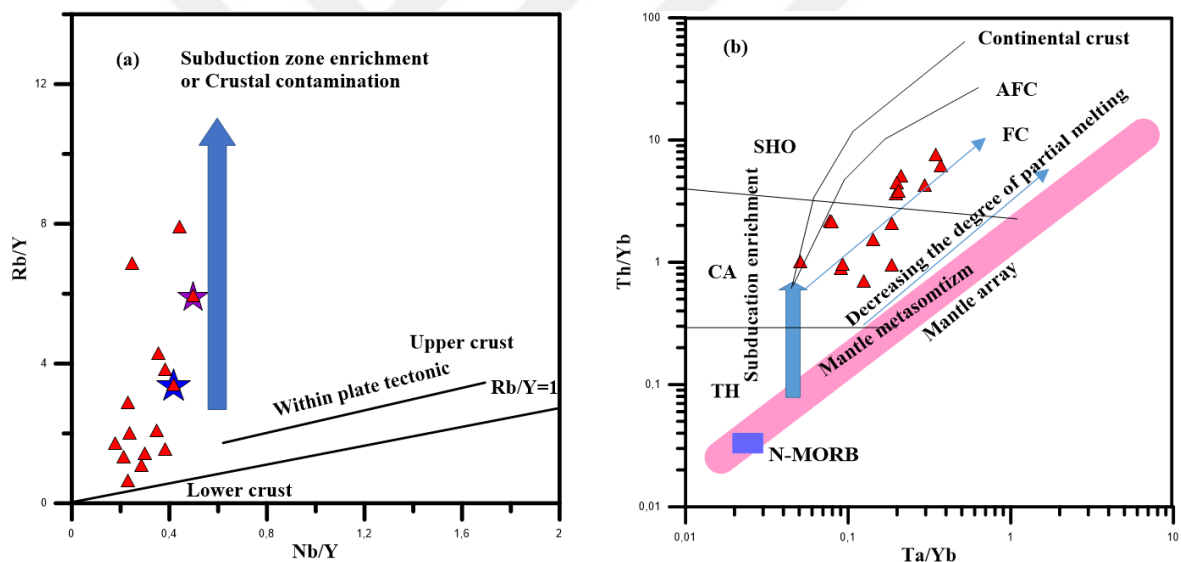


Figure 61. (a) Rb/Y versus Nb/Y for the volcanic samples (upper crust and lower crust are from, (Taylor and McLennan (1985)), (b) Th/Yb versus Ta/Yb diagram (after Pearce et al. 1990) for the Taşlıyayla volcanic rocks. Composition of continental crust and the N-MORB taken are from Taylor and McLennan (1985) and Sun and McDonough (1989) respectively. Vectors displays effects of magma generation process during the evolution of Taşlıyayla volcanic rocks (Pearce et al. 1990). Abbreviations, SHO: Shoshonitic, CA: Calc alkaline, Th: Tholeiitic, AFC: Assimilation Fractional Crystallization FC: Fractional Crystallization.

As mentioned above the Taşlıyayla volcanic rocks exhibits feature of subduction zone because the subduction-related continental arc magma displays LILE enrichment relatively in compared to HFSE, LREE in compared to HREE and negative Nb, Ta, Zr, Hf

and Ti anomalies. All these features indicate to magma with mantle source has been modified by metasomatic fluids derived from the subducted slab or sediments (e.g., Pearce 1983; Hawkesworth et al., 1997; Elburg et al., 2002). So that the enrichment in LILE and negative Nb, Ta and Ti anomalies can be interpreted as a result of the role of asthenosphere melts (OIB) during the magma generation in comparison to typical magma of subduction zone. The retention in Ti-rich residual mineral phases can be related to depletion of some element such as Nb, Ta and Ti (Foley and Wheller 1990; Pearce and Parkinson 1993), whereas the fractional crystallization of apatite and zircon or presence of these phases in the mantle source can be estimated by negative P and Zr anomalies in the primitive mantle diagrams (Guo et al., 2007; Figure 42b).

A Th/Y-Nb/Y plot may provide some useful information that leads to investigate the potential source components involved in the petrogenesis of the magmas (Wilson et al., 1997). Based on the diagram of Th/Y-Nb/Y the Taşlıyayla volcanic rocks define a trend, with variation of Th/Nb ratio range from 0.3 to 2.7 which indicated that the importance of the fractional crystallization processes and crustal assimilation during the magma evolution. The higher ratio of Th/Y is strongly related to metasomatism of the mantle source by subduction zone fluids which taken the trace element signature of a crustal component (Figure 63a). In the Nb/Yb versus  $TiO_2/Yb$  diagram, the Taşlıyayla volcanic rocks displays low  $TiO_2/Yb$  ( $<0.5$ ) and moderate Nb/Yb ( $\sim 1-5$ ) ratios, implying that the melt is a products of a shallow mantle source (MORB-like spinel-lherzolite) (Figure 74d).

The source features of the Taşlıyayla volcanic rocks possible identified by using some diagram of trace element. In the diagram of Nb/Th vs Nb all samples plotted in the subfield of arc volcanic (Figure 63c). In the diagram of Nb/La vs La/Yb the Taşlıyayla volcanic rocks plotted in the field of lithosphere mantle. It has been suggested by Bradshaw and Smith (1994) and Smith et al., (1999) that, the contribution of an OIB in magma source by depletion of some HFSE (such as Nb and Ta) and ratio of Nb/La ratios should be more than 1. According to that the contribution of an OIB has not been detected like asthenospheric mantle because most volcanic samples of Taşlıyayla formation have Nb/La values range from 0.15 to 0.39 and La/Yb values varies from 5.8 to 14.7 whereas a few samples have La/Yb value range from 16 to 21 (Figure 63b). However, the lower ratios of La/Nb in Taşlıyayla volcanic are related to several reasons such as La enrichment in the mantle source by subduction fluid, modified by slab released fluids, or can also be derived

from a lithospheric source, given the metasomatization of mantle source by subduction fluids (illustrated on diagram 63b).

With a view to detect the composition of the main magma of these Taşlıyayla volcanic rocks, we need to approach the percent of mantle source that was formed by a partial melting. As shown in (Figure 62a) the diagram of  $Tb_N/Yb_N$  vs. Th (ppm) displays a variation in the studied rocks with the horizontal line plotted in the field of spinel-bearing lherzolite (low  $Tb_N/Yb_N$ ) (e.g., Wang et al., 2002). The main magma of the volcanic rock of Pontides may be derived from an enriched background that involves subduction and asthenosphere melts. Rare earth element normalized to chondrite (Taylor ve McLennan, 1985), were used here to assess the degree of partial melting and investigate the magma source by using the non-modal Rayleigh partial melting model (Formula 1,2,3: Table 11).

$$C_L/C_O = (1/F)(1-(1-(P_oF/D_o)^{1/P_o})) \quad (1)$$

$$D_o = \sum X_a D_a \quad (2)$$

$$P_o = \sum X_a P_a \quad (3)$$

Where:

F= Degree of partial melting.

$C_L$  = Concentration of some element in the liquid.

$C_o$  = Initial concentration of that element in the liquid.

$D_o$  = Bulk partition coefficient of element between source rock and melt.

$P_o$  = Normative (bulk partition coefficient) of the melt for element (constant during melting).

According to Figure (62b), the original magma of the volcanic rocks could be derived from a spinel-containing lherzolitic mantle source which was metasomatized by 5%. It is determined from the basalt sample 175 of Taşlıyayla volcanic rocks that heavy rare earth element has been partially melted at degree of 20-30% and by 5-10% for light rare earth elements. The similarity with the orientations of the E-MORB mantle composition of McDonough and Sun (1989) and the Ocean Island Basalt of Sun and McDonough (1989) supports the interpretation that these rocks can be derived from an enriched magma, which involves subduction and asthenosphere melts.



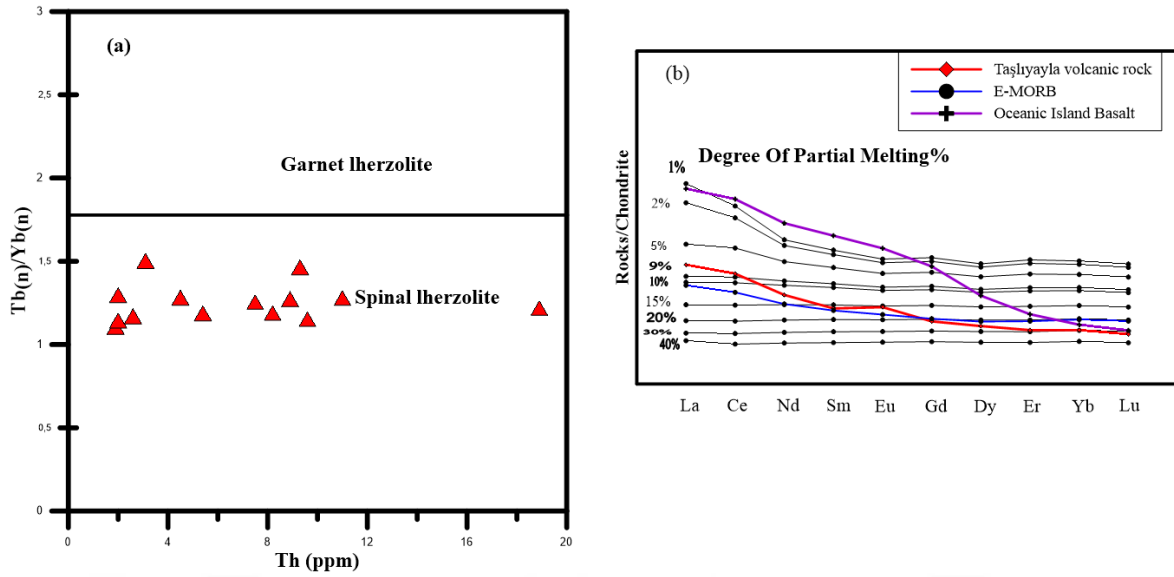


Figure 62.(a)Th(ppm) vs.Tb<sub>N</sub>/Yb<sub>N</sub> for volcanic sample of Taşlıyayla volcanic rocks displays horizontal line separates fields expected for melting spinel–lherzolite as determined for Basin and Range basalts (Wang et al., 2002), (b) Non-modal Rayleigh partial melting model used to determine the main magmas of the Taşlıyayla volcanic (chondrite normalized rare earth element distributions of the melt created by partial melting of the spinal lherzolite source in different degrees (spinal lherzolite , E-type MORB and Ocean Island basalt values are from Sun and McDonough (1989)), the modal composition and melting ratios of the mantle, are from Kelemen et al. 1990, Hart and Dunn, (1993), the partition coefficients are from McKenzie and O’Nions (1991). Chondrite normalized values are from Taylor and McLennan (1985).



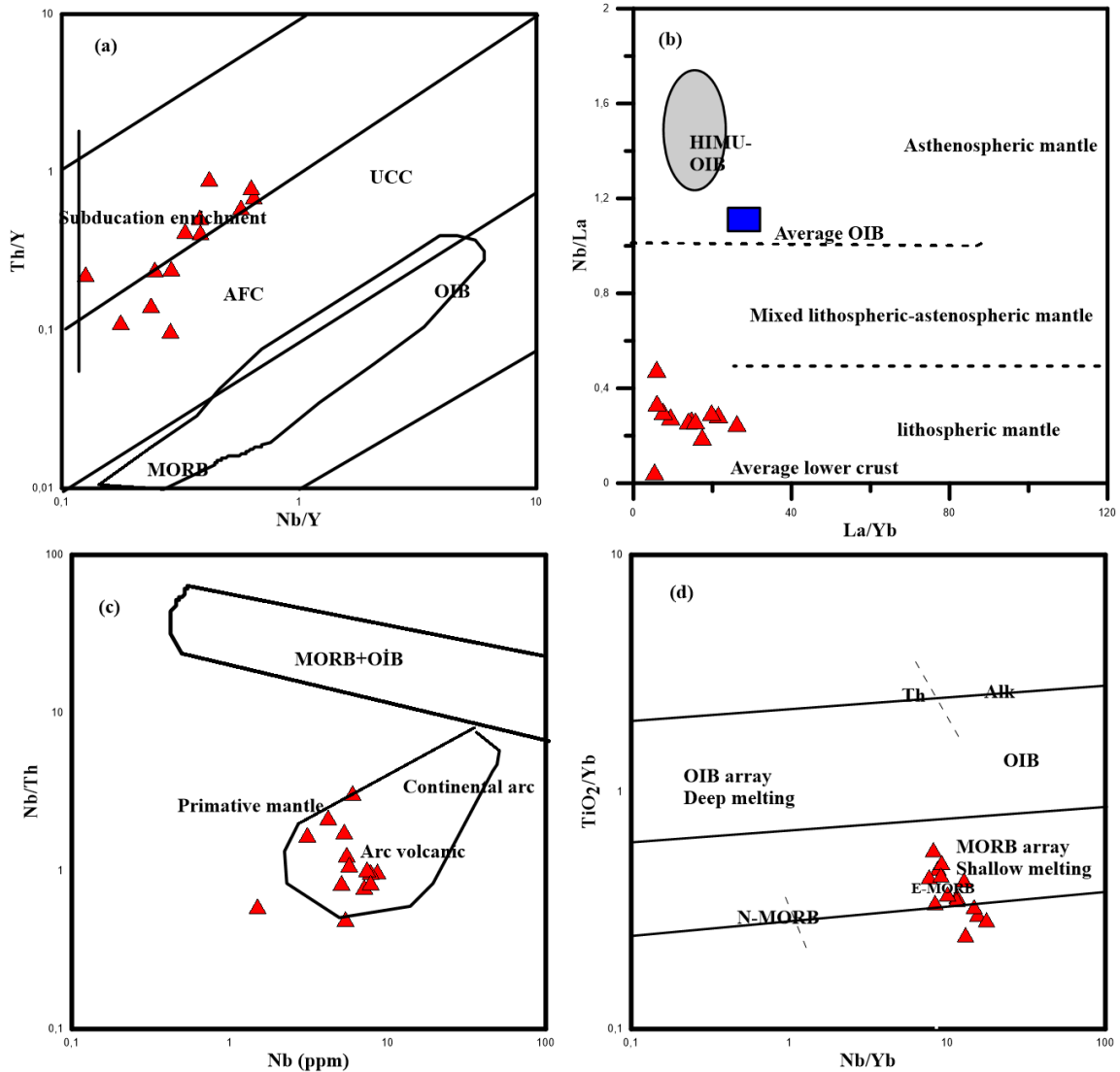


Figure 63. (a) Th/Y vs Nb/Y (Pearce 1983), (b) The Nb/La vs La/Yb variation diagram, (Jahn et al. 1999), (c) Nb/Th vs Nb (ppm) diagram after Hofmann (1988), (d)  $\text{TiO}_2/\text{Yb}$  vs Nb/Yb diagram (after Pearce, 2008), indicating the genesis of volcanic rocks. Composition of OIB and composition of lower crust is taken from Fitton et al (1991) and Chen and Arculus (1995) respectively. Dashed lines that split the fields of asthenospheric, mixed mantle and lithospheric and the HIMU OIB field are after Smith et al. (1999) and Weaver et al. (1987), respectively. Abbreviations, SHO: Shoshonitic, CA: Calc alkaline, Th: Tholeiitic, AFC: Assimilation Fractional Crystallization, FC: Fractional Crystallization, OIB: Oceanic Island Basalt, UCC: Upper Continental Crust.

Table 11. Estimation the degree of partial melting and magma composition for Taşlıyayla volcanic rock and Salman Kaş volcanic rocks by using non-modal Rayleigh partial melting model (Equation 1) and normalized to Chondrite by using the Rare Earth Element. Chondrite normalized value Taylor and McLennan 1985, E-MORB Taylor and McLennan 1989, mantle composition from Kelemen et al. 1990, Hart & Dunn, 1993, the partition coefficients are from McKenzie ve O'Nions (1991).

REE	K <sub>D</sub> Ol	K <sub>D</sub> Kpir	K <sub>D</sub> Spl	K <sub>D</sub> Or	D <sub>0</sub>	P <sub>0</sub>	C <sub>0</sub>	Chondrite	Taşlıyaylı volcanic	E-MORB	Oceanic İslan Basalt
La	0.00007	0.0025	0.0536	0.0005	0.569355	0.51695	1.24	0.37	9.4	17.17	100.82
Ce	0.00001	0.005	0.0858	0.0006	0.922014	0.836806	2.85	0.96	20.9	15.67	83.59
Nd	0.00007	0.01	0.1873	0.001	1.998762	1.814355	1.34	0.71	10.6	12.66	54.15
Sm	0.0007	0.02	0.291	0.291	6.061771	5.482076	0.39	0.23	2.7	11.26	43.29
Eu	0.00095	0.03	0.322	0.322	6.809744	6.155945	0.13	0.09	1.04	10.46	34.48
Gd	0.0012	0.04	0.361	0.361	7.71712	6.974157	0.45	0.31	2.83	9.71	24.9
Dy	0.004	0.05	0.442	0.442	9.49852	8.582093	0.54	0.38	3.24	9.32	14.7
Er	0.009	0.11	0.387	0.3	8.366313	7.537449	0.34	0.25	1.97	9.28	10.52
Yb	0.23	0.11	0.43	0.005	9.067207	8.036486	0.33	0.25	1.96	9.56	8.71
Lu	0.0383	0.17	0.56	0.01	8.375373	7.525419	0.043	0.04	0.28	9.29	7.87
Chondrite Normalized											
REE	C <sub>L</sub> (0.01)	C <sub>L</sub> (0.02)	C <sub>L</sub> (0.05)	C <sub>L</sub> (0.09)	C <sub>L</sub> (0.1)	C <sub>L</sub> (0.15)	C <sub>L</sub> (0.2)	C <sub>L</sub> (0.25)	C <sub>L</sub> (0.3)	C <sub>L</sub> (0.4)	
La	217.8607	148.4756	67.32988	37.54108	33.78736	22.52498	16.89373	13.51	11.17166213	8.719346049	
Ce	140.2259	108.2342	57.67447	33.05376	29.76826	19.85369	14.89028	11.91	9.508881923	7.62800418	
Nd	47.97247	42.4666	30.03707	20.04843	18.33192	12.54162	9.423088	7.54	6.751054852	5.76652602	
Sm	18.51636	17.71654	15.51138	12.99176	12.43121	10.00248	8.122422	6.69	5.622119587	4.372294372	
Eu	14.57166	14.03181	12.5177	10.73325	10.32688	8.517498	7.049098	5.88	4.96831995	4.482758621	
Gd	12.66435	12.26866	11.14075	9.771698	9.452918	7.995247	6.755505	5.72	4.874459366	4.281045752	
Dy	9.936519	9.707438	9.039335	8.193739	7.990517	7.024332	6.143157	5.35	4.648183228	3.779527559	
Er	9.988856	9.735694	9.003617	8.091164	7.874361	6.857743	5.952543	5.16	4.470592796	3.413596765	
Yb	5.820415	5.734279	5.481047	5.155485	5.076252	4.693031	4.331381	3.99	3.672792748	3.100476145	
Lu	6.823078	6.701579	6.3417	5.873051	5.757968	5.195736	4.657024	4.1445	3.661941116	3.175853018	

## 4.2. Gündoğdu Pluton

Different tectonic diagrams are used here to identify the tectonic setting of the Gündoğdu plutonic rocks with their MMEs. In the diagram of the Nb versus Y of Pearce et al., (1984) both rocks and MMEs plotted in the field of volcanic arc granite and (VAG) syn-collisional granites (Syn-COLG) whereas in the diagram of Ta versus Yb both granitoid and MMEs plotted in the VAG field (Figure 64a,b).

Most samples display low ratio of Sr/Y and high Y contents and they plotted in the field of modern volcanic arc in the Sr/Y versus. Y diagram and Ta versus Yb diagram (Figure 64b and c). The degree of arc maturity of Gündoğdu granitoid are related to the abundance of incompatible elements (Brown et al., 1984). The diagram of Rb/Zr versus Nb used here to compare the Gündoğdu pluton with arc-type granitoids (Figure 75d). All granitoid rocks and their MMEs plot in the field of normal arc (Figure 64d), and the samples of studied rocks assign to normal continental arc, because the high ratio of Rb/Zr which displays positive relation with increasing Nb content.

Three main models can be used to interpret the generation of these granitoids rocks with High-K to shoshonitic calc-alkaline affinity; (1) partial melting of mafic lower crust at relatively high pressures (e.g. Roberts and Clemens, 1993) or (2) a magma mixing of crustal- and mantle-derived magmas (e.g., Barbarin, 1999) or (3) fractional crystallization of mantle derived magma. All the data of Gündoğdu pluton can be related to the second model, that attributed to magma mixing of crustal and mantle-derived magma.

Gündoğdu plutons has different sources formed by various degree of partial melting of different sources. The existence of some disequilibrium textures such as sieve and oscillatory plagioclases, poikilitic texture in the Gündoğdu pluton are a good indicator of magma mixing processes (Figure 66). They also display hornblende phenocrysts with eroded edges and skeletal structure indicate that the magma mixture can be effective in the development of these rocks. The existence of MMEs also an indicator of a mixing processes during the magma evolution

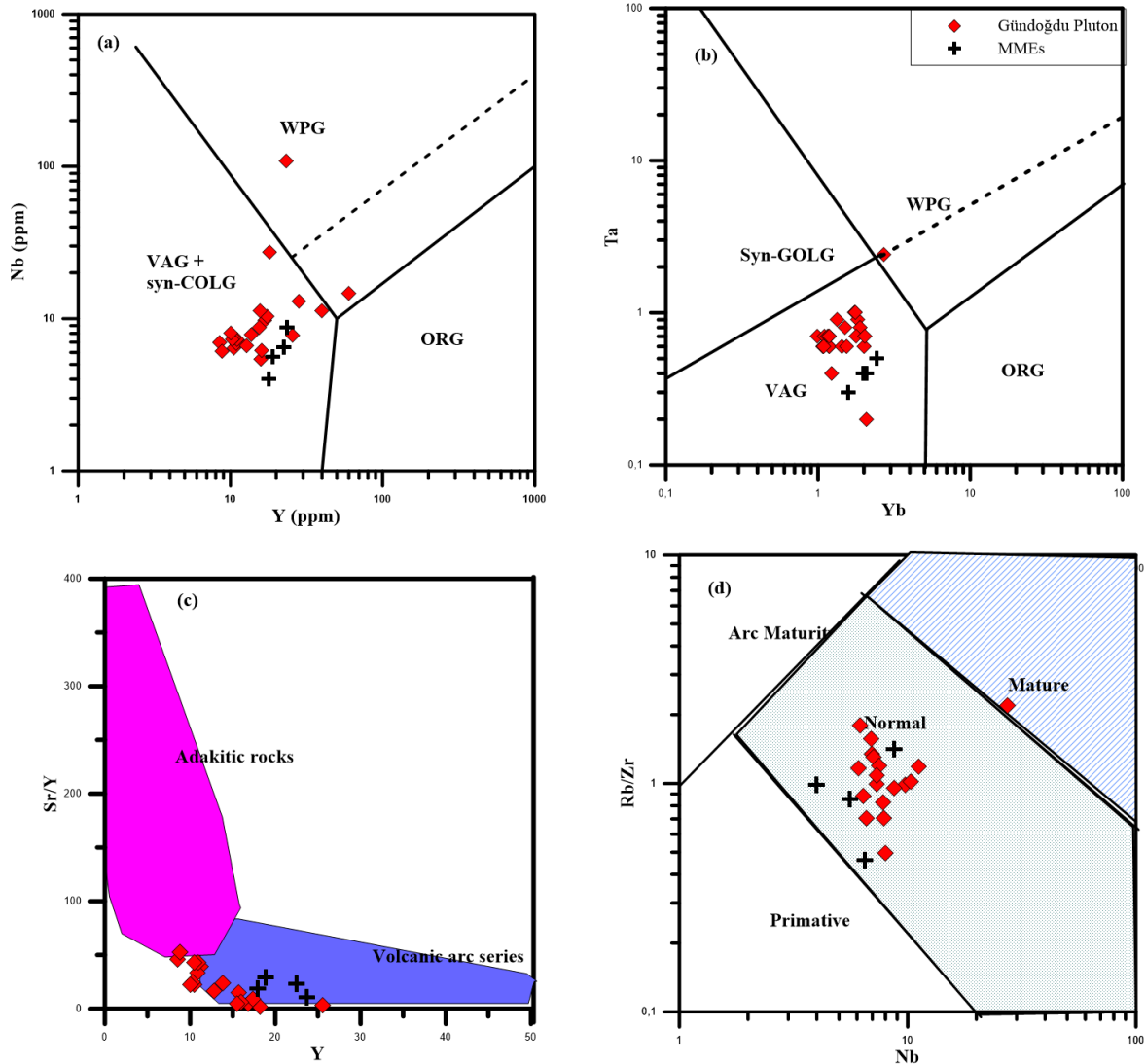


Figure 64. (a, b) Nb-Y and Ta -Nb discrimination diagrams (Pearce et al. 1984) for samples from the Gündoğdu pluton, displaying the fields of volcanic-arc granites (VAG), syn- collisional granites (Syn-COLG), within-plate granites (WPG) and ocean-ridge granites (ORG), (c) Sr/Yvs Y for samples from Gündoğdu pluton, (d) Nb vs Rb/Zr diagram (Brown et al. 1984).

Geochemically, the considerable overlap of the data points of the host rock and their MMEs in the diagram of  $\epsilon\text{Nd}$  (85 Ma) vs  $\text{ISr}$  (85 Ma) indicated to the importance of mixing processes as primary processes during the genesis of rocks (Figure 54a). The isotope analysis displays variations between MMEs and host rocks where host granitic rocks have high Sr isotope value ( $\text{ISr} = 0.708\text{--}0.7118$ ) and MMEs ( $\text{ISr} = 0.7035$ ) whereas  $\epsilon\text{Nd}(t)$  more radiogenic ( $-6.4$  to  $-9.4$  for the host granitic rocks and  $-7.7$  for the MMEs) indicating that mixing of crustal with mantle material during the evolution of parental magma to generate these rocks, (Table 9; Figures 54a). The variation of Nd isotopes also

can be used here to differentiate the magma mixing and autolith hypotheses. The Isr (85) isotopic data also indicate to old continental source/ source rocks were inhomogeneous with a heterogeneous initial isotope composition produced by the mixing of lower-middle crust-derived melts with enriched lithospheric mantle. Moreover, the plots of the element compositions versus isotopic variations can be used as indicator for magma maxing (e.g., Thirlwall and Jones 1993; Chen and Arakawa 2005; Karsli et al., 2010). Paleozoic metamorphic rock lying at the boundary of Gündoğdu pluton the particularly in the western side form possibility candidate sources for the contamination which leads to the high I(Sr) and I(Nd) values.

Linear correlations between SiO<sub>2</sub>, versus some of trace elements also can be used as indicator for magma mixing (Perugini et al., 2004; Karsli et al., 2010; 2012). The samples realize hyperbolic arrays in the diagram of Rb/Sr vs. Ti/Zr (Figure 65a) and linear correlation in the diagram of Ti/Zr Sr/Zr (Figure 65b) all this features can be interpreted as magma mixing processes between two distinct geochemical end-members (mantle derived-magmas and lower crustal components). Considering the isotopic data of the samples, <sup>144</sup>Nd/<sup>143</sup>Nd(i) ratio or <sup>87</sup>Sr/<sup>86</sup>Sr (i) ratios, the Gündoğdu pluton exhibited randomly scattered reflect small negative or positive correlation with SiO<sub>2</sub>, indicating to the importance of crustal assimilation and magma mixing during their genesis (Figure 67a and d). These trends indicating that fractional crystallization and partial melting are the main processes during the magma evolution. However, this magma cannot be directly derived or attributed to only mantle source due to their wide range of SiO<sub>2</sub> (50–75 wt.%) content, and Mg# (11–34) values. Therefore, it is inferred that a parental magma that underwent to several processes explains their generation.

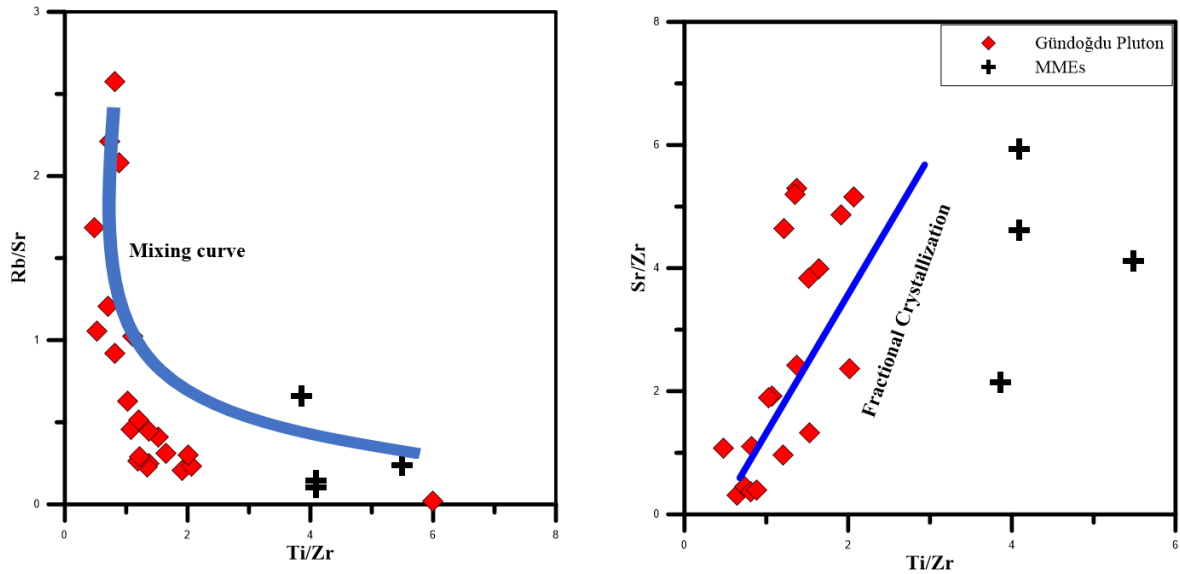


Figure 65. (a) Rb/Sr vs. Ti/Zr diagram, (b) Sr/Zr vs. Ti/Zr diagram for Gündoğdu plutonic rocks which indicating to mixing between two distinct geochemical end-members (i.e. mantle derived-magmas and lower crustal components).

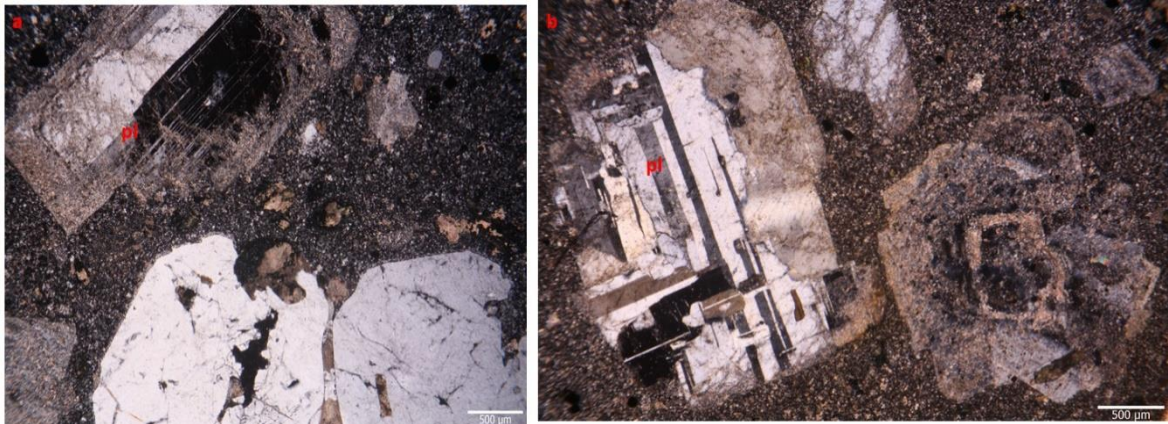


Figure 66. Microphotographs of the Gündoğdu plutonic rocks (a, b) plagioclase with sieve texture showing the change of composition.

The Gündoğdu pluton shows an increasing of  $\text{SiO}_2$  with decreasing  $\text{MgO}$ ,  $\text{CaO}$  and  $\text{Al}_2\text{O}_3$  indicates to fractional crystallization of Plagioclase, Hornblende and Biotite. Increasing of  $\text{SiO}_2$  with decreasing  $\text{TiO}_2$  and  $\text{Fe}_2\text{O}_3$  indicates fractionation of Magnetit and Fe-Ti oxides. The negative correlation between  $\text{SiO}_2$  and  $\text{P}_2\text{O}_5$  indicates fractional crystallization of apatite. Increasing of  $\text{K}_2\text{O}$  and Rb with increasing  $\text{SiO}_2$  also suggests that K-feldspar and biotite are not early-fractionation phases. The variation of trace element trends indicates to the importantace of fractional crystallization during the generation of this pluton and this is also provided by the depletion of Sr, Ba and Eu anomalies.



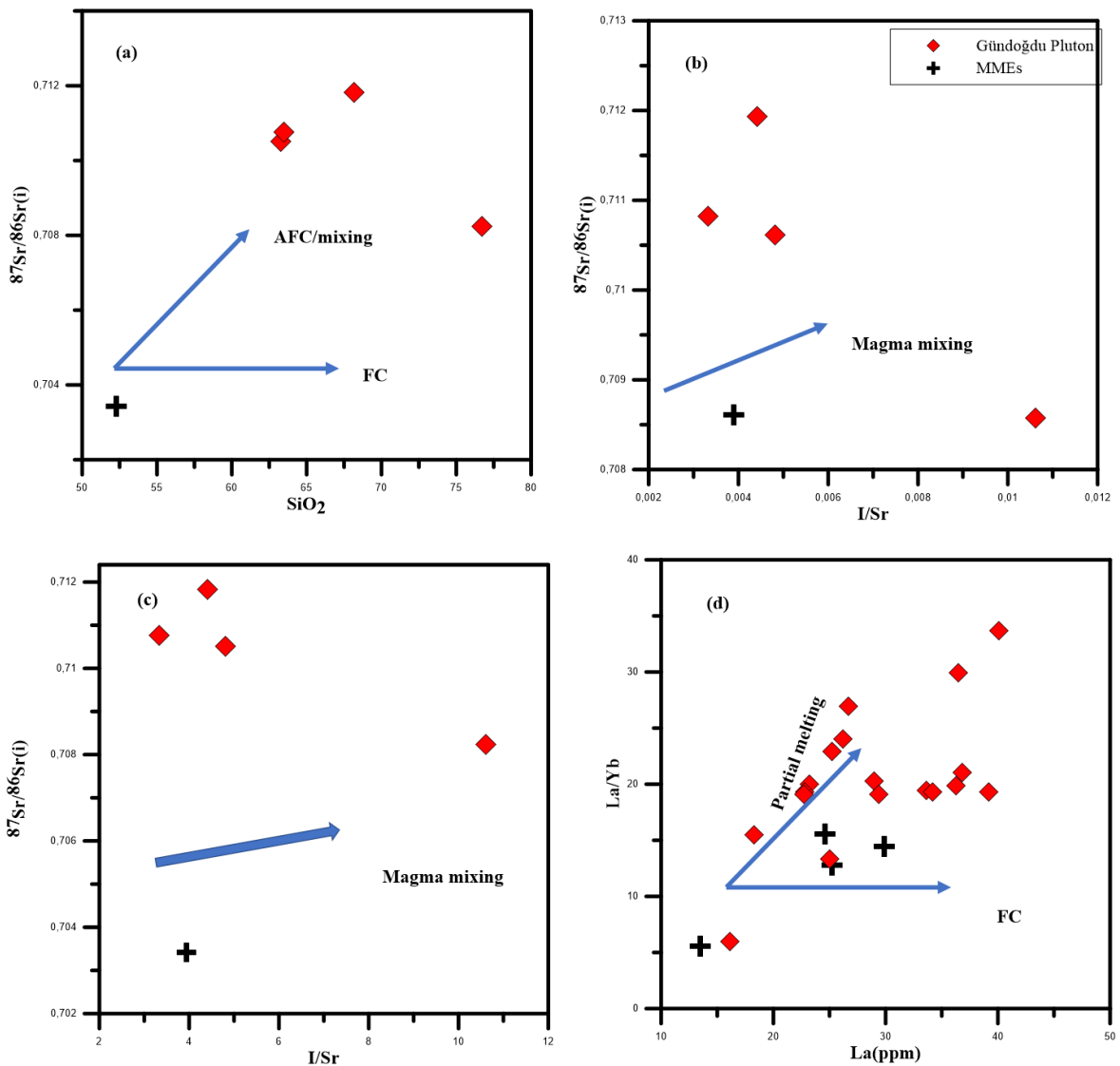


Figure 67. (a)  $\text{SiO}_2$  vs  $I/\text{Sr}$  (85 Ma); (b)  $\text{SiO}_2$  vs  $e\text{Nd}$  (85 Ma) (c)  $1/\text{Sr}$  vs  $I/\text{Sr}$  (85 Ma) and (d)  $\text{La}/\text{Yb}$  ratio vs  $\text{La}$  (ppm) content for the Gündoğdu pluton. Abbreviations, AFC: Assimilation Fractional Crystallization FC: Fractional Crystallization

The negative anomalies of Eu and the depletion of Sr with increasing  $\text{SiO}_2$  leads to fractional crystallization of plagioclase and/or K-feldspar and also indicate to the importance of plagioclase during the fractional crystallization process.

As another indicator of fractional crystallizations has been estimated by the decreasing of  $\text{Al}_2\text{O}_3$ ,  $\text{TiO}_2$ ,  $\text{MgO}$ ,  $\text{P}_2\text{O}_5\text{CaO}$ ,  $\text{Fe}_2\text{O}_3$ , Sr, and increasing of  $\text{K}_2\text{O}$ , Rb, Ba with increasing  $\text{SiO}_2$  (Figure 44) which indicated to fractional crystallization of different phases such as plagioclase, K-feldspar, biotite, amphibole, apatite and titanite. Depletion of

Zr and Y indicates to fractional crystallization of secondary phases such as magnetite, zircon and titanite.

The negative anomalies of Ti in primitive mantle diagram are consistent with fractional crystallization titanite. The Ti anomalies and enrichment of Th and Pb, indicate crustal contamination (Taylor and McLennan, 1985; Karslı et al., 2010; Kaygusuz et al., 2014). Gündoğdu granitoid rocks are characterized by positive anomalies of Pb, pronounced negative Nb–Ta, and enrichment of LILE element relatively to HFSE. That is indicated to subduction related magma and potential minor amount of a crustal contribution during the magma evolution due to the highly fractionation of continental crust, enriched LREE, flat HREE, positive Pb anomalies and negative Nb–Ta anomalies (Taylor and McLennan, 1985; Arslan and Aslan 2006; Kaygusuz et al., 2014).

The variations in volume of the granites compared to the other basic rocks, strongly suggests a limited mantle contribution to the origin of the peraluminous granites, via either crystal fractionation or basic-acid magma mixing. The Gündoğdu plutonic rocks are high-K to shoshonitic and I-type to S type in composition displays vast range of silica content ( $\text{SiO}_2 = 59.44\text{--}75.85$  wt%) and relatively low Mg# (9.01–35). According to these values the chemical composition of Gündoğdu pluton indicates that they are not in equilibrium with essential mantle melt (Karslı et al., 2007; Yang et al., 2007; Aydın 2014).

The Gündoğdu plutonic rocks are also distinguished by pronounced negative anomalies of Ta, Nb and Ti in the spidergrams (Figure 49c and d) and enrichment of LILEs and LREEs, indicating to typical crustal melts and subduction related magmas. The Gündoğdu plutonic rocks displays weak REE fractionation ( $(\text{La}/\text{Yb})_N = 4.02$  to 16.24 for most of granitoid samples and one sample rocks has 22), low Sr/Y ratios (4.7 to 45 and high contents of Y (8 to 25 ppm) and Yb (0.9 to 2.03 ppm). According to these values, it is unlikely to relate this kind of magma to only the crustal-derived melts. However, these features can be interpreted as result to partial melting of mafic lower crust and an enrichment mantle, which was metasomatized by fluids prior to melting (Hawkesworth et al., 1993; Rottura et al., 1998; Dokuz et al., 2010; Kaygusuz et al., 2009). According to ternary diagram of Nb–Y–Ga\*3 (after Eby, 1992), this pluton represent magma generated as a result to interaction of mantle–crust whereas MMEs has a pure mantle source (Figure 68).

Another indicator the Gündoğdu granitoid pluton represents a mixing of mantle and crust, because they display wide range of Y/Nb ratios (0.6-1.5) whereas the Nb/Ta ratios

vary between 7 and 13,1 (Green, 1995; Dokuz et al., 2010). The ratio of Nb/Ta of the MMEs (14–17.4) are similar to their host rocks. The variation of chemical composition of this magma indicate that this magma has different source, such as metagraywackes, amphibolites metabasaltic and metapelites under different melting conditions (Figure 69a-c).

The isotope analysis displays high variation and plotted scattered randomly between MMEs and host rocks. Host granitic rocks have high Sr isotope value ( $ISr = 0.708–0.7118$ ) and MMEs ( $ISr = 0.7034$ ), however,  $\epsilon Nd_{(t)}$  show more radiogenic ( $-6.4$  to  $-9.4$  for the host granitic rocks and  $-7.7$  for the MMEs) indicating to different magma source and imply that to contribution of the crustal contamination and/or magma mixing processes during the evolution of magma and unlike to relate this variation in the elemental of MMEs to only the fractional crystallization. Although the Sr-Nd isotope displays high variation and plotted scattered randomly the isotopic ratio of  $^{206}Pb/^{204}Pb$ ,  $^{207}Pb/^{204}Pb$ ,  $^{208}Pb/^{204}Pb$  of the same pluton reflects a small enriched mantle source which represent the end-member of the mixing process in the genesis. In the diagram of  $^{206}Pb/^{204}Pb_{(i)}$  vs.  $^{207}Pb/^{204}Pb_{(i)}$  and  $^{208}Pb/^{204}Pb_{(i)}$  (Figure 54b and c), all samples from the Gündoğdu pluton plot in the lower continental crust field (Kempton et al., 1997), close to the data of Camiboğazı and Harşit plutons which belong to Late Cretaceous (Karslı et al., 2010a; Kaygusuz et al., 2014). Karslı et al., (2010a) suggested that Harşit pluton have a mixed origin comprised the lower crust and lithospheric mantle. Kaygusuz et al., (2014) suggested that the generation of Camiboğazı pluton probably related to mixing between amphibolitic-type lower crustal with mantle derived magma.

However, according to the  $^{87}Sr/^{86}Sr$  isotope ratios of this pluton and the associated MMEs are not possible to be related that to magma generated from a single, chemically homogeneous source. Therefore, at least two different sources are wanted to evaluate their generation. However, the signature of isotopic ratio of Sr–Nd–Pb, major and trace element features of the Gündoğdu pluton and their MMEs indicate that it is unlikely to relate this magma to only amphibolitic lower crustal source rocks because a different source may have been contributed to the parental magmas such as metagraywackes, meta-igneous, metapelites, and lithospheric mantle. The high Sr-Nd isotope value can be attributed to old continental sources rocks which were inhomogeneous with a heterogeneous initial isotope composition formed as result to

mixing of enriched lithospheric mantle with lower to middle crust-derived melts or can be attributed to the contamination.

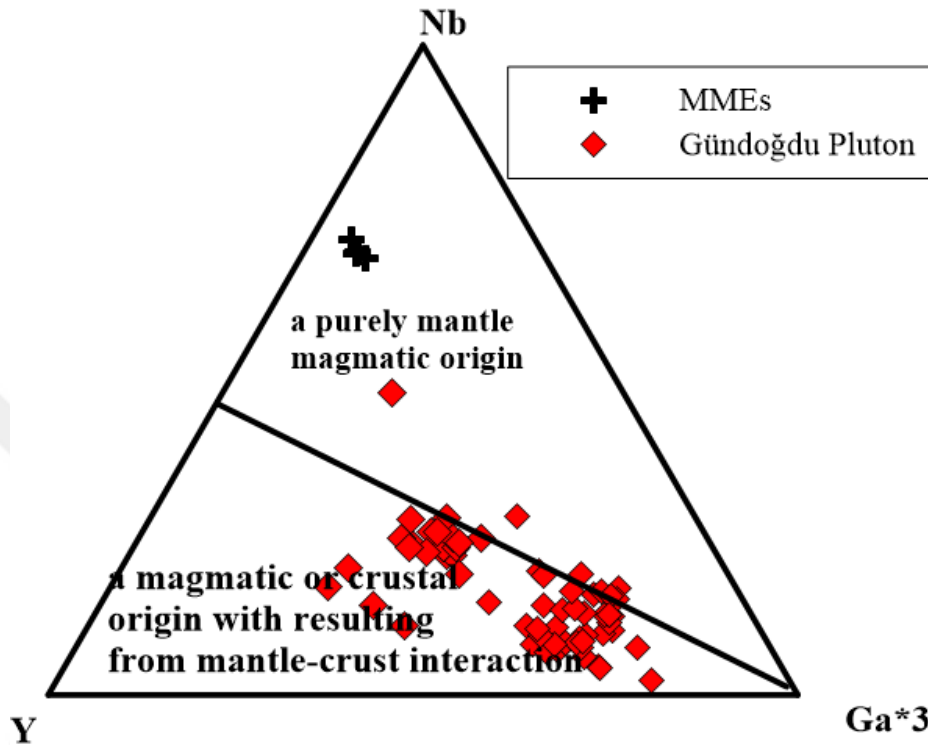


Figure 68. Diagrams of Nb–Y–Ga\*3 (Eby, 1992) for Gündoğdu pluton explained the magma source.

The chemical features of the Gündoğdu pluton is appropriate with the origin by dehydration melting of mafic lower crustal rocks because it has approximately high  $K_2O/Na_2O$ , Mg#,  $Al_2O_3/(FeO_{total} + MgO + TiO_2)$ , and low  $CaO + FeO_{total} + MgO + TiO_2$  (Figure 69). According to the diagrams of (Figure 69) the source of the magmas forming the Gündoğdu Pluton might be the partial melting product of metagreywackes and partially amphibolitic rocks. The contribution of a mantle-derived component can be investigated by chemical composition of MMEs which they have relatively low silica content (44–52%) and relatively high Mg# (27–34). The Gündoğdu granitoid rocks and their MMEs share the properties in terms of mineral content, mineral compositions and correlations between major and trace elements and that might also indicate that MME are fragments of early-crystallizing, chilled magma that was split from the conduit walls

through the later intrusion of the same magma body (Karsli et al., 2012; Kaygusuz et al., 2014).

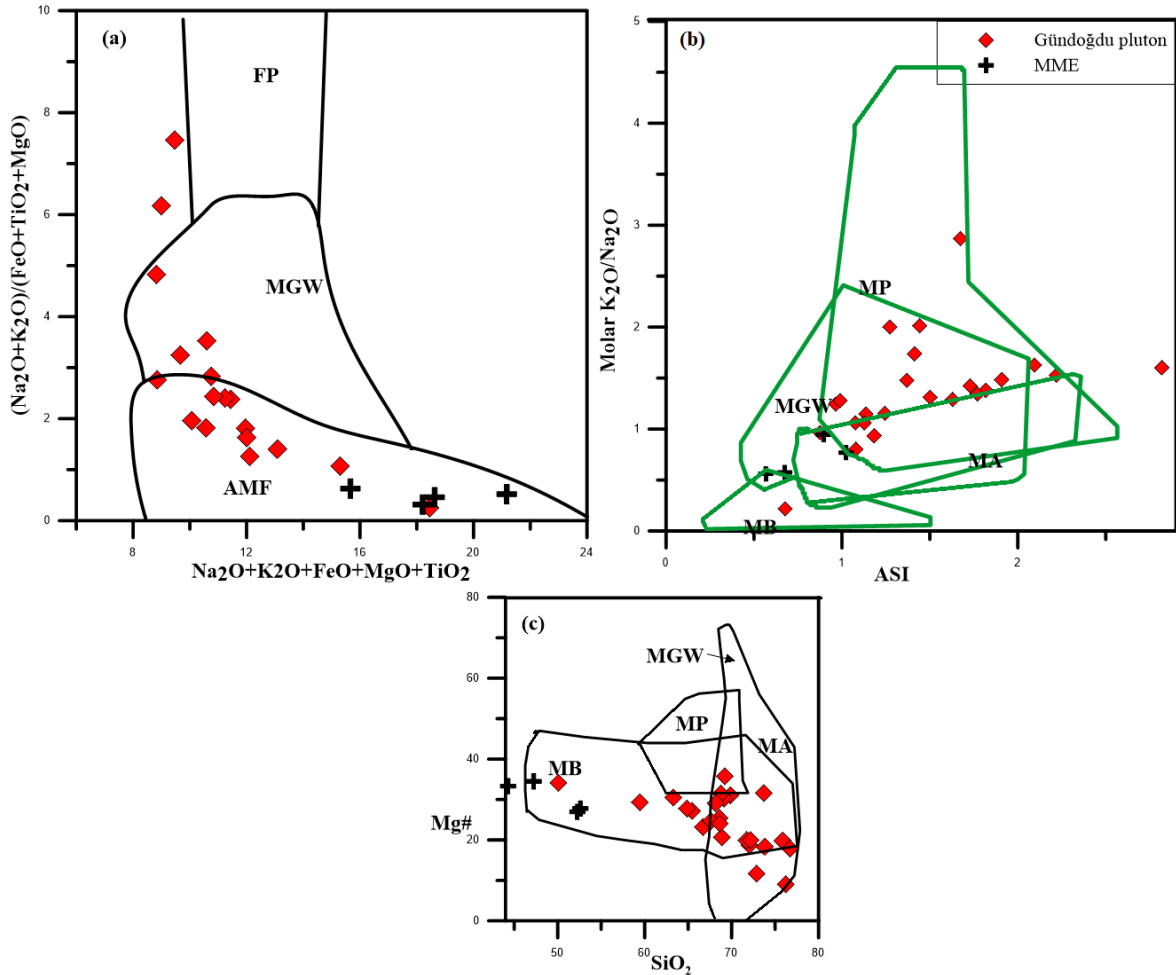


Figure 69. Chemical composition of the Gündoğdu plutonic rocks. (a)  $(\text{Na}_2\text{O}_3+\text{K}_2\text{O}+\text{FeO}+\text{MgO}+\text{TiO}_2)$  vs  $(\text{Na}_2\text{O}_3+\text{K}_2\text{O})/(\text{FeO}+\text{TiO}_2+\text{MnO})$ , (b) ASI vs Molar  $\text{K}_2\text{O}+\text{Na}_2\text{O}_3$ , (c)  $\text{SiO}_2$  vs Mg#. Abbreviation, MB: metabasalts; MA: meta-andesites; MGW: metagreywackes, MP: metapelites; AMP: amphibolites. Sources of data: Vielzeuf and Holloway (1988), Patinˆo Douce and Johnston (1991), Rapp et al. (1991), Gardien et al. (1995), Rapp (1995), Rapp and Watson (1995), Patinˆo Douce and Beard (1996), Stevens et al. (1997), Skjerlie and Johnston (1996), Patinˆo Douce (1997, 1999), Patinˆo Douce and McCarthy (1998).

To define the possibility of magma mixing that took place within Gündoğdu pluton, the researcher proceed isotopic modeling using a simple mixing model by using the lower crust and the mantle as the end members (Figure 75). The parent magma detected from the basaltic mantle was theoretically supposed to represent the mafic end-member and represented by basalt sample of atak Formation (Aydin et al., 2016). Genesis sample of

Pazarcık formation (Şen et al., 2018) from Paleozoic aged in the Eastern Pontides is supposed to be represente the magma derived from the lower continental crustal end member. The isotopic modeling scheme displays a mixing line of Sr and Nd isotop plotted between mantle and local lower crust end-member compositions (Figure 75).

The Gündoğdu samples plot scattered randomly on a curve, suggesting a different petrogenetic processes in addition to magma mixing such crustal contamination. AFC plays role with magma mixing process and fractional crystallization processes. In the diagram of Sr–Nd, different mixing ratios ( $f = 0.1$  to  $0.9$ ) exhibited from depleted mantle (DM) towards lower continental crust (LCC) end-members (Figure 75). Sr–Nd isotope modeling for Gündoğdu Pluton is consistent with a mixed origin 65-60% of lower crust and 35-40% of mantle derived magma. The Sr–Nd isotope modeling of Gündoğdu Pluton indicates that different source and that the magma forming the Gündoğdu Pluton is isotopically homogeneous, but chemically heterogeneous. The possibility of AFC for Gündoğdu pluton was tested using equation of (Depaolo 1981). The “r” value represents the ratio of fractional crystallization to mass assimilation. In the Sr–Nd diagram (Figure 75), some samples plotted between the AFC trajectories drawn for  $r = 0.1$  and  $0.5$ , indicating to small effect of crustal assimilation. The other samples were plotted randomly and suggesting a minor effect of assimilation in the evolution of this pluton and the source are heterogeneous.

### 4.3. Boğalı Pluton

Different tectonic diagrams are used here to identify the tectonic setting of the Boğalı plutonic rocks with their MMEs. According to the diagram of the Nb versus Y or diagram of Ta versus Yb of Pearce et al., (1984) both rocks and MMEs plotted in the field of volcanic arc granite (VAG) with syn-collisional granites (Syn-COLG) and field of volcaic arc granite VAG respectively (Figure 70a, b). Most sample displays low ratio of Sr/Y with enrichment of Y content and they plotted in the field of modern volcanic arc in the diagram of Sr/Y vs. Y and Ta vs Yb diagram (Figure 70b, c). The degree of arc maturity of Boğalı pluton are related to the abundance of incompatible elements (Brown et al., 1984). The diagram of Nb versus Rb/Zr displays all of granitoid rocks of Boğalı pluton and their MMEs plotted in the field of normal arc (Figure 70d), and the samples of



studied rocks assign to normal continental arc, because arc maturity, from primitive to mature can be represented by the high ratio of Rb/Zr and increasing the amount of Nb.

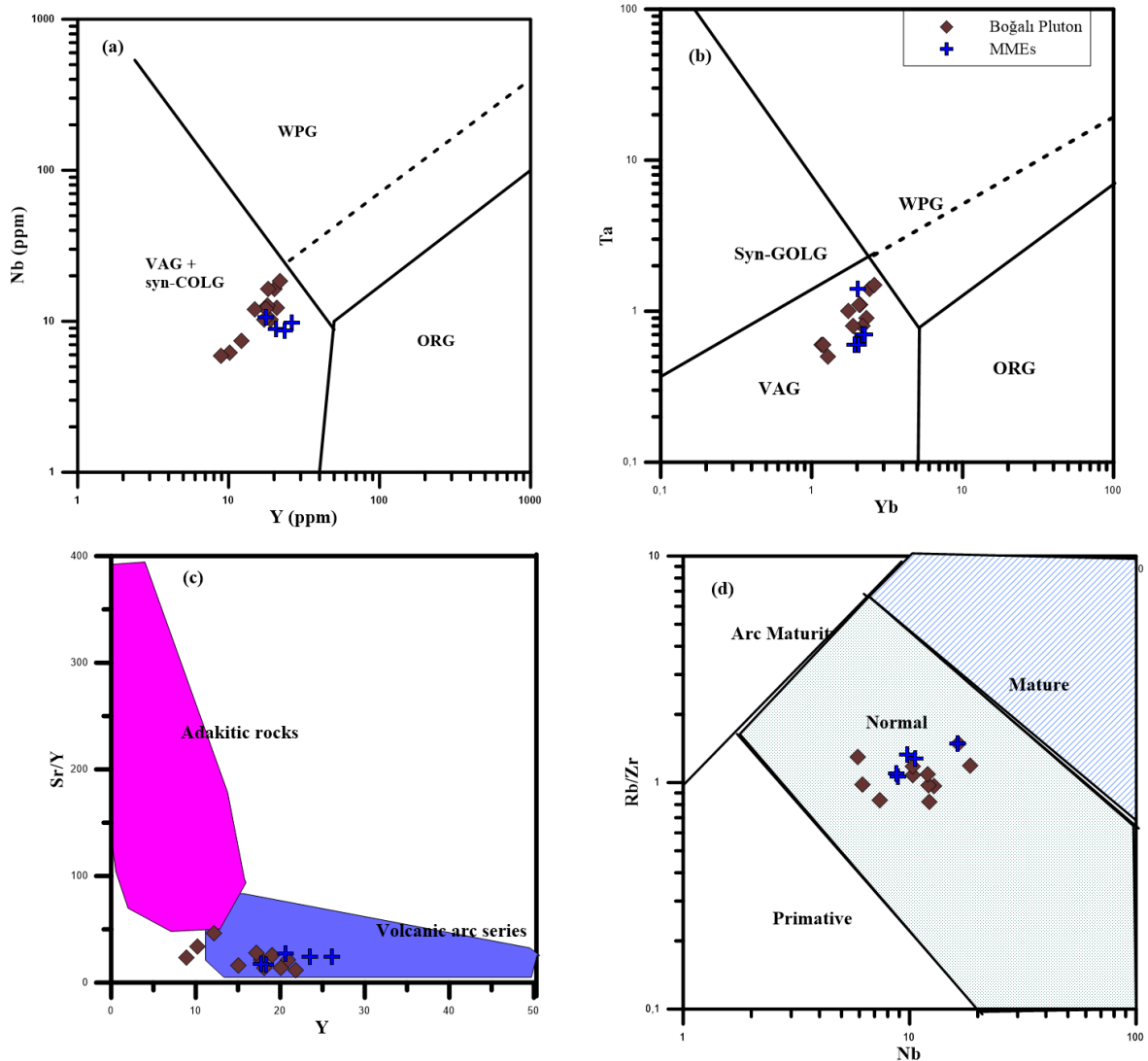


Figure 70. (a, b) discrimination diagrams of Nb vs Y and Ta vs Nb (Pearce *et al.* 1984) of Boğalı pluton, (c) Sr/Y– Y for samples from the Boğalı pluton. (d) Nb vs Rb/Zr diagram (Brown *et al.* 1984). Abbreviation; volcanic-arc granites (VAG), syn-collisional granites (Syn-COLG), within-plate granites (WPG) and ocean-ridge granites (ORG).

The Petrographical and petrochemical properties of Boğalı plutons indicated to produce by mixing of different sources at different degrees of partial melting. The petrographical indicators of the effect of magma mixing during the evolution of the Boğalı pluton can be investigated by existence of MMEs and disequilibrium textures such as sieve in the granitic rocks. Hornblende phenocrysts partly fragmented and with eroded edges and

sometimes skeletal structure indicates that the magma mixture can be effective in the development of these rocks (Figure 73c and d).

Geochemically, the considerable overlap of the data points of the host rock and their MMEs in the diagram of  $\epsilon\text{Nd}$  (85 Ma) vs  $I_{\text{Sr}}$  (82 Ma) indicated to the importance of mixing processes as primary processes (Figure 54a). The isotope analysis in term od Sr and Nd of Boğalı granitic rocks and their MMEs displays variation where host rocks have ( $I_{\text{Sr}} = 0.7061\text{--}0.7063$ ) and MMEs ( $I_{\text{Sr}} = 0.7060$ ) whereas  $\epsilon\text{Nd}_{(t)}$  values ( $-5.1$  to  $-3.9$ ) for the host rocks and  $-5.3$  for the MMEs (Table 9; Figures 54a) indicating to magma mixing and autolith hypotheses. The contribution of mantle material during the generation of pluton can be detected by the increasing the value of  $\epsilon\text{Nd}_{(t)}$  from the MMEs to their host rocks. Moreover, the plots of the element compositions versus isotopic compositions can be used as indicator for magma maxing (e.g., Thirlwall and Jones 1993; Chen and Arakawa 2005; Karsli et al., 2010).

Linear correlations between  $\text{SiO}_2$  versus some of trace element like Rb, Zr,Ti and Zr are indicators of magma mixing processes (Perugini et al. 2004; Karsili et al. 2010;2012). The hyperbolic arrays in the diagram of Rb/Sr vs. Ti/Zr (Figure 71a) and linear correlation between Sr/Zr versus Ti/Zr (Figure 71b) of Boğalı samples explains the mixing processes between two distinct geochemical end-members (i.e. mantle related magmas and components of lower continental crustal). Considering the isotopic data of the samples,  $^{144}\text{Nd}/^{143}\text{Nd}_{(i)}$  ratio and  $^{87}\text{Sr}/^{86}\text{Sr}_{(i)}$  ratios of the Boğalı pluton in comparsion with Gündoğdu pluton exhibited different characterize. It exhibited week correlation with  $\text{SiO}_2$  indicating to insignificant effect of crustal assimilation during the magma genesis (Figure 72a–c). These trends indicating that fractional crystallization and partial melting represents the primary processes during the magma genesis.

Fractional crystallization represents the most important stage during the generation of Boğalı pluton. Major oxide and trace element exhibted negative or positive correlations with increasing of  $\text{SiO}_2$  contents, and that is indicating to the significant of Fractional crystallization during the evolution of magma.

The chemical analysis of Boğalı pluton displays an increasing of  $\text{SiO}_2$  with decreasing MgO, CaO and  $\text{Al}_2\text{O}_3$  indicate fractional crystallization of plagioclase, hornblende and biotite. The positive and negative correlation with increasing of  $\text{SiO}_2$  content indicated to fractional crystallization processes of some phases, which the decreasing of  $\text{TiO}_2$  and  $\text{Fe}_2\text{O}_3$  with increasing  $\text{SiO}_2$  indicates to fractionation of magnetit

and Fe-Ti oxides. The negative correlation between SiO<sub>2</sub> and P<sub>2</sub>O<sub>5</sub> indicates fractional crystallization of apatite.

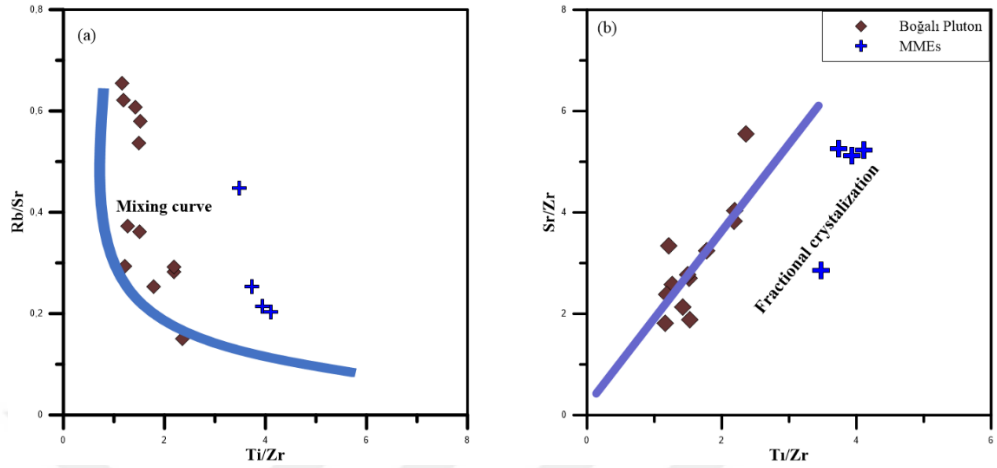


Figure 71. (a) Diagram of Rb/Sr vs. Ti/Zr, (b) linear correlation between Sr/Zr vs Ti/Zr for Boğalı pltonic rocks indicating to mixing process.

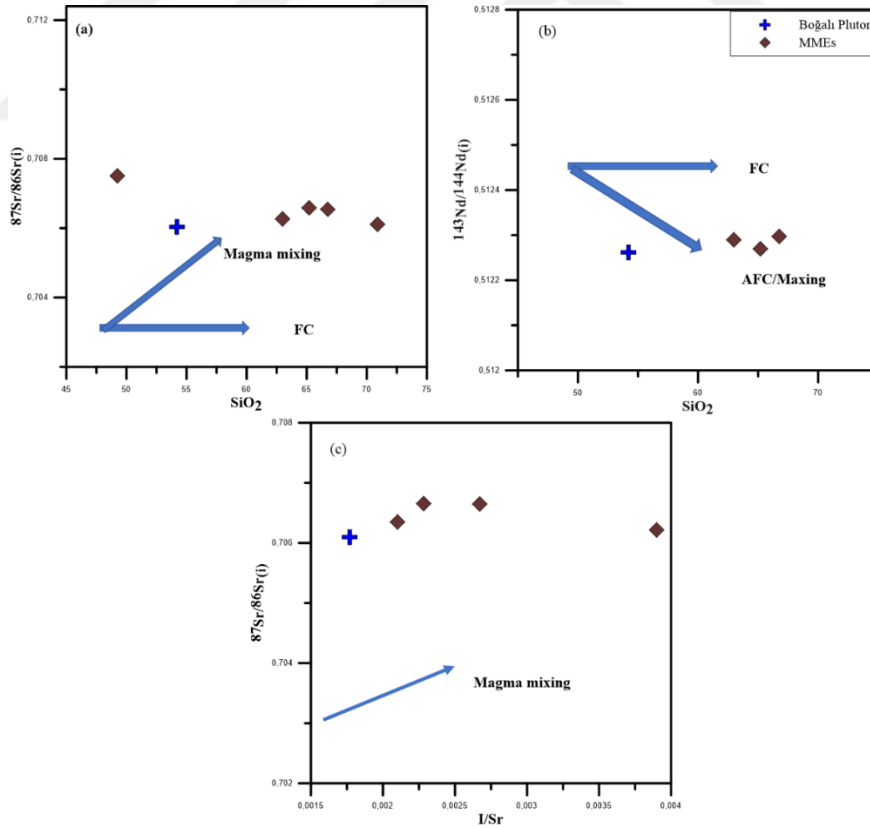


Figure 72. (a) SiO<sub>2</sub> vs I<sub>Sr</sub> (82 Ma); (a) SiO<sub>2</sub> vs eNd (82 Ma) and (c) 1/Sr vs I<sub>Sr</sub> (82 Ma) for the Boğalı pluton. Abbreviations, AFC: Assimilation Fractional Crystallization FC: Fractional Crystallization

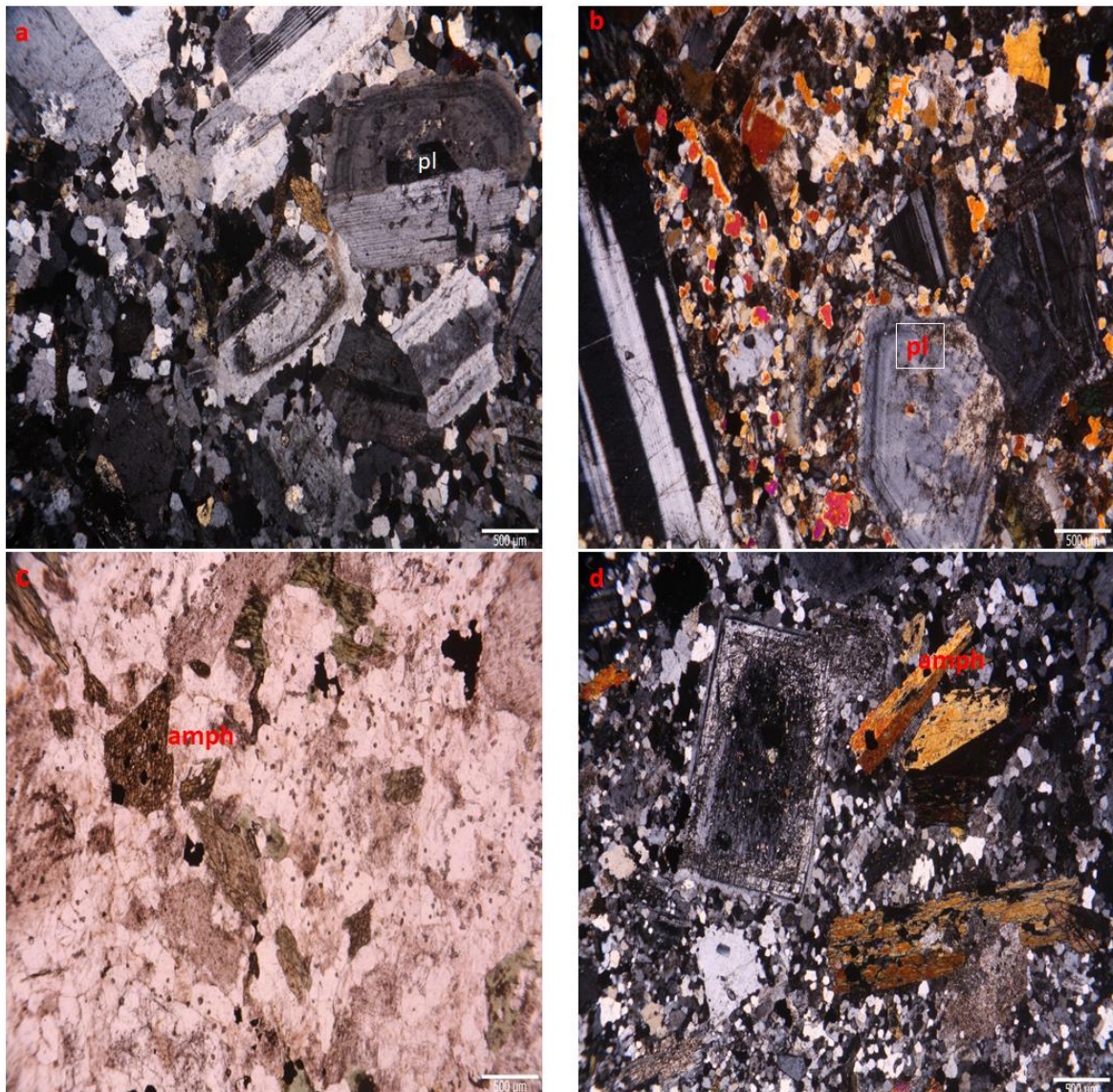


Figure 73. Microphotographs of the Boğalı plutonic rocks (a, b) plagioclase with sieve texture showing the change of composition, (c, d) hornblende with eroded edges and skeletal structure.

The positive correlation between  $K_2O$  and Rb with  $SiO_2$  indicates to fractionation of K-feldspar and biotite and indicating to late-fractionation phases. The variation of major and trace element provided by the depletion of Ba, Sr, and Eu anomalies indicates to fractional crystallization of some common phases. The increasing of  $SiO_2$  with increasing of negative Eu anomalies and decrease of Sr leads to fractional crystallization of plagioclase and/or K-feldspar and indicate that plagioclase represent the most important phase. The increasing of  $K_2O$ , Rb, Ba and decreasing of  $Al_2O_3$ ,  $TiO_2$ , CaO, MgO,  $Fe_2O_3$ ,



P<sub>2</sub>O<sub>5</sub>, Sr with increasing SiO<sub>2</sub> related to the fractional crystallization of common phases such as plagioclase, K-feldspar, amphibole, biotite, apatite and titanite (Figures 50 and 51).

An accessory minerals such as zircon, magnetite and titanite has been crystallized as result to the depletion in Zr and Y. The fractional crystallization of titanite can be related to the negative Ti anomalies in spidergrams. The negative anomalies of Ti may have been result of crustal contamination. The negative anomalies of Nb–Ta, positive anomalies of Pb, enrichment of LILE element relatively to HFSE indicated to subduction signature and contribution of continental crust in the generation of magma because the fractionated continental crust will lead to depletion of Nb-Ta and enrichment of LREE, flat HREE, and a positive anomaly of Pb (Taylor and McLennan, 1985). The Boğalı pluton characterized high Th (9-35ppm) and Pb (5.3-19.1 ppm) and that is indicated to the effect of crustal contamination during the magma evolution (Taylor and McLennan, 1985). The effects of assimilation can be evaluated by ratio of isotopic and elemental. The weak correlation in the diagram SiO<sub>2</sub>, vs <sup>87</sup>Sr/<sup>86</sup>Sr<sub>(i)</sub> and diagram of SiO<sub>2</sub> vs <sup>143</sup>Nd/<sup>144</sup>Nd<sub>(i)</sub> (Figure 72a, b and c), indicating to negligible effect of assimilation process during generation of the rocks.

The samples of the Boğalı pluton are High-K to shoshonitic and I-type in compositions result of mixing of different sources such as meta-igneous rocks including lower/middle crustal or subcontinental mantle sources (Chappell and White, 1992; Roberts and Clemens, 1993; Kaygusuz et al 2014). The Boğalı plutonic rocks displays weak REE fractionation ((La/Yb)<sub>N</sub> = 3.2 to 12.7 for most of granitoid samples and one monzogranite rocks has (18.6), low Sr/Y ratios (11 to 34) for most of granitoid samples and one monzogranite rocks has (46) and the highest of Y contents (8 to 26 ppm) and Yb (1.1 to 2.35 ppm) (Table 8). It is also characterized by broad range of silica content (SiO<sub>2</sub> = 63. – 70.88 wt %), relatively low Mg# (18–29).

As mentioned above the negative Nb anomalies and other HFSE are characteristics of magma created in the subduction zone. All these features indicate to magma obtained from mixing of lower crust and mantle-derived magmas ((e.g. McCulloch and Gamble, 1991; e.g., Barbarin, 1999; Karsli et al., 2010a; Kaygusuz et al 2014). The appearance of MMEs in the Boğalı plutonic rocks are another indicator of mixing/mingling of mafic and felsic magmas (Barbarin and Didier, 1992; Vernon, 1990; Dokus et al 2010). The samples of Boğalı Granitoid rocks displays vast range of Y/Nb ratios (1.6-2,7), indicating to magma has crustal and mantle origin. The Boğalı plutonic rock also displays Nb/Ta ratios varies from 9.8 to 14.8 and these values provided the suggestion of crustal- and mantle-

related magmas because the average Nb/Ta ratios in mantle-derived magma are 17.5 whereas the crustal-derived magmas are 11–12 (Green, 1995; Kaygusuz et al 2014). MMEs displays the Nb/Ta ratios range (14–15.14) which are similar to their host rocks.

However, the Boğalı pluton characterize by  $^{87}\text{Sr}/^{86}\text{Sr}$  isotope ratios (0.7061-0.7065) and  $\epsilon\text{Nd}_{(i)}$  (-5 to -3.9) more chemically homogeneous than that of Gündoğdu pluton and it is not possible to related to melt generated from a single source. There are, two separate magmas at least can explain the generation of Boğalı pluton. The considerable overlap of the data points of the host rock and their MMEs in the diagram of  $\epsilon\text{Nd}$  (85 Ma) vs  $\text{ISr}$  (82 Ma) indicated to the importance of mixing processes as primary processes (Figure 54a). Pb isotope ratios of the granitoid rocks of this pluton also reflect a small enriched mantle source which can be considered as an end-member of the mixing process in the genesis. In the diagram of  $^{206}\text{Pb}/^{204}\text{Pb}_{(i)}$  vs.  $^{207}\text{Pb}/^{204}\text{Pb}_{(i)}$  and  $^{208}\text{Pb}/^{204}\text{Pb}_{(i)}$  (Figure 54b, c) all of the Boğalı plutonic samples plotted in the lower continental crust field close to the data points from the Camiboğazı and Harşit plutons of late cretaceous aged (Kempton et al., 1997; Karşlı et al., 2010a; Kaygusuz et al., 2014; Karşlı et al. 2010a) have detected that the Harşit pluton represented by mixing source between lower crust as a major component and a subcontinental mantle as a minor component. Kaygusuz et al. (2014) suggested that the generation of Camiboğazı pluton probably related to mixing of amphibolitic-type lower crustal with mantle derived end-members. However, this pluton shares the same feature of Harşit and Camiboğazı plutons indicating the mixing processes between amphibolitic lower crustal as parental magma and lithospheric mantle based on the isotopic signatures and the variation of major and trace element of the Boğalı pluton and their MMEs.

The similarity in petrographical and chemical characterize of MMEs and their host rocks in the Boğalı pluton might also indicate that MME represent a fragment of early-crystallizing, chilled magma that was splited from the conduit walls through the later intrusion of the same magma body (Kaygusuz et al. 2014). The MMEs shown a low silica content (53–54,21%), low Ni content 1,6-3,8 and relatively high Mg# (20–30) in comparison to host rocks and that indicated to contribution of a mantle derived magma. It has been indicated by Roberts and Clemens (1993), that the I-type, High-K granitoids formed as result to partial melting of hydrous, calc-alkaline mafic to intermediate metamorphic rocks in the crust (Roberts and Clemens 1993; Dokuz et al 2010; Karşlı et al 2012). The variation in chemical composition of magmas is produced by partial melting of



different source rocks such as amphibolites, under variable melting conditions (Figure 74). Therefore the variation in chemical composition of the Boğalı pluton is compatible with the origin by dehydration melting from mafic lower crustal rocks because it has approximately high  $K_2O/Na_2O$ , Mg#,  $Al_2O_3/(FeO_{total} + MgO + TiO_2)$ , and low  $CaO + FeO_{total} + MgO + TiO_2$  (Figure 74a,b and c). According to the ternary diagram of Nb–Y–Ga\*3 (after Eby, 1992), this pluton has been generated as a result of mixing between mantle–crust (Figure 74d).

It has been used the simple mixing model to evaluate the possibility of mixing process in the Boğalı pluton by using lower crustal and mantle end members (Figure 75). The basalt sample of Çatak Formation (Aydın et al 2016), has been assumed to represent the mafic end-member of the average parent magma from the isotopically basaltic mantle products whereas lower continental crustal end member represented by genesis sample of Pazarçık formation from Paleozoic aged (Şen et al., 2018). The isotopic modeling scheme displays a mixing line of Sr and Nd isotope plotted between mantle and lower crust end-member compositions (Figure 75). The Boğalı samples plotted on a curve suggests a magma mixing process. In the Sr–Nd diagram, displays different mixing ratios ( $f = 0.1$  to  $0.9$ ) from depleted mantle towards lower continental crust end-members and indicated that the Boğalı pluton has mixed origin with a parental magma contain ~25–35% from lower crustal and ~65–75% from mantle.

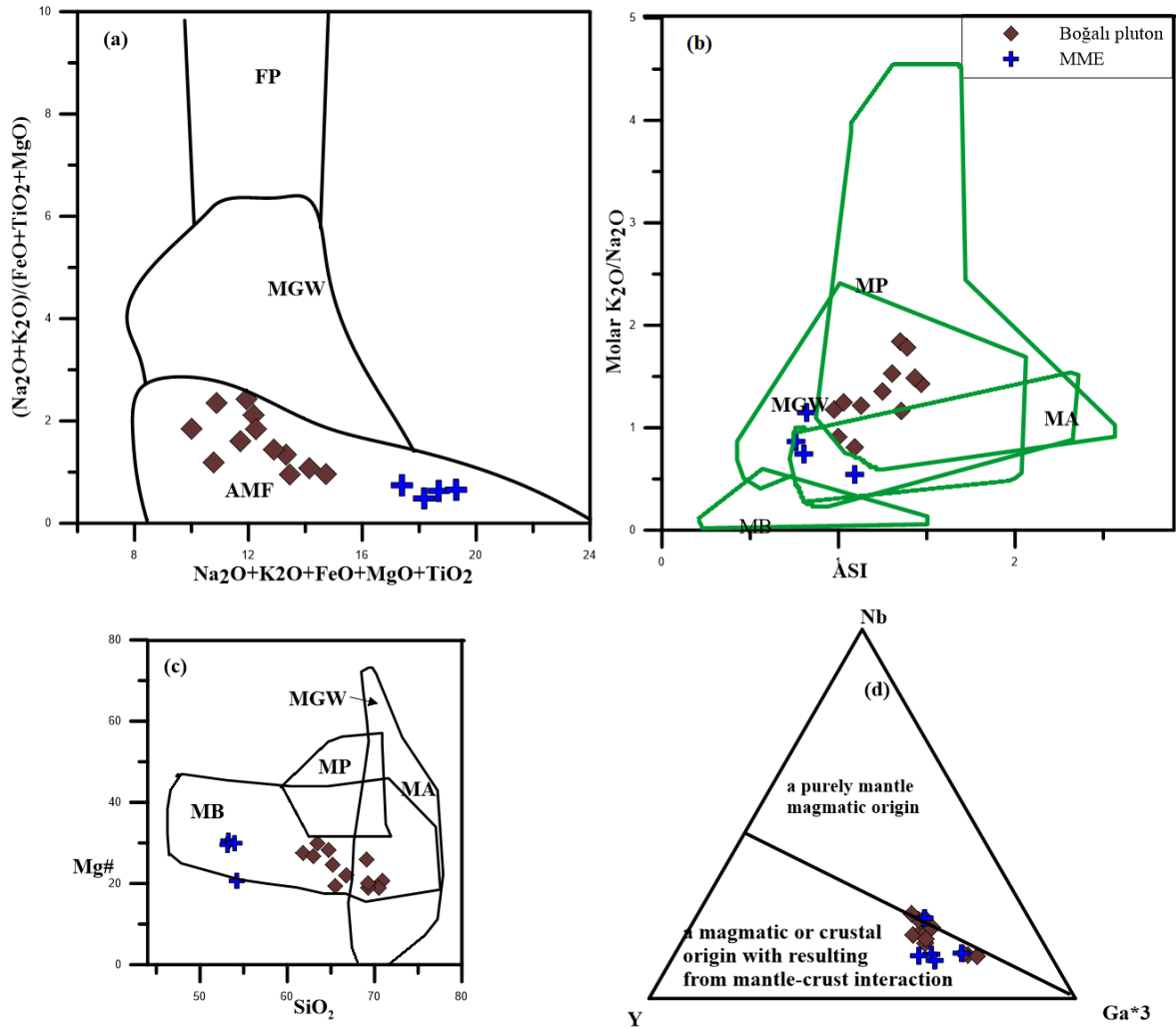


Figure 74. Chemical composition of the Boğalı plutonic rocks, (a)  $(\text{Na}_2\text{O}_3+\text{K}_2\text{O}+\text{FeO}+\text{MgO}+\text{TiO}_2)$  vs  $(\text{Na}_2\text{O}_3+\text{K}_2\text{O}) / \text{FeO}+\text{TiO}_2+\text{MnO}$ , (b) ASI vs Molar  $\text{K}_2\text{O}+\text{Na}_2\text{O}_3$ , (c)  $\text{SiO}_2$  vs Mg#, (d) Nb–Y–Ga\*3 (Eby, 1992). Different diagrams for samples from the Boğalı pluton explained the magma source. Abbreviation, MB: metabasalts; MA: meta-andesites; MGW: metagreywackes, MP: metapelites; AMP: amphibolites. Data sources: Vielzeuf and Holloway (1988), Patinˆo Douce and Johnston (1991), Rapp et al. (1991), Gardien et al. (1995), Rapp (1995), Rapp and Watson (1995), Patinˆo Douce and Beard (1996), Stevens et al. (1997), Skjerlie and Johnston (1996), Patinˆo Douce (1997, 1999), Patinˆo Douce and McCarthy (1998).

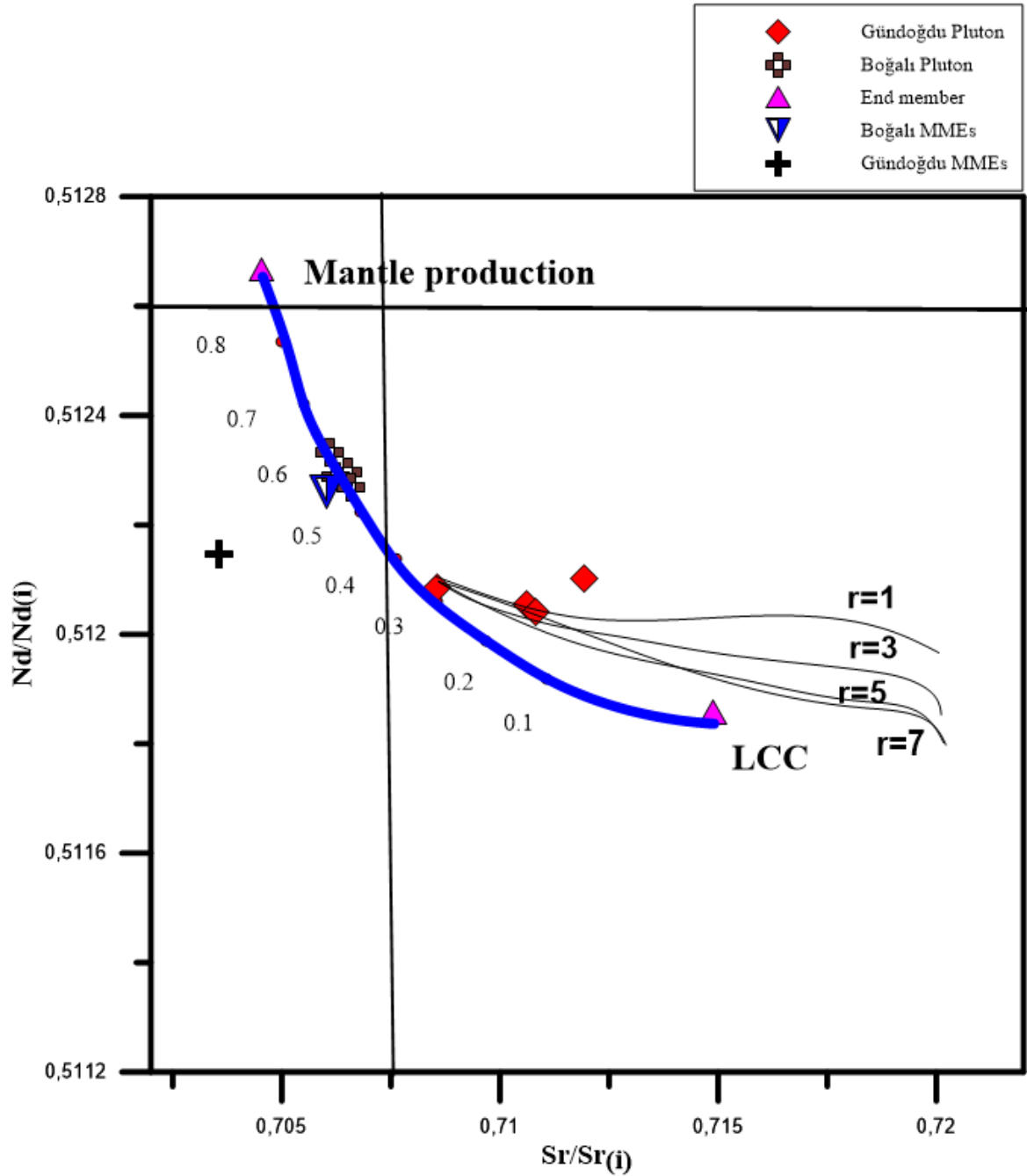


Figure 75.  $^{143}\text{Nd}/^{144}\text{Nd}(i)$  vs  $^{87}\text{Sr}/^{86}\text{Sr}(i)$  plot for samples from the Boğalı and Gündoğdu plutons with simple source mixing lines between Basaltic mantle (BM; Aydın et al., 2017) and local lower crustal (LCC, Gnesis of a Paleozoic age from Tübitak 114Y219, 2018) end members by using two component equation of (Langmuir et al, 1978) and AFC equation of (Depaolo 1981), UUC from Taylor and McLennan (1985).

#### 4.4. P-T Conditions of Crystallization and Emplacement

The changing of pressure (P), and temperature (T) strongly influence crystallization history and mineral compositions in magmatic systems. The P-T are calculated by using the minerals chemistry of plagioclase, clinopyroxene, hornblend and major oxides of zircon and apatite saturation in order to determine the emplacement depths and thermal history of these magma.

##### 4.4.1. Taşlyayla Volcanic Rocks

The graphical method of the Or-Ab-An ternary feldspar isotherm diagram of Fuhrman and Lindsley (1988) has been used to determine the geothermometric estimation (Figure 76). The composition of plagioclase from basalt and andesite shown on a ternary diagram of Or-Ab-An reflected that plagioclase in the core as composition of bytownite (An<sub>80-85</sub>) or in the center as composition of labradorite (An<sub>40-60</sub>) plotted within the 650–700°C temperature curves, whereas in the rim as orthoclase (Or<sub>55-88</sub>) plotted within the 750–800°C temperature curves (Figure 76).

Thermobarometers using clinopyroxene-liquid equilibria equation of (Putirka et al. 1996; Putirka and Condit 2003; Putirka 2008) to determine the crystallization temperatures and depths. Results from clinopyroxene-liquid thermobarometers reflect average pressure and temperature for basaltic rocks equal to (mean =  $8.9 \pm 1.2$  kbar and  $1269 \pm 19^\circ\text{C}$ ; Table 12) which is higher than those of andesitic rocks (mean =  $5.6 \pm 0.9$  and  $1224 \pm 12^\circ\text{C}$ ; Table 12).

Chlorite represent one the volcanic rocks minerals that formed as result to plutonic intrusions. The chlorite temperature estimated based on equations of Cathelineau (1988) and Jowett (1991) and reviewed in table 13. The estimated chlorite temperature for Taşlyayla Volcanic rock ranged between 235-380 T (°C)-Jowett, 213-386 T (°C)-Cathelineau for basaltic rocks whereas the andesitic rocks of same intrusion formed in temperature between 225-257 T (°C)-Jowett, 230-251 T (°C)-Cathelineau.

Table 12. Comparison of calculated P (kbar) and T (°C) conditions after Putirka (2008) using c clinopyroxene liquid in basaltic and andesitic rocks from the Taşlıyayla volcanic rocks (Arakli) area.

Rocks	Number of samples	Mean T (°C)	Max T(°C)	Min T(°C)	Max P (kbar)	Min P (kbar)	Mean P (kbar)
Basaltic	22	1269	1300	1215	12± 1	4± 1.	8,9± 12
Andesitic	20	1224	1291	1173	11.4	0.44	5.6

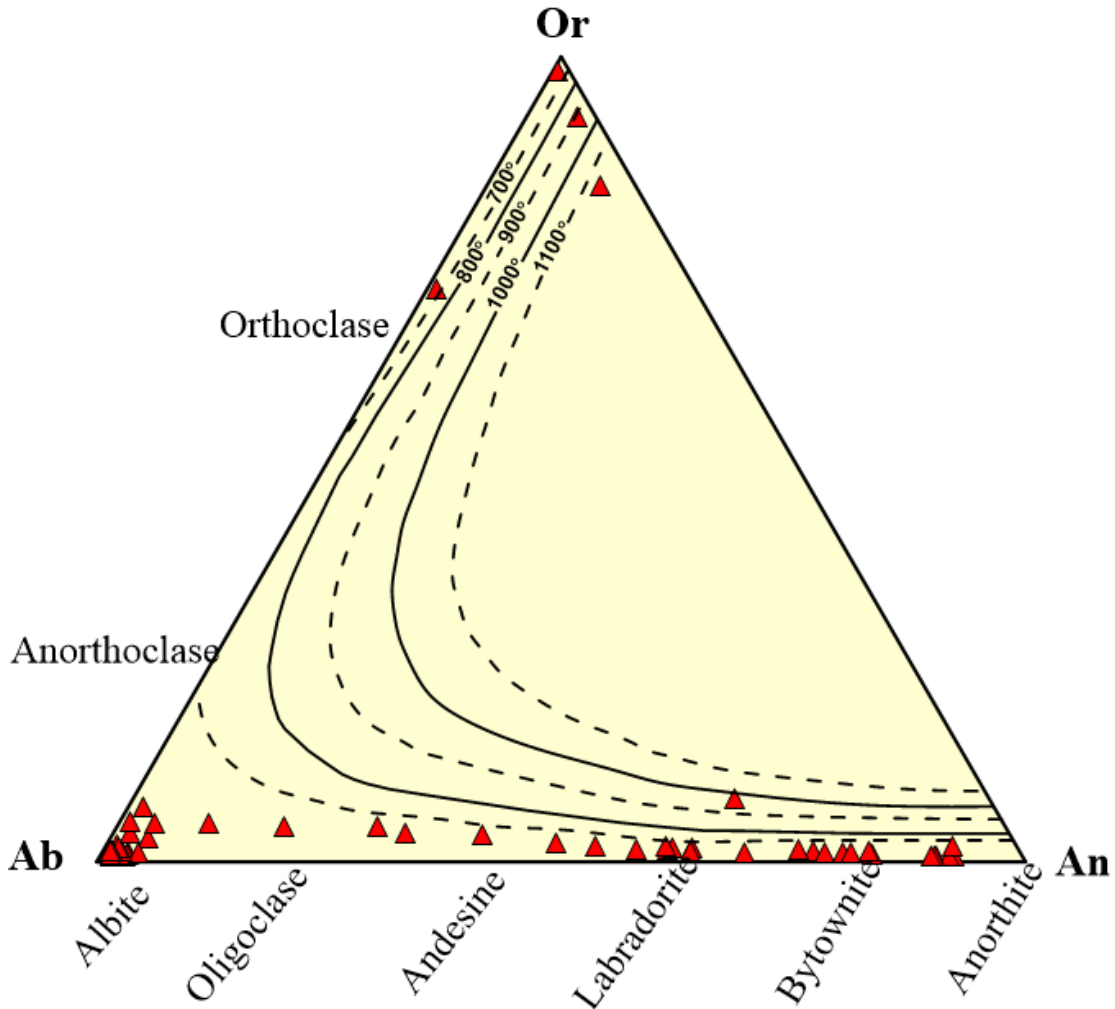


Figure 76. Ternary diagram An–Ab–Or by using the method of (Fuhrman and Lindsley 1988) for the feldspar compositions.

Table 13. Chlorite temperature according to Cathelineau (1988).

Rocks	Number of samples	Mean T (°C) Cathelineau	Min T(°C) Jowett
Basaltic	22	380±	386±
Andesitic	20	245±	250±

#### 4.4.2. Gündoğdu and Boğalı Pluton

The chemical composition of plagioclase from Monzogranit, Diorite, and MMEs (Quartz monzodiorite and monzodiorite) of Gündoğdu pluton on a ternary diagram of Or-Ab-An displays plagioclase samples lies within the 600–700°C temperature curves for composition (An<sub>11-66</sub>), whereas plagioclase in the rim as composition of orthoclase (Or<sub>57-85</sub>) lies within the 650–800°C temperature curves, implying the mixing/mingling of mafic and felsic magmas (Table 14; Figure 77). The Boğalı pluton review same thermometry fearurs similar to that of Gündoğdu pluton but the plagioclase in the rim as composition of orthoclase (Or<sub>57-85</sub>) lies within the 600–650°C temperature curves.

It showed by Piccoli and Candela (1994), (Watson and Green, 1982) and Piccoli et al. (1999) that the apatite crystallization temperature can be estimate by the relationship between the SiO<sub>2</sub> and P<sub>2</sub>O<sub>5</sub> in the initial melt. The minimum temperature for melting determines by this diagram SiO<sub>2</sub> and P<sub>2</sub>O<sub>5</sub> and it is 750-850 for Gündoğdu pluton and lower than 750 Kbar whereas 800-950 for Boğalı pluton lower750 Kbar. The minimum temperature for melting for MMEs of Gündoğdu pluton ranged from 700 to 800 and lower 750K bar whereas MMEs of Boğalı Pluton ranged 800 to 850 and lower 750 Kbar (Figure 78).

Zircon saturation temperatures are calculated major oxides data to detecte temperatures and the effect of composition crustal magma types by using experimental models of the Miller et al. (2003) with the parameters  $M = \frac{[Na + K + 2Ca]}{[Al \times Si]}$  of Watson and Harrison (1983).



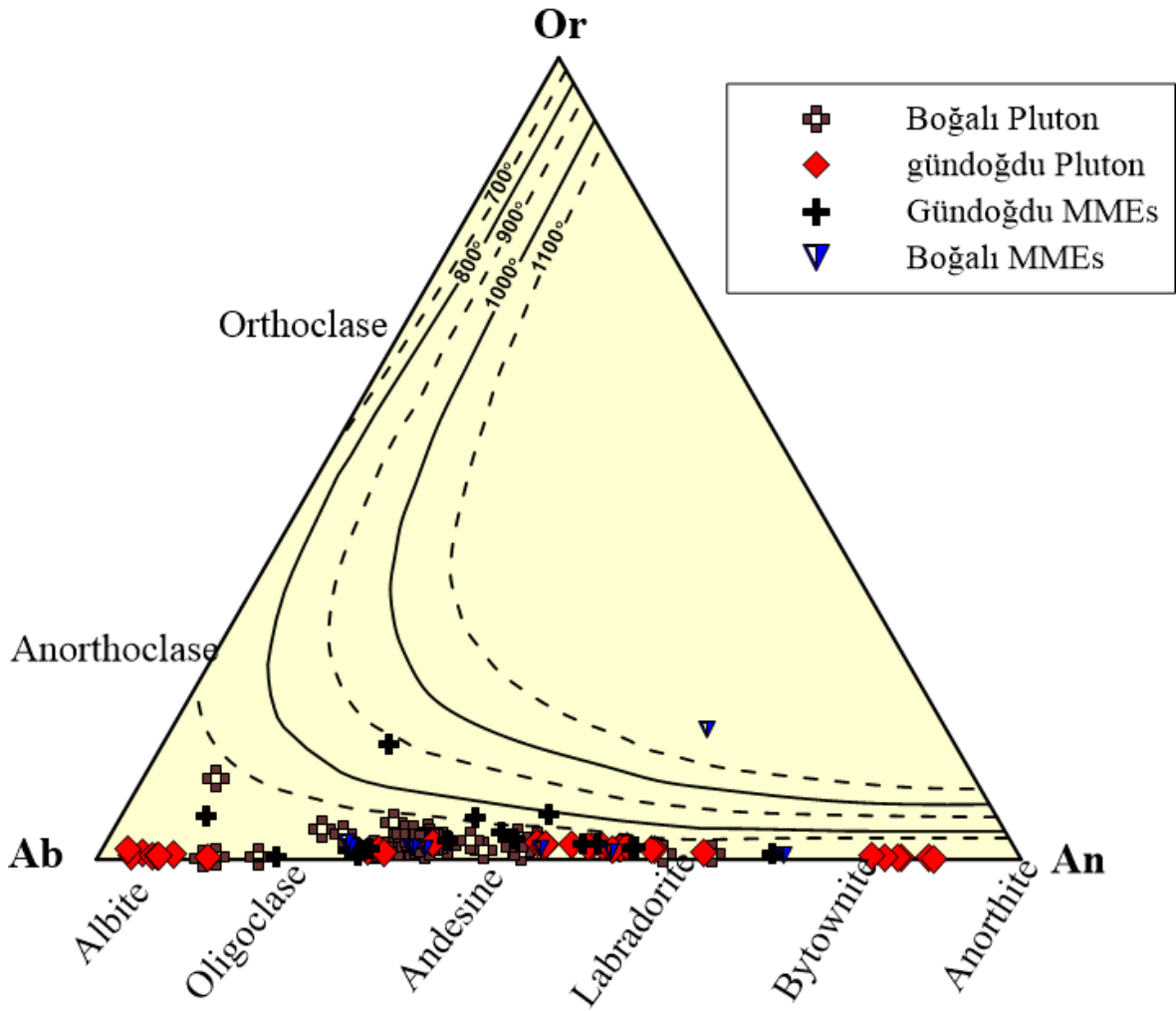


Figure 77. Ternary diagram of An–Ab–Or using the method of (Fuhrman and Lindsley 1988) for the feldspar compositions. Symbols as figure 65

The estimated zircon saturation T (°C) temperatures of (Miller et al. 2003) for Gündoğdu plutonic rocks ranging from 663°C to 835 °C (mean = 765± 5°C) and ranging from 610°C to 695°C (mean = 678 ± 3°C) for their MMEs which is a little bit lower temperature than those of host rocks (Table 14). The estimated zircon saturation T (°C) temperatures of (Miller et al. 2003) for Boğalı plutonic rocks ranging from 726°C to 767°C (mean = 749± 5°C), (Table 14). The estimated zircon saturation temperatures for MME of Boğalı pluton, are ranging from 687°C to 730°C (mean = 701 ± 3°C), they are lower than those of host rocks (Table 14).

The application of Al<sup>(IV)</sup> and Al<sup>T</sup> in hornblende, are used to estimate both thermometer and barometer, respectively, which supports information on terms of

temperatures and pressures that existed during the emplacement of magma within the crust. The pressures obtained from Gündoğdu pluton using the Al content of hornblende (P4; Schmidt 1992) range from 3.93–1.63 kbar (mean =  $2.80 \pm 0.1$  kbar). Additionally, pressures estimated by the various calibrations for granitoid rocks range from 3.4–1.4 kbar (mean =  $2.21 \pm 0.3$  kbar) (P1; Hammarstrom and Zen 1986), from 0.8–3.46 kbar (mean =  $2.22 \pm 0.1$  kbar) (P2; Hollister et al. 1987), from 2.72– 0.71 kbar (mean =  $1.7 \pm 0.5$  kbar) (P3; Johnson and Rutherford 1989), and from 1.5–3.35 kbar (mean =  $2.22 \pm 1.1$  kbar) (P5; Anderson and Smith 1995), respectively (Table 15).

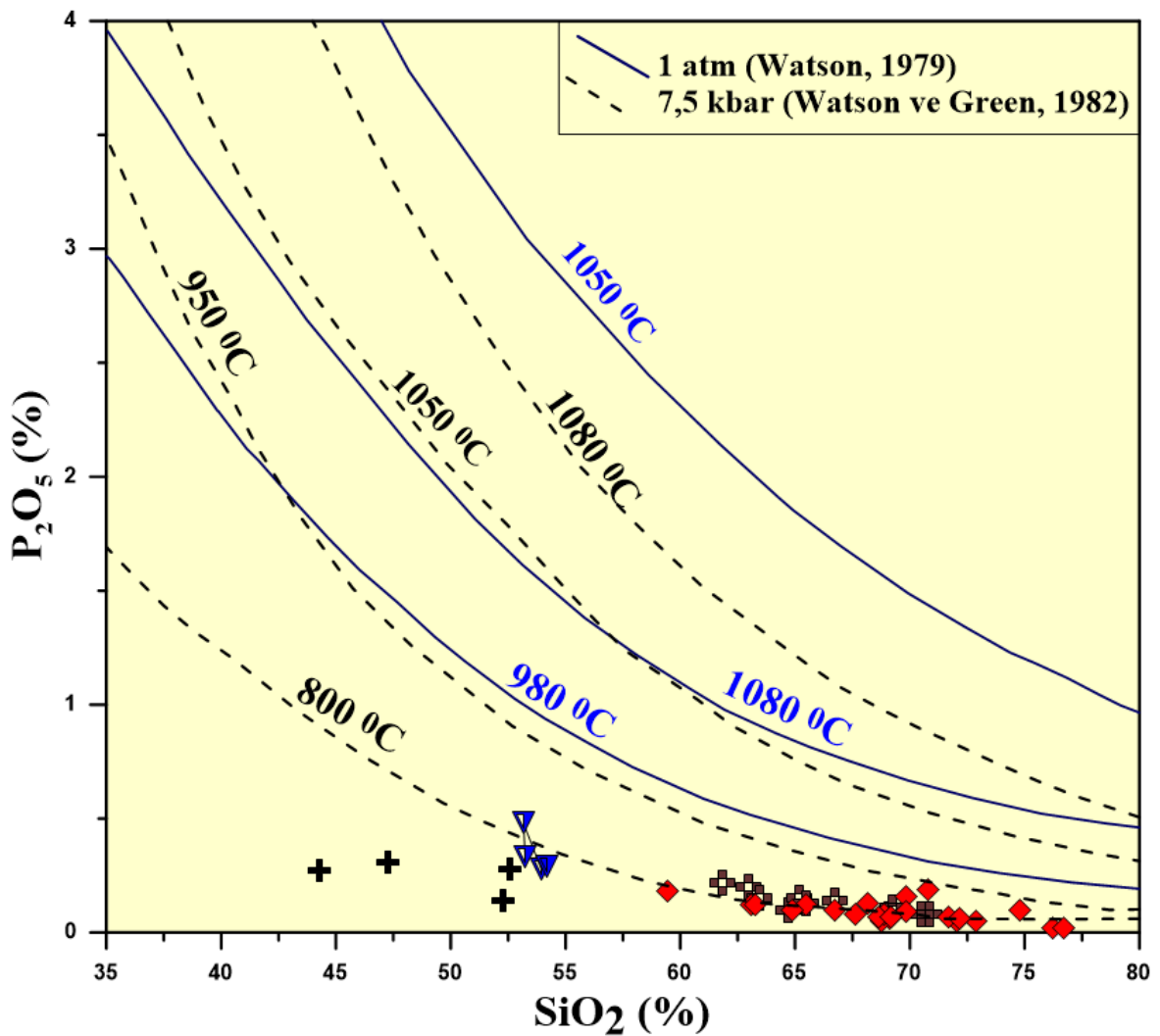


Figure 78. The minimum temperature for melting by this diagram SiO<sub>2</sub> and P<sub>2</sub>O<sub>5</sub> according to pressure (Watson ve Green, 1982). Symbols as in Figure 65.

The obtained pressures from Boğalı pluton and their MMEs using the Al content of hornblende (P4; Schmidt 1992) range from 9.39–1.35 kbar (mean =  $5.50 \pm 2.1$  kbar) to 1.15–3.06.83 kbar (mean =  $2.11 \pm 0.3$  kbar), respectively. Additionally, pressures estimated by the various calibrations for granitoid host rocks and MMEs range from 2.60–9.3 kbar (mean =  $5.07 \pm 0.3$  kbar) to 2.5–0.9 kbar (mean =  $1.49 \pm 0.3$  kbar) (P1; Hammarstrom and Zen 1986), from 10.2–1.27 kbar (mean =  $5.32 \pm 0.1$  kbar) to 2.44–0.17 kbar (mean =  $1.30 \pm 0.1$  kbar) (P2; Hollister et al. 1987), from 7.35–1.06 kbar (mean =  $4.10 \pm 0.5$  kbar) to 1.94–0.24 kbar (mean =  $1.09 \pm 0.1$  kbar) (P3; Johnson and Rutherford 1989), and from 8.7–1.17 kbar (mean =  $4.77 \pm 1.1$  kbar) to 3.16–1.10 kbar (mean =  $2.05 \pm 1.1$  kbar) (P5; Anderson and Smith 1995), respectively (Table 15). Estimating the temperature from hornblende–plagioclase geothermometry by using calculated average pressures by various calibrations (Blundy and Holland, 1990; Holland and Blundy, 1994) are given in (Table 14). The calculated hornblende–plagioclase temperature obtained from the Gündoğdu plutonic rocks is  $659 \pm 30$  °C whereas in Boğalı pluton is  $637 \pm 28$  °C and their MMEs is  $645 \pm 30$  °C (Table 15). The crystallization depth of gündoğdu pluton based on the mean pressure obtained from hornblende barometry values (1.7–2.8 kbar), approximately equal to 6.2–9.2 km (1 kbar = 3.7 km for the continental crust; Tulloch and Challis, 2000), whereas the Boğalı pluton detected as 15.7–20.3 km because the obtained pressure values (4.10–5.5 kbar. According to hornblende barometry crystallization depth of the Boğalı pluton deeper than Gündoğdu pluton.

Table 14. Comparison of calculated temperatures (T, °C) conditions after Fuhrman ve Lindsley, (1988) for two feldspar, hornblend-plagioclase (Blundy and Holland, 1990; Holland and Blundy, 1994), for Zircon (after Mşller et al,2003), Using whole-rocks major oxides for 7,5 k bar after Watson ve Green (1982) and and lower than 1 atmosphere pressure after Watson (1979).

	Two feldspar	Hornblend-Plagioclase	Whole rock Zr(ppm)	Whole rock P2O5%	
				T (°C) 1 atm	T (°C) 7,5 atm
Günderdu pluton	600-700	659± 3°C	765 ± 3°C	Lower than 950	750-850
MME of Günderdu pluton	600-750		678 ± 3°C	Lower than 950	700-800
Boğalı Pluton	600-700	637± 30°C	749 ± 3°C	Lower than 950	800-950
MME of Boğalı Pluton	600-650	645± 28°C	701 ± 3°C	Lower than 950	800-800

Table15. Comparison of calculated pressures (P, kbar) conditions after Hammarstrom and Zen (1986), Hollister et al. (1987), Johnson and Rutherford (1989), Schmidt (1992), and Anderson and Smith (1995) using hornblendes in Granitoid rocks and MME from the Günderdu and Boğalı plutons.

Formation		Hammarstrom and Zen (1986) P1	Hollister et al.(1987) P2	Johnson and Rutherford (1989) P3	Schmidt (1992) P4	Anderson and Smith (1995) P5
Günderdu Pluton	Max p (kbr)	3.4	3,46	2.7	3.93	3.35
	Min p (kbr)	1.04	0.80	0.71	1.63	1.05
	Mean p (kbr)	2,21	2,22	1,70	2,50	2,22
Boğalı Pluton	Max p (kbr)	9.33	10.2	7.35	9.39	8.7
	Min p (kbr)	2.60	1.27	1.06	1.35	1.17
	Mean p (kbr)	5.07	5.32	4.10	5.50	4.77

#### **4.5. Geodynamic Implications.**

The geodynamic evolution of the eastern Pontides orogenic belt in Turkey is still debatable. The onset of subduction, time and direction of subduction of Pontides and the TAP (Tauride–Anatolide Platform) still under discussion. In general, there are three subduction models have been proposed to evaluate in the eastern Pontides. The suggested by (e.g. Adamia et al., 1977; Okay and Şahintürk 1998; Okay et al., 1993; Ustaömer and Robertson, 1996) proposed subduction to northward from the Paleozoic to the end of the Eocene. They argued that the ultramafic rocks which are found in the southern part of the eastern Pontides represents the residual part of the Paleotethys Ocean. Another hand, Şengör and Yılmaz (1981) and Yılmaz (1997) proposed that the Paleotethys was situated north of the Pontides, and that is needed two tectonic models, the first one start in Paleozoic and continue to the Mid-Jurassic with subduction to the southward, followed by subduction to the north from the Upper Cretaceous and continue to the end of the Eocene. According to this model, they suggested that the southern active continental margin of Eurasia represented by the eastern Pontides. They also dated the opening of Neotethys during the lower Jurassic and formed as result to back-arc basin to the eastern Pontides.

In a third model, conversely, some authors proposed that the northern part of Turkey was shaped by in a southerly direction subduction of Paleotethys oceanic lithosphere that was situated in the north of the Pontides (Dewey et al. 1973; Chorowicz et al. 1998; Bektaş et al. 1999; Eyuboglu, 2010). They suggested that the Black Sea represents the residual of the Tethys Ocean whereas the back arc basin represented by an ophiolitic belt in the Axial. Geodynamic evolution of Upper Cretaceous plutonic and volcanic rocks across or along Eastern Pontides is potentially convoluted because of direction of the subduction, crustal contribution, mantle metasomatism, and differentiation.

Generally, the eastern Pontides characterized by extensive mafic-felsic magmatism during the Upper Cretaceous period and was an extensional continental arc (e.g., Arslan et al., 1997; Okay and Şahintürk, 1997). Geodynamic evolution and geochemical features of Late Cretaceous plutonic and volcanic rocks in this study area can be interpreted by parental magmas derived from enriched lithospheric mantle mixed with lower crustal sources which was formed while the environment was under extensional conditions in a subduction zone and slab roll-back of the Tethyan oceanic slab in its vanish stage (i.e., Rice et al. 2009; Çinku et al., 2010; Karsli et al., 2012; Aydın et al., 2016). The suggested geodynamic model conforms well to a northward subduction of the Tethyan oceanic slab, which began in the Turonian-Santonian period in the region (e.g., Şengör and Yılmaz, 1981; Okay and Şahintürk, 1997; Okay and Tüysüz, 1999; Karsli et al., 2010, 2012).

The Taşlıyayla volcanic rocks formation hosts Santonian and Campanian aged plutonic rocks and are the conjugate with Late Cretaceous aged (Turonian) Çatak formations. The Taşlıyayla volcanic rocks consisting of basalt and andesite their age approximately 92.5 Ma is consistent with Çatak and Kızılkaya formations (Güven, 1993; Aydın et al 2016) which represent the first magma generated after a long period of carbonate deposition, and the marginal basin start to open (namely the Black Sea Basin). The Çağlayan Formation that came over these formations contemporaneous with the Campanian aged plutons which were formed in the last stages of the closure of the Neotethyan Ocean.

During the Early Cretaceous the Northern Neotethys Ocean started to splitting due to convergent event between the Arabian Plates and Eurasian Plate, and the initiation of a northward-directed subduction beneath the Eurasian Plate due to convergent movement between Arabian Plates and Eurasian Plate an (e.g., Şengör and Yılmaz, 1981; Okay and Şahintürk, 1997; Okay and Tüysüz, 1999; Karlı et al., 2010, 2012; Aydın et al., 2017). furthermore, the geochronologic ages obtained from the previous studies (Eyüboğlu et al. 2014) point out that the first volcanism with basic characteristic could be in the Early Turonian (~92-94 million years) or earlier (probably the Turonian-Cenomanian; ~92-100) aged. When the fact that the first volcanism reached to the surface until ~10-15 million years after the start of subduction is considered, it can be envisaged that the subduction



must have started at least in the Early Cenomanian or a bit earlier (in the Late Cretaceous; ~110-115 million years).

As mentioned above the Taşlıyayla formation hosting Santonian and Campanian aged plutonic rocks is generated in the same time as the Çatak formation and derived from similar source. They share similar geochemical characters in which were formed by moderate to high degrees of melting of spinel-bearing lherzolites at shallow (~50 km) depths and was modified by the addition of fluids from the subducting oceanic slab (Aydın et al., 2016). The generation of Calc Alkaline magmas can be a result of decompression melting of a continental lithosphere previously modified by subduction and can be attributed to two stage of subduction (e.g. Hawkesworth et al. 1993, 1997; Fan et al., 2003). According to the (Aydın et al., 2016) the first subduction starts at the Early cretaceous with subduction of northern branch of Neotethyan oceanic lithosphere beneath the Eurasia, when the Mid Oceanic Ridge reaches the appropriate depth during subduction, the leading slab will sink more rapidly than the following slab. This subduction would have started to subduct at a relatively higher angle because the subducting oceanic lithosphere would have been the oldest, and that's will lead to ascends the hot asthenosphere to provide isostatic stability, bringing it into contact with the overlying mantle wedge peridotites. This is leads to significant heat flow caused the partial melting of mantle peridotites first, then mixing with lower crust, by mafic melts coming from the underlying mantle, and generate the Taşlıyayla volcanic rock which is the first stage of the subduction (e.g. Hawkesworth et al. 1993; Aydın et al., 2016: Figure 79a). Then the subduction angle will decrease gradually because the subducting crust will be young, and the subduction probably paused shortly when the mid-ocean ridge (MOR) collided with trench (Aydın et al 2016).

The heating of overlying mantle wedge peridotites and mixing with the lower crust to generate the Taşlıyayla volcanic rock and produced a hybrid melt that can be contributed of the composition of the parental magma of Gündoğdu pluton. The second stage of subduction starting with subduction of southern branch of Neotethyan oceanic lithosphere. Along with heat produced previously by underplated basaltic magma (Taşlıyayla formation) might have led to the partial melting and assimilation of lower to middle crustal rocks and create magma of Gündoğdu pluton in the late Santonian- Early Campanian

(Figure 79b). With increasing the age of the subducting oceanic crust, the subduction angle becoming increasingly upright due to the “roll-back” must have caused the volcanism to immigrate from the arc towards the fore-arc basin and the magma source area to immigrate deeper and deeper, towards the time of the Neotethyan Ocean’s being closed totally. According to that the source area would have undergone to extensional forces, at increasing magnitudes, causing decompression in the overriding continental crust. In this way the underplated basaltic magma led to melting of lower crust by creating with the enough amount of heat required for melting above the plagioclase stability field at lower crustal. This heat transfer may have caused to the partial melting of lower/middle crust parts. Then, the hybrid melts, undergoes to fractional crystallization process with minor crustal assimilation, and ascend to shallower crustal levels. Due to the increasing the age and angle of subduction (roll-back) the calc-alkali magmas of Boğalı plutons will be generated (Figure 79c). Based on the geochemical features of the studied Gündoğdu and Boğalı plutons belonging to Late Cretaceous (~85–82 Ma respectively). The slab-roll back and extensional arc model which explains the geodynamic evolution of Late Cretaceous volcanic and plutonic rocks can be schematized in (Figure 79).

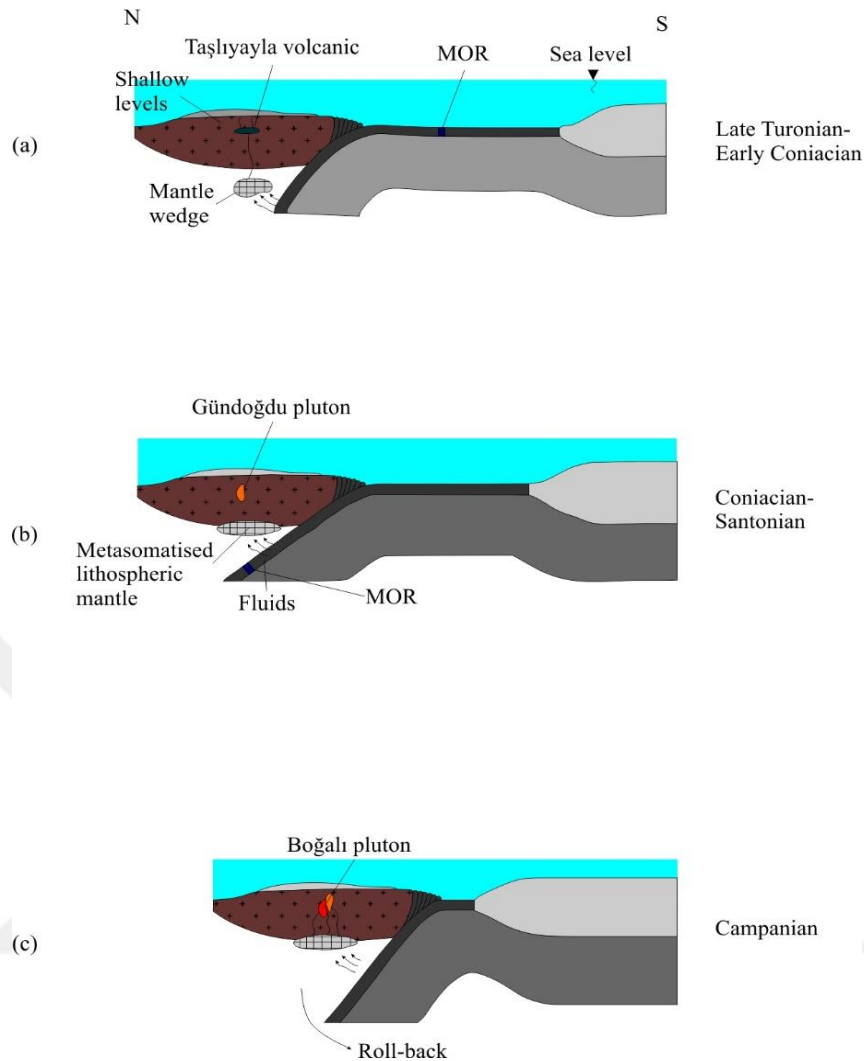


Figure 79. Proposed geodynamic model for Late Cretaceous volcanic and plutonic rocks and evolution of the ESZ (NE Turkey) Modified from (Aydın et al. 2016). Explanations, (a) The initiation of a northward-directed subduction leading Incorporation of slab-derived fluids to the mantle wedge and area of metasomatised spinel-lherzolite mantle and generation of the Taşlıyayla basaltic melt. This subduction would have started to subduct at a relatively higher angle because the subducting oceanic lithosphere would have been the oldest, (b) Subduction angle less angle due to the age and density of oceanic lithosphere and significant amounts of heat flow input from MOR leading Partial melting of the metasomatised mantle and generation of Gündoğdu pluton, (c) An increasing the age of the subducting oceanic crust, the subduction angle becoming increasingly upright due to the “roll-back” must have caused the volcanism to immigrate from the arc towards the fore-arc basin and the magma source area to immigrate deeper and deeper and leading to generation of Boğalı pluton.

## 5. CONCLUSIONS

1. The area of the present study includes volcanic and plutonic rocks that belong to Late Cretaceous and Eocene which are cutted by Basic and Acidic Eocene Dayks.

2. The volcanic rocks of the study area were separated into two formations. The first formation is known as Taşlıyayla volcanic rocks and belong to upper cretaceous, and the second is named as Salman Kaş Volcanic rocks and belong to Eocene.

3. The study area has been studied by Şahin (2005) and is aged the volcanic rocks to Late Cretaceous and named as Taşlıyayla volcanic rocks. The study area occupied 1500 m and unfortunately was covered by vegetation so the rocks outcrop is found in valley floor and road splitting.

4. The Taşlıyayla volcanic rocks consist of Basaltic and andesitic rocks that consist mainly of plagioclase, clinopyroxene, chlorite. These rocks have greyish-blackish aphanitic texture characterize by microcrystalline porphyritic, microlitic porphyritic, glomeroporphyritic, microgranular and intersertal texture.

5. The Gündoğdu pluton cutted by Boğalı pluton is in contact with Eocene Plutonic rocks and Taşlıyayla volcanic rocks. It is also cutted by acidic and basic dayks and displays high of alteration. The main body of Gündoğdu pluton shows high diversity in composition and texture in which it consists of fine grain Granitic, Granodiorite, Monzogranit and Diorite rocks. Generally, this pluton displays porphyritic aphanitic textures, porphyritic phaneritic textures, poikilitic, graphic and rarely myrmekitic textures. It includes MMEs which are diorite and quartz monzodiorite in compositions.

6. Boğalı pluton also cutted by different dayks and contains MMEs are diorite and monzodiorite in compositions. Petrographically the Boğalı Pluton has similar mineralogical and textural characteristics as Gündoğdu Pluton.

7. SHRIMP U-Pb age analysis, the emplacement age is 92.5 Ma (Turonian) for Taşlıyayla volcanic rock, 85.2 Ma (Santonian) for Gündoğdu plutonic rocks, 83.1 Ma (Campanian) for Boğalı plutonic rocks and 44.61 Ma (Eocene) for Salman Kaş Volcanic rocks.

8. The chemical analysis of Taşlyayla volcanic rocks displays negative and positive correlation between major and trace element and SiO<sub>2</sub> indicating fractional crystallization of plagioclase, clinopyroxene, chlorite, Fe-Ti oxides, apatite, and amphibole. The increasing of SiO<sub>2</sub> with increasing K<sub>2</sub>O and Rb indicates that K-feldspar and biotite were not among the early phases of fractionation.

9. Chemically Taşlyayla volcanic rocks shows variation from Calc alkaline to High K shoshonitic magma and the Chondrite-normalized rare earth element patterns have concave-upward shape characterized by negative anomalies of Eu with Eu/Eu\* ranging from 0.49 to 1.14 indicating insignificance of plagioclase fractionation in the evolution of the volcanic rocks, or possibly due to high oxygen fugacity.

10. The Gündoğdu and Boğalı plutons also displays negative and positive correlation between major and trace element and SiO<sub>2</sub> indicating to fractionation of plagioclase, Quartz, K-feldspar, amphibole, Biotite, Fe-Ti oxides and apatite. They are also distinguished by pronounced negative Ta, Nb and Ti anomalies in the spidergrams and enrichment of LILEs and LREEs, indicating typical crustal melts and subduction related magmas.

11. Geochronological and geochemical data indicate that the composition of the Late Cretaceous volcanic rocks and plutonic rocks displays transition from metaluminous-peraluminous and Calc-alkaline to shoshonitic through time (Turonian to Campanian).

12. Both volcanic and plutonic rocks are enriched in LILE and deficient in HFSE, displays concave-upward chondrite-normalized REE patterns with pronounced negative Eu anomalies and show features of arc-related intrusive rocks.

13. Isotopically, the Gündoğdu pluton is distinguished by high <sup>87</sup>Sr / <sup>86</sup>Sr (i) and εNd<sub>(T)</sub> between 0.703552- 0.711929 and -9.6 to -8.4 (85My), respectively, whereas their MMEs <sup>87</sup>Sr / <sup>86</sup>Sr (i) and <sup>143</sup>Nd / <sup>144</sup>Nd (i) 0.703 and -7.5, respectively. They are also characterized by homogeneous in lead isotopic compositions which have <sup>206</sup>Pb/<sup>204</sup>Pb = 18.45–18.50, <sup>207</sup>Pb/<sup>204</sup>Pb = 15.62–15.65, <sup>208</sup>Pb/<sup>204</sup>Pb = 38.12–38.64, whereas their MMEs displays lead isotopic compositions similar to their host rocks and that indicates to source of crustal and mantle components were involved in their genesis.

14. The rocks of Gündoğdu pluton and their MMEs displays a geochemical and Sr–Nd–Pb isotopic features are heterogeneous when compared with Boğalı plutonic rocks.

15. Boğalı Pluton displays a considerable range of initial  $^{87}\text{Sr}/^{86}\text{Sr}$  ratios (0.7061 to 0.7065), whereas isotopic ratios of  $\epsilon\text{Nd}_{(T)}$  values varies from  $-4.75$  to  $-3.9$ . The Boğalı plutonic samples are relatively homogeneous in lead isotopic compositions of  $^{206}\text{Pb}/^{204}\text{Pb}$ ,  $^{207}\text{Pb}/^{204}\text{Pb}$  and  $^{208}\text{Pb}/^{204}\text{Pb}$ . Lead isotopic ratios of the samples are  $^{206}\text{Pb}/^{204}\text{Pb} = 18.18\text{--}18.70$ ,  $^{207}\text{Pb}/^{204}\text{Pb} = 15.62\text{--}15.64$ ,  $^{208}\text{Pb}/^{204}\text{Pb} = 38.05\text{--}38.58$ . The MMEs of Boğalı pluton displays a similar isotopically composition in comparison with their host rock.

16. The crystallization conditions were detected by means of the chemistry of feldspar, Clinopyroxene, for volcanic rocks whereas in plutonic rocks the feldspar, Phosphorus pentoxide hornblende and Zircon minerals were used. The calculated temperature and pressure values of Taşlıyayla volcanic rocks range between  $600\text{--}700$  °C for two feldspars, and  $5.6\text{--}8.9$  kbar,  $1224\text{--}1296$  °C for clinopyroxene. The calculated temperature and pressure values range between  $600\text{--}750$  for feldspar,  $750\text{--}950$  °C for Phosphorus pentoxide,  $750\text{--}769$  °C for zircon and  $2.2\text{--}4.6$  kbar  $639\text{--}739$  °C for hornblend. These also values indicate that the volcanic and plutonic rock were generally crystallized from mid to shallow crustal depths.

17. Based on the tectono-magmatic discrimination diagrams, both volcanic and plutonic formations are magmatic arc in characters.

18. According to the Petrographical properties, major oxid and trace elements the Taşlıyayla volcanic rocks were formed due to several processes such as magma mixing, fractional crystallization, and crustal assimilation. They also indicated that the Taşlıyayla volcanic rocks were formed from moderate to high ( $\sim 10\text{--}30\%$ ) melting of a spinel-bearing lherzolitic mantle.

19. The isotopic compositions of Gündoğdu pluton rather  $\text{Isr}$  or  $\epsilon\text{Nd}(t)$  displays high  $\text{Isr}$  value which indicates different magma source and informed that unlike crystal, fractionation is only the main processes formed the pluton, and the crustal contamination and/or magma mixing played important role during the generating of pluton. The isotopical signatures and trace element features of the Gündoğdu pluton and their MMEs indicates that, it is unlikely to relate this magma to only amphibolitic lower crustal source rocks because there is a different source that may



have been contributed to the parental magmas such as metagraywackes, metaigneous, metapelites, and lithospheric mantle. The high Sr-Nd isotope value can be attributed to old continental source/source rocks, which were inhomogeneous with a heterogeneous initial isotope composition and formed by mixing of enriched lithospheric mantle with lower to middle crust or can be attributed to the contamination. The Sr-Nd isotope signature of MMEs indicate to xenolith source.

20. The Sr–Nd–Pb isotopic compositions of Boğalı pluton and its correlation with SiO<sub>2</sub> indicates a negligible effect of assimilation during the magma generation. It also indicates that the magma mixing, and fractional crystallization were the main processes through the evaluation of the pluton. The Sr–Nd–Pb isotopic signatures and trace element characteristics of the Boğalı pluton and associated MMEs indicate that, it is unlikely to relate this magma to only amphibolitic lower crustal source rocks because the lithospheric mantle may have contributed to the parental magmas.

21. The source of the magmas forming the Gündoğdu Pluton might be the production of partial melting of different source rocks, such as metagraywackes, amphibolite, metabasaltic and metapelite, whereas the Boğalı pluton produced by partial melting of magma derived from amphibolite source.

22. The isotopic modeling scheme displaying the Sr and Nd isotopic bulk mixing lines are plotted between mantle and local lower crust end-member compositions. The Gündoğdu samples plotted scattered randomly on a curve, suggesting a different petrogenetic processes in addition to magma mixing such crustal contamination. AFC plays role in magma mixing process and fractional crystallization processes whereas Boğalı samples plotted on a curve, suggesting a magma mixing process. In the Sr–Nd diagram, various mixing ratios ( $f = 0.1$  to  $0.9$ ) are shown from mantle (DM) towards local lower continental crust (LCC) end-members the Gündoğdu pluton is consistent with a mixed origin with 65-60% of lower crust and 35-40 of mantle derived magma whereas the Boğalı pluton contain ~25–35% of lower crustal-derived and ~65–75% of mantle derived magmas. The Sr–Nd isotope modeling of Gündoğdu Pluton indicates different source and that the magma forming the Gündoğdu Pluton is isotopically homogeneous, but chemically heterogeneous. The possibility of AFC for Gündoğdu pluton tested and found some minor function of assimilation in the evolution of this Gündoğdu pluton and the source are heterogeneous.

23. The geochemical compositions suggest the Taşlıyayla volcanic rocks formed during the first stage of closure of the Neotethyan Ocean as a result of normal stage of subduction during the Turonian from moderate to high degrees of melting of spinel-bearing lherzolites at shallow (~50 km) depths similar to Çatak formations. With ongoing subduction, the slab-derived fluids added to mantle component leading to significant heat flow transferred into the mantle wedge and the overlying lower crust causing partial melting of mantle peridotites in the first place, than lower crust, by mafic melts coming from the underlying mantle. The Gündoğdu and Boğalı Plutons were formed during the last stage closure of the Neotethyan Ocean as a result of extensional arc and slab-roll back model.



## 6. REFERENCES

- Adamia, S. A., Lordkipanidze, M.B. and Zakariadze, G.S., 1977. Evolution of an active continental margin as exemplified by the Alpine history of the Caucasus, Tectonophysics, 40, 183–199.
- Aiglsperger, T., Proenza, J. A., Zaccarini, F., Lewis, J. F., Garuti, G., Labrador, M., and Longo, F., 2015. Platinum group minerals (PGM) in the Falcondo Ni-laterite deposit, Loma Caribe peridotite (Dominican Republic). Mineralium Deposita, 50,1, 105-123.
- Arculus, R. J. and Powell, R., 1986. Source component mixing in the regions of arc magma generation, Journal of Geophysical Research: Solid Earth, 91, B6, 5913-5926.
- Arslan, M., Tüysüz, N., Korkmaz, S. and Kurt, H., 1997. Geochemistry and petrogenesis of the eastern Pontide volcanic rocks, Northeast Turkey, Chemie Der Erde, Geochemistry, 57, 157–187.
- Arslan, M. 2003. Geochemical and petrological characteristics of the eastern Pontide Tertiary volcanism: some implications to geodynamic evolution. In Geology and Mining Potential of Eastern Black Sea Region Symposium Proceedings, Trabzon, 103-105.
- Arslan, M. and Aslan, Z., 2006. Mineralogy, petrography and whole-rock geochemistry of the Tertiary granitic intrusions in the Eastern Pontides, Turkey, Journal of Asian Earth Sciences, 27, 2, 177-193.
- Aydin, F., 2014. Geochronology, geochemistry and petrogenesis of the Macka subvolcanic intrusions: Implications for the Late Cretaceous magmatic and geodynamic evolution of the eastern part of the Sakarya Zone, NE Turkey, Inter Geol Review, 56, 10, 1246-1275.
- Aydin, F., Şen, C., Dokuz, A., Kandemir, R. and Sarı, B., 2015. Petrology and genesis of the Late Cretaceous volcanism in northeastern Turkey: new evidence for the Late Mesozoic geodynamic evolution of the eastern Pontides, TÜBİTAK Project (in Turkish with English abstract), No: 112Y365 (unpublished).
- Aydınçakır, E. and Şen, C., 2013. Petrogenesis of the post-collisional volcanic rocks from the Borçka (Artvin) area: Implications for the evolution of the Eocene magmatism in the Eastern Pontides (NE Turkey), Lithos, 172, 998–1117.
- Bacon, C.R., and Hirschmann, M.M., 1988, Mg/Mn partitioning as a test for equilibrium between coexisting Fe-Ti oxides: American Mineralogist, 73, 57–61.

- Barbarin, B. and Didier, J., 1992. Genesis and evolution of mafic microgranular enclaves through various types of interaction between coexisting felsic and mafic magmas, Transactions of the Royal Society of Edinburgh, Earth Sciences 83, 145–153.
- Barbarin B., 1999. A review of the relationships between granitoid types, their origins and their geodynamic environments, Lithos, 46, 605–626
- Bektaş, O., 1984. The importance of Geodynamic setting and shoshonitic volcanism rocks of Upper Cretaceous in the Eastern Pontides: Karadeniz University (in 1005 Turkish with English abstract), Earth Science Derg., 3, 1-2.
- Bektaş, O., Yılmaz, C., Taslı, K., Akdağ, K. and Özgür, S., 1995. Cretaceous rifting of the eastern Pontide carbonate platform (NE Turkey): the formation of carbonates breccias and turbidites as evidences of a drowned platform. Geologia, 57,1-2, 233-244.
- Bektaş, O., Sen, C., Atici, Y. and Köprübasi, N., 1999. Migration of the Upper Cretaceous subduction-related volcanism towards the back-arc basin of the Eastern Pontide magmatic arc (NE Turkey), Geological Journal, 34, 95-106.
- Blundy, J.D., and Holland, T.J.B., 1990, Calcic amphibole equilibria and a new amphibole-plagioclase geothermometer: Contributions to Mineralogy and Petrology, v. 104, p. 208– 224. doi:10.1007/BF00306444 Anderson, J.L., and Smith, D.R., 1995, The effects of temperature and  $fO_2$  Al-in-hornblende barometer: American Mineralogist, 80, 549–559.
- Boztuğ, D., 2001. Petrogenesis of the composite Kaçkar batholith along a north-south geotraverse between Ardesen (Rize) and Ispir (Erzurum) towns, eastern Black Sea region, Turkey. In Fourth International Turkish Geology Symposium (ITGS IV), September, Adana/Turkey, Abstracts.
- Boztuğ, D., Kuşçu, İ., Erçin, A. İ., Avcı, N. and Şahin, S.Y., 2003. Mineral deposits associated with the pre-, syn- and postcollisional granitoids of the Neo-Tethyan convergence system between the Eurasian and Anatolian plates in NE and Central Turkey. In: Eliopoulou, D. et al. (Ed.), Mineral Exploration and Sustainable Development. Millpress, Rotterdam, 1141–1144.
- Boztuğ, D., Erçin, A.I., Kuruçelik, M.K., Göc, D., Kömür, I. and Iskenderoğlu, A., 2005. Main geochemical characteristics of the composite Kaçkar batholith derived from the subduction through collision to extensional stages of the Neo-Tethyan convergence system in the Eastern Pontides, Turkey, Journal of Asian Earth Sciences, in review.
- Boztuğ, D., Erçin, A.I., Kuruçelik, M.K., Göc, D., Kömür, I. and Iskenderoğlu, A., 2006. Geochemical characteristics of the composite Kaçkar batholith generated in a Neo-Tethyan convergence system, eastern Pontides, Turkey, Journal of Asian Earth Sciences, 27, 286–302.

- Brown, GC., Thorpe, RS. and Webb PC., 1984. The geochemical characteristics of granitoids in contrasting arcs and comments on magma sources. J Geol Soc, 141,413–426.
- Bradshaw, T. K. and Smith, E. I., 1994. Polygenetic Quaternary volcanism at Crater Flat, Nevada, Journal of Volcanology and Geothermal Research, 63,3-4, 165-182.
- Cathelineau, M., 1988. Cation site occupancy in chlorites and illites as a function of temperature, Clay minerals, 23, 4, 471-485.
- Chappell BW., 1999. Aluminum saturation in I- and S-type granites and the characterization of fractionated hapogranites, Lithos, 46, 531–55.
- Chen, B. and Arakawa, Y., 2005. Elemental and Nd-Sr isotopic geochemistry of granitoids from the West Junggar foldbelt (NW China), with implications for Phanerozoic continental growth. Geochimica et Cosmochimica Acta, 69, 5, 1307-1320.
- Chorowicz, J., Collet, B., Bonavia, F. F., Mohr, P., Parrot, J. F. and Korme, T., 1998. The Tana basin, Ethiopia: intra-plateau uplift, rifting and subsidence. Tectonophysics, 295, 3-4, 351-367.
- Çamur, M. Z., Güven, İ. H. and Murat, E. R., 1996. Geochemical characteristics of the Eastern Pontide volcanics, Turkey: an example of multiple volcanic cycles in the arc evolution, Turkish Journal of Earth Sciences, 5, 2, 123-144.
- Çinku, M.C. and Hisarlı, M., 2009. Palaeogeographic evidence for the Jurassic to Middle Eocene tectonic history of the Pontides: New palaeomagnetic data from the Sakarya continent and eastern Pontides, 62nd Geological Kurultai of Turkey. MTA, Ankara 944–945.
- Çoğulu, E., 1975. Gümüşhane ve Rize granitik plutonlarının mukayeseli petrojeolojik ve jeokronolojik etüdü [Petrogeologic and geochronologic investigation of Gümüşhane and Rize granitic plutons and their comparison]. Unpublished Dissertation Thesis, İstanbul Technical University (in Turkish with English abstract).
- Debon F, and Le Fort, P., 1982. A chemical-mineralogical classification of common plutonic rocks and associations, Trans R Soc Edinb Earth Sci, 73,135–149.
- DePaolo, D.J., 1981. Trace element and isotopic effects of combined wallrock assimilation and fractional crystallization. Earth and Planetary Science Letters, 53, 189–202.
- Dewey, J.F., Pitman, W.C., Ryan, W.B.F. and Bonnin, J., 1973. Plate tectonics and evolution of the Alpine system. Geological Society of America Bulletin 84, 3137–3180.
- Davies, J. H. and von Blanckenburg, F., 1995. Slab breakoff: a model of lithosphere detachment and its test in the magmatism and deformation of collisional orogens. Earth and Planetary Science Letters, 129, 1-4, 85-102.

- Debon, F. and Le Fort, P., 1983. A chemical–mineralogical classification of common plutonic rocks and associations, Earth and Environmental Science Transactions of the Royal Society of Edinburgh, 73, 3, 135-149.
- Deer, W.A., Howie, R.A. and Zussman, J., 1992. An Introduction to the Rock Forming Minerals, 2nd ed, Longman, London, 696.
- Dokuz, A., Karsli, O., Chen, B. and Uysal, İ., 2010. Sources and petrogenesis of Jurassic granitoids in the Yusufeli area, Northeastern Turkey: implications for pre- and post-collisional lithospheric thinning of the eastern Pontides, Tectonophysics 480, 259–279.
- Dokuz, A., 2011. A slab detachment and delamination model for the generation of Carboniferous high-potassium I-type magmatism in the Eastern Pontides, NE Turkey: the Kose composite pluton, Gondwana Research, 19, 4, 926–944.
- Dungan, M. A. and Rhodes, J. M., 1978. Residual glasses and melt inclusions in basalts from DSDP Legs 45 and 46: evidence for magma mixing, Contributions to Mineralogy and Petrology, 67, 4, 417-431.
- Eby, G.N., 1992. Chemical subdivision of the A-type granitoids: Petrogenetic and tectonic implications. Geology, 20, 641–644.
- Evcimen, Ö., 2011. U-Pb Geochronology, Petrology and Geodynamic significance of ikizdere pluton (NE-Turkey), 76, In English abstract.
- Elburg, M.A, Bergen, M.V., Hoogewerff, J., Foden, J., Vroon, P., Zulkarmain, I. and Nasution, A., 2002. Geochemical trends across an arc-continent collision zone: magma sources and slab-wedge transfer processes below the Pantar Strait volcanoes, Indonesia, Geochimica et Cosmochimica Acta, 66, 2771-2789.
- Eyüboğlu, Y., Bektas, O., Seren, A., Maden, N., Jacoby, W.R. and Özer, R., 2006. Three axial extensional deformation and formation of the Liassic rift basins in the Eastern Pontides (NE Turkey), Geologica Carpathica, 57, 5, 337-346.
- Eyüboğlu, Y., 2010. Late Cretaceous high-K volcanism in the Eastern Pontides Orogenic Belt, and its implications for the geodynamic evolution of NE Turkey. International Geology Review, 52, 2-3, 142–186.
- Eyüboğlu, Y., Santosh, M., Yi, K., Tüysüz, N., Korkmaz, S., Akaryalı, E., Dudas, F. and Bektaş, O., 2014. The Eastern Black Sea-type volcanogenic massive sulfide deposits: geochemistry, zircon U–Pb geochronology and an overview of the geodynamics of ore genesis, Ore Geology Reviews, 59, 29–54.
- Eyüboğlu, Y., 2015. Petrogenesis and U–Pb zircon chronology of felsic tuffs interbedded with turbidites (Eastern Pontides Orogenic Belt, NE Turkey): implications for Mesozoic geodynamic evolution of the eastern Mediterranean region and accumulation rates of turbidite sequences, Lithos ,212–215, 74–92.



- Fitton, J. G., James, D. and Leeman, W. P., 1991. Basic magmatism associated with late Cenozoic extension in the western United States: Compositional variations in space and time, Journal of geophysical Research: Solid earth, 96, B8, 13693-13711.
- Foley, S. F. and Wheller, G. E., 1990. Parallels in the origin of the geochemical signatures of island arc volcanics and continental potassic igneous rocks: the role of residual titanates, Chemical Geology, 85, 1-2, 1-18.
- Frost, T.P. and Mahood, G.A., 1987. Field, chemical, and physical constraints on mafic—felsic magma interaction in the Lamarck Granodiorite, Sierra Nevada, California. Geological Society of America Bulletin, 99, 272–291.
- Fuhrman, M.L. and Lindsley, D.H., 1988. Ternary feldspar modeling and thermometry, American Mineralogist, 73, 201–215.
- Gardien, V., Thompson, A. B., Grujic, D. and Ulmer, P., 1995. Experimental melting of biotite+ plagioclase+ quartz±muscovite assemblages and implications for crustal melting, Journal of Geophysical Research, Solid Earth, 100, B8, 15581-15591.
- Gedikoğlu, A., 1978. Harşit Granit karmaşığı ve çevre kayalar, Doçentlik Tezi, KTÜ Yer Bilimleri Fakültesi, Trabzon, 161.
- Gedikoglu, A., Pelin, S. and Ozsayar, T., 1979. The main lines of geotectonic development of the East Pontides in the Mesozoic era. Proceedings of the 1st Geol Congr Middle East (GEOCOME), 555-580.
- Gill, J.B., 1981. Orogenic Andesites and Plate Tectonics. Springer-Verlag, Berlin Heidelberg New York, 390.
- Green, T.H., 1995. Significance of Nb/Ta as an indicator of geochemical processes in the crust-mantle system, Chemical Geology, 120, 347–359. doi:10.1016/0009-2541(94)00145-X.
- Guo, Z., Wilson, M. and Liu, J., 2007. Post-collisional adakites in south Tibet: products of partial melting of subduction-modified lower crust, Lithos, 96, 1-2, 205-224.
- Güven, I. H., 1993. 1/250 000 scaled geological and metallogenical map of the Eastern Black Sea Region. General Directorate of Mineral Research and Exploration, Ankara (unpublished).
- Hamilton, W. J., 1842. Researches in Asia Minor, Pontus and Armenia. 2. London, J. Murray, 267.
- Hammarstrom, J.M. and Zen, E., 1986. Aluminium in hornblende: An empirical igneous geobarometer, American Mineralogist, 71, 1297–1313.
- Hart, S.R., 1984. A large scale isotope anomaly in the Southern Hemisphere mantle, Science, 309, 753–757.

- Hart, S. R. and Dunn, T., 1993. Experimental cpx/melt partitioning of 24 trace elements, Contributions to Mineralogy and Petrology, 113, 1, 1-8.
- Hawkesworth, C.J., Gallagher, K., Herot, J.M., and McDermott, F., 1993. Mantle and slab contributions in arc magmas, Annu. Rev. Earth Planet. Sci., 21, 175–2004.
- Hawkesworth, C. J., Turner, S. P., McDermott, F., Peate, D. W. and Van Calsteren, P. 1997. U-Th isotopes in arc magmas, Implications for element transfer from the subducted crust, Science, 276, 5312, 551-555.
- Hey, M. H. 1954. A new review of the chlorites, Mineralogical Magazine and Journal of the Mineralogical Society, 30, 224, 277-292.
- Hibbard, M. J. 1981. The magma mixing origin of mantled feldspars, Contributions to Mineralogy and Petrology, 76, 2, 158-170.
- Hibbard, M.J. 1991. Textural anatomy of twelve magma-mixed granitoid systems. In: Didier, J., Barbarin, B. (Eds.), Enclaves and Granite Petrology, Elsevier, Amsterdam, 431–444.
- Holland, T.J.B. and Blundy, J.D., 1994. Non-ideal interaction in calcic amphiboles and their bearing on amphibole- plagioclase thermometry, Contributions to Mineralogy and Petrology, 116, 433–447.
- Hollister, L.S., Grisson, G.C., Peters, E.K., Stowell, H.H. and Sisson, V.B., 1987. Confirmation of the empirical correlation of Al in hornblende with pressure of solidification of calcalkaline, American Mineralogist, 72, 231–239.
- Irvine, T. N. J. and Baragar, W. R. A., 1971. A guide to the chemical classification of the common volcanic rocks, Canadian journal of earth sciences, 8, 5, 523-548.
- Jahn, B.M., Wu, F., Lo, C.H. and Tsai, C.H., 1999. Crust-mantle interaction induced by deep subduction of the continental crust: geochemical and Sr-Nd isotopic evidence from post-collisional maficultramafic intrusions of the northern Dabie complex, central China, Chemical Geology, 157, 119–146.
- Johnson, M.C. and Rutherford, M.J., 1989. Experimental calibration of the aluminum-in-hornblende geobarometer with application to Long Valley caldera (California) volcanic rocks: Geology, 17, 837–841. doi:10.1130/0091-7613 (1989)017 < 0837: ECOTAI > 2.3.CO;2.
- Karsli, O., Aydın, F. and Sadıklar, M. B., 2004. Magma interaction recorded in plagioclase zoning in granitoid systems, Zigana Granitoid, eastern Pontides, Turkey, Turkish Journal of Earth Sciences, 13, 287–305.
- Karsli, O., Chen, B., Aydın, F. and Şen, C., 2007. Geochemical and Sr–Nd–Pb isotopic compositions of the Eocene Dölek and Sariçiçek Plutons, Eastern Turkey:

implications for magma interaction in the genesis of high-K calc-alkaline granitoids in a post-collision extensional setting, Lithos, 98, 1-4, 67-96.

- Karsli, O., Aydin, F., Uysal, I. and Sadiklar, M. B., 2008. Magma Interaction Processes Inferred from Fe-Ti Oxide Compositions in the Dölek and Sarıçiçek Plutons, Eastern Turkey, Turkish Journal of Earth Sciences, 17, 2, 297-315.
- Karsli, O., Dokuz, A., Uysal, İ., Aydın, F., Chen, B., Kandemir, R. and Wijbrans, J., 2010a. Relative contributions of crust and mantle to generation of Campanian high-K calcalkaline I-type granitoids in a subduction setting, with special reference to the Harşit Pluton, Eastern Turkey, Contributions to Mineralogy and Petrology, 160, 467–487.
- Karsli, O., Dokuz, A., Uysal, İ., Aydın, F., Kandemir, R. and Wijbrans, R.J., 2010b. Generation of the early Cenozoic adakitic volcanism by partial melting of mafic lower crust, Eastern Turkey: implications for crustal thickening to delamination, Lithos, 114, 109–120.
- Karsli, O., Uysal, I., Ketenci, M., Dokuz, A., Aydin, F., Chen, B., Kandemir, R. and Wijbrans, J., 2011. Adakite-like granitoid porphyries in Eastern Pontides, NE Turkey: potential parental melts and geodynamic implications, Lithos, 127, 354–372.
- Karsli, O., Caran, Ş., Dokuz, A., Çoban, H., Chen, B. and Kandemir, R., 2012a. A-type granitoids from the Eastern Pontides, NE Turkey: records for generation of hybrid A-type rocks in a subduction-related environment, Tectonophysics, 530–531, 208–224.
- Karsli, O., Dokuz, A., Uysal, İ., Ketenci, M., Chen, B. and Kandemir, R., 2012b. Deciphering the shoshonitic monzonites with I-type characteristic, the Sisdagi pluton, NE Turkey: magmatic response to continental lithospheric thinning, Journal of Asian Earth Sciences, 51, 45–62.
- Kaygusuz, A., Chen, B., Aslan, Z., Wolfgang, S. and Şen, C., 2009. U–Pb zircon SHRIMP ages, geochemical and Sr–Nd isotopic compositions of the Early Cretaceous I type Sariosman pluton, eastern Pontides, NE Turkey, Turkish Journal of Earth Sciences, 18, 549–581.
- Kaygusuz, A. and Aydınçakır, E., 2011. Petrogenesis of a Late Cretaceous composite pluton from the eastern Pontides: the Dağbaşı pluton, NE Turkey, Neues Jahrbuch für Mineralogie (Abhandlungen), 188, 211–233.
- Kaygusuz, A. and Şen, C., 2011. Calc-alkaline I-type plutons in the eastern Pontides, NE Turkey: U–Pb zircon ages, geochemical and Sr–Nd isotopic compositions, Chemie der Erde-Geochemistry, 71, 59–75.
- Kaygusuz, A., Arslan, M., Wolfgang, S., Sipahi, F. and İlbeyli, N., 2012a. Geochronological evidence and tectonic significance of Carboniferous magmatism

in the southwest Trabzon area, eastern Pontides, Turkey, International Geology Review, 1776–1800.

- Kaygusuz, A., Sipahi, F., İlbeyli, N., Arslan, M., Chen, B. & Aydınçakır, E., 2013. Petrogenesis of the Late Cretaceous Turnagöl intrusion in the eastern Pontides: implications for magma genesis in the arc setting, Geoscience Frontiers, 4, 423–438.
- Kaygusuz, A., Arslan, M., Siebel, W., Sipahi, F., İlbeyli, N., and Temizel, İ. 2014. LA-ICP MS zircon dating, whole-rock and Sr–Nd–Pb–O isotope geochemistry of the Camiboğazı pluton, Eastern Pontides, NE Turkey: Implications for lithospheric mantle and lower crustal sources in arc-related I-type magmatism. Lithos, 192, 271–290.
- Kelemen, P. B., 1990. Reaction between ultramafic rock and fractionating basaltic magma I. Phase relations, the origin of calc-alkaline magma series, and the formation of discordant dunitite, Journal of Petrology, 31, 1, 51–98.
- Kempton, P.D., Downes, H. and Embey-Istzin, A., 1997. Mafic granulite xenoliths in Neogene alkali basalts from the western Pannonian basin: insights into the lower crust of a collapsed orogen, Journal of Petrology, 38, 941–970.
- Keskin, M., Genç, Ş. C. and Tüysüz, O., 2008. Petrology and geochemistry of post-collisional Middle Eocene volcanic units in North-Central Turkey: evidence for magma generation by slab breakoff following the closure of the Northern Neotethys Ocean, Lithos, 104, 1–4, 267–305.
- Ketin, İ., 1966. Anatolia tectonic units, Miner. Res. (in Turkish with English abstract), Expl. Bull, 66, 20–34.
- Ketin, I. and Canitez, N., 1972. Structural geology, Technical University Matbaasi Gumussuyu, Ankara, 66, 20–34.
- Korkmaz, S., Tüysüz, N., Er, M., Musaoğlu, A. and Keskin, İ., 1995. Stratigraphy of the eastern Pontides NE Turkey. In: Erler, A., Ercan, T., Bingöl, E., Örcen, S. (Eds.), Geology of the Black Sea Region, General Directorate of Mineral Research and Exploration, and Chamber of Geological Engineers, Ankara, 59–69.
- Le Maitre RW, Bateman P, Dudek A, Keller J, Lameyre J, Le Bas MJ, Sabine PA, Schmid R, Sorensen H, Streckeisen A, Wooley AR. and Zanettin B. 1989. A classification of igneous rocks and glossary of terms. Blackwell, Oxford, 193.
- Maniar, P. D. and Piccoli, P. M., 1989. Tectonic discrimination of granitoids, Geological society of America bulletin, 101, 5, 635–643.
- McCulloch, M.T., Kyser, T.K., Woodhead, J.D. and Kinsley, L., 1994. Pb–Sr Nd–O isotopic constraints on the origin of rhyolites from the Taupo Volcanic zone of New Zealand: evidence for assimilation followed by fractionation of basalt, Contributions to Mineralogy and Petrology, 115, 303–312.

- McCulloch, M. T., and Gamble, J. A., 1991. Geochemical and geodynamical constraints on subduction zone magmatism. *Earth and Planetary Science Letters*, 102(3-4), 358-374.
- McKenzie, D. A. N. & O'Nions, R. K., 1991, Partial melt distributions from inversion of rare earth element concentrations, *Journal of Petrology*, 32(5), 1021-1091.
- Morimoto, N., 1988. Nomenclature of pyroxenes. *Mineralogy and Petrology*, 39, 1, 55-76.
- Middlemost, E.A.K., 1994. Naming materials in the magma/igneous rock system. *Earth Sci. Rev.* 37, 215–224.
- Miller, C. F., McDowell, S. M., and Mapes, R. W., 2003. Hot and cold granites? Implications of zircon saturation temperatures and preservation of inheritance. *Geology*, 31, 6, 529-532.
- Nelson, S. T. and Montana, A., 1992. Sieve-textured plagioclase in volcanic rocks produced by rapid decompression, *American Mineralogist*, 77, 11-12, 1242-1249.
- Nachit, H., Ibhi, A., Abia, E.A., and Ohoud, M.B., 2005. Discrimination between primary magmatic biotites, reequilibrated biotites and neoformed biotites: *Comptes Rendus Geoscience*, 337, 1415–1420. doi:10.1016/j. crte.2005.09.002.
- Okay, A. I., Celal Sengor, A. M. and Görür, N., 1994. Kinematic history of the opening of the Black Sea and its effect on the surrounding regions, *Geology*, 22, 3, 267-270.
- Okay, A.I. and Leven, E.J., 1996. Stratigraphy and paleontology of the upper Paleozoic sequences in the Pular (Bayburt) region, Eastern Pontides, *Turkish Journal of Earth Sciences*, 5, 145–155.
- Okay, A. I. and Şahintürk, O., 1997. Geology of the Eastern Pontides, In: A. G. Robinson, (Ed.), *Regional and Petroleum Geology of the Black Sea and Surrounding Region*, AAPG Mem, 68, 291-311.
- Okay, A. I. and Tüysüz, O., 1999. Tethyan sutures of northern Turkey, *Geological Society, London, Special Publications*, 156, 1, 475-515.
- Özsayar, T., 1971. Paläontologie und Geologie des Gebietes Östlich Trabzon (Anatolien), *Gieben, Geol. Schrift.*, Gieben, 1.
- Pearce, J. A., and Cann, J. R., 1973. Tectonic setting of basic volcanic rocks determined using trace element analyses. *Earth and planetary science letters*, 19, 2, 290-300.
- Pearce, J.A., 1983. Role of the subcontinental lithosphere in magma genesis at active continental margins. In C. J., Hawkesworth ve M. J. Norry, (eds.), *Continental Basalts and Mantle Xenoliths*, Shiva, Cheshire, 230-249.
- Pearce, J. A., Harris, N. B., and Tindle, A. G., 1984. Trace element discrimination diagrams for the tectonic interpretation of granitic rocks, *Journal of petrology*, 25, 4, 956-983.

- Pearce, J. A. and Parkinson, I. J., 1993. Trace element models for mantle melting: application to volcanic arc petrogenesis, Geological Society, London, Special Publications, 76, 1, 373-403.
- Pearce, J. A., 1996. A user's guide to basalt discrimination diagrams. Trace element geochemistry of volcanic rocks: applications for massive sulphide exploration, Geological Association of Canada, Short Course Notes, 12, 79-113.
- Pearce, J.A., Bender, J.F., De Long, S.E., Kidd, W.S.F., Low, P.J., Güner, Y., Şaroğlu, F., Yılmaz, Y., Moorbath, S. and Mitchell, J.J., 1990. Genesis of collision volcanism in eastern Anatolia Turkey, Journal of Volcanology and Geothermal Research, 44, 189-229.
- Piccoli, P.M. and Candela, P.A., 1994. Apatite in felsic rocks: A model for the estimation of initial halogen concentrations in the Bishop Tuff (Long Valley) and Tuolumne Intrusive Suite (Sierra Nevada Batholith) magmas, American Journal of Science, 294, 92–135. doi:10.2475/ajs.294.1.92
- Piccoli, P.M., Candela, P.A. and Williams, T.J., 1999. Estimation of aqueous HCl and Cl concentrations in felsic systems, Lithos, 46, 591–604. doi:10.1016/S0024-4937(98)00084-X.
- Pelin, S., 1977. Geological study of the area southeast of Alucra (Giresun) with special reference to its petroleum potential. Karadeniz Teknik Üniversitesi Yayın No. 87, Trabzon, 103, (in Turkish with English abstract).
- Perugini, D., Ventura, G., Petrelli, M. and Poli, G., 2004. Kinematic significance of morphological structures generated by mixing of magmas: a case study from Salina Island (southern Italy), Earth and Planetary Science Letters, 222, 3-4, 1051-1066.
- Putirka, K., Johnson, M., Kinzler, R., Longhi, J. and Walker, D., 1996. Thermobarometry of mafic igneous rocks based on clinopyroxene-liquid equilibria, 0–30 kbar, Contributions to Mineralogy and Petrology, 123, 1, 92-108.
- Putirka, K. D., 2008. Thermometers and barometers for volcanic systems, Reviews in mineralogy and geochemistry, 69, 1, 61-120.
- Rapp, R.P., Watson, E.B. and Miller, C.F. 1991. Partial melting of amphibolite eclogite and the origin of Archean trondhjemites and tonalites, Precambrian Research, 51, 1-25.
- Rapp, R.P., 1995. Amphibole-out phase boundary in partially melted metabasalt, its control over liquid fraction and composition, and source permeability, Journal of Geophysical Research, 100, 15601-15610.
- Rapp, R.P. and Watson, E.B., 1995. Dehydration melting of metabasalt at 8e32 kbar: implications for continental growth and crust-mantle recycling, Journal of Petrology, 36, 891-931.

- Rice, S.P., Roberson, A.H.F., Ustaömer, T., İnan, T. and Taslı, K., 2009. Late Cretaceous–Early Eocene tectonic development of the Tethyan Suture Zone in the Erzincan area, eastern Pontides, Turkey, Geol Mag. 146, 4, 567–590.
- Roberts, M. P. and Clemens, J. D., 1993. Origin of high-potassium, calc-alkaline, I-type granitoids, Geology, 21, 9, 825-828.
- Robinson, A.G., Banks, C.J., Rutherford, M.M. and Hirst, J.P.P., 1995. Stratigraphic and structural development of the Eastern Pontides, Turkey, Journal of Geological Society London, 152, 861–872.
- Rojay, B., Heimann, A. and Toprak, V., 2001. Neotectonic and volcanic characteristics of the Karasu fault zone (Anatolia, Turkey): the transition zone between the Dead Sea transform and the East Anatolian fault zone, Geodinamica Acta, 14, 1-3, 197-212.
- Ramos, F.C., 1992. Isotope Geology of the Metamorphic Core of the Central Grouse Creek Mountains, Box Elder County, Utah. UCLA PhD Thesis.
- Rottura, A., Bargossi, G.M., Caggianelli, A., Del Moro, A., Visona, D. and Tranne, C.A., 1998. Origin and significance of the Permian high-K calc-alkaline magmatism in the central-eastern Southern Alps, Italy, Lithos, 45, 329–348.
- Salonsaari, P.T., 1995. Hybridization in the subvolcanic Jaala–Iitti complex and its petrogenetic relation to rapakivi granites and associated mafic rocks of southeastern Finland, Geological Society of Finland Bulletin, 67, 1b, 104.
- Schmidt, M.W., 1992. Amphibole composition in tonalite as a function of pressure: an experimental calibration of the Al- in-hornblende barometer, Contributions to Mineralogy and petrology, 110, 304–310.
- Schultze-Westrum, H. H., 1961. The geological profile of Aksu stream near Giresun: MTA Publ., 57, 63-71.
- Simonetti, A., Shore, M. and Bell, K., 1996. Diopside phenocrysts from nephelinite lavas, Napak Volcano, eastern Uganda; evidence for magma mixing, The Canadian Mineralogist, 34, 2, 411-421.
- Skjerlie, K.P. and Johnston, A.D., 1996. Vapour-absent melting from 10 to 20 kbar of crustal rocks that contain multiple hydrous phases: implications for anatexis in the deep to very deep continental crust and active continental margins, Journal of Petrology, 37, 661-691.
- Smith, E.I., Sanchez, A., Walker, J.D. and Wang, K., 1999. Geochemistry of mafic magmas in the Hurricane Volcanic field, Utah: implications for small and large scale chemical variability of the lithospheric mantle, Journal of Geology, 107, 433-448.



- Stevens, G., Clemens, J.D. and Droop, G.T.R., 1997. Melt production during granulite facies anatexis: experimental data from 'primitive' metasedimentary protoliths, Contributions to Mineralogy and Petrology, 128, 352-370.
- Stimac, J. A. and Pearce, T. H., 1992. Textural evidence of mafic-felsic magma interaction in dacite lavas, Clear Lake, California, American Mineralogist, 77, 7-8, 795-809.
- Streckeisen, A., 1976. To each plutonic rock its proper name, Earth-science reviews, 12, 1, 1-33
- Streck, M. J., 2008. Mineral textures and zoning as evidence for open system processes, Reviews in Mineralogy and Geochemistry, 69, 1, 595-622.
- Sun, S.S. and McDonough W.E., 1989. Chemical and isotopic systematics of oceanic basalts: implications for mantle composition and processes. In: Saunders AD, Norry MJ (eds) Magmatism in the ocean basins, Geol Soc Spec Publ, 313–345.
- Şahin, S. Y., 2005. Transition from Arc-to Post-Collision Extensional Setting Revealed By K-Ar Dating and Petrology: An Example from the Granitoids of the Eastern Pontide Igneous Terrane, Araklı-Trabzon, NE Turkey. Geol. J., 40, 425-440.
- Şahin, S. Y., 2008. Geochemistry of mafic microgranular enclaves in the Tamdere quartz monzonite, south of Dereli/Giresun, Eastern Pontides, Turkey. Chemie der Erde-Geochemistry, 68, 1, 81-92.
- Şengör, A.M.C. & Yılmaz, Y., 1981. Tethyan evolution of turkey: a plate tectonic approach, Tectonophysics, 75, 181–241.
- Şengör, A. M. C., 2003. East Anatolian high plateau as a mantle- supported, north- south shortened domal structure, Geophysical Research Letters, 30.24.
- Şen, C., 1988. Dağbaşı (Trabzon) Bölgesinde yüzeyleyen Alt Bazik (Jura)-Granitoid (Üst Kretase) formasyonlarının petrografik-kimyasal özellikleri. M.Sc. Thesis, KTÜ Fen Bilimleri Enstitüsü, Trabzon, In English abstract.
- Şen, C., Arslan, M. and Van, A., 1998. Geochemical and petrological characteristics of the Pontide Eocene (?) alkaline province, NE Turkey, Turkish Journal of Earth Sciences, 7, 231–239.
- Şen, C., 2007. Jurassic volcanism in the Eastern Pontides: is it rift related or subduction related? Turkish Journal of Earth Sciences 16, 523–539.
- Şen, C., Aydın, F., Dokuz, A., Aydınçakır, E., Dündar, B. and Yılmaz, S., 2018. Petrochemical, Sr-Nd-Pb-O Isotope Geochemistry, Geochronology of the Intrusive Complex of Caykara: New evidence for Late Mesozoic-Early Cenozoic Tectonomagmatic Evolution of the Eastern Part of the Sakarya Zone. TÜBİTAK Project (in Turkish with English abstract), No: 114Y219 (unpublished).

- Taylor, S.R. and McLennan, S.M., 1985. The Continental Crust: Its Composition and Evolution, Blackwell Scientific Publication, Oxford, 312.
- Temizel İ., Arslan M., Abdioğlu E. and Yücel C., 2014. Mineral chemistry and thermobarometry of the Eocene monzogabbroic stocks from the Bafra (Samsun) area in Turkey: implications for disequilibrium crystallization and emplacement condition, International Geology Review, 56,10, 1226–1245.
- Thirlwall, M.F. and Jones, N.W., 1993. Isotope geochemistry and contamination mechanism of Tertiary lavas from Skye, northwest Scotland. In: Hawkesworth, C.J., Norry, M.J. (Eds.), Continental Basalts and Mantle Xenoliths. Shiva, Cheshire, 186–208.
- Tokel, S., 1972. Stratigraphical and volcanic history of the Gümüşhane region, NE Turkey. University College London, UK.
- Topuz, G., Altherr, R., Schwarz, W. H., Siebel, W., Satır, M. and Dokuz, A. 2005. Post-collisional plutonism with adakite-like signatures: the Eocene Saraycık granodiorite (Eastern Pontides, Turkey), Contributions to Mineralogy and Petrology, 150, 4, 441-455.
- Topuz, G., Altherr, R., Siebel, W., Schwarz, W. H., Zack, T., Hasözbeğ, A. and Şen, C., 2010. Carboniferous high-potassium I-type granitoid magmatism in the Eastern Pontides: the Gümüşhane pluton (NE Turkey), Lithos, 116, 1-2, 92-110.
- Tsuchiyama, A., 1985. Dissolution kinetics of plagioclase in the melt of the system diopside-albite-anorthite, and origin of dusty plagioclase in andesites, Contributions to Mineralogy and Petrology, 89, 1, 1-16.
- Tüysüz, O., 1999. Geology of the Cretaceous sedimentary basins of the Western Pontides, Geological Journal, 34, 1- 2, 75-93.
- Ustaömer, T. and Robertson, A. H. F., 1996. Paleotethyan tectonic evolution of the North Tethyan margin in the central Pontides, N Turkey. In International symposium on the geology of the Black Sea Region, Proceedings-I, 24-33.
- Vernon, R.H., 1990. Crystallization and hybridism in microgranitoid enclave magmas: microstructural evidence, Journal of Geophysical Research, 95, 17849–17859.
- Vielzeuf, D. and Holloway, J. R., 1988. Experimental determination of the fluid-absent melting relations in the pelitic system, Contributions to Mineralogy and Petrology, 98, 3, 257-276.
- Watson, E. B., 1979. Zircon saturation in felsic liquids: experimental results and applications to trace element geochemistry. Contributions to Mineralogy and Petrology, 70, 4, 407-419.
- Watson, E.B. and Green, T.H., 1982. Apatite Liquid-partition Coefficients for the Rare Earth Elements and Strontium, Earth and Planetary Science Letters, 56, 405-421.

- Watson, E.B. and Harrison, T.M., 1983, Zircon saturation revisited: Temperature and composition effects in a variety of crustal magma types, Earth and Planetary Science Letters, 64, 295–304. doi:10.1016/0012-821X(83)90211-X.
- Weaver, B.L., Wood, D.A., Tarney, J. and Joron, J., 1987. Geochemistry of ocean island basalt from the South Atlantic: Ascension, Bouvet, St. Helena, Gough and Tristan da Cunda. In: Fitton, J.G ve Upton, B.G.J. (eds), Alkaline Igneous Rocks, Geological Society, London, Special Publications, 30, 253-267.
- Wilson, M., 1989. Igneous Petrogenesis. Oxford University Press, Oxford, 466.
- Wilson, M., Tankut, A. and Guleç, N. 1997. Tertiary volcanism of the Galatia province, north-west Central Anatolia, Turkey, Lithos, 42, 1-2, 105-121.
- Wood, D. A., 1979. A variably veined suboceanic upper mantle—genetic significance for mid-ocean ridge basalts from geochemical evidence. Geology, 7, 10, 499-503.
- Wyllie, P.J., Cox, K.G. and Biggar, G.M., 1962. The habit of apatite in synthetic systems and igneous rocks, Journal of Petrology, 3, 238–243.
- Yang, J. H., Wu, F. Y., Wilde, S. A., Xie, L. W., Yang, Y. H. and Liu, X. M. 2007. Tracing magma mixing in granite genesis: in situ U–Pb dating and Hf-isotope analysis of zircons, Contributions to Mineralogy and Petrology, 153, 2, 177-190.
- Yılmaz, I., 1977. Çaykara granitlerinin petrojenetik ve jeokronometrik etüdü. Tübitak Doğa Bilim Dergisi, (in Turkish with English abstract), 8, 29–35.
- Yılmaz, Y., Tuysuz, O., Yiğitbaş, E., Genc, Ş.C. and Şengor, A.M.C., 1997. Geology and tectonics of the Pontides. In: ROBINSON, A.G. (ed), Regional and Petroleum Geology of the Black Sea and Surrounding Region, American Association of Petroleum Geologists (AAPG) Memoir, 68, 183-226.
- Zankl, H., 1961. Die Geologie der Torrener-Joch-Zone in den Berchtesgadener Alpen, (in German with English abstract), Zeitschrift der Deutschen Geologischen Gesellschaft, 446-462.
- Zindler, A. and Hart, S.R., 1986. Chemical geodynamics, Annual Review of Earth and Planetary Sciences 14, 493–571.

## 7. APPENDIX

Appendix table 1. Description all information about the taken sample from Gündoğdu and Boğalı pluton, Q quartz, Plg-Plagioclase, Amph-Amphibole, Bio-Biotite.

Gündoğdu	Location	GSP location	Highest	Lithology	Rocks name	Texture	Mineralogy	Matrix
BG-15	Bahçecik	37585676 D 4493156 K	1517	Massif granite	Monzogranite	Granular	Q %20, K-Feld %30, plg (An28) %50, Amph > %5, Fe-Ti oksit > %2 epidot ve serisit common	
BG-16	Bahçecik	37585892 D 4493030 K	1526	Massif	Monzogranite	Microgranular prophyritic	Q %10 (kemirilmis), K-Feld % 15, plj (An25) %10, Amph > %2 and fine grain as matriks %63	Q, plg, K-feld, amph and Fe-Ti oxides display sericitization and carbonation
BG-18	Gündoğdu	37586135 D 4492912 K	1642	Massif	Prophyritic Synogranodirite	Fine grain prophyritic	Q %40, K-Feld %10, plg %35, Amph %10, Opak %2, Epd %3 and displays sericitization.	
BG-19	Cörmeler	37586883 D 4491950 K	1600	Massif	Prophyritic Synogranodirite	Fine grain prophyritic	Q %38, K-Feld %12, plg %34, Amph %10, Opak %6 serizitleşme displays sericitization and carbonation	
BG-20	Cörmeler	37586930 D 4491647 K	1607	Massif	Prophyritic Dasit	Mirogranuşar prophyritic	Q %20, plg %30, Amph%10, and matrix %40	Qu, plg, amph and opak
BG-20	Cörmeler	37586930 D 4491647 K	1607	Enclave	Prophyritic Diorite	Mirogranuşar prophyritic	plg %55, Amph%35, Opak %10	
EO-3	Boğalı Yaylası	37589094 D 4494373 K	2476	Massif	Prophyritic Diorite	Prophyritic-Ophitic	plg > %80, Q < %5	
EO-6	Cılar Tepe güneyi	37586856 D 4494482 K	2101	Massif	Synogranodirite	Medium gain (Equigranular)	Q %30, K-Feld %45, plg %10, Amph %10,	

EO-7	Gündoğdu-Bayburt yol ayrımı	37587784 D 4491667 K	1678	Massif	Granodirite	Fine grain ektigranüler)	Biotit %5 Q %30, K-Feld %20, plg (An25) %50, Amph > %2. Sericitazation common	
EO-10	Cörmeler	37586649 D 4492138 K	1525		Prophyritic Diorite	Microgranular prophyritic	K-Feld %5, plg %50, Amph %30, matrix %15	
EO-11	Cörmeler	37586281 D 4492410 K	1684		Monzogranite prophyr	Microgranular prophyritic	Q %30, K-Feld %30, plG %30, Amph %10	
EO-25	Pazarcık	37581669D 4494396 K	1390	Massif	Monzogranite	Fine to medium grain with pokilitic texture	Q %30, K-Feld %30 plG %30, Amph %10	
EO-29	Pazarcık	37581998 D 4494168 K	1480	Massif	Monzogranite	Fine to medium grain	Q %30, K-Feld %40, plg%20, Amph %5, Opak %5 displays sericitazation	
EO-30	Pazarcık	37586100D 4494110 K	1480	Massif	Monzogranite	Granular graine (Equigranular)	Q %40, K-Feld %30, plg%25, Ep >%5	
EO-70	Ispatan kuzeyi	37590567 D 4489932 K	1851		Monzogranite	Medium grain (Equigranular)	Q %33, K-Feld %30, plg %32, Amph %5 displays sericitazation and chloritization	
EO-71	Gündoğdu-Bayburt yol ayrımı	37587985 D 4491230 K	1618		Monzodiorite	Monzonitic prophyritic	Quartz(few), plagioclase, A-feld	Quartz (few)+ Plaj+A feldsapr
EO-74	Gündoğdu	37587922 D	1627	Massif	Monzogranite	Fine grain	Q %15, K-feld %30, plg	



									and carbonation	
BG-20	Cörmeler	37586930 D 4491647 K	1607	Massif	Prophyritic Dazit	Mirogranuŕar prophyritic	Q %20, plg %30, Amph%10, and matrix %40	Qu, plag, amph and opak		
BG-20	Cörmeler	37586930 D 4491647 K	1607	Enclave	Prophyritic Diorite	Mirogranuŕar prophyritic	plg %55, Amph%35, Opak %10			
EO-3	Boęalı Yaylası	37589094 D 4494373 K	2476	Massif	Prophyritic Diorite	Prophyritic- Ophitic	plg >%80, Q <%5			
EO-6	Cılar Tepe güneyi	37586856 D 4494482 K	2101	Massif	Syngranodirite	Medium grain (Equigranular)	Q %30, K-Feld %45, plg %10, Amph %10, Biotit %5			
EO-7	Gündoędu- Bayburt yol ayrımı	37587784 D 4491667 K	1678	Massif	Granodirite	Fine grain (Equigranular)	Q %30, K-Feld %20, plg (An25) %50, Amph > %2. Sericitazation common			
EO-10	Cörmeler	37586649 D 4492138 K	1525		Prophyritic Diorite	Microgranular Prophyritic	K-Feld %5, plg %50, Amph %30, matrix %15			
EO-11	Cörmeler	37586281 D 4492410 K	1684		Prophyritic Monzogranite	Microgranular Prophyritic	Q %30, K-Feld %30, plg %30, Amph %10			



EO-25	Pazarcik	37581669D 4494396 K	1390	Massif	Monzogranite	Fine to medium grain with pokilitic texture	Q %30, K-Feld %30 plg %30, Amph %10	
EO-29	Pazarcik	37581998 D 4494168 K	1480	Massif	Monzogranite	Fine to medium grain	Q %30, K-Feld %40, plg%20, Amph %5, Opak %5 displays sericitization	
EO-30	Pazarcik	37586100D 4494110 K	1480	Massif	Monzogranite	Granular graine (Equigranular)	Q %40, K-Feld %30, plg%25, Ep >%5	
EO-70	Ispatan kuzeyi	37590567 D 4489932 K	1851		Monzogranite	Medium grain (Equigranular)	Q %33, K-Feld %30, plg %32, Amph %5 displays sericitization and chloritization	

EO-71	Gündoğdu-Bayburt yolayırımı	37587985 D 4491230 K	1618		Monzodiorite	Monzonitic prophyritic	Quartz(few), plagioclase, A-feld	Quartz (few)+ Plaj+A feldspr
EO-74	Gündoğdu batısı	37587922 D 4491147 K	1627	Massif	Monzogranite	Fine grain (Equigranular)	Q %15, K-feld %30, plg (An25)%30, Amph %20 carbonation common	
EO-83	Altıncı Yayla	37590406 D 4486677 K	2108	Massif	Diorite	Intersertal texture	plg %55, Amph %30, Biotit %15	
EO-84	Altıncı Yayla	37590987 D 4487261 K	2032	Massif	Granodiorite proph	Fine grain prophyritic	Q %30, K-Feld %15, plj %30, Amf %25 displays sericitization and chloritization	
EO-91	Ziyaret Tepe	37593257 D 4486517 K	2357		Monzogranite proph	Fine grain prophyritic	Q %20, K-Feld %22, plg %38, Amph %20	

Boğalı										
BG-1	Boğalı Yolu	37585532 D 4494855 K	1542	Massif	Monzogranite proph	Fine to medium grain prophyritic	Q %25, K-Feld %40, plg(An32) %25, Amph %9, Opak %1, Plagioclase displays sericitazation alteration.			
BG-1a	Boğalı Yolu	37585532 D 4494855 K	1542	Enclave inside	Quartz Monzonit Porfir	Fine grain prophyritic (Equigranular)	Q %10, K-Feld %30, plg %40, Amph %18, Opak %2 felspar displays sericitazation alteration			
BG-1b*	Boğalı Yolu	37585532 D 4494855 K	1542	Enclave inside	Prophyritic Monzogranit	Fine grain prophyritic	Q %30, K-Feld %30, plg %30, Amph %10, displays sericitazation alteration			

					Prophyritic Quartz Monzonit	Fine prophyritic, pokiolitic texture	Q %10, K-Feld %32, plg %38, Amph %18, Opak %2 Kuvars korozyana uğramıştır	
BG-2	Boğalı Köyü	37587314 D 4497241 K	2053	Massif kçt dokanağında n	Prophyritic Quartz Monzonit	Fine prophyritic	Q %15, K-Feld %50, plg %30, Amph%5	
BG-4-a	Bahçecik- Boğalı	37585474D 4494613K	1537	Massif kütle	Prophyritic Quartz Monzodiyorit	Fine prophyritic	Q %8, K-Feld %10, plg %60, Amph %20, Biot %2	
BG-4-b	Bahçecik- Boğalı	37585474D 4494613 K	1537	Massif kütle	Prophyritic Granite	Fine prophyritic	Q %20, K-Feld %30, plg %40, Amph %10, plgioclase displays albite composition and displays twinning and zoning	
BG-11	Boğalı	37585300 D 4495372 K	1803	Massif	Prophyritic Granite	Microgranular Prophyritic	Q %30, K-Feld %35, plg %30, Amph %5	

EO-18	Bahçecik	37584872 D 4493334 K	1474	Massif	Prophyritic Quartz Monzonit	Microgranular Prophyritic	Q %10, K-Feld %37, plg %50, Amph %1, Opak %2	
EO-19	Bahçecik	37584630 D 4493492 K	1532	Massif	Monzogranit	Medium to large phenocryst	Q %28, K-Feld %24, plg %35, Amph%8, Epi %5	
EO-20	Bahçecik	37584635 D 4493340 K	1545	Massif	Prophyritic Quartz Monzonit	Fine grain prophyritic	Q %18, K-Feld %30, plg %47, Amph %5 Serizitleşme yaygın, kuvars minerallerinin kenar kısmı korozyona ugramış ve	
EO-32	Sulakyurt	37584650 D 4494788 K	1927	Massif	Prophyritic Granite	Fine grain prophyritic	Q %32, K-Feld %28, plg(An33) %30, Amf %10	

App table 2. Microporpe analysis results of Plagioclase in the Taşhyayla formation

	42				Ö38								
SiO <sub>2</sub>	67.96	66.70	67.22	66.66	59.84	67.42	67.31	67.42	66.70	66.4	66.64	67.72	65.8
TiO <sub>2</sub>	0.012	0.008	0.002	0.049	0.00	0.00	0.001	0.005	0.018	0.02	0.00	0.00	0.01
Al <sub>2</sub> O <sub>3</sub>	19.47	19.19	19.05	19.41	20.84	19.25	19.69	19.19	19.39	19.5	19.49	19.4	20.1
Cr <sub>2</sub> O <sub>3</sub>	0.005	0.01	0.00	0.009	0.00	0.004	0.016	0.007	0.009	0.01	0.013	0.00	0.00
FeO	0.37	0.4	0.35	0.69	0.61	0.08	0.058	0.082	0.108	0.06	0.058	0.05	0.17
MnO	0.02	0.00	0.00	0.002	0.004	0.00	0.00	0.00	0.00	0.00	0.00	0.00	0.00
MgO	0.001	0.03	0.03	0.27	0.51	0.005	0.01	0.00	0.00	0.005	0.00	0.00	0.04
CaO	0.74	0.39	0.32	0.71	0.23	0.67	0.50	0.29	0.68	0.60	0.74	0.30	0.97
Na <sub>2</sub> O	12.41	12.20	12.39	12.34	3.13	12.3	12.89	13.0	12.6	12.5	12.7	12.5	11.7
K <sub>2</sub> O	0.09	0.10	0.31	0.14	11.9	0.09	0.08	0.06	0.06	0.09	0.08	0.07	0.48
Sum	101.11	99.05	99.70	100.	97.18	99.8	100.5	100	99.6	99.4	99.7	100	99.4
Si	2.961	2.96	2.97	2.93	2.83	2.96	2.94	2.96	2.95	2.94	2.94	2.97	2.92
Al	1.000	1.00	0.99	1.01	1.16	0.99	1.01	0.99	1.01	1.02	1.01	1.01	1.05
Fe <sub>2</sub>	0.01	0.01	0.01	0.02	0.024	0.003	0.002	0.003	0.004	0.003	0.002	0.002	0.01
Ca	0.03	0.01	0.01	0.03	0.012	0.03	0.024	0.01	0.03	0.02	0.03	0.01	0.04
Na	1.04	1.05	1.06	1.05	0.28	1.05	1.095	1.10	1.08	1.08	1.09	1.07	1.01
K	0.005	0.006	0.01	0.008	0.72	0.005	0.005	0.004	0.004	0.005	0.005	0.004	0.02
Sum	5.06	5.06	5.07	5.08	5.08	5.06	5.093	5.09	5.09	5.08	5.09	5.06	5.07
Al	96.33	97.69	96.97	96.21	28.06	96.59	97.50	98.41	96.7	96.9	96.4	98.2	93.2
An	3.19	1.75	1.38	3.06	1.16	2.93	2.09	1.24	2.87	2.59	3.10	1.33	4.24
Or	0.47	0.55	1.64	0.72	70.76	0.46	0.40	0.33	0.33	0.46	0.43	0.40	2.52

Appendix table 2. Continue.

	150										Gb1									
SiO2	65.64	67.5	67.19	67.71	68.18	66.8	68.23	66.6	67.3	64.82	66.56	66.4	43.4							
TiO2	0.009	0.001	0.00	0.01	0.00	0.02	0.00	0.01	0.00	0.012	0.00	0.00	0.01							
Al2O3	21.4	19.4	19.82	19.9	19.64	20.4	19.76	20.8	19.2	21.61	20.20	19.9	34.5							
Cr2O3	0.008	0.004	0.002	0.001	0.004	0.00	0.006	0.00	0.00	0.00	0.006	0.00	0.009							
FeO	0.49	0.08	0.06	0.07	0.08	0.91	0.03	0.32	0.06	0.10	0.00	0.02	0.70							
MnO	0.01	0.00	0.00	0.00	0.004	0.00	0.00	0.00	0.00	0.00	0.00	0.00	0.005							
MgO	0.13	0.00	0.002	0.00	0.00	0.03	0.00	0.03	0.001	0.04	0.006	0.00	0.05							
CaO	0.89	0.44	0.53	0.38	0.22	0.45	0.29	0.31	0.27	0.38	0.28	0.25	18.8							
Na2O	11.4	1.39	12.5	12.5	12.7	11.6	12.7	12.08	12.7	10.6	12.5	12.2	1.09							
K2O	0.84	0.15	0.15	0.27	0.23	0.59	0.18	0.89	0.16	1.13	0.08	0.16	0.04							
Sum	100.9	100.1	100.2	100.9	101.1	100.9	101.2	101.2	99.7	98.7	99.6	99.07	98.7							
Si	2.87	2.96	2.94	2.95	2.96	2.92	2.96	2.91	2.96	2.88	2.93	2.94	2.04							
Al	1.10	1.007	1.02	1.02	1.007	1.05	1.01	1.07	0.99	1.13	1.05	1.04	1.91							
Fe2	0.01	0.003	0.002	0.003	0.003	0.03	0.001	0.01	0.002	0.004	0.00	0.001	0.02							
Ca	0.04	0.02	0.02	0.01	0.01	0.02	0.01	0.01	0.01	0.01	0.01	0.01	0.95							
Na	0.97	1.05	1.06	1.05	1.07	0.98	1.07	1.02	1.08	0.92	1.07	1.05	0.10							
K	0.04	0.009	0.009	0.01	0.01	0.03	0.01	0.05	0.009	0.06	0.005	0.009	0.00							
Sum	5.07	5.06	5.07	5.07	5.07	5.05	5.07	5.08	5.08	5.03	5.07	5.06	5.04							
Al	91.6	97.2	96.9	96.9	97.8	94.7	97.8	94.0	98.0	91.7	98.3	98.0	9.49							
An	3.94	1.91	2.27	1.64	0.95	2.03	1.24	1.35	1.17	1.84	1.24	1.10	90.2							
Or	4.44	0.80	0.80	1.38	1.20	3.19	0.95	4.55	0.82	6.41	0.42	0.86	0.27							



App table 2. Continue

	Ö31										175									
SiO2	45.0	43.4	44.1	43.5	50.9	46.1	43.3	46.2	46.3	45.7	58.7	55.8	45.9	46.1						
TiO2	0.02	0.00	0.01	0.001	0.20	2.26	0.009	0.02	0.02	0.018	0.006	0.003	0.00	0.00						
Al2O3	33.0	35.0	32.9	34.1	4.57	31.16	34.07	32.28	32.48	32.63	23.87	26.11	32.53	34.24						
Cr2O3	0.00	0.01	0.00	0.00	0.001	0.019	0.016	0.005	0.00	0.008	0.00	0.001	0.00	0.003						
FeO	0.69	0.80	0.83	0.66	16.13	0.74	0.71	0.82	0.84	0.88	0.59	0.64	2.44	1.62						
MnO	0.01	0.00	0.00	0.00	0.54	0.015	0.00	0.023	0.00	0.00	0.00	0.03	0.018	0.15						
MgO	0.04	0.01	0.16	0.04	12.94	0.12	0.04	0.05	0.06	0.06	0.003	0.03	1.65	0.85						
CaO	17.3	18.9	17.4	18.6	12.16	16.77	18.44	16.36	16.42	16.74	6.21	8.71	0.72	0.09						
Na2O	1.86	0.91	1.90	1.10	0.53	2.69	1.12	2.46	2.2	2.12	8.24	6.84	0.16	0.09						
K2O	0.08	0.04	0.16	0.05	0.16	0.17	0.057	0.12	0.13	0.11	0.74	0.53	9.98	10.25						
Sum	98.1	99.2	97.6	98.2	98.19	100.17	97.87	98.4	98.4	98.3	98.4	98.7	93.5	93.4						
Si	2.12	2.03	2.10	2.05	2.59	2.14	2.05	2.17	2.17	2.15	2.68	2.55	2.28	2.27						
Al	1.83	1.93	1.84	1.90	0.27	1.70	1.90	1.78	1.79	1.80	1.28	1.40	1.90	1.99						
Fe2	0.02	0.03	0.03	0.02	0.68	0.02	0.02	0.03	0.03	0.03	0.02	0.02	0.10	0.06						
Ca	0.87	0.95	0.89	0.94	0.66	0.83	0.93	0.82	0.82	0.84	0.30	0.42	0.03	0.005						
Na	0.17	0.08	0.17	0.10	0.05	0.24	0.10	0.22	0.20	0.19	0.72	0.60	0.01	0.009						
K	0.01	0.01	0.01	0.003	0.01	0.01	0.003	0.008	0.008	0.007	0.04	0.03	0.63	0.64						
Sum	5.04	5.04	5.06	5.04	5.29	5.05	5.04	5.05	5.03	5.04	5.06	5.05	5.09	5.05						
Al	16.1	8.02	16.3	9.64	7.21	22.32	9.93	21.26	19.36	18.53	67.75	56.97	2.27	1.39						
An	83.3	91.6	82.7	90.0	91.35	76.73	89.73	78.01	79.87	80.8	28.2	40.1	5.61	0.76						
Or	0.47	0.28	0.92	0.31	1.43	0.93	0.33	0.72	0.76	0.65	4.04	2.91	92.12	97.84						





App table 3. Continue

	175													
SiO2	51.24	53.16	50.32	52.89	50.21	51.5	50.4	52.02	49.71	50.2	48.48	48.65	48.85	52.01
TiO2	0.31	0.31	0.55	0.36	0.17	0.34	0.35	0.45	0.91	0.71	1.02	0.82	0.85	0.43
Al2O3	3.43	2.28	4.99	2.83	4.48	3.56	3.91	1.48	3.85	3.57	5.17	5.13	4.66	1.49
Cr2O3	0.00	0.00	0.008	0.00	0.00	0.014	0.00	0.016	0.002	0.008	0.008	0.006	0.004	0.01
FeO	16.96	13.03	15.80	15.26	17.41	15.82	19.25	10.36	10.93	10.66	10.26	10.09	9.89	9.67
MnO	0.51	0.41	0.54	0.47	0.61	0.55	0.61	0.43	0.27	0.27	0.22	0.19	0.211	0.34
MgO	14.56	15.5	13.51	14.61	12.68	13.92	11.91	14.48	13.95	14.31	13.11	13.33	13.55	14.56
CaO	11.76	13.71	12.41	12.16	12.62	12.63	12.29	20.51	20.47	20.23	21.41	21.11	21.41	21.27
Na2O	0.35	0.19	0.49	0.33	0.33	0.27	0.47	0.38	0.36	0.42	0.38	0.35	0.43	0.41
K2O	0.11	0.07	0.19	0.17	0.17	0.14	0.15	0.02	0.005	0.005	0.005	0.006	0.002	0.01
Sum	99.25	98.66	98.83	99.12	98.71	98.81	99.43	100.17	100.46	100.46	100.06	99.71	99.87	100.22
Si	1.96	1.98	1.97	2.00	2.00	1.97	1.94	1.96	1.95	1.96	1.96	1.97	1.94	1.94
Ti	0.00	0.00	0.01	0.00	0.00	0.01	0.01	0.01	0.01	0.01	0.01	0.01	0.00	0.00
Al	0.09	0.07	0.06	0.03	0.03	0.07	0.07	0.08	0.10	0.08	0.10	0.07	0.11	0.12
Cr	0.01	0.01	0.01	0.00	0.01	0.01	0.01	0.01	0.01	0.01	0.01	0.01	0.03	0.03
Fe2	0.13	0.12	0.11	0.14	0.10	0.10	0.14	0.11	0.12	0.12	0.12	0.12	0.10	0.10
Mg	0.94	0.92	0.92	0.87	0.90	0.90	0.92	0.91	0.93	0.92	0.94	0.92	0.96	0.95
Ca	0.84	0.87	0.89	0.93	0.94	0.92	0.93	0.90	0.85	0.88	0.83	0.88	0.83	0.83
Na	0.01	0.01	0.01	0.01	0.01	0.01	0.01	0.01	0.02	0.01	0.01	0.01	0.01	0.01
Sum	3.99	3.99	3.99	3.99	3.98	3.99	4.02	3.99	4.00	3.99	3.99	3.99	3.99	3.98
Mg#	87.97	88.65	89.07	86.18	90.04	89.59	87.13	88.88	88.20	88.73	88.57	88.73	90.78	90.79
Wo	43.94	45.66	46.44	47.89	48.50	47.75	46.84	46.69	44.51	46.10	43.97	46.00	44.20	44.36
En	49.32	48.18	47.71	44.91	46.37	46.81	46.32	47.38	48.95	47.82	49.62	47.91	50.65	50.51
Fs	6.74	6.17	5.85	7.20	5.13	5.44	6.84	5.93	6.55	6.07	6.40	6.09	5.14	5.13

App table 3. Continue

	54.0	51.18	51.63	50.57	52.47	53.21	50.66	44.42	52.4	53.01	51.22	51.21	51.75	51.49	51.36
SiO2	0.17	0.61	0.54	0.73	0.37	0.31	0.42	0.47	0.18	0.15	0.66	0.56	0.56	0.54	0.59
TiO2	0.63	2.56	1.92	3.09	1.02	0.79	2.72	2.43	0.67	0.59	2.47	2.12	2.12	2.07	2.06
Al2O3	0.009	0.002	0.00	0.00	0.00	0.00	0.00	0.005	0.02	0.01	0.00	0.003	0.004	0.005	0.00
Cr2O3	6.41	10.01	10.15	10.97	9.20	9.72	9.47	8.47	10.21	9.36	10.18	9.89	10.01	10.06	10.02
FeO	0.37	0.24	0.28	0.29	0.36	0.45	0.24	0.43	0.55	0.44	0.24	0.27	0.29	0.32	0.31
MnO	15.48	14.51	14.45	14.21	14.67	14.31	13.87	13.06	13.66	14.14	14.45	14.71	14.73	14.93	14.8
MgO	23.43	20.51	20.25	20.12	21.23	21.21	21.23	24.01	21.78	22.12	20.75	20.52	20.66	20.61	20.83
CaO	0.21	0.41	0.46	0.34	0.41	0.52	0.44	0.31	0.41	0.41	0.36	0.29	0.34	0.33	0.33
Na2O	0.01	0.01	0.07	0.005	0.01	0.007	0.08	0.08	0.01	0.009	0.001	0.007	0.005	0.00	0.003
K2O	100.74	100.06	99.79	100.3	99.79	100.54	99.17	93.70	100.01	100.27	100.36	99.61	100.5	100.3	100.3
Sum	1.94	1.95	1.94	1.94	1.96	2.00	2.00	2.01	1.99	1.99	1.97	1.96	1.92	1.98	1.89
Si	0.01	0.00	0.00	0.00	0.00	0.00	0.00	0.00	0.00	0.00	0.00	0.00	0.00	0.00	0.00
Ti	0.11	0.11	0.11	0.11	0.09	0.01	0.03	0.01	0.04	0.05	0.08	0.08	0.13	0.06	0.16
Al	0.03	0.03	0.03	0.03	0.01	0.00	0.00	0.00	0.00	0.01	0.01	0.01	0.01	0.01	0.04
Cr	0.09	0.09	0.09	0.09	0.10	0.08	0.09	0.06	0.12	0.09	0.12	0.10	0.12	0.10	0.12
Fe2	0.94	0.94	0.94	0.94	0.97	0.90	0.91	0.93	0.87	0.91	0.96	0.94	1.01	0.93	0.98
Mg	0.85	0.84	0.87	0.85	0.82	0.98	0.94	0.97	0.94	0.93	0.83	0.89	0.80	0.90	0.82
Ca	0.02	0.01	0.01	0.01	0.03	0.00	0.00	0.01	0.01	0.01	0.01	0.01	0.01	0.01	0.01
Na	3.99	3.98	3.99	3.99	3.99	3.99	3.99	3.99	3.99	3.99	3.98	3.99	4.01	3.99	4.02
Sum	91.08	91.64	91.40	91.14	90.89	91.47	91.15	94.39	88.09	90.53	89.26	90.46	89.50	90.64	88.74
Mg#	45.17	45.05	46.07	44.97	43.53	50.09	48.52	49.70	48.70	48.19	43.44	46.13	41.59	46.66	42.57
Wo	49.94	50.36	49.29	50.15	51.33	45.65	46.92	47.48	45.19	46.90	50.48	48.73	52.27	48.33	50.96
En	4.89	4.59	4.64	4.88	5.14	4.26	4.56	2.82	6.11	4.91	6.07	5.14	6.14	5.02	6.47
Fs															

175

App table 4. Microprobe analysis result of Chlorite in the Taşlyayla formation.

	150															
SiO2	28.34	28.33	28.05	28.25	31.85	31.03	29.79	28.17	28.16	27.99	28.07	28.74	27.66	27.86	29.10	27.28
TiO2	0.05	0.07	0.08	0.11	0.14	0.10	0.07	0.06	0.05	0.06	0.06	0.08	0.05	0.05	0.07	0.05
Al2O3	18.84	18.74	18.13	18.56	21.36	19.89	20.03	18.90	18.80	18.96	18.65	19.37	19.05	19.42	18.89	19.28
Fe2O3	1.01	0.83	0.56	0.69	6.15	3.92	2.65	0.61	0.89	1.14	1.13	2.03	0.34	0.77	1.56	0.00
FeO	23.93	24.44	24.54	24.48	15.50	19.37	21.25	24.08	23.82	23.30	21.99	21.28	24.00	23.03	22.29	24.13
MnO	0.92	0.96	0.86	0.89	0.71	0.72	0.84	0.88	0.92	0.89	0.79	0.80	0.84	0.75	0.77	0.84
MgO	15.86	15.80	16.04	16.05	12.81	14.41	15.14	16.39	15.89	15.43	16.22	15.33	16.53	16.67	15.85	17.51
CaO	0.15	0.12	0.18	0.17	0.24	0.25	0.23	0.17	0.17	0.16	0.16	0.22	0.16	0.09	0.27	0.05
Na2O	0.00	0.03	0.01	0.03	0.05	0.05	0.02	0.03	0.00	0.04	0.05	0.05	0.06	0.00	0.10	0.00
K2O	0.04	0.07	0.08	0.06	0.10	0.16	0.11	0.08	0.09	0.08	0.08	0.10	0.06	0.04	0.13	0.04
Si	0.943	0.943	0.933	0.940	1.060	1.033	0.991	0.938	0.937	0.932	0.934	0.957	0.921	0.927	0.969	0.908
Ti	0.001	0.002	0.002	0.003	0.004	0.003	0.002	0.002	0.001	0.002	0.002	0.002	0.001	0.001	0.002	0.001
Al	0.55	0.55	0.53	0.54	0.62	0.58	0.58	0.55	0.55	0.55	0.54	0.57	0.56	0.57	0.55	0.56
Fe2+	0.34	0.35	0.34	0.34	0.29	0.31	0.32	0.34	0.34	0.33	0.32	0.32	0.33	0.33	0.33	0.33
Mn	0.01	0.01	0.01	0.01	0.01	0.01	0.01	0.01	0.01	0.01	0.01	0.01	0.01	0.01	0.01	0.01
Mg	0.39	0.39	0.39	0.39	0.31	0.35	0.37	0.41	0.39	0.38	0.41	0.38	0.41	0.41	0.39	0.43
Ca	0.003	0.002	0.003	0.003	0.004	0.004	0.004	0.003	0.003	0.003	0.003	0.004	0.003	0.002	0.005	0.001
Total	2.25	2.25	2.23	2.25	2.31	2.31	2.30	2.26	2.24	2.22	2.22	2.24	2.24	2.25	2.26	2.26





App table 4. Continue

	Ö30					Ö38					Ö42				
SiO2	29.96	29.56	29.32	37.35	29.58	29.14	30.77	30.20	24.95	25.26	25.19	25.16	25.01	25.43	
TiO2	0.08	0.14	0.28	0.0	23.12	0.08	0.12	0.10	0.00	0.03	0.02	0.02	0.01	0.07	
Al2O3	19.78	18.80	18.61	20.60	12.46	19.24	19.16	19.02	19.11	18.85	19.59	19.29	19.79	18.56	
Fe2O3	2.06	2.34	1.44	8.38	11.49	1.25	3.28	2.15	0.00	0.00	0.00	0.00	0.00	0.00	
FeO	22.20	21.82	22.35	10.18	0.00	22.64	20.79	22.07	32.13	32.73	31.15	30.30	29.66	32.55	
MnO	0.77	0.72	0.86	0.18	0.45	0.76	0.65	0.71	0.62	0.50	0.71	0.66	0.59	0.46	
MgO	15.94	14.75	16.28	0.02	1.74	16.91	14.58	15.87	12.74	12.45	13.49	13.69	14.01	12.55	
CaO	0.34	0.44	0.43	23.33	19.63	0.23	0.49	0.36	0.06	0.05	0.02	0.02	0.01	0.09	
Na2O	0.03	0.07	0.04	0.02	0.00	0.00	0.04	0.06	0.00	0.02	0.01	0.00	0.04	0.05	
K2O	0.15	0.18	0.20	0.01	0.09	0.07	0.18	0.13	0.02	0.03	0.07	0.03	0.06	0.03	
Si	0.99	0.98	0.97	1.24	0.98	0.97	1.02	1.01	0.83	0.84	0.83	0.83	0.83	0.84	
Ti	0.002	0.003	0.007	0.002	0.57	0.002	0.003	0.002	0.000	0.001	0.001	0.001	0.000	0.002	
Al	0.58	0.55	0.54	0.61	0.36	0.56	0.56	0.56	0.56	0.55	0.57	0.56	0.58	0.54	
Fe2+	0.33	0.33	0.32	0.247	0.14	0.33	0.33	0.33	0.44	0.45	0.43	0.42	0.41	0.45	
Mn	0.01	0.01	0.01	0.003	0.006	0.01	0.009	0.01	0.009	0.007	0.01	0.009	0.008	0.007	
Mg	0.39	0.36	0.40	0.00	0.04	0.41	0.36	0.39	0.31	0.31	0.33	0.34	0.34	0.31	
Ca	0.006	0.008	0.008	0.41	0.35	0.004	0.009	0.006	0.001	0.001	0.000	0.000	0.000	0.002	
Total	2.33	2.26	2.28	2.51	2.47	2.31	2.31	2.31	2.16	2.16	2.19	2.17	2.18	2.16	

App table 4. Continue

SiO <sub>2</sub>	25.01	25.21	24.85	25.78	28.00	33.34	27.90	25.73	25.32
TiO <sub>2</sub>	0.00	0.06	0.02	0.06	0.09	0.07	0.05	0.04	0.02
Al <sub>2</sub> O <sub>3</sub>	18.48	18.37	19.06	18.87	20.70	21.15	19.77	19.01	19.05
Fe <sub>2</sub> O <sub>3</sub>	0.00	0.00	0.00	0.00	0.74	4.34	1.33	0.00	0.00
FeO	33.16	34.12	33.76	33.44	27.35	18.90	27.39	32.37	29.60
MnO	0.45	0.41	0.66	0.42	0.44	0.51	0.68	0.57	0.77
MgO	11.94	11.17	11.78	11.96	12.41	10.05	10.98	12.07	14.01
CaO	0.05	0.04	0.05	0.03	0.05	0.04	0.07	0.03	0.03
Na <sub>2</sub> O	0.01	0.02	0.02	0.00	0.04	0.09	0.00	0.02	0.00
K <sub>2</sub> O	0.18	0.19	0.03	0.15	1.29	3.47	1.15	0.23	0.04
Si	0.83	0.83	0.82	0.85	0.93	1.11	0.92	0.85	0.84
Ti	0.00	0.002	0.00	0.002	0.002	0.002	0.001	0.001	0.00
Al	0.54	0.54	0.56	0.55	0.61	0.62	0.58	0.55	0.56
Fe <sub>2</sub> <sup>+</sup>	0.46	0.47	0.47	0.46	0.39	0.31	0.39	0.45	0.41
Mn	0.006	0.006	0.009	0.006	0.006	0.007	0.010	0.008	0.01
Mg	0.29	0.27	0.29	0.29	0.30	0.24	0.27	0.29	0.34
Ca	0.001	0.001	0.001	0.001	0.001	0.001	0.001	0.001	0.000
Total	2.14	2.14	2.16	2.18	2.26	2.34	2.20	2.17	2.17

App table 5. Microprobe analysis of Plagioclase in the Gündoğdu pluton and their MMEs.

Monzogranite		Diorite																
BG20		83																
SiO2	69.31	69.43	67.54	68.58	66.77	67.18	67.82	66.93	51.50	53.93	53.28	59.52	56.09	54.49	55.58	52.91	46.54	46.68
TiO2	0.01	0.00	0.00	0.00	0.01	0.02	0.00	0.00	0.06	0.06	0.04	0.02	0.06	0.04	0.04	0.05	0.00	0.02
Al2O3	20.26	19.84	20.30	19.77	21.90	20.74	20.61	21.26	30.22	28.61	29.32	25.37	27.00	28.39	27.83	29.27	33.54	33.54
Cr2O3	0.00	0.02	0.02	0.00	0.00	0.00	0.00	0.00	0.03	0.00	0.02	0.00	0.01	0.00	0.00	0.00	0.02	0.04
FeO	0.02	0.00	0.03	0.12	0.00	0.00	0.03	0.02	0.37	0.40	0.41	0.27	0.41	0.44	0.46	0.49	0.45	0.43
MgO	0.00	0.00	0.00	0.01	0.00	0.00	0.00	0.01	0.03	0.03	0.02	0.02	0.02	0.04	0.04	0.03	0.00	0.02
CaO	1.01	0.78	1.27	0.59	2.62	1.75	1.43	1.43	13.71	12.03	12.58	7.64	9.98	11.46	10.65	12.65	18.03	17.94
Na2O	11.62	11.75	11.50	11.78	10.64	11.12	11.38	11.23	3.93	5.08	4.53	7.44	6.05	5.21	5.58	4.63	1.47	1.50
K2O	0.15	0.11	0.11	0.26	0.05	0.13	0.08	0.09	0.17	0.27	0.24	0.37	0.38	0.29	0.33	0.23	0.05	0.04
Total	102.40	101.93	100.80	101.13	102.00	100.94	101.36	101.02	100.03	100.42	100.44	100.73	100.01	100.41	100.55	100.32	100.17	100.21
Si	2.97	2.98	2.94	2.97	2.88	2.92	2.94	2.91	2.35	2.44	2.41	2.65	2.53	2.46	2.50	2.40	2.14	2.15
Al	1.02	1.00	1.04	1.01	1.11	1.06	1.05	1.09	1.62	1.52	1.56	1.33	1.44	1.51	1.48	1.57	1.82	1.82
Ca	0.05	0.04	0.06	0.03	0.12	0.08	0.07	0.07	0.67	0.58	0.61	0.36	0.48	0.55	0.51	0.62	0.89	0.88
Na	0.96	0.98	0.97	0.99	0.89	0.94	0.96	0.95	0.35	0.45	0.40	0.64	0.53	0.46	0.49	0.41	0.13	0.13
K	0.01	0.01	0.01	0.01	0.00	0.01	0.00	0.00	0.01	0.02	0.01	0.02	0.02	0.02	0.02	0.01	0.00	0.00
An	4.55	3.51	5.72	2.67	11.95	7.92	6.45	6.53	65.22	55.84	59.72	35.45	46.67	53.97	50.39	59.37	86.89	86.63
Ab	94.63	95.91	93.69	95.93	87.80	91.36	93.13	93.00	33.79	42.68	38.90	62.50	51.23	44.39	47.73	3933	12.84	13.13
Or	0.82	0.58	0.59	1.40	0.25	0.72	0.43	0.47	0.99	1.48	1.38	2.05	2.10	1.64	1.87	1.30	0.27	0.24



App table 5. Continue

	Monzodiorite					Quartz monzodiorite					BG 20en							
	61.77	61.84	62.20	61.58	57.92	56.95	54.82	64.08	59.67	53.95	50.01	57.24	53.66	55.11	58.20	53.50	53.72	53.52
SiO <sub>2</sub>	0.00	0.02	0.00	0.00	0.01	0.02	0.00	0.00	0.02	0.00	0.01	0.03	0.00	0.01	0.06	0.01	0.02	0.01
TiO <sub>2</sub>	24.14	24.49	24.18	24.42	23.53	26.95	26.32	23.11	25.96	27.53	31.28	26.76	28.64	28.09	23.69	28.91	28.83	28.87
Cr <sub>2</sub> O <sub>3</sub>	0.00	0.02	0.00	0.02	0.02	0.06	0.00	0.00	0.00	0.00	0.00	0.00	0.04	0.00	0.01	0.00	0.00	0.00
FeO	0.13	0.16	0.09	0.09	2.48	0.35	0.33	0.03	0.24	0.44	0.43	0.34	0.38	0.38	1.16	0.40	0.44	0.47
MgO	0.00	0.00	0.00	0.00	2.00	0.02	0.03	0.00	0.03	0.03	0.06	0.01	0.04	0.01	0.05	0.03	0.03	0.04
CaO	6.04	6.17	5.95	6.29	5.11	9.18	10.19	4.24	7.59	11.11	15.16	9.44	12.10	10.95	4.94	12.20	12.20	12.23
Na <sub>2</sub> O	8.59	8.52	8.55	8.40	7.18	6.57	5.88	9.70	6.94	5.16	3.05	6.35	4.84	5.42	6.87	4.79	4.84	4.81
K <sub>2</sub> O	0.24	0.22	0.26	0.23	0.08	0.62	1.03	0.07	0.39	0.35	0.14	0.46	0.24	0.34	2.46	0.26	0.26	0.27
Total	100.91	101.43	101.25	101.06	98.50	100.75	98.62	101.24	100.86	98.62	100.15	100.62	99.96	100.31	97.50	100.15	100.36	100.22
Si	2.73	2.72	2.73	2.71	2.65	2.55	2.52	2.80	2.64	2.48	2.29	2.56	2.44	2.48	2.69	2.43	2.43	2.43
Al	1.26	1.27	1.25	1.27	1.27	1.42	1.43	1.19	1.36	1.49	1.68	1.41	1.53	1.49	1.29	1.55	1.54	1.54
Ca	0.29	0.29	0.28	0.30	0.25	0.44	0.50	0.20	0.36	0.55	0.74	0.45	0.59	0.53	0.24	0.59	0.59	0.59
Na	0.74	0.73	0.73	0.72	0.64	0.57	0.52	0.82	0.60	0.46	0.27	0.55	0.43	0.47	0.62	0.42	0.42	0.42
K	0.01	0.01	0.01	0.01	0.00	0.04	0.06	0.00	0.02	0.02	0.01	0.03	0.01	0.02	0.15	0.02	0.01	0.02
An	27.63	28.23	27.36	28.92	28.07	42.08	46.22	19.36	36.82	53.25	72.72	43.95	57.23	51.73	24.36	57.61	57.39	57.55
Ab	71.09	70.59	71.22	69.82	71.38	54.55	48.23	80.25	60.91	44.77	26.49	53.50	41.40	46.36	61.22	40.90	41.15	40.93
Or	1.29	1.18	1.43	1.26	0.55	3.37	5.55	0.40	2.26	1.98	0.79	2.55	1.38	1.92	14.42	1.49	1.45	1.52

App table 6. Microprobe analysis of K-feldspar in the Gündoğdu pluton and their MMEs.

	Mozongranite		30	Quartz monzodiorite	
	BG20	50.46		BG20 MME	64.84
SiO <sub>2</sub>	50.60	50.65	63.40	65.30	66.54
TiO <sub>2</sub>	0.08	0.09	0.03	0.00	0.02
Al <sub>2</sub> O <sub>3</sub>	30.18	31.43	18.62	18.42	18.54
Cr <sub>2</sub> O <sub>3</sub>	0.01	0.01	0.00	0.00	0.04
FeO	1.63	1.37	0.41	0.03	0.00
MnO	0.08	0.02	0.00	0.01	0.00
NiO	0.02	0.04	0.00	0.00	0.00
MgO	2.06	1.76	0.18	0.02	0.01
CaO	0.02	0.06	0.24	0.00	0.22
Na <sub>2</sub> O	0.06	0.08	0.41	0.92	4.14
K <sub>2</sub> O	10.51	10.14	14.75	15.12	12.01
Total	95.30	95.69	98.05	99.82	101.53
Si	2.44	2.42	2.98	3.01	2.99
Al	1.71	1.77	1.03	1.00	0.98
Fe	0.07	0.05	0.02	0.00	0.00
Mg	0.15	0.13	0.01	0.00	0.00
Ca	0.00	0.00	0.01	0.00	0.01
Na	0.01	0.01	0.04	0.08	0.36
K	0.65	0.62	0.88	0.89	0.69
An	0.13	0.52	1.29	0.02	1.00
Ab	0.87	1.24	4.02	8.44	34.00
Or	99.00	98.24	94.69	91.54	65.00





App table 7. Continue

Comment	Fe-Ti Oxides												30_Anc			
	30	83	83	83	83	83	83	83	83	83	83	83				
SiO2	0.06	0.06	0.06	0.06	0.09	0.08	0.06	0.08	0.06	0.06	0.06	0.02	0.06	0.45	0.05	0.04
TiO2	4.31	0.10	0.20	2.13	0.81	0.76	0.29	1.26	2.11	46.12	0.01	46.12	0.01	4.84	4.35	4.32
Al2O3	1.32	0.09	0.13	0.89	0.11	0.35	0.31	0.28	1.79	0.00	0.06	0.00	0.06	0.60	1.27	1.27
Cr2O3	0.009	0.000	0.008	0.048	0.041	0.000	0.063	0.021	0.026	0.000	0.004	0.000	0.004	0.007	0.015	0.084
FeO	80.34	85.97	84.84	82.25	84.95	83.56	85.26	83.96	81.32	42.99	86.60	42.99	86.60	79.59	78.76	79.99
MnO	0.62	0.05	0.09	0.32	0.21	0.12	0.03	0.21	0.18	4.67	0.03	4.67	0.03	0.32	1.38	1.45
NiO	0.00	0.00	0.00	0.01	0.00	0.00	0.04	0.00	0.04	0.00	0.00	0.00	0.00	0.00	0.00	0.02
MgO	0.11	0.02	0.01	0.03	0.006	0.00	0.008	0.00	0.01	0.04	0.00	0.04	0.00	0.03	0.33	0.44
CaO	0.02	0.03	0.02	0.02	0.21	0.03	0.17	0.09	0.07	0.05	0.02	0.05	0.02	0.07	0.006	0.004
Na2O	0.005	0.00	0.01	0.001	0.00	0.00	0.03	0.02	0.01	0.008	0.003	0.008	0.003	0.01	0.003	0.00
K2O	0.00	0.03	0.006	0.00	0.00	0.005	0.008	0.00	0.008	0.00	0.02	0.00	0.02	0.009	0.003	0.00
Total	87.29	86.61	85.84	86.69	87.23	85.85	87.18	86.77	86.39	94.27	87.14	94.27	87.14	86.54	86.66	88.08
Si	0.003	0.003	0.003	0.004	0.003	0.005	0.004	0.005	0.004	0.001	0.003	0.001	0.003	0.025	0.003	0.002
Ti	0.17	0.004	0.009	0.08	0.03	0.03	0.01	0.05	0.08	1.58	0.00	1.58	0.00	0.20	0.18	0.17
Al	0.08	0.006	0.009	0.05	0.008	0.02	0.02	0.02	0.11	0.00	0.004	0.00	0.004	0.04	0.08	0.08
Fe	2.14	1.99	2.00	2.07	2.01	2.02	1.99	2.03	2.07	1.64	1.99	1.64	1.99	2.20	2.09	2.07
Mg	0.009	0.002	0.001	0.003	0.00	0.00	0.001	0.00	0.001	0.003	0.00	0.003	0.00	0.003	0.02	0.03
Ca	0.002	0.002	0.001	0.001	0.01	0.002	0.01	0.006	0.005	0.003	0.002	0.003	0.002	0.004	0.00	0.00
Na	0.001	0.00	0.002	0.00	0.00	0.00	0.004	0.002	0.001	0.001	0.00	0.001	0.00	0.001	0.00	0.00
K	0.00	0.003	0.00	0.00	0.00	0.00	0.001	0.00	0.001	0.00	0.002	0.00	0.002	0.001	0.00	0.00

App table 7. Continue

	Biotite		Chlorite	
	BG20	30_Anc	BG20	30_Anc
SiO2	38.99	48.23	SiO2	26.65
TiO2	4.41	0.12	TiO2	0.02
Al2O3	12.38	30.78	Al2O3	20.71
Cr2O3	0.00	0.00	Cr2O3	0.00
FeO	16.08	3.09	FeO	19.31
MnO	0.25	0.14	MnO	1.20
NiO	0.00	0.01	NiO	0.00
MgO	13.6	2.95	MgO	17.55
CaO	0.07	0.06	CaO	0.02
Na2O	0.10	0.08	Na2O	0
K2O	8.80	9.12	K2O	0.035
Total	94.5	94.58	Total	85.6
Si	5.87	6.46	Si	5.59
Ti	0.50	0.01	Ti	0.004
Al	2.19	4.86	Al	5.12
Fe	1.99	0.33	Fe	3.39
Mg	3.05	0.59	Mg	5.49
Ca	0.01	0.00	Ca	0.005
Na	0.02	0.02	Na	0
K	1.69	1.56	K	0.009
%Al	30.33	84.06		
%Fe	27.51	5.71		
%Mg	42.14	10.22		

App table 8. plgioclase microprobe analysis of Boğalı pluton and their MMEs.

Monzogranite																		
BG1																		
SiO2	62.60	59.74	59.99	66.41	67.28	62.17	60.05	61.17	54.50	57.11	59.43	59.58	59.70	60.31	58.84	59.43	59.29	60.53
TiO2	0.00	0.04	0.00	0.00	0.00	0.00	0.00	0.02	0.00	0.02	0.00	0.00	0.00	0.00	0.00	0.01	0.01	0.00
Al2O3	22.68	24.60	24.47	21.45	22.60	23.46	24.88	24.23	26.50	26.79	24.99	25.28	25.24	24.36	25.59	24.76	25.19	23.95
FeO	0.24	0.22	0.19	0.05	0.08	0.24	0.20	0.18	0.29	0.28	0.23	0.21	0.22	0.18	0.24	0.23	0.21	0.21
MgO	0.00	0.01	0.00	0.00	0.01	0.00	0.00	0.01	0.03	0.01	0.02	0.00	0.02	0.00	0.01	0.01	0.02	0.01
CaO	4.86	7.06	6.93	2.89	1.62	5.48	7.43	6.42	9.90	9.39	7.48	7.51	7.48	6.81	8.05	7.21	7.61	6.40
Na2O	8.79	7.67	7.87	10.78	9.23	8.59	7.48	7.76	6.00	6.22	7.48	7.56	7.55	8.06	7.30	7.75	7.54	8.30
K2O	0.67	0.45	0.39	0.06	1.73	0.56	0.61	0.83	0.41	0.50	0.49	0.41	0.21	0.37	0.29	0.31	0.28	0.21
Total	99.90	99.86	99.86	101.67	102.57	100.52	100.66	100.65	97.65	100.33	100.15	100.64	100.45	100.15	100.31	99.76	100.17	99.67
Si	2.79	2.68	2.69	2.88	2.89	2.75	2.67	2.71	2.52	2.56	2.66	2.65	2.66	2.69	2.63	2.67	2.65	2.71
Al	1.19	1.30	1.29	1.10	1.14	1.22	1.30	1.27	1.45	1.42	1.32	1.33	1.32	1.28	1.35	1.31	1.33	1.26
Fe	0.01	0.01	0.01	0.00	0.00	0.01	0.01	0.01	0.01	0.01	0.01	0.01	0.01	0.01	0.01	0.01	0.01	0.01
Ca	0.23	0.34	0.33	0.13	0.07	0.26	0.35	0.31	0.49	0.45	0.36	0.36	0.36	0.33	0.39	0.35	0.36	0.31
Na	0.76	0.67	0.68	0.91	0.77	0.74	0.65	0.67	0.54	0.54	0.65	0.65	0.65	0.70	0.63	0.67	0.65	0.72
K	0.04	0.03	0.02	0.00	0.09	0.03	0.03	0.05	0.02	0.03	0.03	0.02	0.01	0.02	0.02	0.02	0.02	0.01
An	22.54	32.89	32.01	12.86	7.94	25.26	34.23	29.92	46.58	44.21	34.62	34.65	34.96	31.17	37.25	33.37	35.25	29.51
Ab	73.74	64.62	65.86	86.83	81.97	71.67	62.41	65.49	51.13	52.99	62.65	63.11	63.89	66.78	61.13	64.90	63.20	69.31
Or	3.72	2.49	2.13	0.30	10.09	3.07	3.36	4.59	2.29	2.80	2.72	2.24	1.15	2.04	1.62	1.73	1.55	1.18

App table 8. Continue.

	Monzogranite			Quartz monzonite														
	BG1			BG4A														
SiO <sub>2</sub>	57.61	55.55	59.24	59.56	60.20	58.84	59.43	59.29	60.53	49.86	50.84	57.93	58.98	55.95	58.88	58.45	55.86	
TiO <sub>2</sub>	0.02	0.00	0.01	0.00	0.01	0.00	0.01	0.01	0.00	0.02	0.00	0.00	0.01	0.00	0.01	0.01	0.00	
Al <sub>2</sub> O <sub>3</sub>	24.46	24.34	25.32	25.42	25.07	25.59	24.76	25.19	23.95	30.20	29.05	24.56	24.17	24.76	27.01	24.33	24.70	26.35
FeO	0.17	0.24	0.17	0.23	0.26	0.24	0.23	0.21	0.21	0.25	0.29	0.17	0.21	0.21	0.44	0.27	0.15	0.17
MgO	0.01	0.02	0.00	0.01	0.00	0.01	0.01	0.02	0.01	0.00	0.00	0.00	0.00	0.00	0.00	0.02	0.00	0.01
CaO	6.83	7.31	7.80	7.63	7.30	8.05	7.21	7.61	6.40	13.30	12.33	7.06	6.20	6.90	9.22	6.78	6.97	9.10
Na <sub>2</sub> O	7.43	7.06	7.42	7.40	7.56	7.30	7.75	7.54	8.30	3.67	4.29	7.53	8.06	7.50	6.02	7.79	7.39	6.12
K <sub>2</sub> O	0.56	0.36	0.38	0.39	0.36	0.29	0.31	0.28	0.21	0.10	0.12	0.28	0.24	0.25	0.16	0.28	0.29	0.27
Total	97.11	94.92	100.40	100.64	100.79	100.31	99.76	100.17	99.67	97.51	96.99	97.54	98.36	98.65	98.85	98.40	97.97	97.96
Si	2.66	2.63	2.64	2.65	2.67	2.63	2.67	2.65	2.71	2.33	2.38	2.66	2.70	2.67	2.54	2.68	2.66	2.56
Al	1.33	1.36	1.33	1.33	1.31	1.35	1.31	1.33	1.26	1.66	1.60	1.33	1.29	1.32	1.45	1.30	1.33	1.42
Fe	0.01	0.01	0.01	0.01	0.01	0.01	0.01	0.01	0.01	0.01	0.01	0.01	0.01	0.01	0.02	0.01	0.01	0.01
Ca	0.34	0.37	0.37	0.36	0.35	0.39	0.35	0.36	0.31	0.67	0.62	0.35	0.30	0.33	0.45	0.33	0.34	0.45
Na	0.66	0.65	0.64	0.64	0.65	0.63	0.67	0.65	0.72	0.33	0.39	0.67	0.71	0.66	0.53	0.69	0.65	0.54
K	0.03	0.02	0.02	0.02	0.02	0.02	0.02	0.02	0.01	0.01	0.01	0.02	0.01	0.01	0.01	0.02	0.02	0.02
An	32.62	35.64	35.97	35.51	34.08	37.25	33.37	35.25	29.51	66.28	60.92	33.57	29.41	33.21	45.45	31.95	33.70	44.41
Ab	64.18	62.25	61.95	62.32	63.91	61.13	64.90	63.20	69.31	33.11	38.37	64.84	69.23	65.34	53.64	66.48	64.65	54.03

App table 8. Continue

Monzodiorite											
BG4A-MME											
SiO <sub>2</sub>	61.82	61.06	59.45	49.60	56.92	50.55	62.99	60.56	57.18		
TiO <sub>2</sub>	0.00	0.00	0.00	0.01	0.02	0.03	0.02	0.00	0.02		
Al <sub>2</sub> O <sub>3</sub>	23.84	25.40	24.86	31.64	29.35	31.05	23.91	25.73	27.49		
FeO	0.15	0.20	0.24	0.73	0.24	0.69	0.29	0.22	0.36		
MnO	0.04	0.02	0.02	0.04	0.05	0.03	0.02	0.02	0.00		
NiO	0.00	0.03	0.04	0.00	0.02	0.02	0.00	0.00	0.00		
MgO	0.00	0.02	0.00	0.01	0.00	0.28	0.00	0.00	0.01		
CaO	5.74	7.12	7.17	15.55	9.95	10.94	5.58	7.52	9.94		
Na <sub>2</sub> O	8.54	7.72	7.68	2.94	4.39	2.71	8.55	7.58	5.96		
K <sub>2</sub> O	0.28	0.29	0.27	0.10	0.13	2.55	0.37	0.24	0.25		
Total	100.42	101.87	99.74	100.62	101.07	98.85	101.73	101.92	101.21		
Si	2.74	2.68	2.67	2.26	2.52	2.34	2.75	2.66	2.54		
Al	1.25	1.31	1.31	1.70	1.53	1.69	1.23	1.33	1.44		
Fe	0.01	0.01	0.01	0.03	0.01	0.03	0.01	0.01	0.01		
Ca	0.27	0.33	0.34	0.76	0.47	0.54	0.26	0.35	0.47		
Na	0.73	0.66	0.67	0.26	0.38	0.24	0.72	0.64	0.51		
K	0.02	0.02	0.02	0.01	0.01	0.15	0.02	0.01	0.01		
An	26.67	33.22	33.50	74.07	55.14	57.96	25.96	34.94	47.28		
Ab	71.77	65.19	64.98	25.36	44.01	25.96	72.01	63.71	51.31		
Or	1.56	1.58	1.52	0.57	0.85	16.08	2.03	1.35	1.41		

App table 9. K-Feldspar microprobe analysis of Boğalı Pluton and their MMEs.

Monzogranite		32																	
BG1		64.98	65.16	65.14	65.61	65.17	65.24	65.34	66.00	65.13	65.38	63.97	64.12	63.99	63.72	62.78	63.02	63.17	63.55
SiO <sub>2</sub>	0.02	0.01	0.00	0.01	0.01	0.03	0.03	0.01	0.01	0.01	0.02	0.02	0.02	0.02	0.00	0.00	0.01	0.01	0.00
TiO <sub>2</sub>	17.95	18.22	18.00	18.07	17.93	18.32	18.06	18.40	18.20	18.38	17.71	17.54	17.40	17.52	17.51	17.90	17.48	17.65	
Al <sub>2</sub> O <sub>3</sub>	0.05	0.13	0.09	0.16	0.07	0.14	0.06	0.09	0.06	0.12	0.13	0.27	0.09	0.04	0.07	0.10	0.08	0.10	
FeO	0.00	0.04	0.00	0.02	0.00	0.00	0.00	0.08	0.06	0.01	0.02	0.01	0.02	0.01	0.00	0.00	0.03	0.02	
MnO	0.00	0.00	0.01	0.00	0.00	0.00	0.00	0.00	0.00	0.00	0.00	0.01	0.01	0.00	0.00	0.00	0.01	0.00	
MgO	0.01	0.10	0.05	0.05	0.01	0.13	0.00	0.14	0.13	0.13	0.05	0.03	0.02	0.00	0.00	0.12	0.01	0.04	
CaO	0.74	1.92	1.12	2.02	0.85	0.89	0.40	2.49	1.87	2.65	1.40	0.51	0.70	0.61	0.77	1.40	0.97	1.56	
Na <sub>2</sub> O	15.21	13.77	14.89	13.76	15.31	14.98	15.66	13.02	13.47	12.56	13.74	14.71	14.45	14.46	14.58	13.38	14.05	13.23	
K <sub>2</sub> O	99.02	99.39	99.35	99.72	99.38	99.75	99.60	100.26	98.95	99.27	97.05	97.29	96.69	96.41	95.71	95.95	95.84	96.20	
Total	3.02	3.01	3.01	3.01	3.02	3.01	3.02	3.01	3.01	3.00	3.02	3.03	3.03	3.03	3.01	3.00	3.02	3.02	
Si	0.00	0.00	0.00	0.00	0.00	0.00	0.00	0.00	0.00	0.00	0.00	0.00	0.00	0.00	0.00	0.00	0.00	0.00	
Ti	0.98	0.99	0.98	0.98	0.98	1.00	0.98	0.99	0.99	1.00	0.98	0.98	0.97	0.98	0.99	1.01	0.99	0.99	
Al	0.00	0.01	0.00	0.01	0.00	0.01	0.00	0.00	0.00	0.00	0.01	0.01	0.00	0.00	0.00	0.00	0.00	0.00	
Fe	0.00	0.00	0.00	0.00	0.00	0.00	0.00	0.00	0.00	0.00	0.00	0.00	0.00	0.00	0.00	0.00	0.00	0.00	
Mg	0.00	0.00	0.00	0.00	0.00	0.00	0.00	0.00	0.00	0.00	0.00	0.00	0.00	0.00	0.00	0.00	0.00	0.00	
Ca	0.00	0.00	0.00	0.00	0.00	0.01	0.00	0.01	0.01	0.01	0.00	0.00	0.00	0.00	0.00	0.01	0.00	0.00	
Na	0.07	0.17	0.10	0.18	0.08	0.08	0.04	0.22	0.17	0.24	0.13	0.05	0.06	0.06	0.07	0.13	0.09	0.14	
K	0.90	0.81	0.88	0.81	0.90	0.88	0.92	0.76	0.79	0.74	0.83	0.89	0.87	0.88	0.89	0.81	0.86	0.80	
An	0.05	0.48	0.24	0.25	0.04	0.68	0.00	0.68	0.69	0.67	0.27	0.15	0.08	0.00	0.00	0.62	0.06	0.23	
Ab	6.87	17.37	10.21	18.19	7.81	8.24	3.70	22.39	17.28	24.13	13.36	5.00	6.86	5.98	7.43	13.63	9.46	15.17	
Or	93.08	82.16	89.54	81.56	92.14	91.08	96.30	76.93	82.04	75.20	86.37	94.85	93.05	94.02	92.57	85.75	90.48	84.60	





App table 10. amphibole microprobe analysis of Boğah Pluton and MMEs.

Comment	Monzogranite											Quartz mozonite											Monzodiorite	
	BG1	50.81	50.63	50.85	53.24	52.25	45.51	46.81	44.89	51.66	44.68	48.23	50.27	54.19	52.01	54.08	54.13	52.21	55.11	54.69	BG4A_MME			
SiO2	0.72	0.74	0.71	0.01	0.37	1.34	1.20	1.25	0.13	1.24	1.19	0.78	0.24	0.63	0.21	0.33	0.51	0.10	0.19					
TiO2	4.07	4.62	4.37	4.55	3.58	7.42	6.39	7.22	2.68	7.04	6.45	4.85	2.17	3.27	2.26	2.49	3.32	1.88	1.97					
Cr2O3	0.00	0.00	0.00	0.00	0.00	0.01	0.00	0.03	0.00	0.00	0.02	0.06	0.03	0.01	0.02	0.01	0.04	0.00	0.02					
FeO	10.46	10.84	10.75	9.71	10.38	12.50	12.18	12.29	9.03	11.30	12.42	11.03	10.02	11.24	9.73	10.31	12.17	9.56	10.09					
MnO	1.19	1.27	1.20	0.06	1.14	0.86	0.92	0.84	1.37	1.13	1.02	1.24	0.53	0.67	0.47	0.59	0.58	0.52	0.50					
NiO	0.01	0.00	0.01	0.02	0.01	0.00	0.00	0.00	0.00	0.00	0.02	0.01	0.01	0.02	0.00	0.00	0.00	0.00	0.01					
MgO	16.22	15.63	15.82	14.73	16.45	13.01	13.80	12.97	16.14	12.94	14.03	15.33	16.83	16.20	16.76	17.00	15.26	17.39	17.36					
CaO	12.01	11.84	11.89	10.59	12.18	11.35	11.33	10.96	11.55	11.01	11.70	11.92	12.32	11.21	12.46	12.25	11.72	12.54	12.34					
Na2O	0.83	0.96	0.88	0.78	0.70	1.34	1.19	1.34	0.47	1.39	1.26	1.08	0.50	0.99	0.55	0.54	0.80	0.39	0.49					
K2O	0.37	0.41	0.39	0.30	0.24	0.83	0.68	0.78	0.13	0.76	0.70	0.42	0.16	0.27	0.16	0.23	0.26	0.10	0.13					
Total	96.69	96.96	96.88	93.99	97.30	94.21	94.54	92.63	93.19	91.53	97.05	96.99	97.03	96.54	96.72	97.91	96.88	97.63	97.79					
Si	7.09	7.06	7.08	7.46	7.21	6.64	6.78	6.66	7.38	6.69	6.80	7.02	7.44	7.24	7.44	7.38	7.27	7.49	7.44					
Ti	0.08	0.08	0.07	0.00	0.04	0.15	0.13	0.14	0.01	0.14	0.13	0.08	0.03	0.07	0.02	0.03	0.05	0.01	0.02					
Al	0.67	0.76	0.72	0.75	0.58	1.28	1.09	1.26	0.45	1.24	1.07	0.80	0.35	0.54	0.37	0.40	0.55	0.30	0.32					
Fe	1.22	1.26	1.25	1.14	1.20	1.53	1.47	1.52	1.08	1.41	1.46	1.29	1.15	1.31	1.12	1.18	1.42	1.09	1.15					
Mg	3.37	3.25	3.29	3.08	3.38	2.83	2.98	2.87	3.44	2.89	2.95	3.19	3.44	3.36	3.44	3.45	3.17	3.52	3.52					
Ca	1.79	1.77	1.78	1.59	1.80	1.77	1.76	1.74	1.77	1.77	1.77	1.78	1.81	1.67	1.83	1.79	1.75	1.83	1.80					
Na	0.23	0.26	0.24	0.21	0.19	0.38	0.33	0.39	0.13	0.40	0.35	0.29	0.13	0.27	0.15	0.14	0.22	0.10	0.13					
K	0.07	0.07	0.07	0.05	0.04	0.15	0.12	0.15	0.02	0.14	0.13	0.08	0.03	0.05	0.03	0.04	0.05	0.02	0.02					
Ca+Na	2.02	2.03	2.01	1.80	1.99	2.15	2.09	2.13	1.90	2.17	2.11	2.07	1.94	1.94	1.98	1.93	1.96	1.93	1.93					
Na+K	0.29	0.33	0.31	0.26	0.23	0.53	0.46	0.53	0.15	0.55	0.47	0.37	0.16	0.32	0.18	0.18	0.26	0.12	0.15					
Mg#	73.44	71.99	72.41	73.00	73.86	64.98	66.88	65.30	76.11	67.13	66.82	71.24	74.97	71.99	75.44	74.61	69.09	76.43	75.40					

App table 11. Fe-Ti oxides microprobe analysis of Boğalı Pluton and MMEs.

	32												
	BG1								BG4A	BG4en			
SiO2	0.06	0.03	0.07	0.04	0.03	0.05	0.05	0.05	0.05	0.05	0.10	0.21	0.19
TiO2	0.31	0.08	0.06	0.15	0.05	0.15	0.11	0.11	0.09	0.04	5.67	3.16	0.09
Al2O3	0.45	0.07	0.26	0.20	0.12	0.14	0.14	0.14	0.06	0.08	0.35	0.80	0.12
Cr2O3	0.01	0.01	0.05	0.04	0.00	0.01	0.06	0.06	0.01	0.01	0.02	0.00	0.01
FeO	84.53	85.00	84.10	86.29	86.30	79.54	78.24	65.46	81.15	85.33	79.87	77.49	84.67
MnO	0.15	0.07	0.11	0.13	0.07	0.36	0.31	5.08	0.11	0.12	0.27	0.58	0.07
MgO	0.00	0.01	0.00	0.00	0.00	0.00	0.01	0.03	0.02	0.01	0.05	0.26	0.02
CaO	0.01	0.00	0.43	0.00	0.02	0.00	0.01	0.14	0.02	0.04	0.23	0.03	0.01
Na2O	0.00	0.03	0.02	0.00	0.00	0.00	0.00	0.00	0.00	0.02	0.01	0.05	0.00
K2O	0.00	0.01	0.01	0.00	0.00	0.01	0.01	0.02	0.03	0.00	0.01	0.01	0.07
V2O3	0.32	0.31	0.29	0.28	0.31	0.24	0.24	0.24	0.28	0.29	0.57	0.36	0.28
Total	85.86	85.64	85.41	87.16	86.91	80.48	79.18	79.65	87.61	85.99	86.91	82.99	85.53
Si	0.00	0.00	0.00	0.00	0.00	0.00	0.00	0.02	0.32	0.00	0.02	0.01	0.01
Ti	0.01	0.00	0.00	0.01	0.00	0.01	0.01	0.37	0.00	0.00	0.06	0.14	0.00
Al	0.03	0.00	0.02	0.01	0.01	0.01	0.01	0.02	0.00	0.01	0.01	0.05	0.01
Fe	2.01	1.99	1.97	2.00	2.00	1.99	1.99	2.11	2.31	1.99	2.06	2.08	2.00

App table 12. Biotite and Chlorite microprobe analysis.

Biotite	Chlorite		Monzodiorite BG4A_Anc	Monzonite		Monzogranite 32
	Quartz BG4A	Quartz monzonite BG4A		Quartz BG4A	Quartz monzonite BG4A	
SiO2	38.24	36.9	35.4	27.5	27.24	28.0
TiO2	4.58	3.20	4.16	0.01	0.06	0.94
Al2O3	12.5	15.4	13.1	18.6	19.68	16.5
Cr2O3	0.00	0.00	0.00	19.1	19.02	17.8
FeO	16.51	16.05	15.9	0.77	1.11	0.76
MnO	0.24	0.62	0.53	0.00	0.01	0.00
NiO	0.00	0.00	0.00	18.9	18.3	15.6
MgO	13.3	13.1	12.8	0.09	0.08	0.64
CaO	0.00	0.00	0.04	0.00	0.00	0.01
Na2O	0.11	0.08	0.10	0.01	0.00	0.90
K2O	8.90	9.33	8.12	0.00	0.00	0.00
Sum	94.33	94.3	88.4	85.2	85.6	81.3
Si	5.80	5.60	5.69	5.78	5.68	6.12
Ti	0.52	0.36	0.50	4.64	4.85	4.3
Al	2.23	2.75	2.48	0.00	0.00	0.15
Fe	2.06	1.95	1.87	0.10	0.14	0.36
Mg	3.01	2.96	3.06	3.25	3.18	2.88
Ca	3.25	0.00	0.00	0.13	0.19	0.14
Na	0.03	0.02	0.03	5.93	5.72	5.07
K	1.72	1.80	1.66	0.02	0.01	0.15
Mg/(Mg+Fe)	0.59	0.60	0.62			
Mg#	59.39	60.2	62.0			
Fe/(Fe+Mg)	0.40	0.39	0.37			
Fe#	40.60	39.7	37.9			
10*TiO2	45.88	32.0	41.6			
FeO+MnO	16.76	16.69	16.5			

**App table 13.** SHRIMP U-Pb zircon age result Of Taşlıyayla volcanic rocks

Spot	207Pb/206Pb Age	207Pb/235U Age	206Pb/238U Age	208Pb/232Th Age	Concordance
BC10 02	227,845	94,54070705	88,63529426	87,17151077	93%
BC10 04	188,97	101,6619201	92,84204349	92,1636293	90%
BC10 06	255,62	99,45941641	92,82306375	94,4072977	93%
BC10 07	77,87	92,7195528	92,1890754	93,74104209	99%

Concordia Age = 92.5 ±4.6 Ma  
 (95% confidence, decay-const. errs included)  
 MSWD (of concordance) = 8.5,  
 Probability (of concordance) = 0.003

X-Y Weighted Mean:  
 X = 0.1008±0.0045 2s  
 Y = 0.01446±0.00036  
 X-Y error correlation = +0.556  
 MSWD = 1.05, Probability =0.38

App table 14. SHRIMP U-Pb zircon age result Of Gündoğdu Pluton.

Spot	Age $^{207}\text{Pb}/^{235}\text{U}$	Age $2\sigma$	$^{207}\text{Pb}/^{235}\text{U}$	Age $^{206}\text{Pb}/^{238}\text{U}$	Age $2\sigma$	$^{206}\text{Pb}/^{238}\text{U}$
70-471-R	86	29	83,3	4,4		
70-471-C	93	55	93	13		
70-476-R	110	54	103	17		
70-476-C	87	75	86	26		
70-477-R	97	14	88,7	4		
70-477-C	90	66	89	14		
70-473-R	81	17	83,6	3,7		
70-473-C	78	34	78,5	8,4		
70-484-R	83	24	78,7	8,4		
70-484-C	270	170	122	11		
70-485-R	133	68	109	12		
70-485-C	87	28	84,4	6,5		
70-483-R	114	70	99	10		
70-483-C	91	25	89,7	8,1		
70-486-R	84	19	80,4	4,8		
70-486-C	98	30	92	5,7		
70-482-R	83	36	86,8	9,6		
70-482-C	97	44	99	39		
70-494-R	77	17	76,5	7,3		
70-494-C	103	30	103,3	9,2		
70-490-R	92	26	89,9	9		
70-490-C	106	46	102	11		
70-491-R	87	42	90,9	9		
70-491-C	80	32	82,5	7,7		
70-492-R	78	23	81,1	6,3		
70-492-C	91	30	86,8	5,6		
70-493-R	80	12	81,3	2,9		
70-493-C	81	19	83,8	5,1		

App table 15. SHRIMP U-Pb zircon age result Of Boğalı pluton.

Spot	Age $^{207}\text{Pb}/^{235}\text{U}$	Age $2\sigma$ $^{207}\text{Pb}/^{235}\text{U}$	Age $^{206}\text{Pb}/^{238}\text{U}$	Age $2\sigma$ $^{206}\text{Pb}/^{238}\text{U}$
BG4-279-R	80	34	83,2	7
BG4-279-C	86	24	78,6	7
BG4-277-R	85	27	81,6	4
BG4-277-C	81	25	77,6	6,1
BG4-276-R	106	32	96	11
BG4-276-C	84	48	84,9	8,4
BG4-278-R	95	33	89	8,9
BG4-282-R	98	35	87,4	7,1
BG4-282-C	85	58	89	14
BG4-283-R	84	25	79,9	8,2
BG4-283-C	82	16	81,6	6,4
BG4-287-R	81	26	73,6	6,8
BG4-287-C	75	17	79,9	5,2
BG4-286-R	86	14	85,7	5,4
BG4-286-C	86	15	81	14
BG4-289-R	85	35	88,2	9
BG4-289-C	93	49	90,4	9,2
BG4-292-R	76	20	76	6,6
BG4-292-C	76	47	82	14
BG4-295-R	164	78	76	19
BG4-295-C	93	47	93	8,9
BG4-296-C	97	42	93	14
BG4-297-R	147	31	88	7,6
BG4-297-C	88	72	91	13
BG4-299	86	14	84,9	5,7

App table 16. SHRIMP U-Pb zircon age result Of Salmankaş volcanic rocks.

Spot	$^{207}\text{Pb}/^{206}\text{Pb}$	Age	$^{207}\text{Pb}/^{235}\text{U}$	Age	$^{206}\text{Pb}/^{238}\text{U}$	Age	$^{208}\text{Pb}/^{232}\text{Th}$	Age	Concordance
BH-1 01		82	46	45,5	48			99%	
BH-1 02		89	45	44,7	48			99%	
BH-1 03		107	47	46	45,9			98%	
BH-1 04			45	45,4	47			101%	
BH-1 05		18	45	45,2	47,6			100%	
BH-1 06		78	45	44,1	46,6			98%	
BH-1 07		1	43	43,3	43,5			101%	
BH-1 08		37	44	44,3	46,1			101%	

## **8. RESUME**

Born on 25-10-1987, Yaser ALMASHRAMAH completed his primary education at Abu Bakir Alsadeeq primary and continued to Oqba bin Nafie high school in Dhamar city, Yemen. After completion he gained scholarship to University of Aleppo in Syria, and finally graduated in 2006 with a BSc in Geology. In 2011, he finished his master's degree at Lund University, Sweden. Geological department. In 2014 he started his PhD studies at Karadeniz Technical University in Trabzon, Turkey, Geological Engineering. His native language is Arabic, he also speaks fluent English, and has intermediate proficiency in Turkish.